의학 박사학위 논문

저산소 유도 지질대사 효소 발현이 mTOR 신호에 의한 줄기세포 행동에 미치는 영향

The effect of hypoxia-induced lipid metabolic enzymes expression on mTOR signaling-regulated behavior of stem cells

2018년 2월

서울대학교 대학원

수의학과 수의생명과학 전공
(수의생리학)

이 현 직

저산소 유도 지질대사 효소 발현이 mTOR 신호에 의한 줄기세포 행동에 미치는 영향

2018년

이 현 직

수의학 박사학위 논문

저산소 유도 지질대사 효소 발현이 mTOR 신호에 의한 줄기세포 행동에 미치는 영향

The effect of hypoxia-induced lipid metabolic enzymes expression on mTOR signaling-regulated behavior of stem cells

2018년 2월

지도교수: 한 호 재

서울대학교 대학원

수의학과 수의생명과학 전공
(수의생리학)

이 현 직

Doctoral Thesis

The effect of hypoxia-induced lipid metabolic enzymes expression on mTOR signaling-regulated behavior of stem cells

Hyun Jik Lee

Advisor: Ho Jae Han, D.V.M. Ph.D.

Major in Veterinary Biomedical Sciences
(Veterinary Physiology)
Department of Veterinary Medicine
The Graduate School
Seoul National University

February 2018

ABSTRACT

The effect of hypoxia-induced lipid metabolic enzymes expression on mTOR signaling-regulated behavior of stem cells

Hyun Jik Lee

Major in Veterinary Biomedical Science

Department of Veterinary Medicine

The Graduate School

Seoul National University

Nutrient metabolic regulation by hypoxia is an essential physiological process to maintain the behavior of stem cell. Especially, lipid metabolism in the stem cells plays key roles in the regulations of cellular energetics, stemness and behavior. Previous investigators suggested that mitophagy and O-GlcNAc signaling induced by hypoxia are closely associated with metabolic regulation. However, the effect of hypoxia-induced mitpohagy and O-GlcNAc signaling on lipid metabolism of stem cell and the mechanism how lipid metabolism controls behavior are not completely described yet. Threfore, present study aimed to 1) investigate the effect of hypoxia on lipid metabolic enzymes expression and the mechanism how lipid metabolite controls stem cell behavior, and 2) demonstrate the effect of hypoxia-regulated mitophagy and O-GlcNAc signaling on the lipid metabolic enzymes expression in stem cells and its associated mechanism.

Results were as followings:

1. I investigated the effect of hypoxia on lipid metabolic enzyme in umbilical cord blood-derived human mesenchymal stem cells (UCB-hMSCs). In the present study, hypoxia treatment induces UCB-hMSC proliferation, and expression of two lipogenic enzymes: fatty acid synthase (FASN) and stearoyl-CoA desaturase-1 (SCD1). I further confirmed that FASN but not SCD1 is a key enzyme for regulation of UCB-hMSC proliferation and migration.

This finding indicates that FASN-produced palmitic acid stimulates proliferation and migration of UCB-hMSC under hypoxia. I demonstrated that hypoxia increased FASN expression via HIF-1α/SREBP1 pathway. In addition, I observed that hypoxia stimulated mTOR phosphorylation at Ser2481 and Ser2448 residues, whereas inhibition of FASN by cerulenin blocked hypoxia-induced mTOR phosphorylation, proliferation and migration in UCB-hMSCs. *RAPTOR* siRNA transfection significantly inhibited hypoxia-induced proliferation and migration. Hypoxia-induced mTOR also regulated cell cycle and cytoskeletal regulatory proteins. Taken together, these results suggest that hypoxia-induced FASN controls proliferation and migration in UCB-hMSCs through mTORC1 activation. [*Stem Cells*. 2015 33(7):2182-2195]

2. To identify the major mitophagy regulator involving in hypoxia-induced lipid metabolic enzyme expression, I investigated the effect of hypoxia on mitophagy regulator expressions including PINK1, BNIP3, NIX and FUNDC1. And, my data presented that hypoxia reduced mitochondria marker expression in a time-dependent manner and increased mRNA and protein expression levels of BNIP3 and NIX. In addition, BNIP3 silencing induced abberent regulation of mitochondrial ROS production, mitochondrial membrane potential and ER stress markers expression. I demonstrated that hypoxia-induced BNIP3 expression was regulated by CREB binding protein-mediated transcriptional actions

of HIF-1α and FOXO3. Silencing of BNIP3 expression by siRNA transfection inhibited hypoxia-induced SREBP1/FASN-dependent free fatty acid synthesis and mTOR activation. In addition, BNIP3-silenced UCB-hMSC lost hypoxia preconditioning-induced phosphorylation of cofilin-1 and migration. In mouse skin wound healing model, transplantation of BNIP3-silenced UCB-hMSC delayed wound healing, recovered by palmitic acid. Collectively, these data suggest that hypoxia-induced BNIP3 expression via HIF1α and FOXO3 activation is a major mitophagy regulator for inducing the FASN-dependent lipogenesis, which is critical for migration and survival of UCB-hMSCs. [*Redox Biol*. 2017 13:426-443]

3. I examined the effect of glucosamine-induced O-GlcNAcylation on lipid metabolic enzyme expression and survival of mESCs under hypoxia. My data showed that hypoxia treatment increased mESCs apoptosis in a time-dependent manner. And, hypoxia also slightly increased the O-GlcNAc level. Glucosamine treatment as an O-GlcNAc inducer further enhanced the O-GlcNAc level and prevented hypoxia-induced mESC apoptosis, which was suppressed by an O-GlcNAc transferase inhibitor ST045849. Hypoxia regulated several lipid metabolic enzymes while glucosamine increased expression of glycerol-3-phophate acyltransferase-1 (GPAT1), a lipid metabolic enzyme producing lysophosphatidic acid (LPA). I further investigated signaling

pathway how glucosamine controls GPAT1 expression. Glucosamine increased O-GlcNAcylation of Sp1, which subsequently leads to Sp1 nuclear translocation and GPAT1 expression. Silencing of GPAT1 by *Gpat1* siRNA transfection reduced glucosamine-mediated anti-apoptosis in mESCs with mTOR dephosphorylation. Indeed, LPA prevented mESCs from undergoing hypoxia-induced apoptosis and increased phosphorylation of mTOR and its substrates (S6K1 and 4EBP1). Moreover, mTOR inactivation by rapamycin increased pro-apoptotic proteins expressions and mESC apoptosis. Furthermore, transplantation of non-targeting siRNA and glucosamine-treated mESCs increased cell survival and inhibited flap necrosis in mouse skin flap model. Conversely, silencing of GPAT1 expression reversed protective effects of glucosamine. Based upon these findings, present study suggests that upregulation of O-GlcNAc level by glucosamine treatment enhances hypoxia-induced GPAT1 expression through Sp1 activation, which leads to mTOR-mediated protection of mESCs against hypoxic damage. [*Cell Death Dis*. 2016 24;7:e2158]

In conclusion, present study presented that 1) the HIF-1α/FASN/mTORC1 axis is a key pathway linking hypoxia-induced lipogenesis with UCB-hMSC behavior, 2) BNIP3 is a major factor regulating mitophagy and lipogenesis induced by hypoxia, and 3) O-GlcNAc signaling enhanced by glucosamine suppresses hypoxia-induced mESC apoptosis through GPAT1 upregulation.

Keywords: Stem cells, Hypoxia, Lipogenesis, O-GlcNAcylaiton, Mitophagy, FASN, GPAT1, BNIP3

Student Number: 2013-21541

CONTENTS

LIST OF FIGURES

LIST OF TABLES

ABBREVIATIONS

ACC1	Acetyl-coenzyme A carboxylase 1
BCA	Bicinchoninic acid
BNIP3	Bcl2/adenovirus E1B 19kDa protein-interacting protein 3
BrdU	Bromodeoxyuridine
CBP	CREB-binding protein
CCCP	Carbonyl cyanide m-chlorophenyl hydrazine
CDK	Cyclin-dependent kinase
CHIP	Chromatin immunoprecipitation
CHOP	CCAAT-enhancer binding protein homologous protein
CM-H_2DCF-DA	2',7'-dichlorodihydrofluorescein diacetate
CPT1	Carnitine palmitoyltransferase 1
CTCF	Corrected total cell fluorescence
DGAT1	Diglyceride acyltransferase 1
DIC	Differential interference contrast
eIF-2α	Eukaryotic initiation factor 2 α
ER	Endoplasmic reticulum
ESC	Embryonic stem cell
FA	Fatty acid
FASN	Fatty acid synthase

FBS	Fetal bovine serum
FFA	Free fatty acid
FITC	Fluorescein isothiocyanate
FOXO3	Forkhead box, class O3
FUNDC1	FUN14 domain containing 1
GlcN	Glucosamine
GlcNAc	N-acetyl D-glucosamine
GPAT1	Glycerol-3-phosphate acyltransferase 1
H&E	Hematoxylin and eosin
HBP	Hexosamine biosynthetic pathway
HBP	Hexosamine biosynthetic pathway
HIF-1α	Hypoxia-inducible factor-1 α
hMSC	uman mesenchymal stem cell
hMSCs	Human mesenchymal stem cells
HNA	Human nuclear antigen
HRP	Horseradish peroxidase
HSCs	Hematopoietic stem cells
LIF	Leukemia inhibitory factor
LIR	LC3 interacting region
LPA	Lysophosphatidic acid
LPAAT	Lysophosphatidic acid acyltransferase
MAGL	Monoacylglycerol lipase
mESC	Mouse embryonic stem cell

MnSOD	mitochondrial superoxide dismutase
mTOR	Mammalian target of rapamycin
mTORC1	mTOR complex 1
mTORC2	mTOR complex 2
mtROS	Mitochondrial ROS
N.S	Not statistically significant
NAC	N-acetyl cysteine
NF-κB	Nuclear factor κB
NSCs	Neural stem cells
NT	Non targeting
O-GlcNAcylation	O-linked β-N-acetyl glucosaminylation
OGT	O-GlcNAcylation transferase
PA	Palmitic acid
PBA	4-phenylbutyrate
PBS	Phosphate buffered solution
PCR	Polymerase chain reaction
PI	Propidium iodide
PINK1	PTEN-induced putative kinase1
PMSF	Phenylmethylsulfonylfluoride
Ptx	Pertussis toxin
PVDF	Polyvinylidene fluoride
RAPTOR	Regulatory-associated protein of
RICTOR	Rapamycin-insensitive companion of

	mTOR
ROS	Reactive oxygen species
S.E	Standard error of mean
SCAP	SREBP1 cleavage activating protien
SCD1	Stearoyl-CoA desaturase-1
SDS-PAGE	Sodium dodecyl sulfate polyacryl-amide gel electrophoresis
SGLT	Na+/glucose cotransporte
siRNA	Small interfering RNA
SREBP1	Sterol regulatory element binding protein 1
TBST	Tris-buffered saline containing 0.1% Tween-20
TCA	Trichloroactetic acid
TMRE	Tetramethylrhodamine ethyl ester
UCB	Umbilical cord blood
UCB-hMSCs	Umbilical cord blood-derived hMSCs

BACKGROUND

1. Hypoxia

A. Hypoxia as a stem cell regulator

The concept of stem cell niche was firstly proposed by Schofield in 1978 (Schofield. 1978). Stem cell niche includes a variety cellular environment such as cells, oxygen, blood vessel, extra-cellular matrix, nutrient and the three-dimensional space. Stem cells in the body are exposed to low oxygen pressure due to the physiological distribution of vessels. As shown in the Fig. 1, several scientists investigating the concentration of oxygen *in vivo* reported that the concentration of oxygen in stem cell niche is between <1-8% as a physiological normoxia (Simon et al., 2008). And, it has been known that self-renewal ability of stem cell depends on the signals from hypoxic microenvironment (Mohyeldin et al., 2010). Many investigators reported the variety of responses of stem cells against hypoxia, which is dependent on cell types and oxygen concentration (Eliasson et al., 2010; Ezashi et al., 2005; Mohyeldin et al., 2010). In addition, the control of oxygen signaling in stem cell has a potential to regulate migration, differentiation, proliferation and survival of stem cells (Covello et al., 2006; Dall et al., 2016; Shi et al., 2014; Simon & Keith. 2008). Reactive oxygen species (ROS)

induced by cellular oxidative stress is a byproduct of metabolism (Bigarella et al., 2014). The main sites of ROS generation are mitochondria, endoplasmic reticulum, and plasma membrane (Di Meo et al., 2016). ROS functions as a oxygen signaling which mediates the cellular physiology and bio-energetic metabolism in the stem cell (Liang et al., 2014). The metabolic regulation of ROS has been considered as an important strategy for functional regulation in stem cell (Burgess et al., 2014; Liang & Ghaffari. 2014). Taken together, these findings suggest that control of extracellular oxygen concentration and intracellular oxygen signaling has a capacity to control stem cell metabolism and behavior.

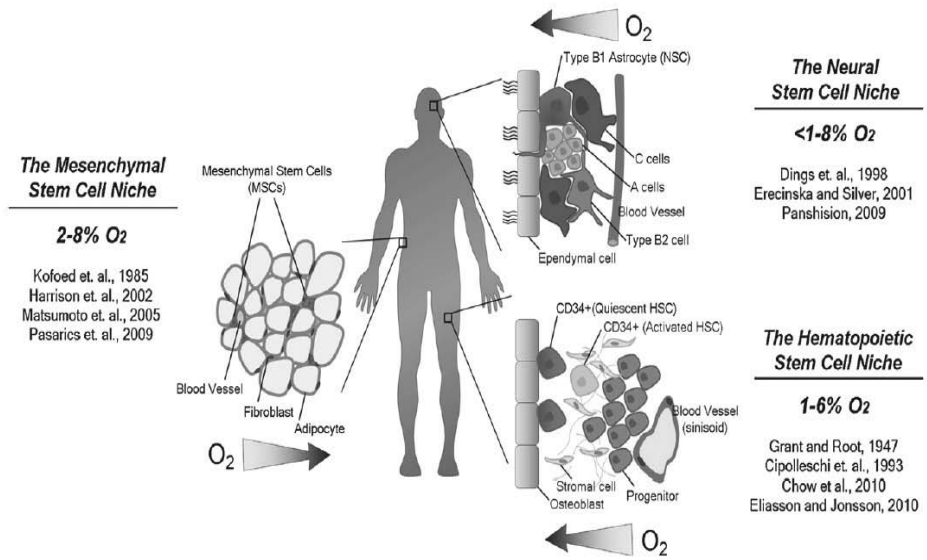

Figure 1. Hypoxia conditions in various stem cell niches. The schematic model shows the various hypoxic niches for neural stem cells (NSCs), mesenchymal stem cells (MSCs) and hematopoietic stem cells (HSCs) in the adipose tissue, the subventricular zone and the bone marrow, repectively. Red-colored cells in the figure indicate MSCs, NSC and CD34-positive HSCs. Various oxygen concentration is measured from body tissues and adjacent blood vessels, where NSCs, MSCs and HSCs reside have been reported in previous studies (Mohyeldin et al., 2010).

B. Hypoxia inducible factor (HIF)

HIFs are the member of bHLH-PAS family, and binds to DNA consensus sequence, known as a hypoxia response element (HRE), in the promoter region of genes. It forms heterodimer complex consisting of HIF-α subunits (HIF-1α, 2α, and 3α), and β subunit (ARNT). HIF's activity is dependent on the stabilization of subunit of HIF. HIF-α subunit is mainly controlled by post-translational modification by prolyl 4-hydroxylases (PHDs) (Palomaki et al., 2013). The proline hydroxylation of HIF-α subunits by PHD under normoxia is necessary for interaction between HIF and Von Hippel-Lindau tumor suppressor protein (pVHL), and then HIF-α interacted with pVHL is degraded by ubiquitin-mediated proteosomal degradation process. Under hypoxia, conversely, oxidative stress inhibits the PHDs activation, and then HIF-α subunits are stabilized. HIFs induce transcriptional response in the various types of cells under hypoxia, which is involved in cellular metabolism and hypoxic adaptation (Palomaki et al., 2013). Many previous researchers investigating the role of HIF-1α in stem cell under hypoxia reported that HIF-1α induced by hypoxia acts as a regulator of differentiation, self-renewal, and survival (Keith et al., 2007; Palomaki et al., 2013; Ramirez-Bergeron et al., 2001). In addition, hypoxia-stabilized HIF alters both glucose and lipid metabolism (Papandreou et al., 2006; Xie et

al., 2012a). Unlike glucose metabolism, however, the detailed mechanism how hypoxia induces lipid metabolic conversion in stem cells is not fully understood yet.

2. Lipid metabolism

A. Lipid metabolism in stem cells

Energy production is necessary to keep the cellular homeostasis and match the cell-specific energetic demands. To ensure stem cell self-renewal and tissue regeneration, stem cells have to maintain the balance between anabolic- and catabolic metabolic pathway (Folmes et al., 2013). Study of stem cell metabolism has been focused on the role of glycolysis and oxidative metabolism in differentiation and cell survival. As a previous report showing the emergent lipid metabolic profile of neural stem cells (NSCs) and its crucial role in NSC activity (Knobloch et al., 2013), the potential of lipid metabolism in the stem cell control has attracted the interest of stem cell researchers. In addition, several previous investigators presented the lipid metabolism-derived fatty acid and lipid metabolites including lysophosphatidic acid (LPA), sphingosine-1-phosphoate as essential energy sources and cellular signaling regulators of stem cells (Jung et al., 2015; Ryu et al., 2014; Ryu et

al., 2015a).

B. Fatty acid synthase (FASN)

Lipogenesis is dependent on the activity of rate limiting enzymes for fatty acid synthesis process, such as FASN and acetyl-CoA carboxylase (ACC). SREBP1 is a transcription factor that binds to sterol regulatory element on promoter region. SREBP1 induces the lipid biosynthesis regulating enzymes. SREBP1 activity is dependent on intracellular sterol levels (Gasic. 1994). Mammalian cells have two distinct SREBP genes, SREBP1 and SREBP2. SREBP1 is responsible for lipogenesis, but SREBP2 is involved in cholesterol metabolism. There has been a previous report showing the protective role of SREBP1-dependent lipogenesis in hypoxic cell death (Jung et al., 2012). In addition, SREBP1 contributes to lipid metabolic switch and somatic cell reprogramming (Wu et al., 2016b). FASN is a major lipogenic multi-protein enzyme which catalyze the palmitic acid production form acetyl-CoA and malonyl-CoA. It has been known that FASN controls growth, proliferation and survival in the normal, cancer and stem cells (Fig.2) (Folmes et al., 2013; Veigel et al., 2015). In addition, a previous researcher reported that FASN is upregulated by hypoxia treatment, which is associated with hypoxia-induced chemoresistance in tumor cells (Furuta et al., 2008a). In stem cells, suppression of

FASN reduces proliferation in NSCs and expression of stemness markers in glioma stem cells (Knobloch et al., 2013; Yasumoto et al., 2016). These evidences of lipogenesis-dependent stem cell fate provide a new insight into the potential role of lipid metabolism in stem cell regulation.

C. Glycerol-3-phosphate acyltransferase (GPAT)

The GPAT is a lipid metabolic enzyme which catalyzes the initial step in glycerolipid synthesis. GPAT1 is a major mitochondrial isoform which produces bio-active lipid metabolite, LPA. In liver cells, GPAT1 incorporates the synthesized fatty acid into triacylglycerol and reduces the fatty acid oxidation (Wendel et al., 2013). Although the role of GPAT1 in stem cell regulation remains poorly understood, there are several reports investigating the effect of LPA in mesenchymal stem cells. Those reports showed that LPA stimulates proliferation, migration and anti-apoptosis in mesenchymal stem cells (Kang et al., 2015; Li et al., 2017; Liu et al., 2009a). Collectively, lipid metabolic regulation will provide a novel strategy for enhancing the therapeutic potential of stem cells.

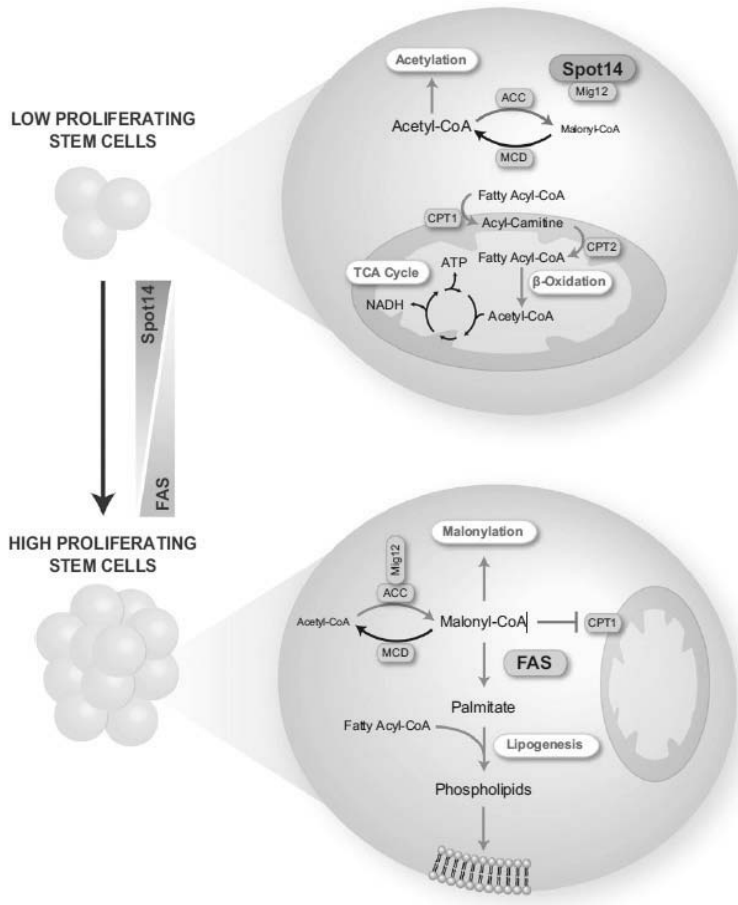

Figure 2. Role of fatty acid metabolism in stem cell proliferation. The schematic model shows the FASN-dependent lipogenesis plays a key role in stem cell proliferation. In quiescent and low proliferating stem cells, Spot14 acts as a metabolic brake by buffering the FASN-medited fatty acid production. In high proliferating stem cells, however, FASN is upregulated by Spot14 downregulaiton, which leads to lipogenesis.

3. Mitophagy

A. Definition of mitophagy

Mitochondria are the major metabolic organelles controlling cellular energetic metabolism. To maintain the healthy mitochondria, eukaryotes have a mechanism to remove the damaged and unwanted mitochondria (Liu et al., 2014b). Mitophagy, mitochondrial selective autophagy, plays a key role in clearance of mitochondria in response to the various stressful environments, such as nutrient status, oxygen concentration and death signal. Mitophagy includes receptor-mediated mitophagy and receptor-independent migophagy (Fig. 3). In the mitophagy-deficient cells, ROS production and oxidative stress are increased, which is closely involved in mitochondrial dysfunction and shortened life span (Kurihara et al., 2012; Richard et al., 2013). In the stem cells, PINK1/Parkin-dependent mitophagy has a critical role in mitochondrial metabolic switch that determines somatic reprogramming in induced pluripotent stem cells (iPSCs) (Vazquez-Martin et al., 2016). In addition, mitochondrial clearance by mitophagy in red blood cells and hematopoietic stem cells regulates the suppression of ROS production, survival, red blood cells maturation (Joshi et al., 2013). However, it remains unknown

that which mitophagy regulator contributes to hypoxia-induced mitophagy in stem cells. Therefore, further investigation into the role of mitophagy in stem cell physiology and metabolism under hypoxia is needed for development of efficient metabolic regulation in stem cells.

B. Bcl2/adenovirus E1B 19 kDa protein interacting protein 3 (BNIP3) and NIX-mediated mitophagy

BNIP3 is the first identified mitophagy receptor as a Bcl-2 interacting protein (Chen et al., 1997a; Matsushima et al., 1998). BNIP3 is localized to mitochondria and ER. They regulate the ROS accumulation or mitochondrial respiration, which is associated with programmed cell death or necrosis (Bursch et al., 2008; Sowter et al., 2001). BNIP3 contains a LC3 interacting region (LIR) which interacts with LC3 (Novak et al., 2011). There are several previous reports investigating the effect of hypoxia on mitophagy receptors regulation. According to previous studies, BNIP3 is a mitophagy receptor involving in hypoxia-induced mitophagy (Liu et al., 2014b). Hypoxia-induced transcription factors, HIF1α and FOXO3, transcriptionally regulate expression of BNIP3 and NIX (Chinnadurai et al., 2008; Sowter et al., 2001). The phosphorylation of BNIP3 at Ser17 and Ser24 residues stimulates the binding to LC3,

which leads to subsequent mitophagy (Zhu et al., 2013). A recent report demonstrated that BNIP3 induction through MAPK activation has a protective effect on UVB-inducd cell apoptosis (Moriyama et al., 2017). Conversely, antoher report showed that hypoxia-induced BNIP3 induces apoptosis (Burton et al., 2009). Therefore, further investigation using stem cells is needed to deeply understand the role of BNIP3-dependent mitophagy in stem cell physiology and metabolism regulated by hypoxia.

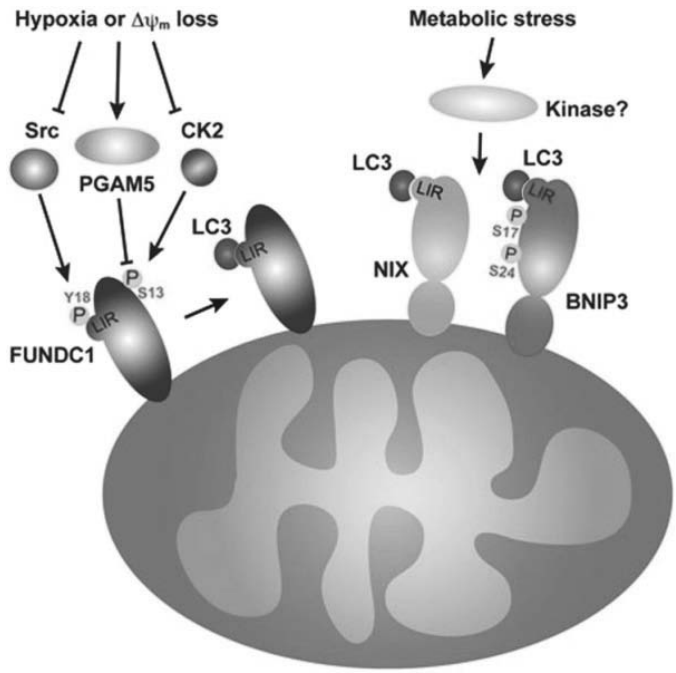

Figure 3. Receptor-mediated mitophagy in mammalian cells. Mitophagy receptors, such as BNIP3, NIX and FUNDC1, are interacted with LC3 via LIR. LIRs in the BNIP3 and FUNDC1 can be reversibly phosphorylated by stress-induced kinases. Hypoxia and carbonyl cyanide m-chlorophenyl hydrazine (CCCP) dephosphorylate Ser13 and Tyr18 residues of FUNDC1. Dephosphorylated FUNDC1 interacts with LC3. Phosphorylation of Ser17 and Ser24 of BNIP3 is induced by metabolic stress. Phosphorylated BNIP3 has a higher affinity to LC3, leads to BNIP3-mediated mitophagy (Liu et al., 2014b).

4. β-linked N-acetyl glucosamine (O-GlcNAC) modification

O-GlcNAcylation is the dynamic post translational modification which attaches a single O-GlcNAc moiety to Ser/Thr residues of cytosolic and nuclear proteins. As shown in the Fig. 4, O-GlcNAc is the product generated by hexosamine biosynthesis pathway (HBP) (Hart et al., 2007; Hart et al., 2011). O-GlcNAcylation signaling is the responsive to nutrient availability and cellular stress. In addition, the impairment of O-GlcNAcylation signaling is closely associated with pathogenesis of cancer, diabetic mellitus and neurodegeneration (Yang et al., 2017). O-GlcNAcylation is tightly controlled by two enzymes, one is the O-GlcNAc transferase (OGT) which transfer O-GlcNAC moiety to the hydroxyl group of the Ser/Thr residues and another one is the O-GlcNAcase (OGA) which catalyzes the hydrolysis of O-GlcNAc moiety. A single pair of O-GlcNAcylation-associated enzymes controls hundreds of cellular proteins in response to nutritional and hormonal signals (Yang & Qian. 2017). OGT and OGA are heavily presented in nucleus and cytosol, respectively (Lubas et al., 1997; Wells et al., 2002). A previous study demonstrated that OGT O-GlcNAcylates transcription factors, such as nuclear factor κB (NF-κB), Sp1 and CREB (Golks et al., 2007; Rexach et al., 2012; Yang et al., 2001).

Previous researchers studying the effect of endogenous O-GlcNAcylation on hypoxia-regulated cellular functions demonstrated that augmentation of endogous O-GlcNAcylation signling by OGT accumulation or glucosamine treatment induces vascular endothelial inflammatory response and prevents against hypoxia-induced Na^+/glucose cotransporter (SGLT) dysfunction in renal proximal tubule cells (Liu et al., 2014a; Suh et al., 2014). A previous report showed that suppression of O-GlcNAcylation inactivates Oct4, which leads to disruption of pluripotency and re-programming in embryonic stem cells (Jang et al., 2012). Also, O-GlcNAcylation upregulation enhances anti-apoptosis of cardiac stem cell with post hypoxic stress (Zafir et al., 2013). Those findings indicate that O-GlcNAcylation acts as an essential factor to control of stem cell physiology.

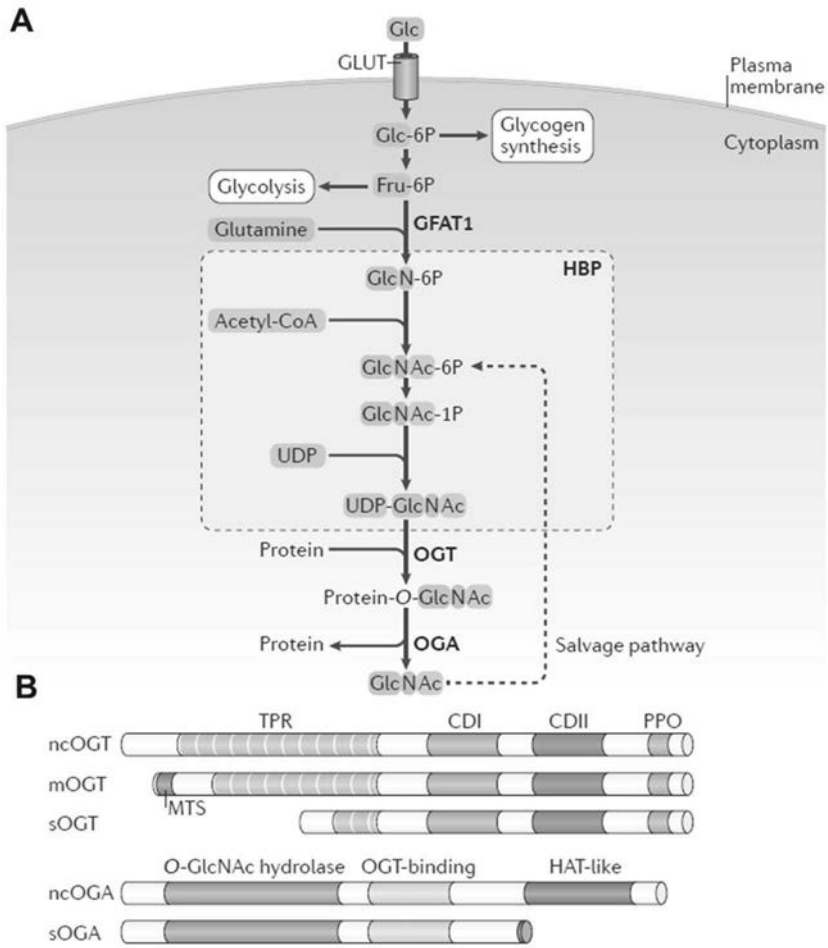

Figure 4. Regulation of O-GlcNAcylation of protein through HBP.

(A) Schematic model shows the nutrient flux through HBP contro O-GlcNAcylaiton of protein. 2~5% of glucose is enterd into the HBP. Glutamine-fructose-6-phsphoate amidotransferase 1 (GFAT1) catalyses Fructose-6-phosphate, the rate-limiting step of the HBP. (B) Schematic model presents OGT and OGA isoforms. OGTs are nucleocytoplasmic (ncOGT), mitochondrial (mOGT) and short (sOGT) isoforms (Yang & Qian. 2017).

5. Mammalian target of rapamycin (mTOR) as a metabolic regulator

A. Definition of mTOR

mTOR is a 289 kDa Ser/Thr kinase that nucleates two distinct complexs, mTOR complex 1 (mTORC1) and mTOR complex 2 (mTORC2) (Saxton et al., 2017). mTORC1 has five components: mTOR, regulatory-associated protein of mTOR (RAPTOR), mammalian lethal with Sec13 protein 8 (mLST8), proline-rich Akt substrate 40 kDa (PRAS40) and DEP-domain-containing mTOR-interacting protein (DEPTOR) (Laplante et al., 2009; Peterson et al., 2009). And, mTORC2 contains mTOR, rapamycin-insensitive companion of mTOR (RICTOR), DEPTOR, mammalian stress-activated protein kinase interacting protein (mSIN1), protein observed with Rictor-1 (PROTOR) and mLST8 (Saxton & Sabatini. 2017). mTOR signaling is associated with cellular physiology. For example, mTORC1 signaling controls protein synthesis, proliferation, growth, lipid and nucleotide synthesis, autophagy (Ma et al., 2008; Porstmann et al., 2008; Saxton & Sabatini. 2017). mTORC2 signaling regulates cytoskeletal remodeling, migration and survival (Jacinto et al., 2004; Sarbassov et al., 2005; Saxton & Sabatini. 2017). Previous investigators reported many extra- and

intracellular factors regulates mTORC1 and mTORC2 activites. Growth factors, amino acids and excessive nutrient status activate mTORC1. However, the effect of oxidative stress on mTOR signaling is still controversial (Schneider et al., 2008; Zhao et al., 2017). It has been reported that substrates of mTORC1 and mTORC2 are S6K1, PGK, SGK, RSK, Akt, 4EBP1 and eIF4G (Hay et al., 2004; Wang et al., 2015). Activated mTOR signaling by $CoCl_2$-induced hypoxic stress leads to HIF-1 stabilization (Hudson et al., 2002). This report supports that mTOR signaling is linked to hypoxic adaptation. Also it has been known that mTOR controls cellular metabolism, which is closely involved in diabetes, obesity, aging and neurodegenerative disease as well as cancer (Blenis. 2017). Taken together, those findings present the mTOR as a nutrient sensor and metabolic regulator controlling pathogenesis of metabolic disease and cancer as well as cellular physiological process.

B. Role of mTOR signaling in stem cells

Many previous researchers have showed the key roles of mTOR signaling in stem cell function. Deletion of the C-terminal six amino acids of mTOR resulted in decreased cell size and cell cycle arrest in embryonic stem cells (Murakami et al., 2004). mTOR signaling inhibition by rapamycin treatment increased clonogenic capacity by

preventing stem cell senescence via mitochondrial superoxide dismutase (MnSOD), and subsequent suppression of ROS generation (Iglesias-Bartolome et al., 2012). mTOR singnaling pathway contributes to self-renewal of hematopotietic stem cells (HSCs) and human ESCs (Huang et al., 2012; Zhou et al., 2009). Activation of YAP/TAZ singaling in stem cells stimulated mTOR signaling to promote transition-amplifying (TA) cells proliferation (Hu et al., 2017). In addition, mTORC1 signaling suppression contributes to switch of T cell metabolism to fatty acid oxidation and formation of stem cell-like memory T cells (Scholz et al., 2016). Based upon those findings, mTOR signaling coordinates anti-aging, self-renewal and immune modulation of stem cells. However, the effect of mTOR regulation on stem cell under hypoxia has not been fully described yet. Therefore, further investigation is required for uncovering the relationship between mTOR and hypoxia-regulated stem cell behavior.

6. Stem cells

A. Definition of stem cells

Stem cells are defined as progenitor cells having capacity of self-renewal and differentiation into the various differentiated somatic cells of all body organs and tissues (Smith. 2001; Weissman et al., 2001). Stem cells are classified into the totipotent-, pluripotent-, multipotent stem cells. Potency of stem cell indicates its potential to generate differentiated progeny. For example, totipotent stem cells have a capacity to divide into the all differentiated cells in the body including embryonic tissues (Mitalipov et al., 2009). Pluripotent stem cells including embryonic stem cells (ESCs) have a potential to produce the three germ layers (ectoderm, endoderm and mesoderm)(Henningson et al., 2003). Embryonic stem cells have a capacity to produce all somatic lineages and germ-line chimeras. Multipotent stem cells, such as adult stem cells, have a limited differentiation potential which generates multiple lineages of somatic cells (Mikkola et al., 2003). Multipotent stem cells exist within the specialized tissue like adipose tissue, bone marrow and umbilical cord blood (UCB). In addition, stem cells have a clonality which means proliferative capacity for self-renewal (Weissman et al., 2001).

B. ESCs

ESCs are pluripotent stem cells which have a self-renewal capacity. Human ESCs are isolated from inner cell mass of blastocysts at the embryonic days 4 or 5 (Thomson et al., 1998). Isolated human ESCs are cultivated on feeder cells (mouse embryonic fibroblast) or matrigel to prevent from differentiation into other cells. Cultured ESCs without feeder cell layer or matrigel forms embryonic body which is a multi-cell layer mass containing differentiated and un-differentiated cells. Embryonic bodies have an ability to differentiate into the three germ layers. In the case of mouse ESCs (mESCs), leukemia inhibitory factor (LIF) is required to maintain the undifferentiation state. LIF binds to gp130 receptor in plasma membrane in the mESCs, which activates the Janus kinases (JAK)/signal transducers and activators of transcription (STAT) pathway (Lowe et al., 1995). Moreover, basic fibroblast growth factor (FGF) can sustain undifferentiated status of ESCs via Activin/Nodal signaling-mediated OCT4 expression (Honda et al., 2009). Another report showed that bone morphogenetic protein 4 (BMP4) can replace the LIF by induction of inhibitors of differentiation (Id) genes (Ying et al., 2003). ESCs provide a drug test platform to investigate the regulatory mechanism of differentiation into the specialized differentiated cells and assess

the developmental cell toxicity (Hou et al., 2013; Liu et al., 2009b). Despite this advantage of ESCs, high rate of cell death remains a barrier to ESC application. Therefore, many researchers are investigating the strategy to increase the survival rate of ESC during cultivation and modulation of stem cell fate.

C. Human UCB-derived mesenchymal stem cells (hUCB-MSCs)

Umbilical cord (UC) of human is a tubular structure organ which allows the exchange the oxygen and nutrients between the embryo and maternal placenta. Umbilical vein in the umbilical cord includes progenitor cells of the fetus, called umbilical cord blood (UCB) cells, which are derived from the trophoblast and other non-embryonic tissues (Flynn et al., 2007). UCB cells in the umbilical vein are considered as a potential stem cell or progenitor source which can be used for cell therapy and research. MSCs in the UCB source is identified as transplantable progenitor cells having a being of great therapeutic potential (Horwitz et al., 1999). According to many researchers addressing the MSC behavior, MSCs can be isolated from fat, urine, bone marrow as well as UCB (Schosserer et al., 2015; Wagner et al., 2005). UCB-hMSCs have the advantages of high yield of cells relative to other MSC sources and being free

from the ethical concerns. UCB-hMSCs are long and spindle shaped adherent cells, which are positive for CD29, CD44, CD73, CD90, CD105 and HLA-ABC, but negative for CD14, CD34, CD45, CD74, CD106 and HLA-DR (Qiao et al., 2008). The differentiation potential of MSCs is demonstrated by *in vitro* assay of multi-lineage differentiation into adiopocytes, osteocytes and chondrocytes. Considering that UCB-hMSCs have multipotent differentiation potential and self-renewal capacity, it has been considered as a good candidate for therapeutic stem cell and gene therapy. Transplantation of UCB-hMSCs into the damaged organ and wound site stimulate vascular repair, immune modulation and tissue regeneration (Gao et al., 2016; Gu et al., 2017; Lee et al., 2016). Migratory and survival abilities of MSC is an important factor determining the therapeutic efficiency of UCB-hMSCs transplantation therapy (Kim et al., 2010b; Li et al., 2010). It has been demonstrated that several growth factors, cytokines and chemokines can regulate the migratory ability of stem or progenitor cells (Asahara et al., 1999; Llevadot et al., 2001; Unzek et al., 2007). Based upon these findings, the further investigation into the development of strategy for enhancing the migratory and survival ability of UCB-hMSC is needed for successful UCB-hMSCs therapy.

CHAPTER I.

Regulation of proliferation and migration in UCB-hMSCs by hypoxia-induced HIF-1α/FASN/mTORC1 pathway

Manuscript is published in *Stem Cells*. 2015 33(7):2182-2195

1. INTRODUCTION

There are indications that the fate of embryonic and adult stem cells is controlled by oxygen signaling. In early-stage pregnancy, the uterine surface where a fertilized egg is attached has a low oxygen level (< 2 % O_2 saturation) (Genbacev et al., 1997). In addition, various adult stem cells such as HSCs, MSCs, and NSCs are thought to reside in niches characterized by low oxygen levels (< 1-8 % O_2 saturation). It is likely that most stem cell niches have low oxygen levels, although further investigation into oxygen characteristics of other stem cell compartments is needed (Harrison et al., 2002; Kofoed et al., 1985; Mohyeldin et al., 2010).

However, details of the hypoxia-related mechanisms that induce changes in stem cell function have not been fully described. Recently, interest in metabolic mechanisms and into differences between the metabolic profiles of stem and normal cells has increased. Reports on stem cell research have suggested several metabolic pathways as regulatory elements in stem cell maintenance; elements that maintain stem cell self-renewal by balancing energetic and biosynthetic requirements cooperatively (Ito et al., 2014). Interestingly, lipid metabolism as a key modulator of stem cell maintenance has also been suggested. The FASN, a key enzyme in *de novo* lipogenesis, may be involved in balancing redox

reactions through its ability to consume reducing equivalents (e.g., NADPH), which in turn may limit the need for oxidizing power (Kuhajda et al., 1994; Menendez et al., 2007). Indeed, treatment of supra-physiological levels of exogenous dietary FAs, such as palmitic and oleic acids, can reduce FASN inhibition-induced cancer cell death (Menendez et al., 2004). Although, FASN upregulation could be a mechanism for improving a hypoxia-induced redox imbalance, few authors have reported on this hypothesis.

The HIF-1α is a crucial factor in hypoxia adaptation and acts via regulation of cellular energy metabolism, including alteration of nutrient metabolism-associated gene expressions that enhance stem cell survival (Krishnamurthy et al., 2004; Rey et al., 2011). Previous reports on the HIF activation pathway and the genes regulated by HIF have provided insight into hypoxia adaptation and regulation of hypoxia-mediated function. In addition, hypoxia-induced HIF activation regulates both lipid and carbohydrate metabolism (Papandreou et al., 2006; Xie et al., 2012b). Compared to carbohydrate metabolism, however, lipid metabolism alteration under hypoxic condition has not been fully described. mTOR, a nutrient sensing molecule, is a factor potentially involved in proliferation, migration, survival, and differentiation of various cell types (Kumar et al., 2014; Murakami et al., 2004; Xiang et al., 2011). However, details of the signaling pathways involved in mTOR regulation of stem cell function have not been fully described.

Therefore, further investigation of HIF and mTOR roles in various cells and conditions is required to elucidate how hypoxia-mediated metabolic changes are linked to specific changes in cellular behavior.

Recent human MSC research may lead to diverse, new clinical applications including cell replacement and immunomodulatory therapies. In particular, UCB-hMSCs have attracted the interest of stem cell investigators because: (1) UCB-hMSCs are inexpensive, easily and non-invasively obtained; (2) they are the most abundant non-embryonic source of stem cells; (3) there are few ethical concerns related to UCB-hMSC research, and (4) there is less immunogenicity associated with UCB-hMSCs than with other stem cells (Le Blanc et al., 2003; Qiao et al., 2008; Yang et al., 2004). Furthermore, investigations into the physiological regulation of UCB-hMSCs may result in promising clinical applications of stem cells. In particular, an improved description of the relationship between hypoxia and stem cell metabolism will help to reduce the effort needed to sustain, develop, and control hMSCs *ex vivo*, and may result in therapeutic advantages in regenerative medicine. The aims of the present study were to identify the hypoxia-inducible lipid metabolic enzyme that regulates UCB-hMSCs proliferation and migration and to investigate the signaling pathway that the enzyme uses to control functional changes in UCB-hMSCs.

2. MATERIALS & METHODS

2.1. Materials

The UCB-hMSCs were provided by Medipost (Seoul, Korea) and were isolated as reported previously (Qiao et al., 2008). The provided UCB-hMSCs are positive for HLA-AB and characterized to express CD73 and CD105, but not CD14, CD34, or CD45. Fetal bovine serum (FBS) was purchased from Bio Whittaker (Walkersville, MD, USA), and FASN, HIF-1α, SCAP, Lamin A/C, β-actin, RhoA GTPase, Rac1 GTPase, Cdc42 GTPase, F-actin, profilin1/2, p-cofilin1 (Ser3), RICTOR, CDK2, CDK4, cyclin D1, cyclin E, and c-myc antibodies were acquired from Santa Cruz Biotechnology (Santa Cruz, CA, USA). RAPTOR, HIF-2α, SREBP1 and mTOR antibodies were purchased from Abcam (Cambridge, MA, USA), and SCD1 antibody was obtained from Thermo Fisher (Waltham, MA, USA). Horseradish peroxidase (HRP)-conjugated IgG was obtained from Jackson Immunoresearch (West Groove, PA, USA). The p-mTOR (Ser2448, Ser2481) antibodies were purchased from Cell Signaling Technology (Beverly, MA, USA), and the HRP-conjugated rabbit anti-goat IgG was purchased from Santa Cruz Biotechnology. Rapamycin, cerulenin, and mitomycin C were acquired from Sigma-Aldrich (St. Louis, MO, USA), and

CAY10566 was obtained from Cayman (Ann Arbor, MI, USA). Small interfering RNAs (siRNAs) for *HIF-1α*, *HIF-2α*, *RAPTOR*, and *RICTOR* were purchased from Cosmo Genetech (Seoul, Korea). All experiments were performed with 8-10 passages of the tested cells.

2.2. UCB-hMSC culture

The UCB-hMSCs were cultured with α-minimum essential medium (α-MEM; Thermo Fisher). Cells were grown in 10% FBS with a 1% antibiotics mixture. Cells were cultured in 35, 60, or 100 mm diameter culture dishes, or in 6- or 12-well plates in an incubator kept at 37° C with 5% CO_2. The medium was changed to serum-free medium. After 24 h of incubation in serum-free medium, cells were washed twice with phosphate buffered solution (PBS), and placed in medium that included supplements.

2.3. Hypoxia treatment

Prior to treatment, UCB-hMSCs were washed with PBS, and the serum-free medium was replaced with α-MEM. A modular incubation chamber (Billups-Rothenberg, Del Mar, CA, USA) was used for hypoxia treatment. The gas used in the hypoxia experiments included 2.2% O_2, 5.5% CO_2, and 92.3% N_2. The

incubation chamber was purged with the hypoxia gas at a flow rate 5 L/min for 30 min prior to its placement in a conventional incubator at 37° C.

2.4. Mouse skin wound-healing model

Procedures involving animal followed the National Institutes of Health Guidelines for the Humane Treatment of Animals and were conducted with approval from the Institutional Animal Care and Use Committee of Seoul National University (SNU-140123-6). Eight-week-old male Institute for Cancer Research (ICR) mice were used. Mice were anesthetized with a 2:1 mixture of Zoletil™ (20 mg/kg; Virbac Laboratories, Carros, France) and xylazine HCl (10 mg/kg; Rompun®, Bayer, Leverkusen, Germany). Mouse skin wound healing was performed as described previously (Dunn et al., 2013; Lee et al., 2011). Experimental animals were divided into five groups: wild-type mice that received vehicle (group 1, n=6); UCB-hMSC transplantation mice that received UCB-hMSCs pretreated with either vehicle (group 2, n=6) or 2 μM cerulenin (group 5, n=6) prior to incubation under normoxic conditions for 24 h; and hypoxia-treated UCB-hMSC transplantation mice that received UCB-hMSCs pretreated with either vehicle (group 3, n=6) or 2 μM cerulenin (group 4, n=6) prior to incubation under normoxic condition for 24 h.

Skin wounds were created by using a 6 mm diameter biopsy punch. For treatment, 70 μL of PBS containing vehicle or UCB-hMSCs (n=1× 10^6) with vehicle or cerulenin were injected into the dermis surrounding the wound site. Transplanted UCB-hMSCs were pretreated with bromodeoxyuridine (BrdU; 2 μM) for 24 h prior to injection. Silicone rings were attached to the peri-wound area by using surgical glue and a 6-0 nylon suture. All wound images were obtained at the same distance from the subject (30 cm) with a digital camera system (D50; Nikon, Tokyo, Japan). Wound size was determined by using ImageJ software (developed by Wayne Rasband, National Institutes of Health, Bethesda, MD; available at http://rsb.info.nih.gov/ij/).

At post-injection day 11, all mice were euthanized and skin tissues from the area containing the wound were excised. Excised tissues were embedded in O.C.T compound (Sakura Finetek, Torrance, CA, USA) and frozen. Embedded tissue slices (10 μm thick) underwent hematoxylin and eosin (H&E) staining and immunohistochemical analysis. Samples for immunohistochemical analysis were immunostained with BrdU and propidium iodide (PI). Immunostained cells were visualized by using fluorescence microscopy and the results were analyzed with MetaMorph software (Universal Imaging, West Chester, PA, USA).

2.5. Western blot analysis

Harvested cells were washed twice with ice-cold PBS prior to incubation in lysis buffer [1 mM EDTA, 1 mM EGTA, 20 mM Tris (pH 7.5), 1% Triton X-100, 1 mg/mL aprotinin, and 1 mM phenylmethylsulfonylfluoride (PMSF)] for 40 min on ice. The lysates were then cleared by centrifugation (15000 rpm at 4° C for 50 min). The Bradford method was used to determine protein concentration (Bradford. 1976). Samples containing 10 μg of protein were prepared for 10% sodium dodecyl sulfate polyacryl-amide gel electrophoresis (SDS-PAGE) and then transferred to a polyvinylidene fluoride (PVDF) membrane. Protein-containing membranes were washed with tris-buffered saline containing 0.1 % Tween-20 (TBST) solution [10 mM Tris-HCl (pH 7.6), 150 mM NaCl, and 0.1 % Tween-20] blocked with 5% skim milk or 5% bovine serum albumin (BSA) for 30 min. Blocked membranes were washed with TBST solution and incubated with primary antibody overnight at 4° C. The membranes were then washed and incubated with HRP-conjugated secondary antibody. The western blotting bands were visualized by using enhanced chemiluminescence (Amersham Pharmacia Biotech, Little Chalfont, United Kingdom). Densitometric analysis was carried out by using ImageJ software.

2.6. Nuclear fraction preparation

Prior to harvesting, cells were washed twice with ice-cold PBS. Harvested cells were resuspended in buffer A [137 mM NaCl, 8.1 mM Na_2HPO_4, 2.7 mM KCl, 1.5 mM KH_2PO_4, 2.5 mM EDTA, 1 mM dithiothreitol, 0.1 mM PMSF, and 10 mg/mL leupeptin (pH 7.5)]. Suspended cells were lysed mechanically by performing homogenization with a 23-gauge needle. Cell lysates were centrifugated at 8000 r/min for 5 min at 4° C. The obtained pellet, as a nuclear fraction, was then lysed with buffer A containing 1% (v/v) Triton X-100.

2.7. GTP-RhoA, Rac1, and Cdc42 affinity precipitation

Affinity precipitation assay kits (EMD Millipore, Billerica, MA, USA) were used to determine the activation of RhoA, Rac1, and Cdc42 according to the manufacturer's instruction. Cells were incubated for 5 min in ice-cold Mg^{2+} lysis buffer (EMD Millipore). The lysates were then incubated for 1 h with agarose beads interacted with either Rho-binding domain of rhotekin (GST-Rhotekin-RBD) or Cdc42/Rac-binding domain (GST-PAK-PBD). Subsequently, the bound RhoA, Rac1, and Cdc42 proteins were diluted with 2× Laemmli sample buffer and assessed by western blotting.

2.8. mRNA isolation and reverse transcription polymerase chain reaction

RNA was extracted from UCB-hMSCs by using the RNeasy Plus Mini Kit (Quiagen, Valencia, CA, USA). Reverse transcription (RT) was performed sequentially with 1 μg of RNA by using a Maxime RT premix kit (iNtRON Biotechnology, Sungnam, Korea). By using a polymerase chain reaction (PCR) kit (iNtRON Biotechnology), cDNA was amplified with the *SREBP1*, *SCAP*, and β*-actin* genes.

2.9. Real-time PCR

FASN, *SCD1*, *SCD5*, *GPAT1*, *GPAT2*, *GPAT3*, *GPAT4*, *CPT1*, *MAGL*, *SREBP1*, *SCAP*, and β*-actin* gene expressions were measured by using a Rotor-Gene 6000 real-time thermal cycling system (Corbett Research, Mortlake, Australia) with a QuantiMix SYBR kit (Phile Korea Technology, Daejeon, Korea) and the addition of sense and antisense primers and cDNA. Data were collected by using the manufacturer's software (Corbett Research). After performing real-time PCR, melting curve analysis was utilized to confirm the identity and specificity of the products. Normalization was performed by using β*-actin* as the endogenous control. Sequences of the primers used are described in Table 1.

Table 1. Sequences of primers used for PCR.

Gene	Identification	Sequence (5'-3')	Size (bp)
FASN	Sense	AACCTGCACTTCCATAGCCC	294
	Antisense	ATGCTCAGGAAAGCCAGGTC	
SCD1	Sense	TGGTTTCACTTGGAGCTGTG	167
	Antisense	GGCCTTGGAGACTTTCTTCC	
SCD5	Sense	CTTGACGTCACTGACCTGCT	236
	Antisense	TTGTCATAGGGCCGGTTTCC	
GPAT1	Sense	AACCCCAGTATCCCGTCTTT	154
	Antisense	CAGTCACATTGGTGGCAAAC	
GPAT2	Sense	GGCTGACGGAGGAGATACTG	178
	Antisense	AGTTGTGCCAGGTGTGTGAG	
GPAT3	Sense	ACAGCAGCCTCAAAAACTGG	153
	Antisense	CAATGGGGGAAGTATGGTTG	
GPAT4	Sense	TGCCAAATGGGAGGTTTAAG	128
	Antisense	GCCACCATTTCTTGGTCTGT	
MAGL	Sense	CTCATTTCGCCTCTGGTTCTTG	226
	Antisense	GTGAGACGGCATTCAGCAGTTG	
CPT1	Sense	CGTCTTTTGGGATCCACGATT	100
	Antisense	TGTGCTGGATGGTGTCTGTCTC	
SREBP1	Sense	TCTTGAAGCCTTCCTGAGCG	289
	Antisense	GGGAGGGCTTCCTGTAGAGA	
SCAP	Sense	CAGTGCTGTCAAGTGTGTGC	133
	Antisense	AGCCCATGGTTGTAGAAGGC	
β-actin	Sense	AACCGCGAGAAGATGACC	351
	Antisense	AGCAGCCGTGGCCATCTC	

2.10. Transfection of small interfering RNA (siRNA)

Prior to hypoxia treatment, siRNAs specific for *HIF-1α*, *HIF-2α*, *RAPTOR*, *RICTOR*, or non-targeting (NT) were transfected to UCB-hMSCs for 24 h with hyperfectamine (QIAGEN, Valencia, CA, USA) according to the manufacturer's instructions. The concentration of each transfected siRNA was 25 nM. The NT siRNA was used as the negative control. The siRNA sequences are described in Table 2.

Table 2. Sequences of siRNAs used for gene silencing.

Target gene	Sequence 5'-3'
HIF-1α	GCCGCUCAAUUUAUGAAUATT UAUUCAUAAAUUGAGCGGCTT
	GCCUCUUUGACAAACUUAATT UUAAGUUUGUCAAAGAGGCTT
	CCACCACUGAUGAAUUAAATT UUUAAUUCAUCAGUGGUGGTT
	GCUGGAGACACAAUCAUAUTT AUAUGAUUGUGUCUCCAGCTT
HIF-2α	GCGCAAAUGUACCCAAUGATT UCAUUGGGUACAUUUGCGCTT
	CGCUCAGCCUAUGAAUUCUTT AGAAUUCAUAGGCUGAGCGTT
	CCCAGAUCCACCAUUACAUTT AUGUAAUGGUGGAUCUGGGTT
	GGAGCUAACAGGACAUAGUTT ACUAUGUCCUGUUAGCUCCTT
RAPTOR	CGAGAUUGGACGACCAAAUTT AUUUGGUCGUCCAAUCUCGTT
	GGUGAACUGAACUGGAUCUTT AGAUCCAGUUCAGUUCACCTT
	CCGAGAAUGAGGAGCAUAUTT AUAUGCUCCUCAUUCUCGGTT
	GCGUCACACUGGAUUUGAUTT AUCAAAUCCAGUGUGACGCTT
RICTOR	CACCCUCUAUUGCUACAAUTT AUUGUAGCAAUAGAGGGUGTT
	GCAGACUCUAUGCAACAAATT UUUGUUGCAUAGAGUCUGCTT
	CGAGGACCUAAGCCUUAUATT UAUAAGGCUUAGGUCCUCGTT
	GCCUUAAGUUAUGCAUCAUTT AUGAUGCAUAACUUAAGGCTT
Non-targeting	UUCUCCGAACGUGUCACGUTT ACGUGACACGUUCGGAGAATT

2.11. Measurement of cellular or extracellular free fatty acid levels

Cellular or extracellular free fatty acid (FFA) levels of UCB-hMSCs were measured by using a FFA quantification kit (Biovision, Mountain View, CA, USA) according to the manufacturer's instructions. Briefly, 1 × 10^6 cells and 50 μL of medium were collected and acetyl-CoA synthetase (ACS) reagent, enzyme mix,

and enhancer were added to the sample. Mixtures were incubated for 30 min and FFA levels were detected by using a microplate reader (at γ = 550 nm).

2.12. Cell number count and viability assay.

Cells were washed twice with ice-cold PBS prior to incubation with a 0.05 % Trypsin and 0.5 mM EDTA solution. Detached cells were treated with soybean trypsin inhibitor (0.05 mg/mL) to quench trypsin. To exclude dead cells, 0.4 % trypan blue was added to the cell suspension. Subsequently, unstained live cells were counted by using a Petroff-Hausser counting chamber.

To calculate the cell viability, use the formula as follows. Cell viability = {1- (number of trypan blue-stained cell ÷ number of total cells) × 100}.

2.13. Incorporation of [^{3}H] thymidine

The UCB-hMSCs were washed with PBS and maintained in serum-free medium. After the indicated treatment, the cells were treated with 1 μCi of [methyl-^{3}H]-thymidine (Amersham Biosciences) and incubated for 1 h at 37° C. The cells were then washed twice with ice-cold PBS, fixed in 10% trichloroactetic acid (TCA) at room temperature for 30 min, and washed with 5% TCA. The acid-insoluble substance was dissolved in 2 N NaOH for 12 h at room temperature. The level of [^{3}H]-thymidine incorporated with DNA was measured by using a liquid scintillation counter. All data were normalized from absolute counts to percentage of controls.

2.14. MTT (3-(4,5,Dimethyl thiazolyl-2)-2,5-diphenyl tetrazolium bromide) cell proliferation assay

The UCB-hMSCs were cultured in a 6-well plate. Prior to harvesting, each well was treated with 100 pg/mL of MTT reagent (Sigma-Aldrich). Harvested cells were washed with PBS and incubated with dimethylsulfoxide (Sigma-Aldrich) for 10 min. Absorbance at 540 nm was measured by using an enzyme-linked immunosorbent assay-plate reader.

2.15. Immunofluorescence staining

Cells were fixed with 3.7% paraformaldehyde for 10 min, followed by permeabilization with 0.1% Triton X-100 in PBS followed by washing with PBS. Cells were incubated with 1% FBS to decrease non-specific binding of antibody, and then incubated with 1:100 dilution of primary antibody. Next, the cells were incubated for 1 h with either fluorescein isothiocyanate (FITC) conjugated anti-rabbit and anti-mouse IgG antibody or Alexa Fluor® goat anti-rabbit IgG counterstained with either PI or Alexa Fluor 488-conjugated phalloidin (Invitrogen, Carlsbad, CA, USA) in PBS containing 1%. Images were obtained by using a FluoView™ 300 fluorescence microscope (Olympus, Tokyo, Japan). I calculated the corrected total cell fluorescence (CTCF, ImageJ arbitrary unit) for quantification of protein expression by using ImageJ software. The equation used to determine CTCF is: CTCF = Integrated density − (Area of selected cell × Mean fluorescence of background readings). Three independent experiments were performed and 60 cells (20 cells per experiment) were used for statistical analysis.

2.16. Wound healing cell migration assay

The UCB-hMSCs were seeded at 1 × 10^4 cells to each well of

an ibidi insert dish (ibidi, Martinsried, Germany), which has two silicon reservoirs separated by a 500 μm thick wall (Chieng-Yane et al., 2011). Cells were incubated in culture medium until full confluence was attained. Cells were incubated in serum-free medium for 24 h, and then the silicon reservoir insert was gently removed with sterile forceps. After hypoxia treatment for 24 h, cells were visualized by using an Olympus View™ fluorescence microscope with a 100× objective.

2.17. Oris™ cell migration assay

Cells were seeded at 1 × 10^4 cells per 100 μL in each well of an Oris™ plate (Platypus Technologies, Fitchburg, WI) and incubated for 24 h. Subsequently, the medium was change to serum free medium. After the well' s insert plug was removed gently, plates were incubated in a hypoxic condition for various periods. Cells were then stained with calcein AM (5 μM) for 30 min. The cells that had migrated into the denuded well area were measured by using a microplate reader at excitation and emission wavelengths of 485 and 515 nm, respectively.

2.18. Live cell imaging

Cells were stained with DAPI (2 μg/mL) in an ibidi insert dish. After removal of the silicon reservoir, cells were washed with PBS

and serum-free medium was added. The dish was then placed in a temperature and CO_2 control chamber (Tokai, Tokyo, Japan). Differential interference contrast (DIC) and DAPI images were obtained over a 24 h period at 5 min intervals by using an Olympus IX81-ZDC zero-drift microscope and a Cascade 512B camera (Roper Scientific, Tucson, AZ, USA). The imaging devices were operated by using the multidimensional acquisition package of MetaMorph software (Molecular Devices, Sunnyvale, CA, USA). To determine cell migration distance, a constant threshold for each image was maintained. Analysis of cell migration distance was performed by using MetaMorph software (Molecular Devices).

2.19. Statistical analysis

Experimental data are summarized as a mean ± standard error (S.E). Differences among groups were tested by using ANOVA, and Comparisons of some treatment means with either control or hypoxia-treatment means were performed by applying the Bonferroni-Dunn test. A test result with a p value <0.05 was considered significant.

3. RESULTS

3.1. Hypoxia promotes UCB-hMSC proliferation and migration

To determine the effect of hypoxia on UCB-hMSC proliferation, UCB-hMSCs were incubated under hypoxic conditions for various periods (0-72 h). The [^{3}H]-thymidine incorporation levels in the treated UCB-hMSCs increased in24 h of hypoxia treatment and decreased during the remaining 48-72 h of hypoxia treatment. After 72 h of hypoxia, the [^{3}H]-thymidine incorporation levels of the UCB-hMSCs were lower than that of the control cells (Fig. 5A).The effect of hypoxia treatment on proliferation was further elucidated by counting cells. However, the number of cells after 48 h of hypoxia was similar to that of the control, and was lower than that of control after 72 h (Fig. 5B). To investigate the effect of hypoxia on UCB-hMSCs migration, I performed ibidi insert dish assay and Oris migration assay. As shown in Figs. 6A-6C, hypoxia stimulated F-actin reorganization and UCB-hMSCs migration. Hypoxia also facilitated translocation of UCB-hMSC into the denuded area for cell migration. I quantified the percentage of migration by using the Oris migration assay. Cell migration under hypoxic condition for 12 and 18 h increased to 133.8 % and 147.5%

of the each normoxia control level, respectively (Fig. 6B). The maximum increase in F-actin expression was observed after 24 h of hypoxia treatment (Fig. 6D). By adding mitomycin C, cell proliferation inhibitor, I confirmed that hypoxia-induced UCB-hMSC proliferation did not affect UCB-hMSC migration (Fig. 6E). In addition, long-term exposure (48-72 h) to hypoxia reduced viability (Fig. 7),

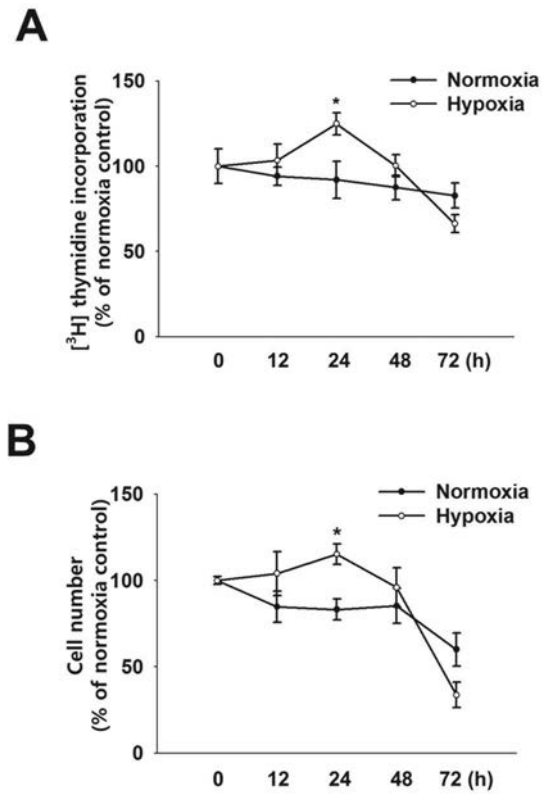

Figure 5. Effect of hypoxia on UCB-hMSCs proliferation. (A) Cells were exposed to hypoxia for 0–72 h and then pulsed with 1 μCi of [^{3}H]-thymidine for 1 h prior to counting. Data are reported as a mean ± standard error (S.E.) of three independent experiments with duplex dishes. * indicates $p < 0.05$ vs. normoxia control. (B) The number of cells was measured directly by using a counting chamber. Cells stained by trypan blue are excluded. Data are reported as a mean ± S.E of three independent experiments with duplex dishes. * indicates $p < 0.05$ vs. normoxia control.

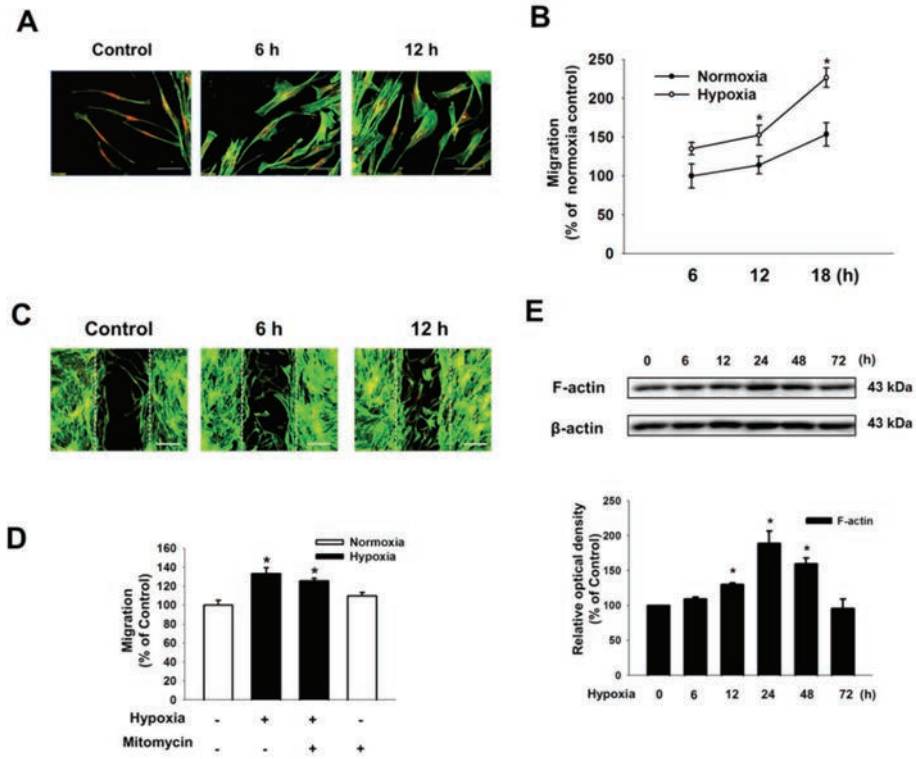

Figure 6. Effect of hypoxia on migration of UCB-hMSCs. (A) Cells were exposed to hypoxia for 0-12 h. F-actin was stained with phalloidin and counterstained with PI. Scale bars, 50 μm (magnification, ×600). (B) Migration of hypoxia-treated cells for 6-18 h was measured with an Oris™ migration assay kit. Data are reported as a mean ± S.E. n=10. (C) Cells cultured in ibidi insert dish were exposed to various periods of hypoxia. Scale bars, 100 μm (magnification, ×100) (D) F-actin expression was detected by western blotting. (E) Cells were pretreated with mitomycin C (1 μg/mL) before being exposed to hypoxia for 24 h. * indicates p < 0.05 vs. control. * indicates p < 0.05 vs. control.

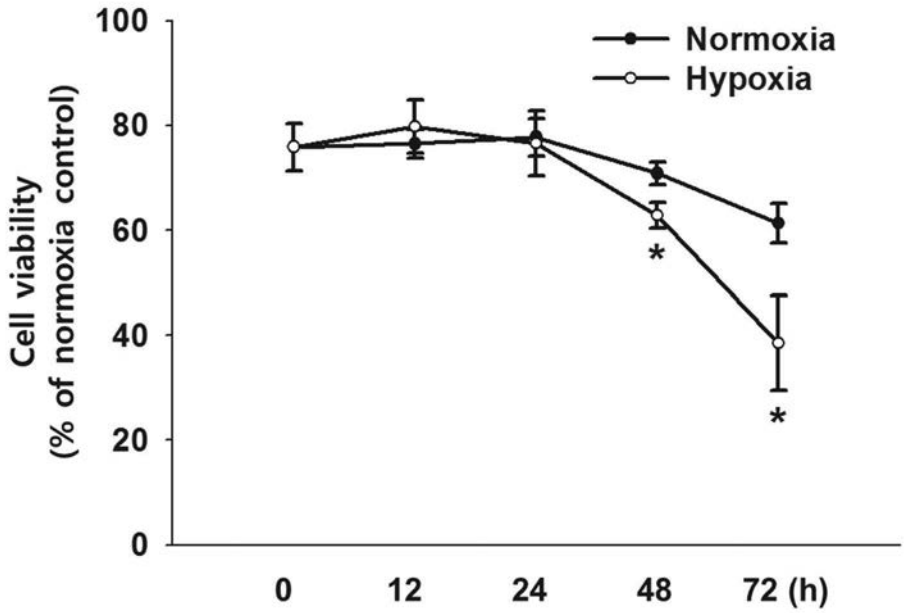

Figure 7. Effect of hypoxia on survival of UCB-hMSCs. UCB-hMSCs were incubated under hypoxic conditions for various periods (0 - 72 h). The viability of UCB-hMSCs was determined by cell viability assay. Data are reported as a mean ± S.E of three independent experiments with duplex dishes. * indicates $p < 0.05$ vs. normoxia control.

3.2. Hypoxia predominantly stimulates lipogenic enzymes expressions in UCB-hMSCs

To determine whether hypoxia treatment affects lipid metabolism of UCB-hMSCs, I screened for lipid metabolic enzymes mRNA expressions in UCB-hMSCs under hypoxic condition for 24 h Hypoxia treatment increased *FASN,* (stearoyl-CoA desaturase 1) *SCD1*, and *SCD5* mRNA expression levels, but failed to regulate other lipid metabolic enzymes, including (glycerol-3-phosphate acyltransferase 1) *GPAT1, GPAT2, GPAT3, GPAT4*, (carnitine palmitoyltransferase 1) *CPT1*, and (monoacylglycerol lipase) *MAGL* mRNA expression levels (Fig. 8). In addition, I observed that FASN and SCD1 protein expression levels increased in a time-dependent manner but only during the initial 24 h of hypoxic incubation (Fig. 9A). Immunofluorescence staining results showed an approximate two-fold increase in the fluorescence intensity of FASN and SCD1 in hypoxia-treated UCB-hMSCs (Figs. 9B and 9C).

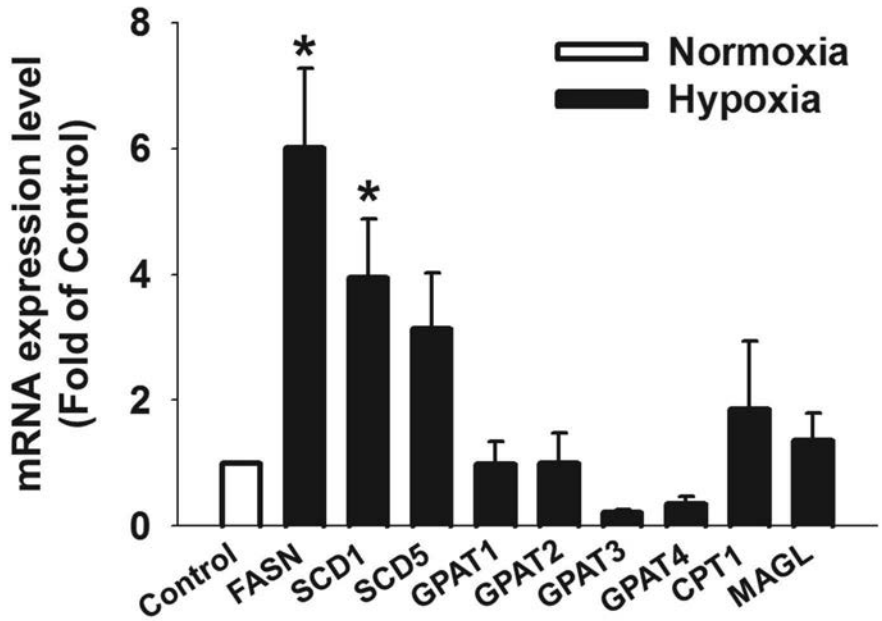

Figure 8. Effect of hypoxia on UCB-hMSC lipid metabolic enzyme expression. (A) Cells were exposed to hypoxia for 24 h, after which *FASN, SCD1, SCD5, GPAT1, GPAT2, GPAT3, GPAT4, CPT1, MAGL* and *β-actin* mRNA were amplified by PCR and quantified using real-time PCR. Each mRNA expression was normalized by *β-actin* mRNA expression. Data are reported as a mean ± S.E. n=5. * indicates $p < 0.05$ vs. control.

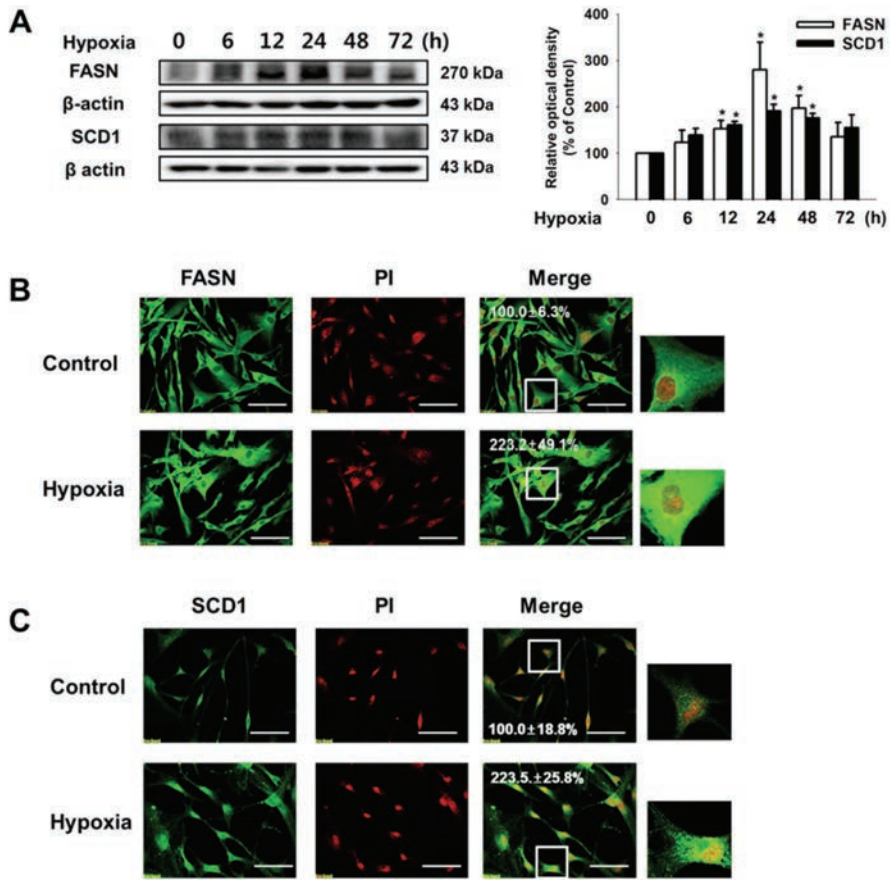

Figure 9. Effect of hypoxia on UCB-hMSC lipid metabolic enzyme expression. (A) Cells were treated for various periods (0-72 h) in a hypoxic condition. FASN and SCD1 proteins were detected by western blotting. n=3. (B, C) Fluorescence densities (ImageJ arbitrary units) of FASN and SCD1 in the cellular region were measured by using confocal fluorescence microscopy. Scale bars, 100 μm (magnification, ×400). The quantification data for the immunofluorescence images were the mean ± S.E. n=3 * indicates $p < 0.05$ vs. control.

3.3. Hypoxia-induced FASN expression regulates UCB-hMSCs proliferation and migration

To determine whether FASN and SCD1 regulate UCB-hMSCs proliferation under hypoxic condition, I examined cell numbers after 24 h of hypoxic incubation and with various concentrations of the FASN inhibitor cerulenin (100 nM-10 μM) or the SCD1 inhibitor CAY10566 (1 nM-1 μM). The number of UCB-hMSCs decreased at cerulenin concentrations $\geq$ 2 μM (Fig. 10A). Conversly, inhibition of SCD1 by CAY10566 did not affect the number of UCB-hMSCs (Fig. 10B). In mESCs, however, CAY10566 (10 nM-1 μM) pretreatment reduced cell viability (Fig. 10C). To clarify the effect of FASN on hypoxia-induced UCB-hMSCs proliferation and migration, cells were incubated under hypoxic condition for 24 h and with cerulenin (2 μM) or palmitic acid (10 μM) pretreatment. Hypoxia treatment increased levels of cellular- (cell lysates) and extracellular (medium) FAs, but their levels decreased with the addition of cerulenin (Fig. 11A). Cerulenin pretreatment also reduced hypoxia-induced UCB-hMSC numbers and [^{3}H]-thymidine incorporation levels, but both were recovered by palmitic acid treatment (Figs. 11B and 11C). Cerulenin inhibited hypoxia-induced cell migration. However, palmitic acid treatment rescued the cerulenin-induced suppression of cell migration (Fig. 12A). The above effects of cerulenin and palmitic acid were confirmed by

performing Oris migration assays for quantification (Fig. 12B). To confirm the effect of FASN on hypoxia-induced UCB-hMSCs migration *in vivo*, I performed mouse skin wound healing assay. The wound area was more significantly reduced by hypoxia-pretreated UCB-hMSCs than that of the addition of UCB-hMSCs alone. However, in both cases co-treatment with cerulenin slowed skin wound healing (Fig 13A), which is reconfirmed by histological evaluation through the hematoxylin and eosin staining (Fig. 13B). Immunohistochemistry results showed that hypoxia pretreatment stimulated migration of BrdU-positive UCB-hMSCs into the wound site, and cerulenin inhibited the migration of transplanted UCB-hMSCs into the wound site (Fig. 14).

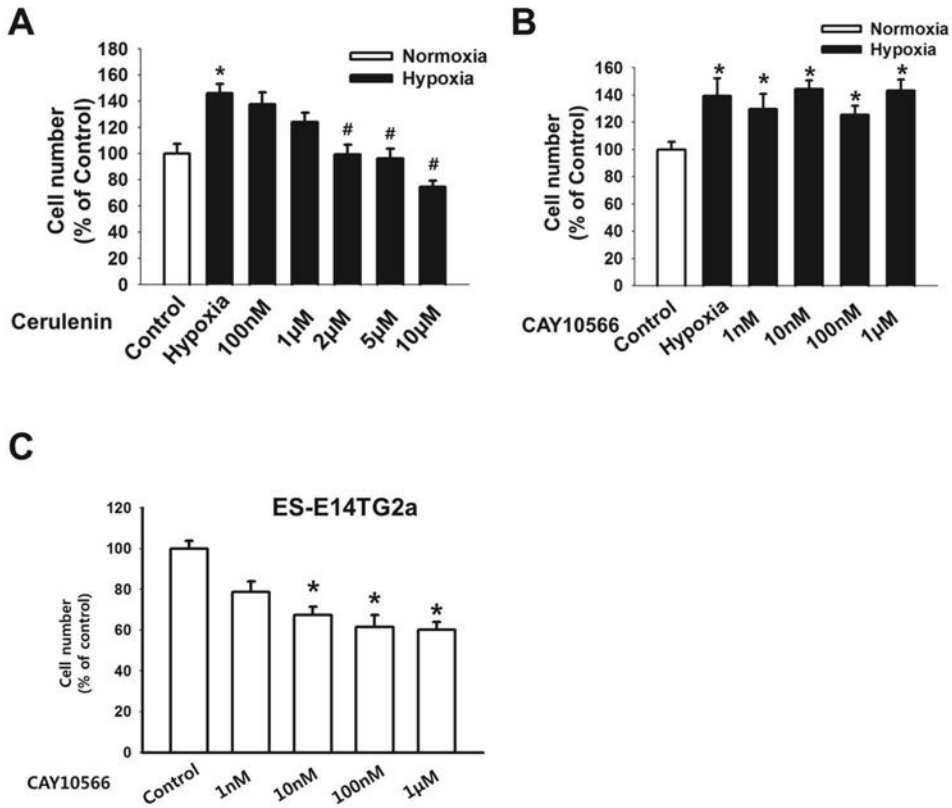

Figure 10. Role of FASN in hypoxia-induced proliferation in UCB-hMSCs. (A, B) Cells were treated with various concentrations of cerulenin (100 nM–10 μM) or CAY10566 (1 nM–1 μM) for 30 min prior to hypoxia treatment. The number of cells was determined by using a counting chamber. Data are reported as a mean ± S.E. n=6. * indicates $p < 0.05$ vs. control, and # indicates $p < 0.05$ vs. hypoxia treatment alone. (C) Cells were treated with various concentrations of CAY10566 (1 nM–1 μM) for 24 h in a normoxic condition. The number of cells was determined by using a counting chamber. Data are reported as a mean ± S.E. n=6. * indicates $p < 0.05$ vs. control.

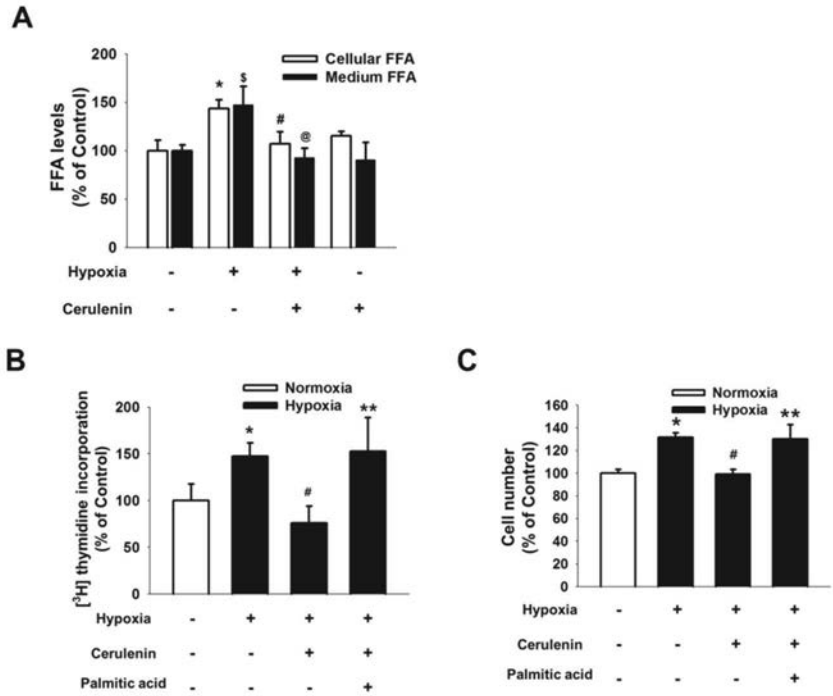

Figure 11. Role of hypoxia-induced FASN in FFA production proliferation of UCB-hMSCs. (A) FFA levels were measured by using a FFA quantification kit. n=8 * indicates $p < 0.05$ vs. cellular FFA of control group, $ indicates $p < 0.05$ vs. medium FFA control, # indicates $p < 0.05$ vs. cellular FFA of hypoxia, and @ indicates $p < 0.05$ vs. medium FFA of hypoxia. (B) Cells were pretreated with cerulenin or palmitic acid for 30 min prior to hypoxia treatment for 24 h and then pulsed with 1 μCi of [^{3}H]-thymidine for 1 h. n=9. (C) The number of cells was determined by using a counting chamber. n=6. Data are reported as a mean ± S.E. * indicates $p < 0.05$ vs. control, # indicates $p < 0.05$ vs. hypoxia, and ** indicates $p < 0.05$ vs. hypoxia with cerulenin.

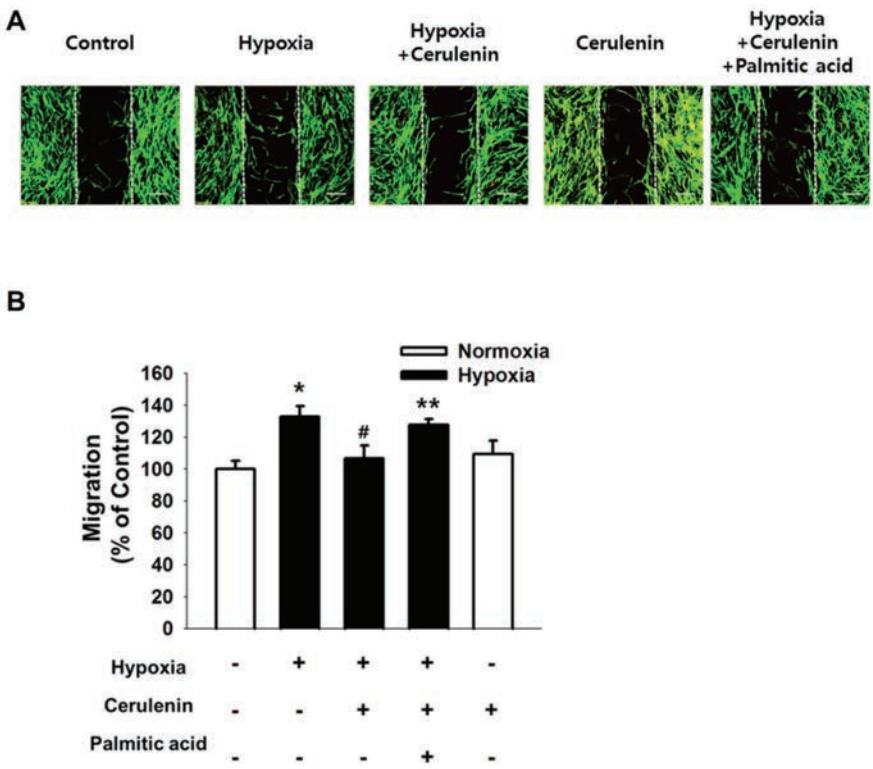

Figure 12. Role of hypoxia-induced FASN in migration of UCB-hMSCs. (A) Cells were pretreated with cerulenin or palmitic acid for 30 min prior to hypoxia treatment for 24 h. Cells cultured in ibidi dish were immunostained with phalloidin and PI, after which they were visualized by using fluorescence microscopy. Scale bars, 100 μm (magnification, $\times$100). (B) Migration of hypoxia-treated cells was quantified by using an Oris™ migration assay kit. Data are reported as a mean $\pm$ S.E of three independent experiments with duplex dishes. * indicates $p < 0.05$ vs. control, # indicates $p < 0.05$ vs. hypoxia alone, and ** indicates $p < 0.05$ vs. hypoxia with cerulenin.

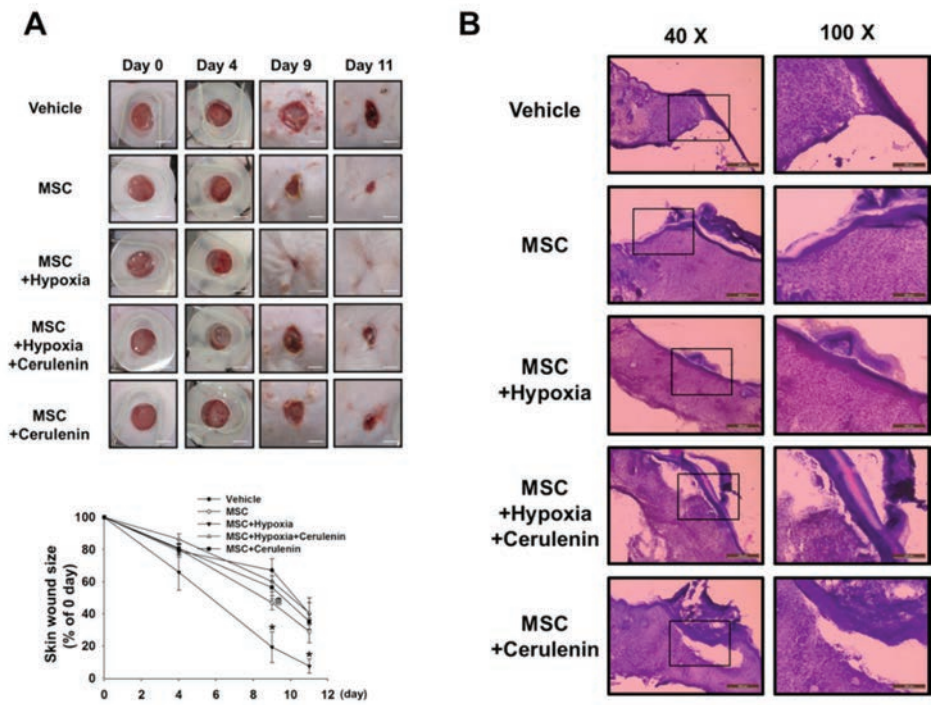

Figure 13. Role of hypoxia-induced FASN expression in mouse skin wound healing. (A) Representative gross images of skin wound healing was obtained at days 0, 4, 9, and 11 after treatment. Wound sizes compared with original wound sizes at day 0 were quantified by using ImageJ software n=6. @ indicates $p < 0.05$ vs. vehicle group and * indicates $p < 0.05$ vs. UCB-hMSC group. Scale bars, 2 mm. (B) Tissues containing wound sites were dissected at day 11 after wound creation, and then stained with hematoxylin and eosin. Representative histological images are shown. Scale bars, 500 μm (magnification, ×40) and 200 μm (magnification, ×100). Abbreviations: C, crust; Ep, epidermis; D, dermis; GT, granulated tissue; and CL, cornified layer.

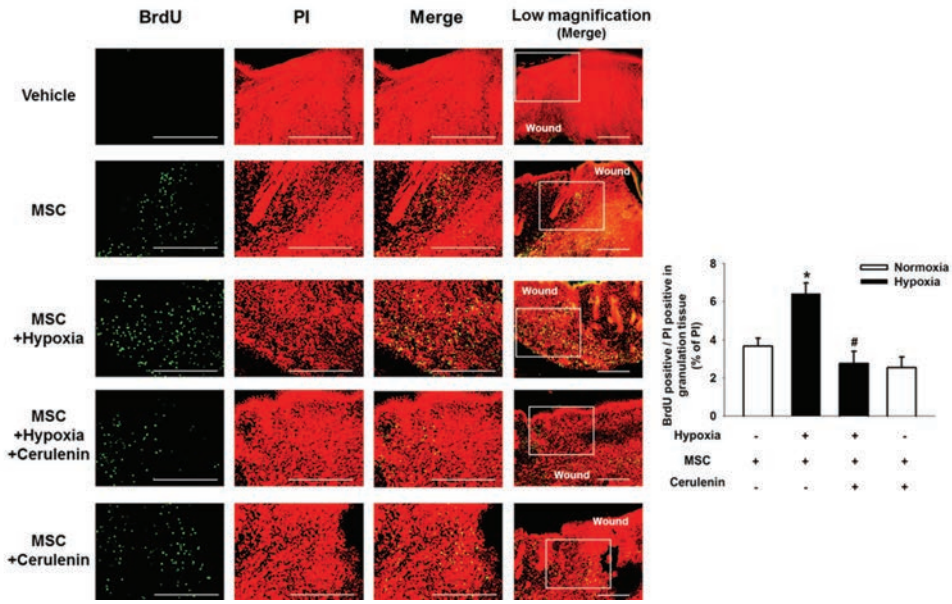

Figure 14. Role of hypoxia-induced FASN in UCB-hMSC survival.

UCB-hMSCs harboring BrdU were injected into the dermis surrounding the wound site. Transplanted UCB-hMSCs were immunostained with BrdU (green) and PI (red) for nuclear counter staining, which was visualized by using confocal microscopy. The relative numbers of BrdU-positive and PI-positive cells were analyzed by using MetaMorph software. Error bars indicate a mean ± S.E. n=6 * indicates $p < 0.05$ vs. UCB-hMSC group, and # indicates $p < 0.05$ vs. hypoxia-pretreated UCB-hMSC group. Scale bars for high (×400) and low (×200) magnification, 200 μm.

3.4. HIF-1α/SCAP/SREBP1 pathway leads to hypoxia-induced FASN expression

To identify how hypoxia induces FASN expression, I screened HIF-1α, HIF-2α, SREBP cleavage activating protein (SCAP), and (sterol regulatory element-binding protein 1) SREBP1 protein expressions during various periods of hypoxia treatment. As shown in Figs. 15A-15C, protein expressions of HIF-1α and HIF-2α were upregulated in a time dependent manner during hypoxia treatment. Moreover, real time PCR results indicated that hypoxia treatment increased *SCAP* and *SREBP1* mRNA expressions with RT-PCR. In support of those mRNA expression results, hypoxia treatment also increased SCAP and mature SREBP1 protein expressions during the initial 24 h of hypoxia treatment, but both expression levels decreased during the remaining 48-72 h incubation period (Fig. 15C). Hypoxia treatment also promoted nuclear translocation of mature SREBP1 (Fig. 16A), which were confirmed by immunofluorescence staining results. Fluorescence intensity within the nuclear region increased to 153% of the control level after 24 h of hypoxia treatment (Fig. 16B). In addition, Hypoxia-induced SREBP1 maturation and FASN expression were suppressed by HIF-1α silencing and fatostatin pretreatment (Figs. 17A and 17B).

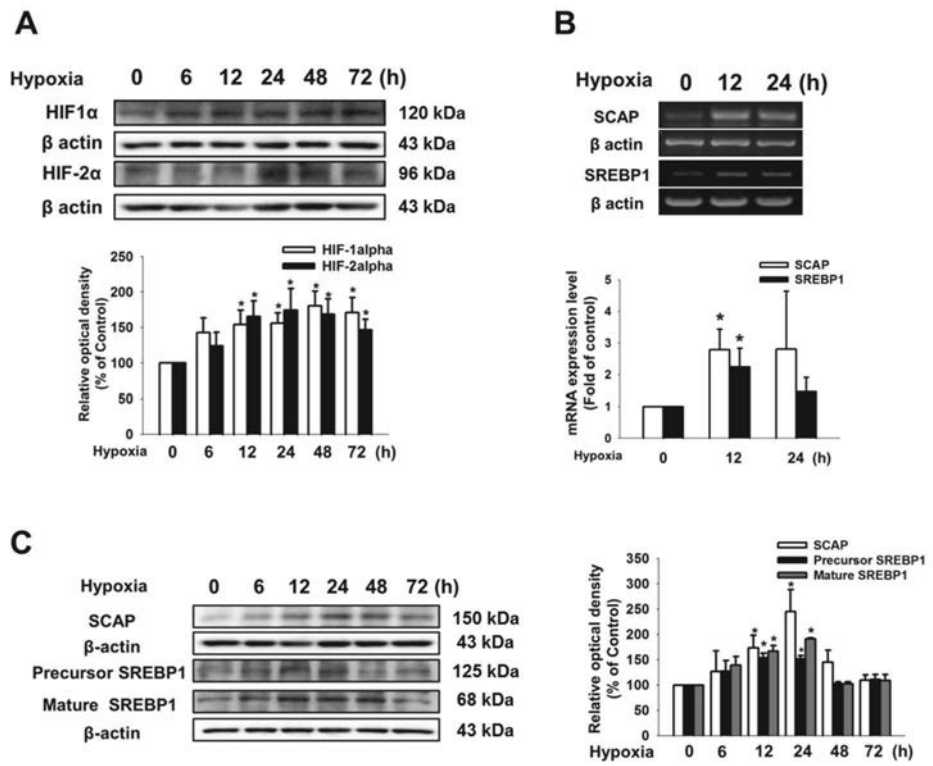

Figure 15. Involvement of HIF-1α, SCAP, and SREBP1 in hypoxia-induced FASN expression. (A) Cells were exposed to hypoxia for 0-72 h, after which HIF-1α and HIF-2α were detected by western blotting. n=3(B) Total mRNA sample from UCB-hMSCs was reverse transcribed and *SCAP* and *SREBP1* genes were amplified by PCR after 0-24 h of hypoxia exposure. The mRNA expression was quantified by using real-time PCR. n=3. (C) Cells were exposed to hypoxia for 0-72 h and SCAP, precursor SREBP1, and mature SREBP1 were then detected by western blotting. Data are reported as a mean ± S.E. * indicates $p < 0.05$ vs. control.

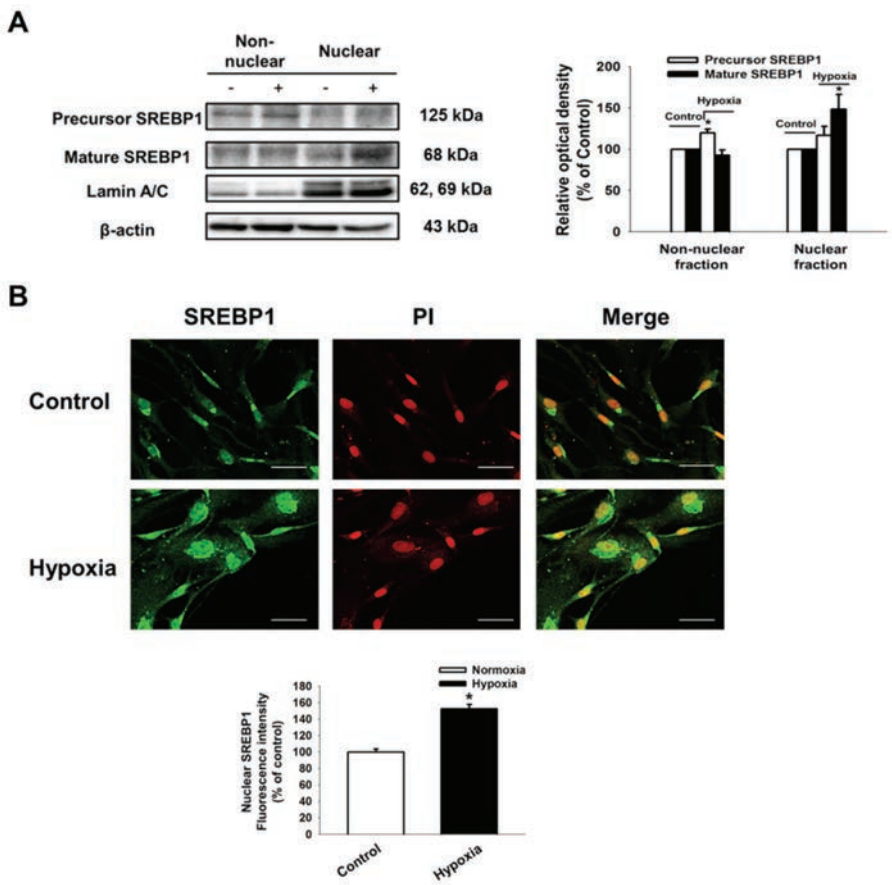

Figure 16. Effect of hypoxia on nuclear translocation of SREBP1. (A) Cells were exposed to hypoxia for 24 h. Precursor SREBP1, mature SREBP1, lamin A/C and β-actin were detected by western blotting. (B) Cells were exposed to hypoxia for 0 or 24 h and SREBP1 was detected by immunostaining with SREBP1 antibody. Fluorescence intensity (ImageJ arbitrary units) in the nuclear region was quantified by using ImageJ software. n=3. Data are presented as a mean ± S.E. Scale bars, 50 μm (magnification, ×600). * indicates $p < 0.05$ vs. control.

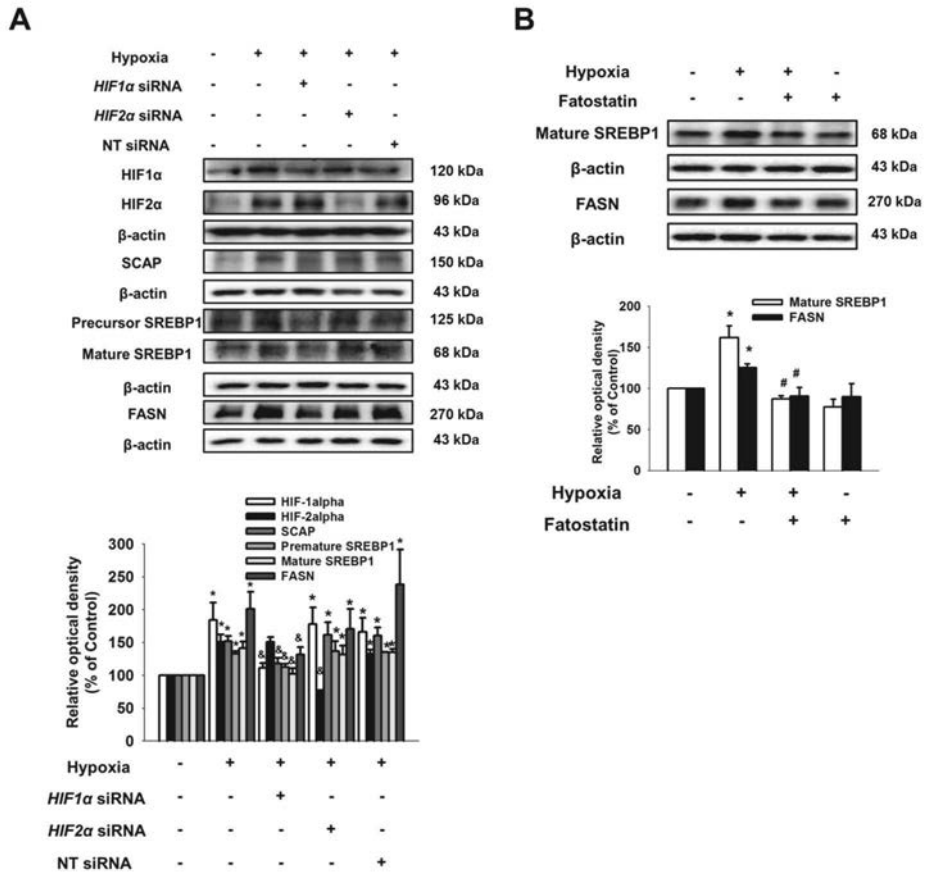

Figure 17. Regulatory role of HIF−1α in hypoxia−induced SCAP, SREBP1 and FASN expressions. (A) Cells were transfected for 24 h with either *HIF−1α*, *HIF−2α*, or NT siRNAs prior to hypoxia treatment for 24 h. HIF−1α, HIF−2α, SCAP, SREBP1, FASN, and β−actin were detected by western blotting. n=3. (B) Cells were pretreated with fatostatin (20 μM) for 30 min prior to hypoxia treatment. Precursor SREBP1, mature SREBP1, FASN, and β−actin were detected by western blotting. n=3. *indicates $p < 0.05$ vs. control, and # indicates $p < 0.05$ vs. hypoxia treatment.

3.5. FASN expression under hypoxia treatment is an upstream regulator of hypoxia-induced mTOR phosphorylation

To elucidate the interaction between hypoxia-induced FASN and the mTOR signaling pathway, I measured mTOR phosphorylation in UCB-hMSCs over various periods (0-72 h) of hypoxia treatment. Hypoxia increased the phosphorylation of mTOR in 24 and 48 h of incubation (Fig. 18A). After 24 h of hypoxia treatment, fluorescence intensity of p-mTOR (Ser2448 and Ser2481) increased to 356 % and 153% of the control level, respectively (Figs. 18B and 18C). Cerulenin pretreatment decreased hypoxia-induced phosphorylation of mTOR 4EBP1 and p70S6K1, but those effects were inhibited by the addition of palmitic acid (Figs. 19A and 19B). These results indicate that hypoxia regulates mTOR activation of UCB-MSCs via FASN activation. As shown in Fig. 19C, I assessed HIF-1α, SREBP1, and FASN expressions following 24 h of hypoxia or rapamycin (10 nM) treatment to determine whether hypoxia-induced mTOR activation also regulates FASN expression. The rapamycin treatment did not inhibit HIF-1α, SREBP1, or FASN expressions. Based upon these results, it is implicated that hypoxia-induced FASN expression is an upstream regulator of mTOR activation.

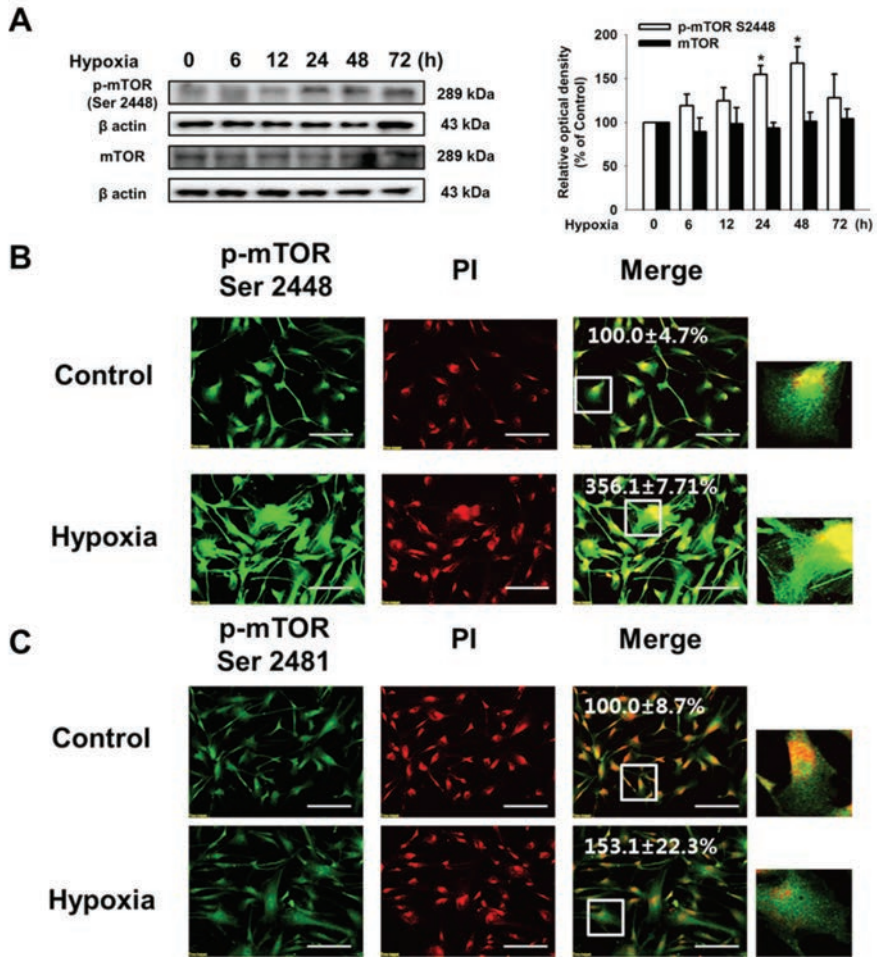

Figure 18. Effect of hypoxia on hypoxia-induced mTOR phosphorylation. (A) Cells were exposed to hypoxia for 0-72 h after which p-mTOR and mTOR were detected by western blotting. n=3. (B, C) Cells were exposed to hypoxia for 24 h, immunostained with p-mTOR (Ser2448 and Ser2481) antibodies and PI. Fluorescence images were acquired by using confocal fluorescence microscopy. Quantitative data are presented as a mean ± S.E. n=3. Scale bars, 100 μm (magnification, ×400). * indicates $p < 0.05$ vs. control.

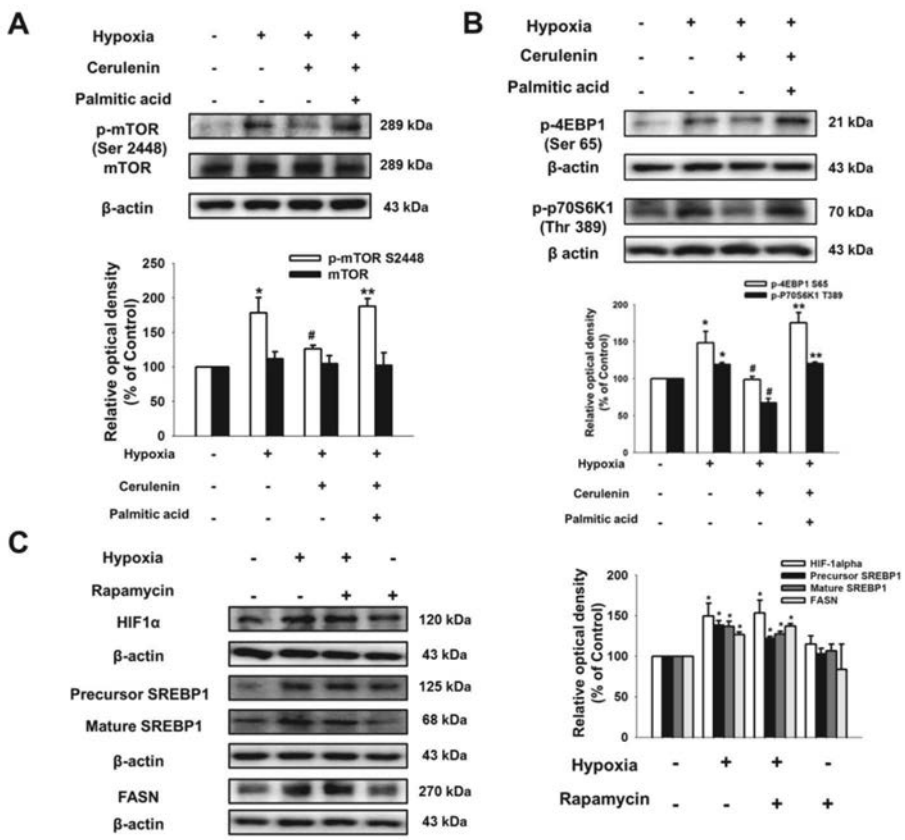

Figure 19. Role of FASN in hypoxia-induced mTOR phosphorylation. (A, B) Cells were pretreated with cerulenin (2 μM) or palmitic acid (10 μM) for 30 min prior to hypoxia treatment for 24 h and p-mTOR, mTOR, p-4EBP1 (Ser65), p-p70S6K1 (Thr389), and β-actin were detected by western blotting. n=3. (B) (C) Cells were pretreated with rapamycin (10 nM) for 30 min prior to hypoxia exposure for 24 h, and HIF-1α, precursor SREBP1, mature SREBP1, FASN, and β-actin were detected by western blotting. n=3. * indicates $p < 0.05$ vs. control, # indicates $p < 0.05$ vs. hypoxia, and ** indicates $p < 0.05$ vs. hypoxia with cerulenin.

3.6. Hypoxia-induced mTORC1 activation promotes UCB-hMSCs proliferation via expression of cell cycle regulatory proteins

I then assessed how hypoxia-induced mTOR activation regulates UCB-hMSCs proliferation. Hypoxia increased cell cycle regulatory proteins including cyclin-dependent kinase 2 (CDK2), CDK4, cyclin D1, and cyclin E levels in a time-dependent manner in the initial 24 h of hypoxia treatment (Fig. 20A). Pretreatment with rapamycin reduced the hypoxia-induced CDK2, CDK4, cyclin D1, cyclin E and c-myc expression levels (Figs. 20B and 20C). To determine which type of mTOR signaling pathway regulates cell proliferation under hypoxic conditions, I treated UCB-hMSCs with *RAPTOR*-, and *RICTOR*-specific siRNA as well as with rapamycin. As shown in Fig. 21, hypoxia-induced RAPTOR, CDK2, CDK4, cyclin D1 and cyclin E expression levels were inhibited to the greatest extent by *RAPTOR*-specific siRNA. I further assessed the role of mTOR in hypoxia-induced cell proliferation by using [^{3}H]-thymidine incorporation and MTT proliferation assays, and by counting cells. Hypoxia-induced UCB-hMSC proliferation was significantly inhibited by *RAPTOR* siRNA pretreatment (Figs. 22A-22C). These results suggest that the mTOR complex 1 signaling pathway predominantly controls hypoxia-induced UCB-hMSCs proliferation.

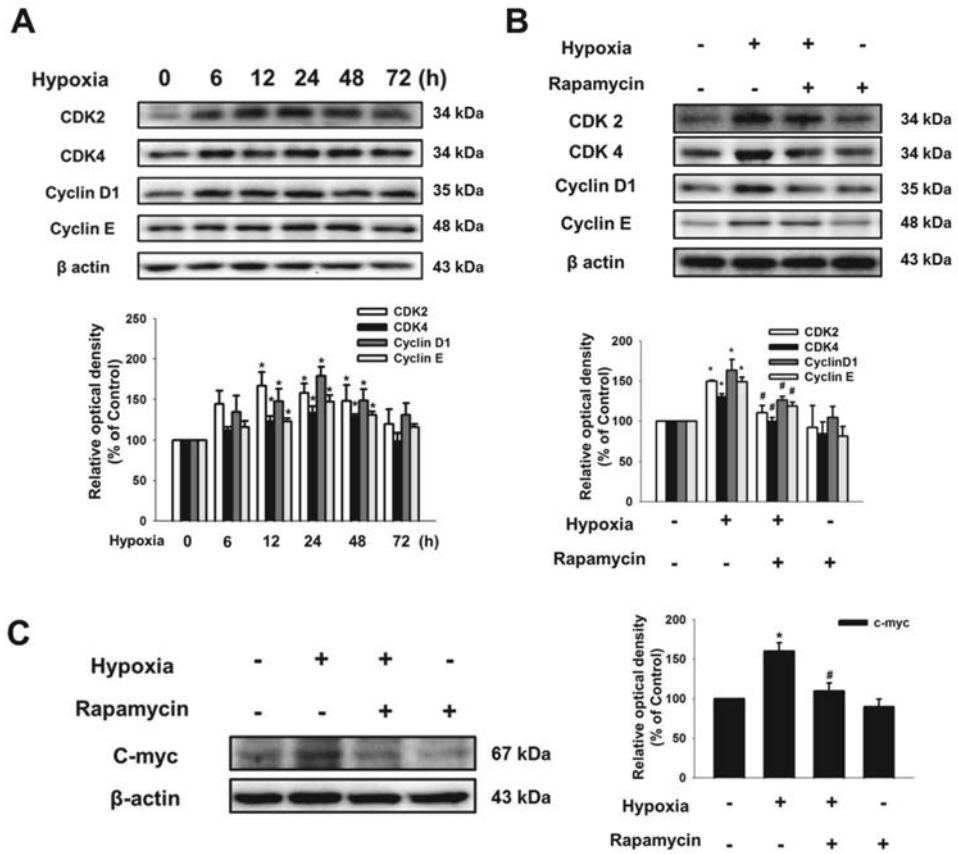

Figure 20. Role of hypoxia-activated mTOR on UCB-hMSC proliferation. (A) Cells were incubated in a hypoxic condition for 0–72 h. Total protein was extracted and blotted with CDK2, CDK4, cyclin D1, and cyclin E. n=3. * indicates $p < 0.05$ vs. control. (B, C) Cells were pretreated with rapamycin (10 nM) for 30 min prior to hypoxia treatment for 24 h, after which cell cycle regulatory proteins (CDK2, CDK4, cyclin D1, cyclin E, and c-myc) were detected by western blotting. n=3. * indicates $p < 0.05$ vs. control, # indicates $p < 0.05$ vs. hypoxia.

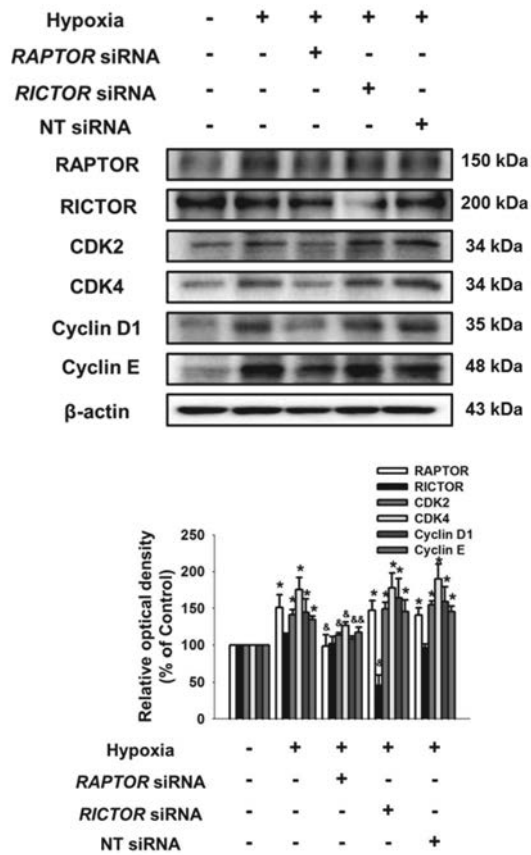

Figure 21. Role of hypoxia-induced RAPTOR on cell cycle regulator proteins. Cells were transfected with *RAPTOR*, *RICTOR* or NT siRNAs for 24 h prior to hypoxia treatment. RAPTOR, RICTOR, CDK2, CDK4, cyclin D1, and cyclin E were detected by western blotting. Data are reported as a mean ± S.E. n=3. * indicates $p < 0.05$ vs. control, # indicates $p < 0.05$ vs. hypoxia alone, and ## indicates $p < 0.05$ vs. hypoxia with NT siRNA.

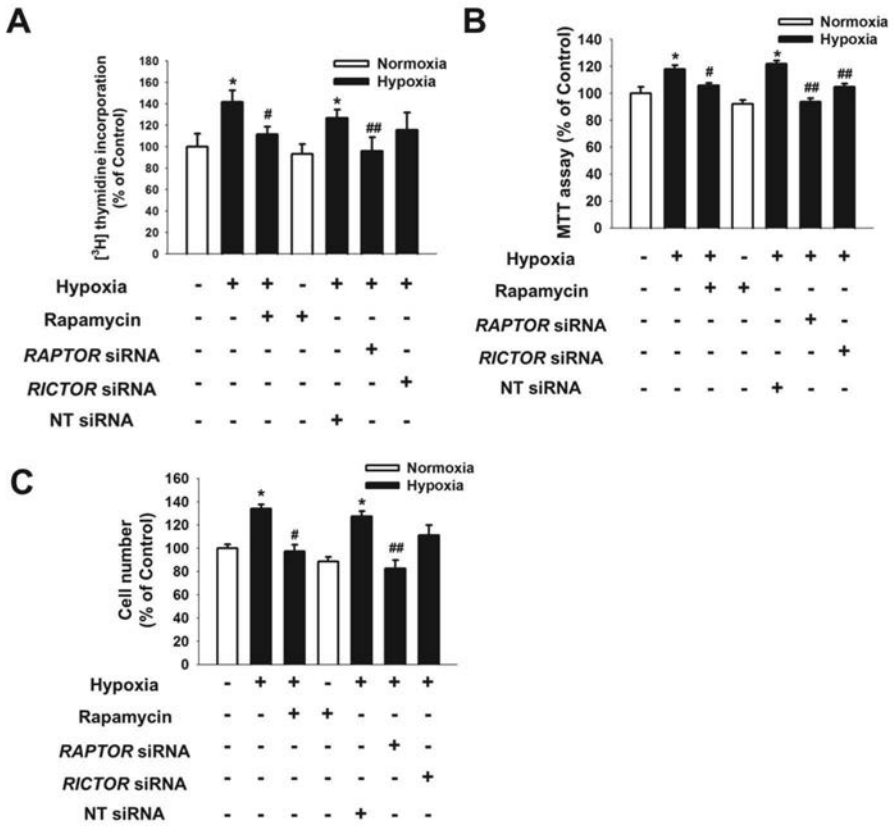

Figure 22. Role of hypoxia-induced RAPTOR in proliferation of UCB-hMSCs. (A-C) Cells were pretreated with rapamycin (10 nM) for 30 min and transfected with *RAPTOR*, *RICTOR*, or NT siRNA for 24 h prior to 24 h of exposure to hypoxia. (A) Cells were pulsed with 1 μCi of [^{3}H]-thymidine for 1 h prior to counting. n=9. (B) MTT proliferation assay reduction was detected at an absorbance of 545 nm by using a microplate reader. (C) Cells were counted by using a counting chamber. Data are reported as a mean ± S.E. n=9. * indicates $p < 0.05$ vs. control, # indicates $p < 0.05$ vs. hypoxia, and ## indicates $p < 0.05$ vs. hypoxia with NT siRNA.

3.7. Hypoxia-induced mTORC1 promotes UCB-hMSCs migration via p-cofilin1, profilin1/2, and Rho GTPase

Next, I investigated the effect of hypoxia-induced mTORC activation on UCB-hMSC migration. Through immunofluorescence staining, I further determined that the fluorescence intensity of proflilin1/2 and p-cofilin1 increased to 191 % and 188 % of control level, respectively (Figs. 23A and 23B). And, hypoxia treatment also increased proflin1/2 expression and cofilin1 phosphorylation, both of which were suppressed by rapamycin treatment (Fig. 23C). Moreover, RhoA GTPase was activated by hypoxia treatment, but Rac1 GTPase and Cdc42 GTPase were inactivated by hypoxia (Fig. 24A). As shown in Fig. 24B, hypoxia-induced F-actin expression decreased via silencing of *RAPTOR.* However, *RICTOR* siRNA treatment did not affect F-actin expression. Regulation of cell migration by RAPTOR was quantified by using the oris migration assay, which was visualized by using the ibidi insert dish assay (Figs. 25A and 25B). I performed live cell imaging to monitor cell migration and determine cell migration distance. The UCB-hMSCs cultured under hypoxic condition exhibited a significant increase in cell the migration distance. Meanwhile, migration distance of UCB-hMSCs that were transfected with *RAPTOR* siRNA was less than that of the control cells (Fig. 25C). Collectively, hypoxia-induced

cell migration is predominantly dependent on RAPTOR and is regulated by the F-actin regulatory protein.

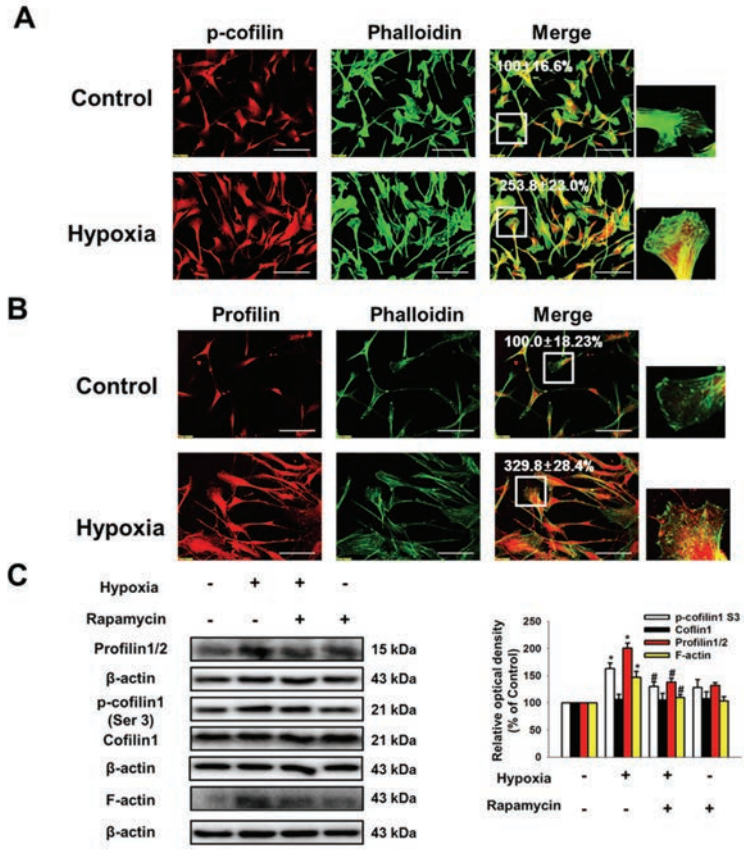

Figure 23. Role of hypoxia-activated mTOR in p-cofilin and proflilin expressions. (A, B) Cells were exposed to hypoxia for 24 h and immunostained with p-cofilin1 (Ser3), profilin1/2 antibodies, and phalloidin. n=3. Scale bars, 100 μm (magnification, ×400). (C) Cells were pretreated with rapamycin (10 nM) for 30 min prior to hypoxia for 24 h. Samples were blotted with p-cofilin1 (Ser3), cofilin1, profilin1/2, and F-actin. Data are presented as a mean ± S.E. * indicates $p < 0.05$ vs. control, # indicates $p < 0.05$ vs. hypoxia alone.

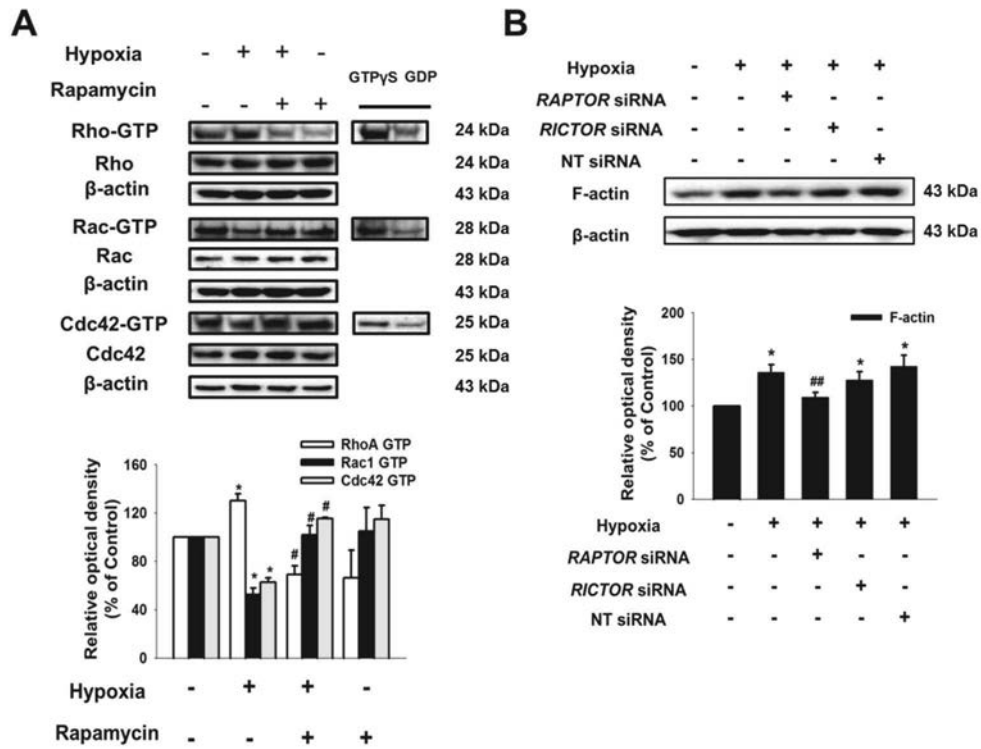

Figure 24. Role of hypoxia-activated mTOR in GTPases activation and F-actin expression. (A) Cells were treated with hypoxia for 24 h, after which activations of RhoA, Rac1, and Cdc42 GTPases were measured with an affinity precipitation. RhoA, Rac1, and Cdc42 protein expressions were detected by western blotting. n=3. * indicates $p < 0.05$ vs. control, # indicates $p < 0.05$ vs. hypoxia, (B) Cells were transfected with *RAPTOR*, *RICTOR*, or NT siRNAs prior to hypoxia. F-actin expression was detected by western blotting. n=3. * indicates $p < 0.05$ vs. control, # indicates $p < 0.05$ vs. hypoxia, ## indicates $p < 0.05$ vs. hypoxia with NT siRNA.

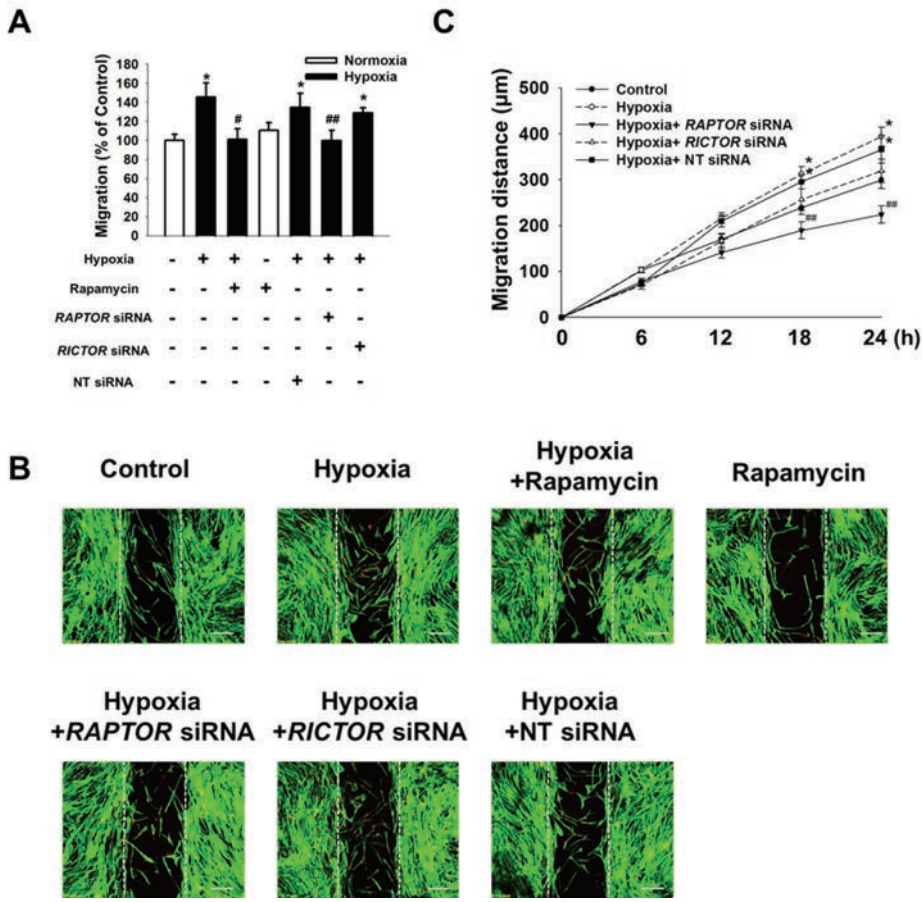

Figure 25. Role of hypoxia-activated mTOR in UCB-hMSC migration.

(A) Cells were pretreated with rapamycin (10 nM) for 30 min and were transfected with *RAPTOR*, *RICTOR*, or *NT* siRNA for 24 h prior to hypoxia treatment. Cell migration was detected with an Oris™ migration assay kit. n=9. * indicates $p < 0.05$ vs. control, # indicates $p < 0.05$ vs. hypoxia, and ## indicates $p < 0.05$ vs. hypoxia with NT siRNA. (B) Cells were immunostained with phalloidin and PI and then observed via confocal fluorescence microscopy. Scale bars, 100 μm (magnification, ×100). (C) Migration distance was measured by using MetaMorph software.

Accumulated cell migration distance is presented as a line graph. n=9. Data are presented as a mean ± S.E. * indicates $p < 0.05$ vs. control and ## indicates $p < 0.05$ vs. hypoxia with NT siRNA.

4. DISCUSSION

In the present study, I demonstrated that hypoxia-induced upregulation of FASN via the HIF-1α/SCAP/SREBP1 pathway, regulates UCB-hMSCs proliferation and migration through mTORC1 activation (Fig. 26). My data showed the long term of hypoxia incubation impairs stem cell functions in UCB-hMSCs, which can be explained by absence of ROS scavenger system of *in vivo.* Indeed, it has been reported that microenvironments, including stem cell niches, can affect stem cell function and ROS reduction (Ito et al., 2004; Jang et al., 2007; Suda et al., 2005; Wang et al., 2013). In addition, I screened expression of lipid metabolic enzymes under hypoxic condition to confirm the effect of hypoxia in UCB-hMSCs lipid metabolism. Lipogenic enzymes such as FASN and SCD1 have critical roles in a variety of cell activities (Ben-David et al., 2014; Knobloch et al., 2013). FASN was higher than that of other lipid metabolic enzymes under hypoxic condition, and FASN inhibition abolished hypoxia-induced UCB-hMSCs proliferation. However, in contrast mouse embryonic stem cells (mESCs), inhibition of SCD1 did not affect to UCB-hMSCs proliferation. These results indicate the importance of FASN on hypoxia-induced regulation of UCB-hMSCs and metabolic differences between UCB-MSCs and mESCs.

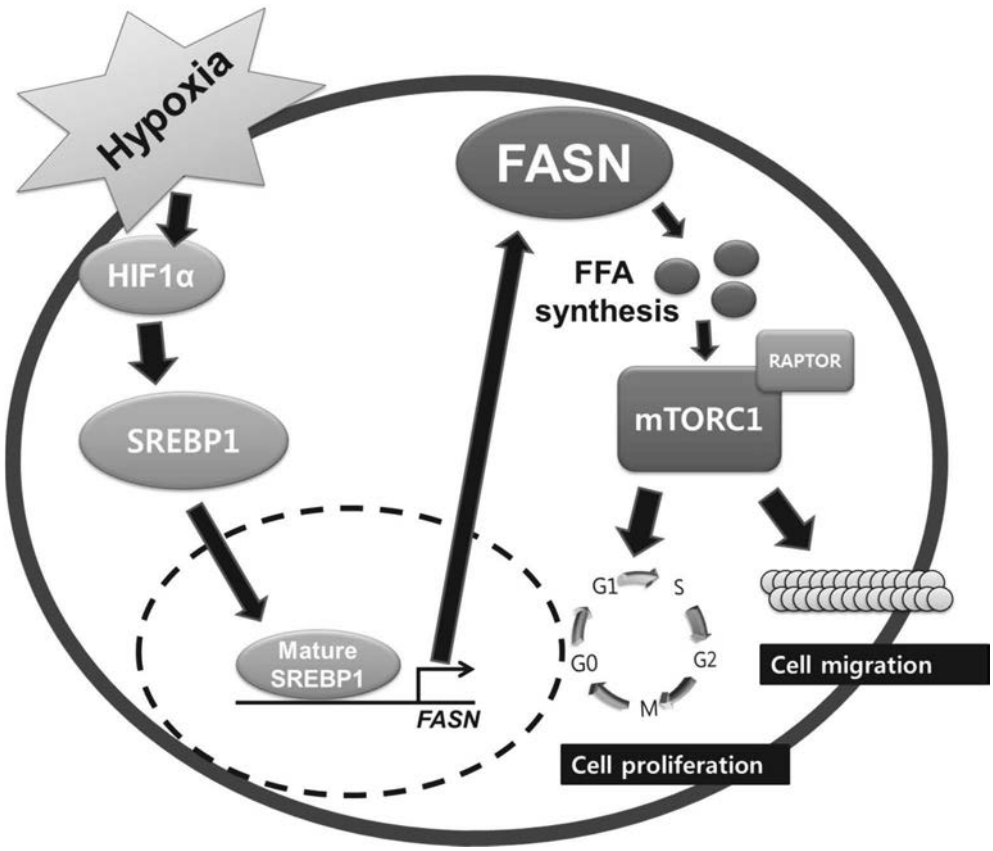

Figure 26. The schematic model for mechanism involved in the role of hypoxia-induced FASN in proliferation and migration of UCB-hMSCs. Hypoxia induces HIF-1α expression, leads to activation of SREBP1. Mature SREBP1 translocates into the nucleus, which is followed by FASN expression. FASN induction increases FFA production and RAPTOR-dependent mTORC1 activation. Finally, activated mTORC1 stimulates proliferation and migration in UCB-hMSCs.

Although identification of the factor making UCB-hMSCs are insensitive to SCD1 inhibition requires further study, it is postulated that the low endogenous level of ER stress in UCB-hMSCs may be a critical factor (Kim et al., 2010a). In addition, several studies have reported that HIF is associated with FASN expression, but the detailed mechanism that regulates FASN expression by HIF is unclear (Furuta et al., 2008b; Rankin et al., 2009). Indeed, the results of my study revealed that hypoxia-induced FASN, SCAP, and SREBP1 expressions are HIF-1α, not HIF-2α, dependent. In addition, it is demonstrated that activated SREBP1 by hypoxia in nucleus interacts with FASN promoter suggesting that SREBP1 may have a direct role in hypoxia-induced FASN expression (Furuta et al., 2008b). Taken together, hypoxia stimulates FASN expression via HIF-1α/SCAP/SREBP1 pathway. Besides, several recent studies reported that alteration of cellular metabolites ratios, such as NADP/NADPH, by hypoxia has also an important role in the regulation of various stem cell functions such as cell cycle and self-renewal activities (Cipolleschi et al., 2014), (Marzi et al., 2013). These findings indicate that change of cellular metabolite ratios may be another pathway, in addition to the HIF1α/SCAP/SREBP1 pathway, involved in the regulation of lipid metabolism in UCB-hMSCs.

Through this study, I have shown that hypoxia-induced FASN stimulates FFA production as well as proliferation and migration. In

addition, several studies reported that FAs and FA derivatives inhibited and uncoupled oxidative phosphorylation of various cells (Brustovetskii et al., 1991; Samartsev et al., 2002; Ventura et al., 1995). Based upon these reports, there appears to be a close interaction among FAs, their bioactive metabolites and functions including proliferation and migration in UCB-hMSCs. In addition, I found that palmitic acid treatment rescues inhibition of mTOR phosphorylation as well as restriction of UCB-hMSC proliferation and migration. Although some studies have focused on the role of mTOR in regulating stem cell growth, survival, and proliferation, there are inconsistent results being reported whether hypoxia activates or inactivates mTOR signaling. For instance, Humar *et al.* demonstrated that hypoxia-induced mTOR activation is important for vascular cell proliferation and angiogenesis (Humar et al., 2002). Conversely, Vadysirisack *et al.* found that hypoxia-inducible REDD1 is essential for hypoxia-induced inhibition of mTORC1 (Vadysirisack et al., 2012). Consistent with those results, I have shown that FASN is critical for hypoxia-induced mTOR phosphorylation, which is followed by promotion of UCB-hMSCs function. Several studies have shown that phosphorylation of mTOR can be indicative of mTOR activation (Hornberger et al., 2007; Moschella et al., 2007; Rosner et al., 2010). Although I did not identify the mechanism that regulates mTOR via FASN, I suggested that palmitic acid produced by FASN may be associated with the

providing ATP sources, as well as with the providing support to cellular membranes, lipid rafts, and extracellular signals (Beneteau et al., 2008; Currie et al., 2013).

There are several reports showing that the role of mTOR in cell proliferation and migration is dependent on the type of mTORC (Guertin et al., 2007; Gulhati et al., 2011; Zhou et al., 2011). In this study, I found that hypoxia induces both proliferation and migration of UCB-hMSCs, and those effects are RAPTOR-dependent. In addition, my result showed that hypoxia increases RAPTOR, not RICTOR, expression; thus suggesting that hypoxia-induced RAPTOR is responsible for mTORC1-dependent UCB-hMSC proliferation and migration. Furthermore, I found that hypoxia-induced mTOR activation regulates expression of c-myc, a potent cell cycle regulatory transcription factor, which can be associated with hypoxia-mediated UCB-hMSCs proliferation. Wang *et al.* reported that rapamycin-induced mTOR inactivation could reduce c-myc expression in T cells (Wang et al., 2011). Moreover, my results also showed that hypoxia-induced mTOR activation upregulates F-actin regulatory proteins, such as p-cofilin, profilin and Rho GTPase, thus indicating that F-actin organization via the actions of actin regulatory proteins is important for hypoxia-induced cell migration (Gulhati et al., 2011). In support of those results, I observed that the number of UCB-hMSCs with a high level of organized F-actin and with extended cell bodies increased

after hypoxia treatment. Particularly, my results showed that hypoxia-induced mTOR activation increased RhoA activity, but not Rac1 and Cdc42, which reveals contradictory with commonly known role of Rac1. However, it has been also reported that the contribution of small GTPases in migration appears cell-type specific (Abecassis et al., 2003; Filippi et al., 2007; Luckashenak et al., 2013). Liu *et al.* demonstrated that inhibition of cell migration by rapamycin is mainly RhoA, not Rac1 and Cdc42, dependent (Liu et al., 2010). In addition, several studies have reported that activated Rho GTPase antagonizes Rac1 and Cdc42 GTPases activities in migrating cells (Baird et al., 2005; Boulter et al., 2012; Ohta et al., 2006). Collectively, these findings indicate that RhoA-dependent F-actin organization plays a critical role in hypoxia-induced UCB-hMSC migration.

CHAPTER II

Regulatory role of BNIP3-mediated mitophagy under hypoxia in FASN-dependent free fatty acid production enhancing therapeutic potential of UCB-hMSCs

Manuscript is published in *Redox Biol*, 2017 13:426-443

1. INTRODUCTION

Metabolic alteration of stem cells under hypoxia is prerequisite to controlling stem cell function activated by oxygen signaling (Ito & Suda. 2014; Ryu et al., 2015b). Many investigators have shown that, in regenerative medicine, stem cell regulation with hypoxia has many advantages for stem cell functional regulation compared to that with normoxia (Abdollahi et al., 2011; Lavrentieva et al., 2010). However, the essential metabolic factor that enhances and sustains the functional regulation of stem cells by hypoxia has been incompletely described. Investigation to unveil the relationships between metabolism and stem cell physiology under hypoxia is required to optimize stem cell-based therapy for clinical application in regenerative medicine. As several investigators recently demonstrated, FA and its metabolites, such as sphigosine-1-phosphate and LPA produced within the stem cell have the capacity to control the metabolism and behavior of stem cells, although it is reported that the role of FA oxidation in ATP synthesis is insignificant (Fillmore et al., 2015; Kang et al., 2015; Lee et al., 2015; Sun et al., 2016). Thus, the interest in the role of lipid metabolism regulation by hypoxia is increasing. Some studies investigating lipid metabolic changes induced by hypoxia reported that hypoxia stimulates FA uptake, *de novo* FA synthesis, and FA

metabolite synthesis (Ader et al., 2008; Cao et al., 2014). However, there are few studies investigating the role of lipid metabolism altered by hypoxia in stem cell regulation. Despite ROS accumulation, which causes ischemic injury, the detailed mechanism involved in how stem cells exposed to hypoxia maintain lipid metabolism and function is not fully described. An investigation into factors protecting against impairment of lipid metabolism shift under high ROS accumulation conditions should provide novel insight into the control of stem cells under hypoxia.

Mitophagy is mitochondria-specific autophagy that removes mitochondria in order to maintain mitochondrial quality (Liu et al., 2014b). It has been shown that mitophagy prevents mitochondrial dysfunction, inflammation, apoptosis, and severe oxidative stress, which are closely associated with pathological progress of neurological and metabolic diseases (Hammerling et al., 2017; Wallace. 2005). Mitophagy is mediated by two mitophagy regulator types, mitophagy receptor and E3 ubiquitin ligase. In addition, some investigators have reported that hypoxia-induced metabolic stress stimulates mitophagy (Liu et al., 2014b; Wu et al., 2015). Mild oxidative stress specifically induces mitophagy without nonspecific autophagy, whereas a high ROS level stimulates both autophagy and mitophagy as a negative-feedback mechanism to reduce mitochondria-derived ROS production (Frank et al., 2012; Kurihara et al., 2012; Scherz-Shouval et al., 2011). Many researchers have

attempted to demonstrate the mechanism for the initial stimulation of mitophagy by oxidative stress. Several mitophagy regulators including mitophagy receptors, such as BNIP3, NIX, FUN14 domain containing 1 (FUNDC1), PINK1/Parkin, which induce mitophagy in mammalian cells under hypoxia, have been identified (Lin et al., 2014; Sowter et al., 2001; Wu et al., 2016a). However, there have been no studies investigating the contribution of such mitophagy regulators to mitophagy induced by hypoxia in stem cells. Since there are few studies demonstrating the role of mitophagy in stem cell differentiation, further investigation is required to elucidate the relationships between mitophagy and stem cell regulation under hypoxia (Joshi & Kundu. 2013). In addition, uncovering the molecular mechanism involved in mitophagy regulation of lipid metabolism in stem cells under hypoxia can answer the question: What is the key player in the induction and maintenance of lipid metabolism in stem cells under hypoxia?

Clinical application of hMSCs has been considered a promising therapeutic strategy for scarless wound healing and ischemic injury (Doi et al., 2016; Liew et al., 2012). The hMSC effect is associated with cell replacement and paracrine effects leading to angiogenesis and damaged tissue repair (Boomsma et al., 2012; Dimarino et al., 2013; Rocheteau et al., 2015). UCB-hMSCs are the most abundant non-embryonic cell source and have generated remarkable interest in researchers studying stem cell-based therapy, because of their

multiple differentiation potential and immune modulation capacity, as they can be obtained easily and non-invasively without ethical concerns (Qiao et al., 2008; Wang et al., 2009). Therefore, investigation into the regulation of UCB-hMSC physiological function under hypoxia may improve the therapeutic effect of UCB-hMSCs in regenerative medicine. The aim of my investigation is to identify the detailed regulatory mechanism of a major mitophagy regulator controlling lipid metabolism and therapeutic potential of UCB-hMSCs under hypoxia.

2. MATERIALS & METHODS

2.1. Materials

The UCB-hMSCs, obtained from Medipost (Seoul, Korea, http://www.medi-post.com). The UCB-hMSCs were positive for HLA-AB but not for HLA-DR, and characterized to express CD73, CD105, but not CD14, CD34, and CD45. FBS and antibiotics for UCB-hMSC cultivation were purchased from Hyclone (Logan, UT, USA) and Gibco (Grand Island, NY, USA), respectively. COX4, α-SMA , F-actin and SREBP1 antibodies were purchased from Abcam (Cambridge, MA, USA). LC3B, NIX and HIF-1α antibodies were obtained from Novus Biologicals (Littleton, CO, USA). BNIP3, β-tubulin, β-actin, PINK1, Lamin A/C, CBP, FASN, p-cofilin1, cofilin1 and caspase-9 antibodies were purchased from Santa Cruz (Paso Robles, CA, USA). p-S6, p-eIF2α, eIF2α, p-mTOR, mTOR, p-S6K1, cleaved caspase-3 and FOXO3 antibodies were purchased from Cell Signaling Technology (Danvers, MA, USA). HNA antibody was acquired from EMD Millipore (Billerica, MA, USA). Horseradish peroxidase (HRP)-conjugated rabbit anti-mouse and goat anti-rabbit secondary antibodies were obtained from Thermo Fisher (Waltham, MA, USA). Alexa fluor 488- and 555-conjugated secondary antibodies and PI were purchased from Life

Technologies (Gaithersburg, MD, USA). CAY10566 was obtained from Cayman chemical (Ann Arbor, MI, USA). Cerulenin, C646 and fatostatin were acquired from Sigma-Aldrich (St. Louis, MO, USA). siRNAs for *PINK1*, *BNIP3*, *NIX* , *FOXO3* and non-targeting were purchased from Dharmacon (Lafayette, CO, USA). *HIF1A* siRNA was obtained from Gene Pharma (Gene Pharma, Shanghai, China). All reagents used in the present study were of the highest quality commercially available forms.

2.2. Cultivation of UCB-hMSCs

The detailed protocol for UCB-hMSCs cultivation is described in Materials and Methods section of CHAPTER I.

2.3. Hypoxia treatment

The detailed protocol for hypoxia is described in Materials & Methods section of CHAPTER I.

2.4. Western blot analysis

The detailed protocol for western bolot analysis is described in Materials & Methods section of CHAPTER I.

2.5. Preparation of mitochondrial fraction sample

Mitochondrial isolation was performed by using a commercial mitochondrial isolation kit (Thermo Fisher) according to the manufacturer's manual. Briefly, harvested samples were incubated in Reagent A for 2 min on ice. Subsequently, the cell lysate sample was incubated with Reagent B for 5 min. Next, Reagent C was added to the lysate sample. The cell lysate sample was centrifugated at 3000×*g* for 15min. Supernatant was used as a cytosolic fraction. The pellet was lysed with 2% CHAPS in Tris-buffered saline (25mM Tris, 0.1M NaCl, pH7.2) solution and used as a mitochondrial fraction for 30 min on ice.

2.6. Preparation of nuclear fraction sample

The detailed protocol for nuclear fractionation is described in Materials & Methods section of CHAPTER I.

2.7. Reverse transcription-polymerase chain reaction (PCR) and real-time PCR

RNA was extracted by using a MiniBEST Universal RNA

extraction kit (TaKaRa, Otsu, Shiga, Japan). RNA (1 μg) was reverse-transcribed with a Maxime RT-PCR PreMix kit (Intron Biotechnology, Seongnam, Korea) to produce the cDNA sample. Reverse transcription was performed for 1 h at 45° C and 5 min at 95° C. The cDNA sample was amplified with a QuantiNova SYBR kit (Life Technologies) and mRNA primers for *FASN*, *SCD1*, *SCD5*, *GPAT1*, *GPAT3*, *GPAT4*, *MAGL*, *DGAT1*, *CPT1A*, and *ACTB*. The expression of *ACTB* mRNA was used for normalization of gene expressions.. The primer sequences are described in Table 3. Amplification of cDNA was carried out by using a Rotor-Gene 6000 real-time thermal cycling system (Corbett Research, Mortlake, NSW, Australia). Real-time PCR was performed as follows: 10min at 95° C for DNA polymerase activation and 50 cycles of 15 sec at 94° C, 20 sec at 55° C, and 30 sec at 72° C. The identity and specificity of the PCR product was validated by performing melting curve analysis. Quantification analysis was performed by using the Rotor-Green 6000 Series Software package (Corbett Research).

Table 3. Sequences of primers used for RT-PCR and real-time PCR.

Gene	Identification	Sequence (5'-3')	Size (bp)
PINK1	Sense	GCCTCATCGAGGAAAAACAGG	114
	Antisense	GTCTCGTGTCCAACGGGTC	
BNIP3	Sense	GCCATCGGATTGGGGATCTAT	150
	Antisense	GCCACCCCAGGATCTAACAG	
NIX	Sense	GGACTCGGCTTGTTGTGTTG	194
	Antisense	TAGCTCCACCCAGGAACTGT	
FASN	Sense	CCGAGACACTCGTGGGCTA	209
	Antisense	CTTCAGCAGGACATTGATGCC	
SCD1	Sense	TTCGTTGCCACTTTCTTGCG	218
	Antisense	AAGTTGATGTGCCAGCGGTA	
SCD5	Sense	GACCTGCTTGCTGATCCTGT	237
	Antisense	AGGGCTGATGTGCTTGTCAT	
GPAT1	Sense	AGGACGCAACGTCGAGAAC	176
	Antisense	GCAGTACCTCCATCATCCCAAG	
GPAT3	Sense	GTACATGCCTCCCATGACTAG	195
	Antisense	GATCCGTTGCCCACGATCATC	
GPAT4	Sense	TCTGGAACAGCAGCAAATAC	115
	Antisense	TCTTCATCTGCCTCTCTAGT	
MAGL	Sense	TCGTCAGGGATGTGTTGCAG	155
	Antisense	AGGCGAAATGAGTACCATGCC	
DGAT1	Sense	GGCTTTCACGGGCATGAT	116
	Antisense	CTATTGGCTGTCCGATGATGA	
CPT1A	Sense	ATCAATCGGACTCTGGAAACGG	121
	Antisense	TCAGGGAGTAGCGCATGGT	
SREBF1	Sense	GTGGCGGCTGCATTGAGAGTG AAG	362
	Antisense	AGGTACCCGAGGGCATCCGAG AAT	
β-actin	Sense	AACCGCGAGAAGATGACC	351
	Antisense	AGCAGCCGTGGCCATCTC	

2.8. Transfection of siRNA

Prior to treatment of reagent or hypoxia, 20 nM of siRNAs specific for *PINK1*, *BNIP3*, *NIX*, *FOXO3,* and NT with transfection reagent TurboFect™ (Thermo Fisher) were added to UCB-hMSCs, which were then incubated for 24 h in a conventional cell incubator at 37° C in 5% CO_2. The siRNAs sequences used in this study are described in Table 4. The siRNAs of *PINK1*, *BNIP3* and *NIX* were

significantly decreased their mRNA expressions, respectively (Fig. 27).

Table 4. Sequences of siRNAs used for gene silencing.

Target gene	Sequence 5'-3'	Supplier
PINK1	GCAAAUGUGCUUCAUCUAA	Dharmacon
	GCUUUCGGCUGGAGGAGUA	
	GGACGCUGUUCCUCGUUAU	
	GAGACCAUCUGCCCGAGUA	
BNIP3	UCGCAGACACCACAAGAUA	Dharmacon
	GAACUGCACUUCAGCAAUA	
	GGAAAGAAGUUGAAAGCAU	
	ACACGAGCGUCAUGAAGAA	
NIX	GACCAUAGCUCUCAGUCAG	Dharmacon
	CAACAACAACUGCGAGGAA	
	GAAGGAAGUCGAGGCUUUG	
	GAGAAUUGUUUCAGAGUUA	
HIF1A	GCCGCUCAAUUUAUGAAUATT UAUUCAUAAAUUGAGCGGCTT	GenePharma
	GCCUCUUUGACAAACUUAATT UUAAGUUUGUCAAAGAGGCTT	
	CCACCACUGAUGAAUUAAATT UUUAAUUCAUCAGUGGUGGTT	
	GCUGGAGACACAAUCAUAUTT AUAUGAUUGUGUCUCCAGCTT	
FOXO3	GCACAGAGUUGGAUGAAGU	Dharmacon
	GUACUCAACUAGUGCAAAC	
	CGAAUCAGCUGACGACAGU	
	UAACUUUGAUUCCCUCAUC	
Non-targeting (NT)	UAGCGACUAAACACAUCAA	Dharmacon
	UAAGGCUAUGAAGAGAUAC	
	AUGUAUUGGCCUGUAUUAG	
	AUGAACGUGAAUUGCUCAA	

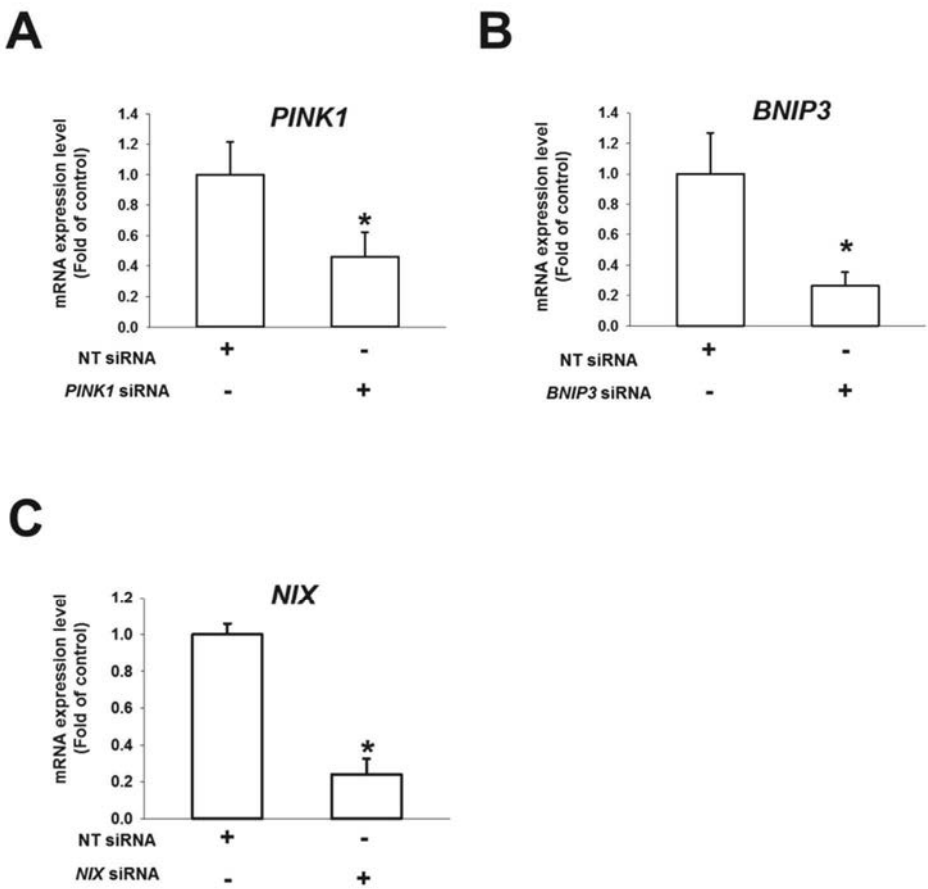

Figure 27. The effect of siRNAs on mRNA expressions of PINK1, BNIP3 and NIX. (A–C) UCB–hMSCs were transfected with PINK1, BNIP3 and NIX siRNAs for 24 h. The mRNA expressions of PINK1, BNIP3 and NIX were analyzed by qPCR. The mRNA expression levels were normalized with *ACTB* mRNA expression level. Data are presented as a mean ± S.E. n = 4.

2.9. Co-immunoprecipitation

To confirm the formation of a protein complex in a cell lysate sample, I performed co-immunoprecipitation with a commercial co-immunoprecipitation kit (Thermo Fisher) according to manufacturer's manual. Harvested cells were lysed with IP lysis buffer and incubated for 5 min on ice. Cell debris was cleared by centrifugation at 13,000×*g*, 4° C for 10 min. Supernatant sample was collected. Determination of protein concentration of lysate sample was performed with a BCA quantification assay (Thermo Fisher). CBP antibody was immobilized with AminoLink Plus coupling resin (Thermo Fisher) for 2 h. Immobilized resin was washed with a commercial wash buffer and incubated with cell lysate for 6 h at 4° C. IgG antibody was provided in an IP kit and used as a negative control to assess the degree of non-specific binding to resin. Protein samples were analyzed by western blot analysis.

2.10. Measurement of cellular FFA production

The detailed protocol for FFA measurement is described in Materials & Methods section of CHAPTER I.

2.11. CHIP assay

CHIP assay was performed by using EZ-CHIP-Chromatin immunoprecipitation kit (EMD Millipore, Billerica, MA, USA) according to the manufacturer's manual. Briefly, samples lysed by SDS lysis buffer were incubated with HIF-1α, FOXO3, normal IgG, and Pol III-specific antibodies overnight at 4° C. Normal IgG and Pol III-specific antibodies were used as negative and positive controls, respectively. Immunoprecipitated protein-chromatin complex samples were eluted with elution buffer provided with the kit {1% SDS, 50mM Tris-HCl (pH7.5), 10 mM EDTA}. Eluted samples were incubated with 5 M NaCl at 65° C for 4h and subsequently incubated with RNase A at 37° C for 30 min. Eluates were incubated with 0.5 M EDTA, 1M Tris-HCl, and proteinase K at 45° C for 2 h. DNA was acquired by using DNA purification column and amplified by real-time PCR with primer. The primer sequences and target consensus sequences for CHIP assay are described (Table 5 and Fig. 28).

Table 5. Sequences of CHIP primers used for PCR.

Gene	Identification	Sequence (5'-3')	Size (bp)
BNIP3 promoter for HIF-1α	Sense	CTTCCCTGCACGTCCTCAC	171
	Antisense	CCGGGTTCTCCTTTGAAGGG	
BNIP3 promoter for FOXO3	Sense	TCCCGAGACGCTCAGCTC	168
	Antisense	TCCATCCTGCTAGTGGGGAA	

Human *BNIP3* promoter (1000bp from TSS)

```
1000 GAAGAAAGACTTTTGATCAAAAGCGGGAAATGAGAAAGCGACTTTCCTCTGAAAAGTGCC
 940 TCCCAGTCCCGAGGCTGCGAGGCCCCCACGCCAGGCTGGCTCCCACGGAAGCCGGGCACC
 880 CACCCGGCCCGACCAAGCGCCACTCCGCCCCGTGGACGGGGCGTCCCACCCCGGGGACGC
 820 CCGCCCCACACCGCGTTTGCACCCCGGAGGCCCCTTGCCGCAGAGGCGGACGGCGCGCCT
 760 CTCCCGGGCCCCTGGGGTCCGCGCCTCCCTCGGGCAGACTCTTTCGACTCTGCTCGAGCC
 700 TCCGCTTCTTCCTGCGGGCGGACGCCCCGGACACAACGGGCCCCGCTGTTCACGCAGGGG
 640 CGCCCCGGCGGGGCGGGCAAAGACCCGGGGACGCGGTCCCGTCCCGAGACGCTCAGCTCC
 580 GGCCCACCGCTCGCAGCTCCCGCCCCGGGCGCAGGTCCCGACCCCACGGGCCGTCTCGGA
 520 GCCGCAGCGGCCGCTTCCCTGCACGTCCTCACGCCCCCCGCACGGACGCCGCCAGCCCCG
 460 CGCCTCAGTTTCCCCACTAGCAGGATGGAAAGACGGGCCCCGCCCCGAAGCGTAGCGGCG
 400 TCTCCGTGGTAGCCAGTGCCCAGAGAGTCCGCCGGTCCCACCGCCCCTTCAAAGGAGAAC
 340 CCGGCCCACCGCCCGCCGCGGCGGCGACCGCGCAGCCCACTCGTCACGCGGCCCGCGGCG
 280 TCCAGCCCGGGCCGGCTCACCTCAGGCGGTCGCTGCCGCCCTCGCGCCTGCGCGCCCCTC
 220 GCCCCGCCCCTCTCCCCGCCCGCGTCCCGCGCACCGCAGGCCTCTGCCCCTCGCCCACCG
 160 CAGGACCCGCCCCGCGCACGCGCCGCACGTGCCACACGCACCCCACGCCCCTGCGCACGC
 100 GCAGGCCCCAAGTCGCGGCCAATGGGCGACGCGGCCGCAGATCCGCCCGGCCCCGCCCTG
  40 CCCTGTGAGTTCCTCCGGCCGGGCTGCGGGGCTCCGCTCA
```

Figure 28. Binding sequences of FOXO3 and HIF-1α to Human BNIP3 promoter. Consensus sequences of FOXO3 (GGAAAGA) and HIF-1α (CGTG) on Human *BNIP3* gene promoter (1000 bp from transcription starting sequence) are described.

2.12. Immunocytochemistry

The detailed protocol for immunocytochemistry is described in Materials & Methods section of CHAPTER I.

2.13. Trypan blue exclusion cell viability assay

The detailed protocol for trypan blue exclusion cell viability assay is described in Materials & Methods section of CHAPTER I.

2.14. AnnexinV / PI apoptosis detection

To evaluate apoptosis of UCB-hMSCs, annexinV-FITC and PI-double staining analysis was performed by using an annexinV-FITC apoptosis detection kit (BD Bioscience, Franklin Lakes, NJ, USA) according to the supplier's instructions. After treatment, UCB-hMSCs were collected and counted by using a Petroff-Hausser cell counting chamber. Cells (1×10^5) were suspended in binding buffer supplied by a commercial kit. AnnexinV-FITC (5 μL) and PI (5 μL) were added to the cell suspension solution, which was then incubated for 15 min at room temperature. UCB-hMSC apoptosis was measured by using flow cytometry (Beckman Coulter, Fullerton, CA, USA). Cells (3×10^3) that had similar side scatter and forward scatter levels were measured by using flowing software (developed

by Perttu Terho, Turku, Finland). AnnexinV-negative and PI-negative (Q3) cells were considered viable. AnnexinV-negative and PI-positive (Q1), annexinV-positive and PI-positive (Q2), and annexinV-positive and PI-negative (Q4) were considered as late apoptotic or necrotic, apoptotic, and early apoptotic cells, respectively. To determine the percentage of total apoptotic cells, the following formula was used: Apoptotic cells=Q1+Q2+Q4.

2.15. Measurement of intracellular ROS production

UCB-hMSCs were detached and then counted by using a Petroff-Hausser counting chamber. Cells (1×10^6) were incubated in PBS solution containing 10 μM of CM-H_2DCFDA (Thermo Fisher) at 37° C and 5% CO_2 for 30 min. Cells were washed with PBS twice, then loaded into a 96-well plate. Fluorescence intensity of intracellular ROS was assessed by using a luminometer (Victor3; Perkin-Elmer, Waltham, MA, USA) at excitation and emission wavelengths of 485 and 535nm, respectively.

2.16. Measurement of mitochondrial ROS production

To measure the mitochondrial ROS production and mitochondrial membrane potential, a MitoSOX™ (Life Technologies) staining kit

was used. After treatment, UCB-hMSCs were incubated in 5 μM of MitoSOX™ for 10min in a conventional cell incubator kept at 37° C and with 5% CO_2. Cells were washed with PBS twice and detached with 0.05% trypsin solution. Collected cells were washed and analyzed by using a flow cytometer (Beckman Coulter). Cells (3×10^3) that had similar side scatter and forward scatter levels were measured by using Flowing Software (developed by Perttu Terho, Turku, Finland).

2.17. Measurement of mitochondrial volume and mitochondrial membrane potential

To measure the mitochondrial volume and membrane potential, a Mitotracker™ (Life Technologies) staining kit and tetramethylrhodamine ethyl ester (TMRE; Sigma-Aldrich) were used, respectively. After treatment, UCB-hMSCs were incubated in 200 nM of Mitotracker™ or 200 nM of TMRE for 15min at room temperature. Live UCB-hMSCs were washed with PBS solution twice and detached by using 0.05% trypsin solution. Subsequently, cells were washed with PBS twice. Fluorescence intensities of Mitotracker™ or TMRE were detected by using flow cytometry. Cells (5×10^3) that had similar side scatter and forward scatter levels were measured by using Flowing Software (developed by

Perttu Terho, Turku, Finland).

2.18. ibidi™ insert dish migration assay

The detailed protocol for ibidi™ insert dish migration assay is described in Materials & Methods section of CHAPTER I.

2.19. Oris™ migration assay

The detailed protocol for Oris™ migration assay is described in Materials & Methods section of CHAPTER I.

2.20. Mouse skin wound healing model

The general protocol for mouse skin wound healing model is described in CHAPITER I. Experimental groups are described as follows. *BNIP3* siRNA or NT siRNA-transfected UCB-hMSCs were pretreated with hypoxia or PA for 24 h. Experimental mice were divided into six groups: mice given vehicle (group 1, n=6); mice given NT siRNA-transfected UCB-hMSCs (group 2, n=6); mice given NT siRNA-transfected UCB-hMSCs with hypoxia pretreatment (group 3, n=6); mice given *BNIP3* siRNA transfected UCB-hMSCs with hypoxia pretreatment (group 4, n=6); mice given

BNIP3 siRNA-transfected UCB-hMSCs with hypoxia and PA pretreatment (group 5, n=6); and mice given *BNIP3* siRNA-transfected UCB-hMSCs (group 6, n=6).

2.21. Histological examination

Slide samples were fixed with 4% paraformaldehyde (Lugen Sci, Seoul, Korea) and stained with H&E for 5 min. Samples were washed with 95% and 100% ethanol three times and incubated in xylene for 5 min. All H&E stained sample images were acquired by using light microscopy. Histological evaluation and re-epithelization scoring were performed in a blind fashion. The scoring of re-epithelization during wound healing with H&E-stained tissue samples was evaluated by determining the percentage of tissue showing the qualitative features of re-epithelization according to a method described previously (Rajabi et al., 2007). The re-epithelization histological scoring was quantified according to the criteria provided in Table 6.

Table 6. Scoring of histological changes in skin wound healing.

Score	Re-epithelialization
0	Absence of ephithelial proliferation in > 70 % of the tissue
1	Poor epidermal organization in > 60 % of the tissue
2	Incomplete epidermal organization in > 40 % of the tissue
3	Moderate epithelial proliferation in > 60 % of the tissue
4	Complete epidermal remodeling in > 80 % of the tissue

2.22. Immunohistochemistry

The detailed protocol for immunohisochemistry is described in Materials & Methods section of CHAPTER I.

2.23. Statistical analysis

All data shown in the results are presented as a mean ± S.E. Statistical differences among experimental samples were analyzed by using analysis of variance. Comparisons of treatment groups with control groups were performed by using the Bonferroni−Dunn test. A p−value < 0.05 was considered statistically significant.

3. RESULTS

3.1. Effect of hypoxia on mitophagy

To determine the effect of hypoxia on mitophagy in UCB-hMSCs, the cells were incubated under hypoxia for various durations (0-48 h). First, I measured mitochondrial volume in UCB-hMSCs under hypoxia by using a mitochondria specific fluorescent dye, Mitotracker™. The fluorescence intensities of Mitotracker™ in the 24 and 48 h hypoxia-treated UCB-hMSCs decreased to 40.2% and 23.6%, respectively, of the control level (Fig. 29A). COX4 protein expression decreased in a time-dependent manner during the 24-48 h of hypoxia (Fig. 29B). Immunofluorescence results showed that 24 h of hypoxia stimulated co-localization of COX4 with LC3B (Fig. 29C). In addition, I observed that ATP production in hypoxia-treated cells decreased to 73.2% of the control level (Fig. 29D). I checked the mRNA expressions of mitophagy regulator genes, such as *PINK1*, *BNIP3*, *NIX* and *FUNDC1*, to determine the effect of hypoxia on expression of mitophagy regulators in UCB-hMSCs. As shown in the figure 1D, *PINK1*, *BNIP3*, and *NIX* mRNA expressions in UCB-hMSC significantly increased, whereas *FUNDC1* mRNA expression was reduced by hypoxia. PCR and western blotting results showed that, among the tested genes, *BNIP3* expression

was increased to the greatest extent by hypoxia (Figs. 30A and 30B).

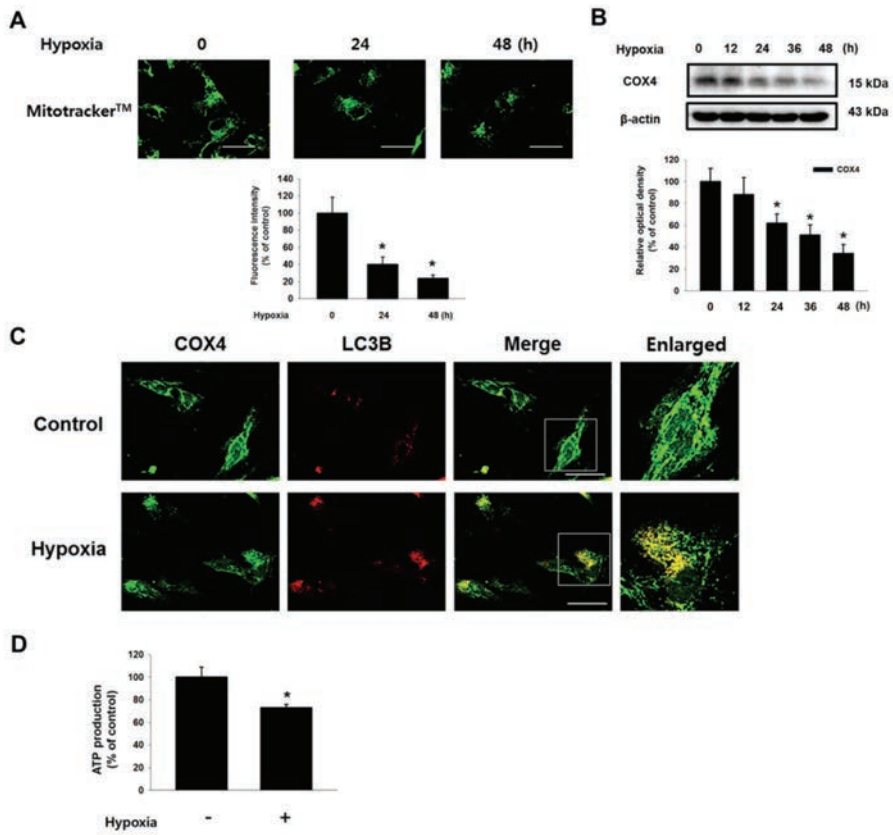

Figure 29. Effects of hypoxia on mitophagy in UCB-hMSCs. (A) UCB-hMSCs were incubated with various times of hypoxia (0-48 h). Cells were stained with Mitotracker™. $n=6$ (magnification, ×1200). Scale bars, 50 μm. (B) The expressions of COX4 and β-actin were detected by western blot. $n=4$. (C) UCB-hMSCs were exposed to 24 h of normoxia or hypoxia. Cells were immuno-stained with COX4 and LC3B-specific antibodies (magnification, ×600). Scale bars, 37.5 μm. Cellular ATP level is measured. n=5. Quantitative data are presented as a mean ± S.E. * indicates $p < 0.05$ vs. control, # indicates $p < 0.05$ vs. hypoxia.

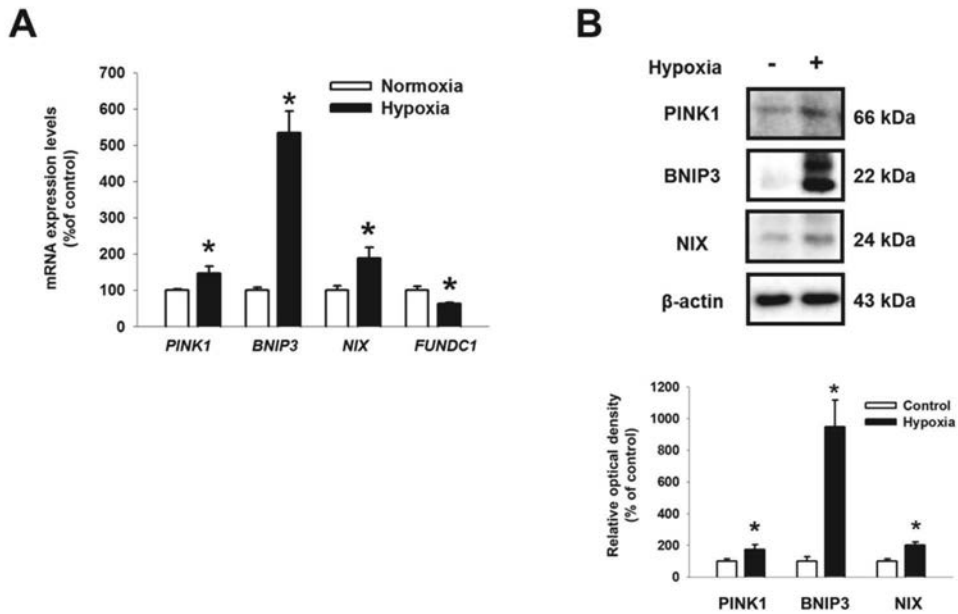

Figure 30. Effects of hypoxia on mitophagy regulators in UCB-hMSCs. (A) The mRNA expressions of *PINK1*, *BNIP3*, *NIX* and *FUNDC1* were analyzed by quantitative real-time PCR (qPCR). $n=5$. (B) The protein expressions of PINK1, BNIP3, NIX and β-actin were assessed by western blot. $n=4$. Quantitative data are presented as a mean ± S.E. Western blot data were normalized by β-actin, and qPCR data were normalized by β-*actin* mRNA expression level. All images are representative. * indicates $p < 0.05$ vs. control, # indicates $p < 0.05$ vs. hypoxia.

3.2. Role of BNIP3 in hypoxia-induced mitophagy

I transfected *PINK1*, *BNIP3*, *NIX,* and NT siRNAs, and assessed COX4 expression in UCB-hMSCs to confirm the effect of mitophagy regulators induced by hypoxia on mitophagy in UCB-hMSCs under hypoxia. The western blot and immunofluorescence staining results showed the decrease in COX4 expression by hypoxia was significantly recovered by *BNIP3* siRNA transfection (Figs. 31A and 31B). The fluorescent intensity of Mitotracker™ in the *BNIP3* siRNA-transfected UCB-hMSCs under hypoxia was higher than that in NT siRNA-transfected UCB-hMSCs under hypoxia (Fig. 31C). In addition, hypoxia increased BNIP3 expression in the mitochondrial fraction and co-localization of BNIP3 with LC3B (Figs. 32A and 32B). Collectively, my results suggest that BNIP3 upregulation by hypoxia mainly induces mitophagy via LC3B in UCB-hMSCs.

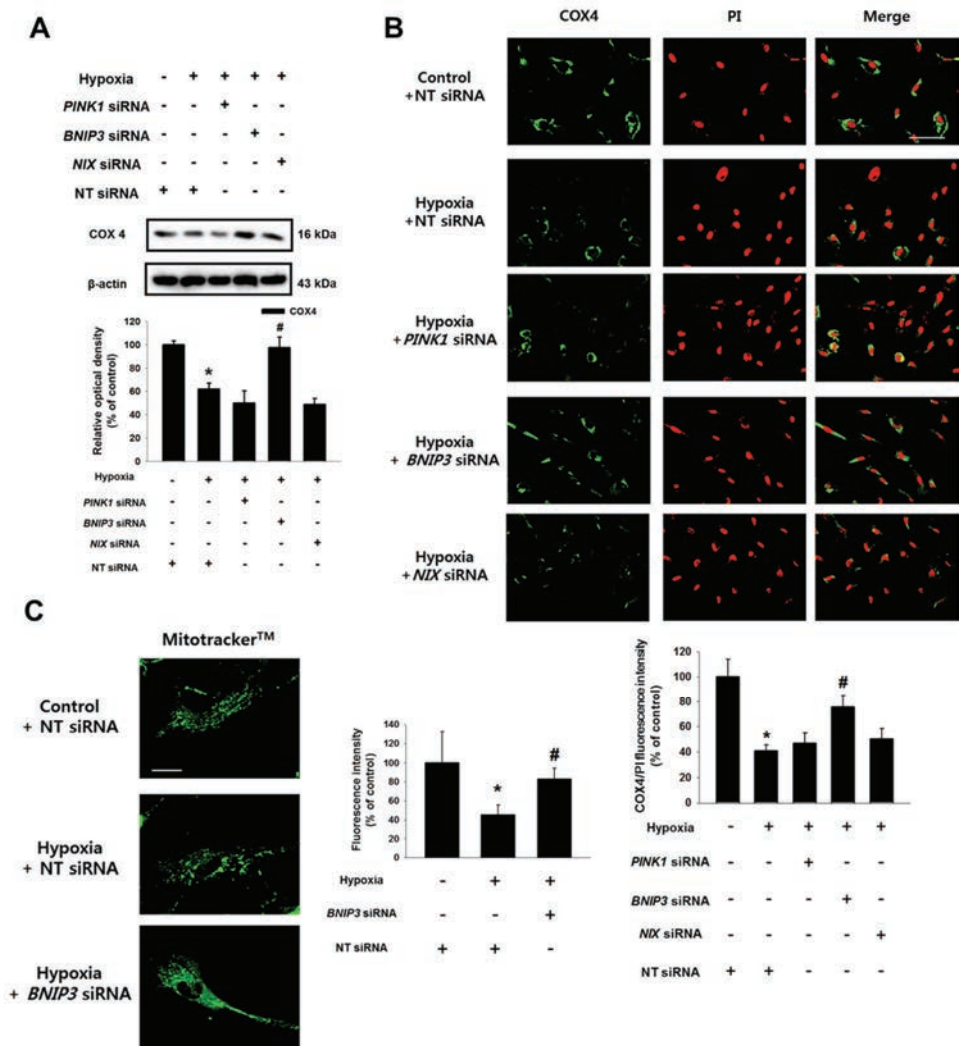

Figure 31. Role of BNIP3 in hypoxia-induced mitophagy of UCB-hMSCs. (A, B) *PINK1*, *BNIP3*, *NIX* or non-targeting (NT) siRNAs were transfected to UCB-hMSCs prior to hypoxia. COX4 and β-actin expressions were assessed by western blot. *n=4* (A). Cells were immunostained with COX4 and PI. *n=3* (magnification, ×400). All scale bars, 50 μm. COX4 fluorescence intensity was analyzed by luminometer. *n=5* (B). (C) *BNIP3* siRNA was transfected to

UCB-hMSCs prior to hypoxia treatment for 24 h. Cells were stained with Mitotracker™. $n=6$ (magnification, ×1200). Scale bars, 50 μm. Data are presented as a mean ± S.E. * indicates $p < 0.05$ vs. control, # indicates $p < 0.05$ vs. hypoxia.

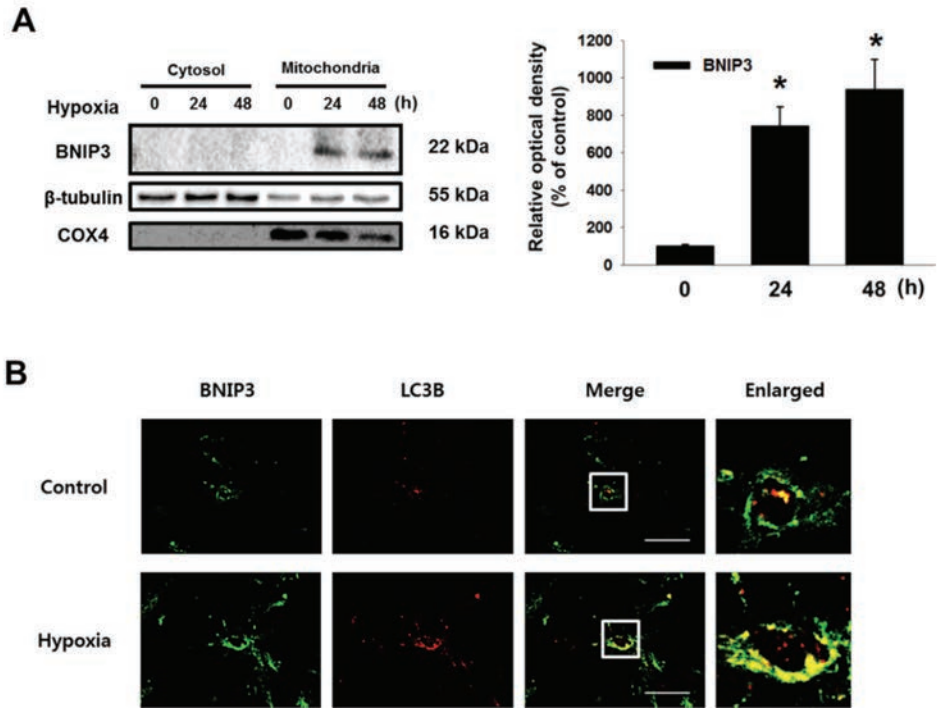

Figure 32. Effect of hypoxia on BNIP3-mediated mitophagy. (A) BNIP3, β-tubulin and COX4 with cytosol and mitochondrial fractionized sample were detected by western blot. BNIP3 was normalized by COX4 expression. n=3. (B) Cells were incubated with hypoxia or normoxia for 24 h. Cells were immune-stained with BNIP3 and LC3B specific antibodies. (magnification, ×600). Scale bars, 37.5 μm. Quantitative data are presented as a mean ± S.E. All blot and confocal images are representative. * indicates $p < 0.05$ vs. control.

3.3 Role of BNIP3 in the regulation of ROS accumulation in UCB-hMSCs under hypoxia

Furthermore, I investigated the role of mitophagy regulators induced by hypoxia in ROS production and functions determining therapeutic efficiency of UCB-hMSC transplantation, such as apoptosis, and migration. As shown in figure 33A, the intracellular ROS levels in hypoxia-treated UCB-hMSCs, measured by using a general oxidative stress indicator, 2', 7'-dichlorodihydrofluorescein diacetate (CM-H_2DCF-DA), increased to 225.5% of the control level, and that of *BNIP3* siRNA-transfected UCB-hMSCs under hypoxia increased further to 380.5% of the control level. Moreover, I performed flow cytometry analysis with MitoSOX™, a mitochondrial ROS-sensitive dye, to determine the role of BNIP3 in mitochondrial ROS production. The number of MitoSOX™-positive cells in *BNIP3* siRNA-transfected UCB-hMSCs under hypoxia was higher than that in hypoxia-pretreated UCB-hMSCs (Fig. 33B). I also assessed the effect of mitophagy regulated by BNIP3 under hypoxia on the uptake of the mitochondrial membrane potential-sensitive fluorescent dye, TMRE. The flow cytometry results with Mitotracker™ and TMRE showed that the decrease in Mitotracker™-positive cells and the increase in TMRE-positive cells by hypoxia were reversed by silencing of BNIP3 expression (Figs. 34A and 34B). A chemical inhibitor of oxidative

phosphorylation, carbonyl cyanide m-chlorophenyl hydrazine (CCCP) was used as a negative control for mitochondrial membrane potential collapse.

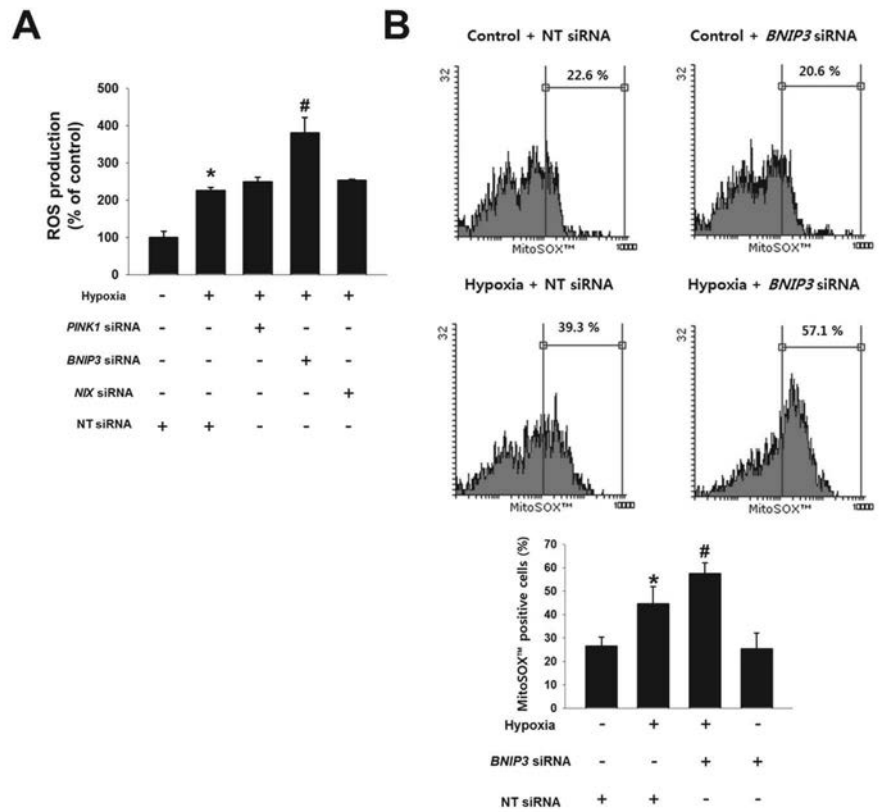

Figure 33. Role of hypoxia-induced BNIP3 in the mitochondrial ROS accumulation. (A) *PINK1*, *BNIP3*, *NIX* or NT siRNAs were transfected to UCB-hMSCs prior to hypoxia treatment for 48 h. Intracellular ROS level was measured by using CM-H_2DCF-DA staining. $n=6$. (B) *BNIP3* and NT siRNAs were transfected to UCB-hMSCs prior to hypoxia treatment for 48 h. MitoSOX™ (were analyzed by flowcytometer. $n=4$. Data are presented as a mean ± S.E. * indicates $p < 0.05$ vs. control or normoxia, # indicates $p < 0.05$ vs. hypoxia.

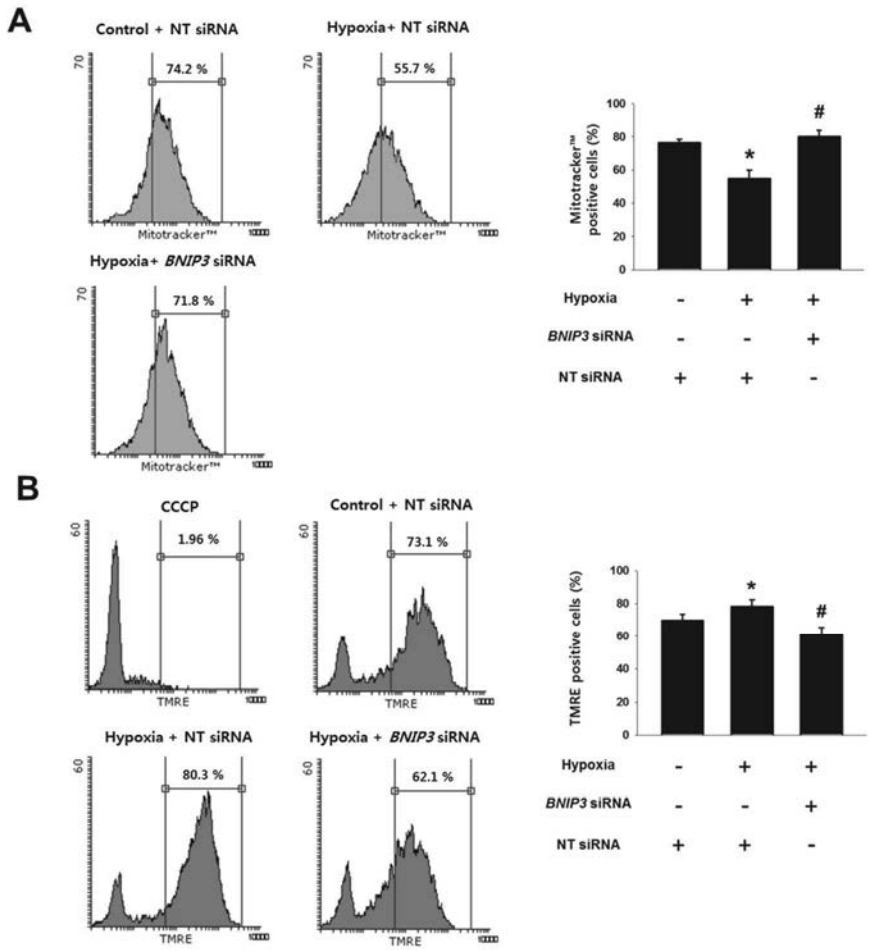

Figure 34. Role of hypoxia-induced BNIP3 in the mitophagy and mitochondrial membrane potential. (A) *PINK1*, *BNIP3*, *NIX* or NT siRNAs were transfected to UCB-hMSCs prior to hypoxia treatment for 48 h. or Mitotracker™ (A) or TMRE-positive cells (B) were analyzed by flowcytometer. $n=4$. Cells were pretreated CCCP (50 uM) for 2 h (B). Data are presented as a mean ± S.E. * indicates $p < 0.05$ vs. control or normoxia, # indicates $p < 0.05$ vs. hypoxia.

3.4 Role of BNIP3 in the apoptosis and migrationn in UCB-hMSCs under hypoxia

In addition, I investigated the effect of mitophagy regulators induced by hypoxia on apoptosis and migration in UCB-hMSCs. The cell viability results, measured by trypan blue exclusion assay, showed the viability of UCB-hMSCs at 72 h of hypoxia was lower than that of UCB-hMSCs at 72 h of normoxia, and the viabilities of *BNIP3* siRNA-transfected UCB-hMSCs at 48 and 72 h of hypoxia were significantly lower than those of UCB-hMSCs at 48 and 72 h of hypoxia (Fig. 35A). And, I performed AnnexinV and PI double staining flow cytometry analysis with 48 h of normoxia or hypoxia-treated UCB-hMSCs. I showed the number of annexinV-positive apoptotic cells of BNIP3-silenced UCB-hMSCs under hypoxia to be higher than that of UCB-hMSCs under hypoxia (Fig. 35B). To determine the effect of mitophagy regulators induced by hypoxia on UCB-hMSC migration regulated by hypoxia pretreatment, I performed ibidi™ insert dish and Oris™ migration assays. As shown in figures 36A and 36B, hypoxia pretreatment increased UCB-hMSC migration that had been abolished by *BNIP3* siRNA transfection. These findings suggest that mitophagy induced by BNIP3 is critical for reducing the mitochondrial ROS (mtROS) production, mitochondrial membrane potential, and enhancing anti-apoptosis and migration in UCB-hMSC under hypoxia.

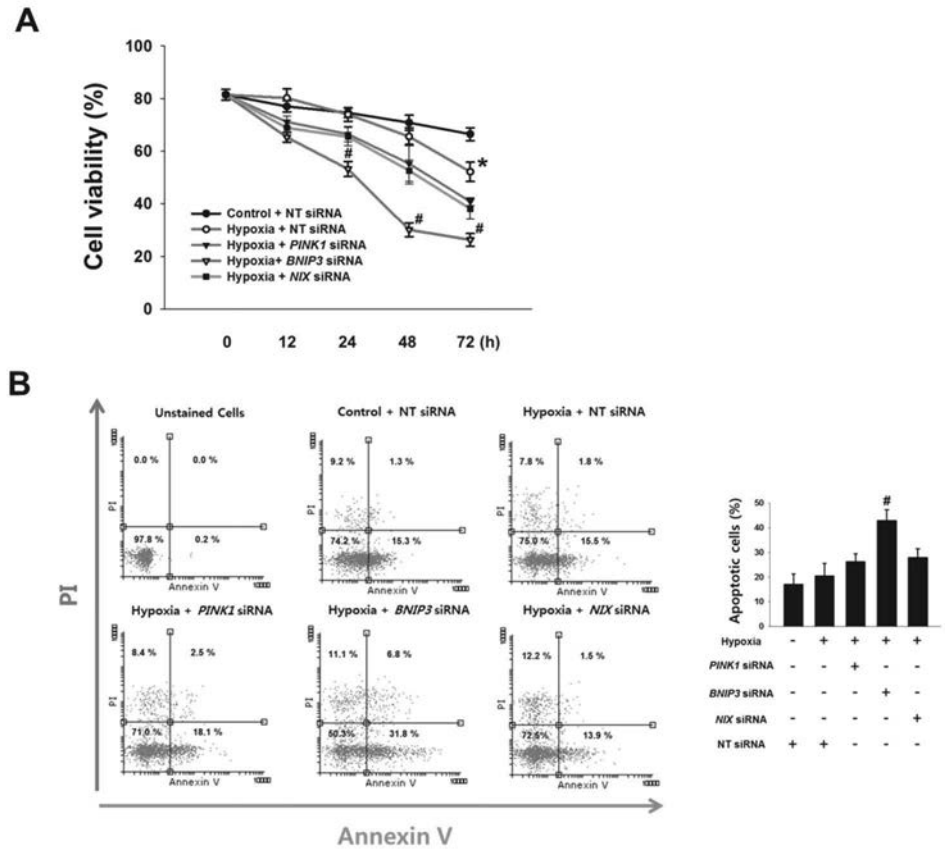

Figure 35. Role of BNIP3 in the apoptosis of UCB-hMSCs under hypoxia. (A) UCB-hMSCs transfected with *PINK1*, *BNIP3*, *NIX* or NT siRNAs were exposed to various durations of hypoxia (0-72 h). Cell viability was measured by trypan blue exclusion assay. $n=5$. (B) *PINK1*, *BNIP3*, *NIX* or NT siRNAs were transfected to UCB-hMSCs prior to hypoxia treatment for 48 h. Apoptotic cells were detected by annexinV/PI analysis. $n=4$. * indicates $p < 0.05$ vs. control, # indicates $p < 0.05$ vs. hypoxia.

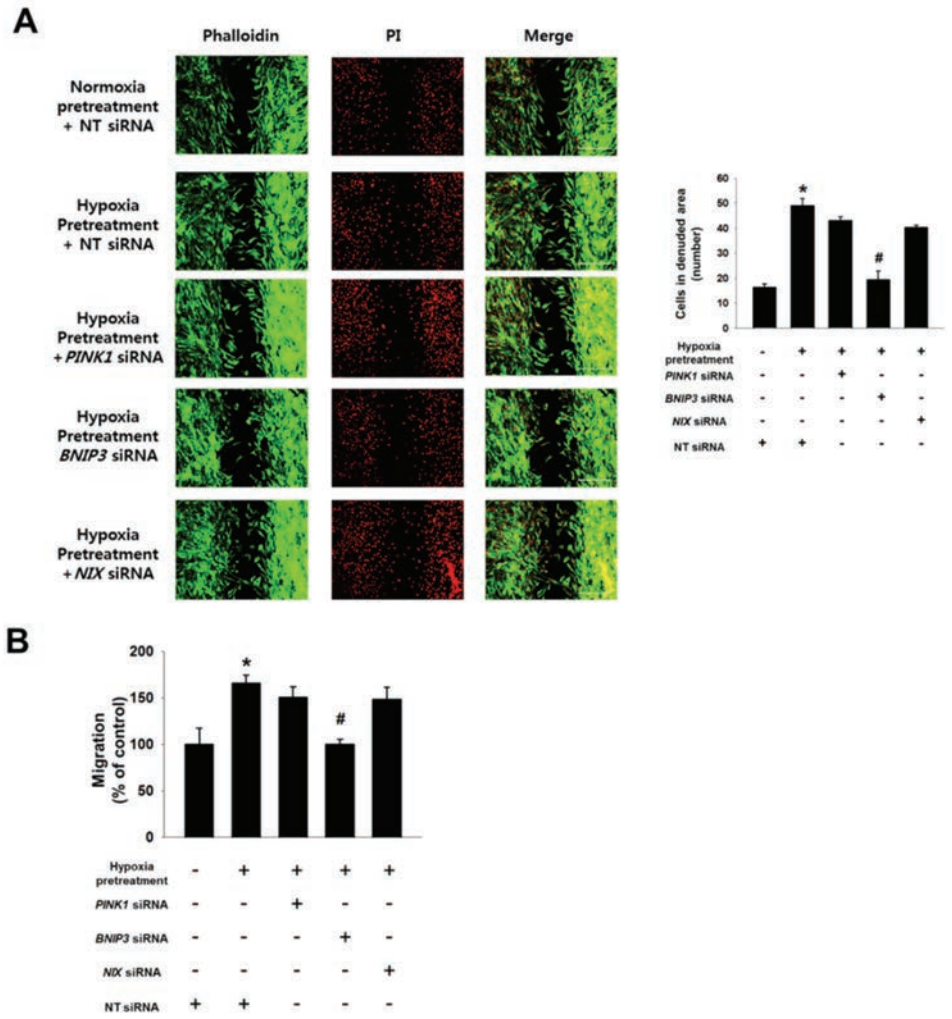

Figure 36. Role of BNIP3 in the migration of UCB-hMSCs with hypoxia pretreatment. (A) UCB-hMSCs were cultured in ibidi™ insert dish, and siRNAs were transfected to cells prior to hypoxia pretreatment for 24 h. Migrated cells under normoxia for 24 h were visualized by immunostaining with phalloidin and PI. *n=4* (magnification ×100). All scale bars, 200 μm. (B) UCB-hMSC migration was measured by Oris™ migration assay. *n=8.* Data are

presented as a mean ± S.E. * indicates $p < 0.05$ vs. normoxia pretreatment, # indicates $p < 0.05$ vs. hypoxia pretreatment.

3.5. Involvement of HIF-1α, FOXO3 in BNIP3 expression

HIF-1α and FOXO3 have been well recognized as major transcription factors controlling UCB-hMSC physiology under hypoxia (Liu et al., 2011; Zhang et al., 2013). Although previous investigations have reported that HIF-1α or FOXO3 are involved in BNIP3 expression under hypoxia (Choi et al., 2016; Feng et al., 2016), their roles in BNIP3 expression seem to vary with cell type (Bakker et al., 2007; Chourasia et al., 2015; Mammucari et al., 2007). To demonstrate the detailed mechanism regulating BNIP3 expression in UCB-hMSCs under hypoxia, I investigated the roles of HIF-1α and FOXO3 in BNIP3 regulation. Then, I confirmed that hypoxia stimulated HIF-1α expression in a time-dependent manner (Fig. 37A). To investigate the role of hypoxia-induced ROS in expressions and activations of HIF-1α and FOXO3, I pretreated a general ROS scavenger, N-acetyl cysteine (NAC) to block the ROS production in UCB-hMSCs under hypoxia. Western blot with nuclear fraction and immunofluorescence results showed ROS produced by hypoxia increased HIF-1α localization in the nucleus (Fig. 37B and 37C). As shown in figures 38A and 38B, mRNA and protein expressions of BNIP3 were increased by hypoxia but abolished by *HIF-1A* siRNA transfection. In addition, I further determined the role of FOXO3 in BNIP3 expression in UCB-hMSCs under hypoxia. Western blot with nuclear fraction results showed

ROS production under hypoxia stimulated FOXO3 localization in the nucleus (Fig. 39A). In addition, enhanced BNIP3 expression by hypoxia was partially abolished by silencing of FOXO3 expression (Figs. 39B and 39C). These results suggest that HIF-1α and FOXO3 induced by ROS production are major factors regulating BNIP3 expression under hypoxia.

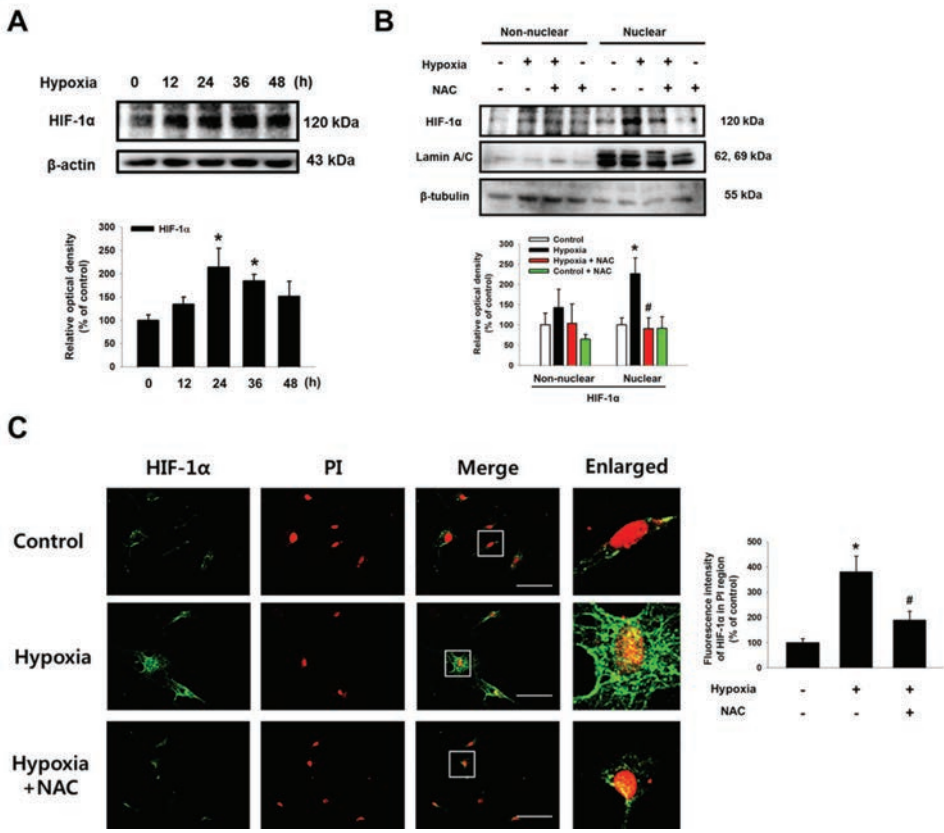

Figure 37. Effect of hypoxia on HIF−1α expression and nuclear translocation. (A) UCB−hMSCs were incubated with various durations of hypoxia (0–48 h). The protein expressions of HIF−1α and β−actin were detected by western blot. *n=4.* (B) UCB−hMSCs were pretreated with NAC (5 mM) for 30 min prior to hypoxia incubation for 24 h. The protein expressions of HIF−1α, lamin A/C and β−tubulin in non−nuclear and nuclear fractionized cell samples were assessed by using western blot. *n=3.* (C) UCB−hMSCs were immune−stained with HIF−1α and PI (magnification×600). Scale bars, 37.5μm.

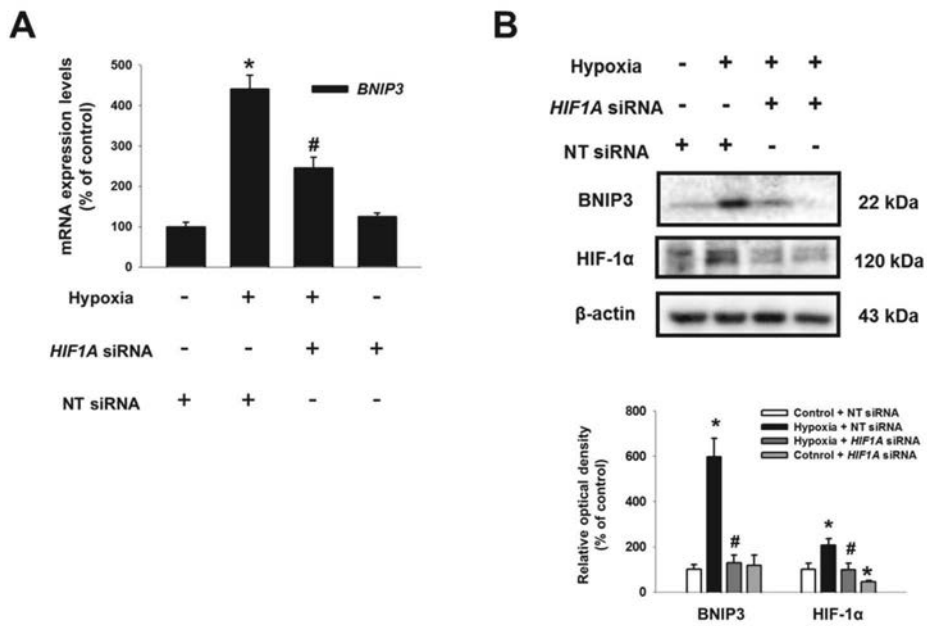

Figure 38. Role of HIF−1α in hypoxia−induced BNIP3 expression. (A) *HIF1A* or NT siRNAs were transfected to cells prior to hypoxia treatment for 24 h. The mRNA expression of *BNIP3* was analyzed by qPCR. *n=6.* (B) The protein expressions of BNIP3 and HIF−1α were detected by western blot. *n=4.* . Quantitative data are presented as a mean ± S.E. All blot and confocal images are representative. * indicates $p < 0.05$ vs. control, # indicates $p < 0.05$ vs. hypoxia.

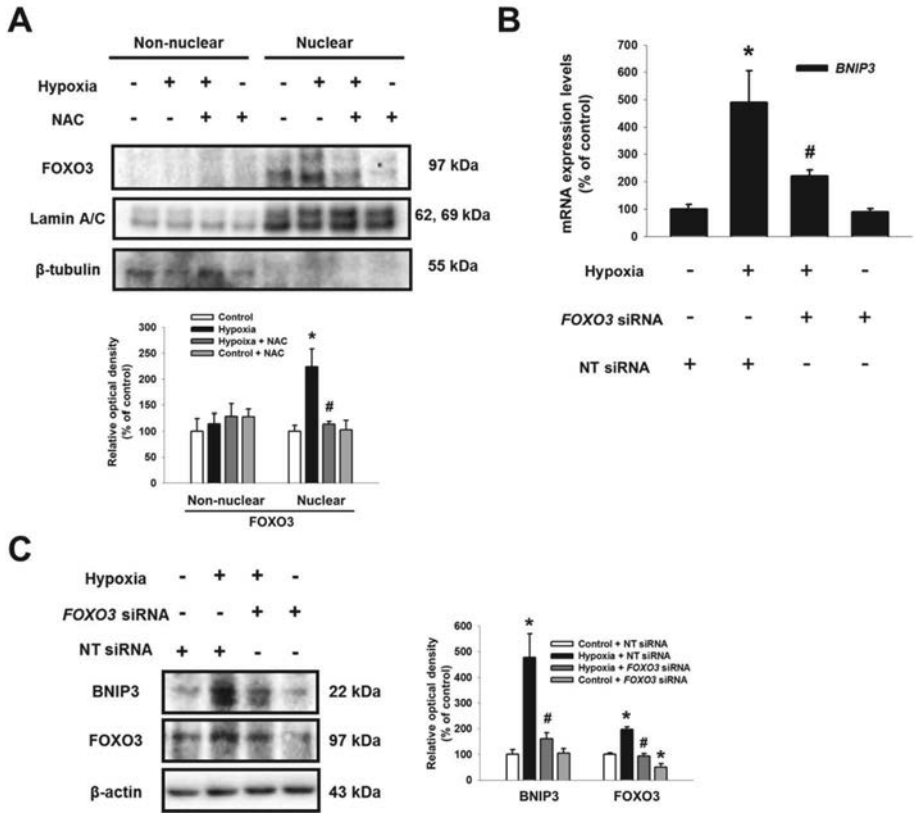

Figure 39. Role of FOXO3 in hypoxia-induced BNIP3 expression.

(A) NAC (5 mM) pretreated to UCB-hMSCs prior to hypoxia treatment for 24 h. FOXO3, lamin A/C and β-tubulin proteins expressions were assessed by western blot. *n=3.* (B) *FOXO3* siRNA transfected to UCB-hMSCs prior to hypoxia treatment for 24 h. The *FOXO3* mRNA expression was measured by qPCR. qPCR data were normalized by *β-actin* mRNA expression level. *n=6.* (C) BNIP3, FOXO3 and β-actin expressions were detected by western blot. n=3. Data are presented as a mean ± S.E. * indicates $p < 0.05$ vs. control, # indicates $p < 0.05$ vs. hypoxia.

3.6. Involvement of CBP in the bindings of HIF−1α and FOXO3 to the *BNIP3* promoter

Subsequently, I observed that hypoxia stimulates the interaction of CREB−binding protein (CBP) with HIF−1α and FOXO3 (Fig. 40A). To determine the role of CBP in BNIP3 expression under hypoxia, I pretreated C646, a CBP/p300 inhibitor, to UCB−hMSCs prior to hypoxia treatment. As shown in figures 40B and 40C, mRNA and protein expressions of *BNIP3* increased by hypoxia were reversed by C646 pretreatment. Moreover, I investigated the role of CBP in the interaction of HIF−1α and FOXO3 with the *BNIP3* promoter. CHIP assay results showed CBP inactivation by C646 pretreatment interrupted the binding of HIF−1α and FOXO3 to their consensus sequences in the *BNIP3* promoter (Figs. 41A and 41B). Overall, my results indicate that the interaction of CBP with HIF−1α and FOXO3 stimulated by hypoxia has a critical role in the binding of HIF−1α and FOXO3 to the *BNIP3* gene promoter, leading to transcriptional regulation of BNIP3 expression in UCB−hMSCs.

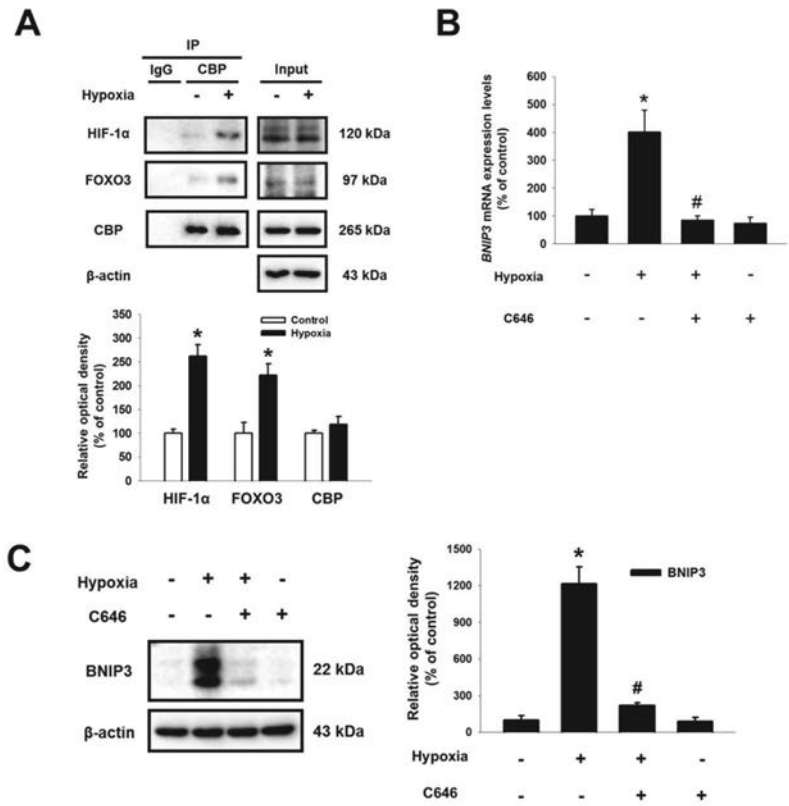

Figure 40. Involvement of CBP in BNIP3 expression regulated by HIF-1α and FOXO3 under hypoxia. (A) UCB-hMSCs were incubated with hypoxia for 24 h. Co-immunoprecipitation of HIF-1α and FOXO3 with IgG and CBP were shown. *n=3.* (B) CBP (20 μM) was pretreated to UCB-hMSCs, and cells were incubated with hypoxia for 24 h. The *BNIP3* mRNA expression level was analyzed by qPCR. *n=6.* (C) BNIP3 and β-actin protein expressions were analyzed by western blot. Data are represented as a mean ± S.E. *n=4.* * indicates $p < 0.05$ vs. control, # indicates $p < 0.05$ vs. hypoxia.

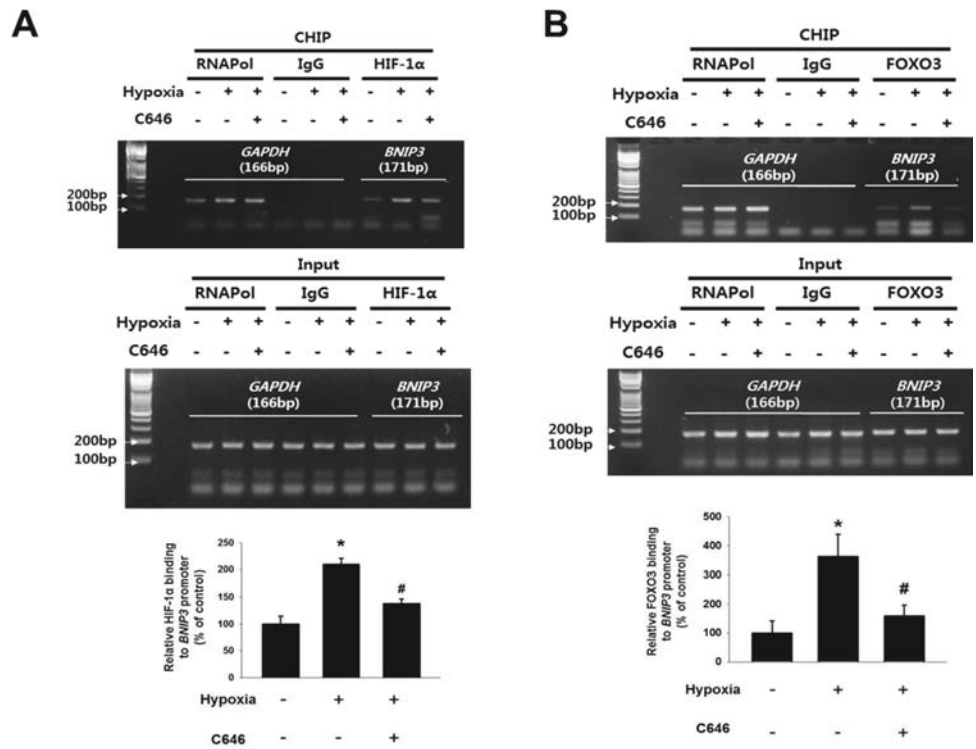

Figure 41. Role of CBP in the bindings of HIF−1α and FOXO3 to *BNIP3* gene promoter. (A, B) Sample DNA was immune−precipitated with RNA polymerase, IgG, HIF−1α and FOXO3 specific antibodies. CHIP (top panel) and lysate (bottom panel) samples were amplified with the primers of *GAPDH* and *BNIP3* promoters. Quantitative CHIP data was analyzed by qPCR, and shown in the right panel. $n=4$. Western blot data were normalized by β−actin, and qPCR data were normalized by β−*actin* mRNA expression level. Quantitative data are presented as a mean ± S.E. * indicates $p < 0.05$ vs. control, # indicates $p < 0.05$ vs. hypoxia.

3.6. Effect of BNIP3-induced FASN on hypoxia-induced survival and migration in UCB-hMSCs

To confirm the role of BNIP3 expression induced by hypoxia in lipid metabolism, I examined mRNA expressions of lipid metabolic enzymes including *FASN*, *SCD1*, *SCD5*, *GPAT1*, *GPAT3*, *GPAT4*, *MAGL*, diglyceride acyltransferase 1 (*DGAT1*), and *CPT1A* in UCB-hMSCs under hypoxia. As shown in figure 42A, I observed an increase in FFA-producing enzymes including *FASN* and *SCD1*. Particularly, mRNA expression of *FASN* in UCB-hMSCs under hypoxia increased to 225.3% of the control level. I further confirmed that hypoxia stimulated production of cellular FFA in UCB-hMSCs after 24 and 48 h (Fig. 42B). In addition, upregulated cellular FFA production and mRNA expressions of *FASN* and *SCD1* by hypoxia were reversed by silencing BNIP3 expression (Figs. 42C and 42D). In addition, AnnexinV and PI double staining flow cytometry results showed that FASN inhibition by cerulenin (a FASN inhibitor) but not by CAY10566 (a SCD1 inhibitor) increased apoptosis of UCB-hMSC exposed to hypoxia (Fig. 43). There was no significant difference between groups treated with normoxia or hypoxia. The results of ibidi™ insert dish and Oris™ migration assays showed that hypoxia pretreatment stimulated UCB-hMSC migration, abolished by pretreatment of cerulenin, but not by CAY10566 (Figs. 44A and 44B). These results suggest that

FASN-dependent FFA production is important for the regulation of apoptosis and migration in UCB-hMSCs under hypoxia.

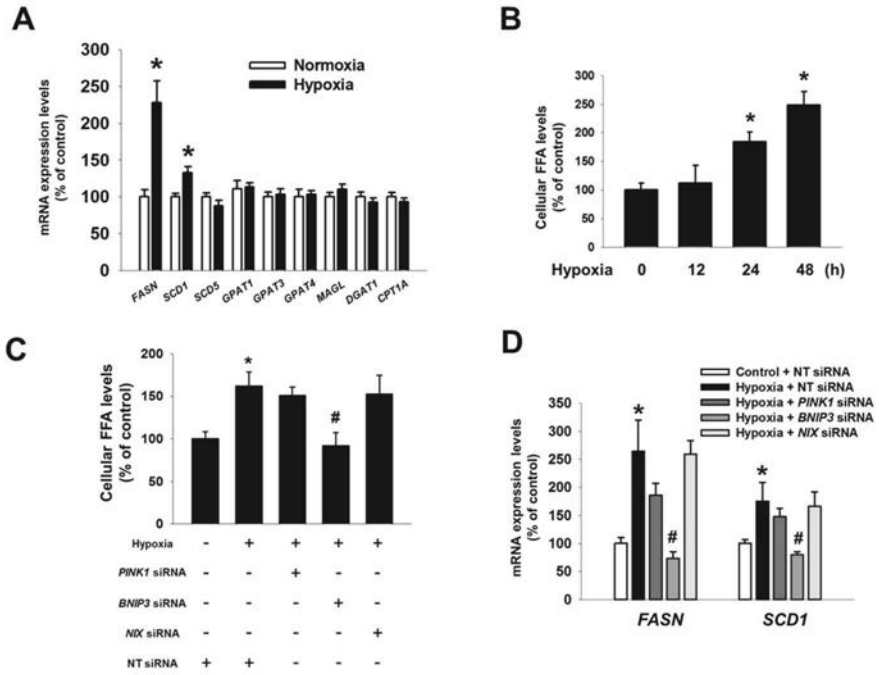

Figure 42. Role of BNIP3 on hypoxia-induced production of FFA and expressions of FASN and SCD1 in UCB-hMSCs. (A) UCB-hMSCs were incubated with hypoxia for 24 h. The mRNA expressions of *FASN*, *SCD1*, *SCD5*, *GPAT1*, *GPAT3*, *GPAT4*, *MAGL*, *DGAT1*, *CPT1A* were analyzed by qPCR. *n=5.* (B) UCB-hMSCs were treated with hypoxia (0 - 48 h). FFA level was measured with FFA detection kit. *n=6.* (C) Cells were transfected with *PINK1*, *BNIP3*, *NIX* or NT siRNAs, treated with hypoxia for 24 h. *n=6.* (D) The *FASN* and *SCD1* mRNAs expressions level were assessed by qPCR. *n=6.* Data are presented as a mean ± S.E. * indicates $p < 0.05$ vs. control, # indicates $p < 0.05$ vs. hypoxia.

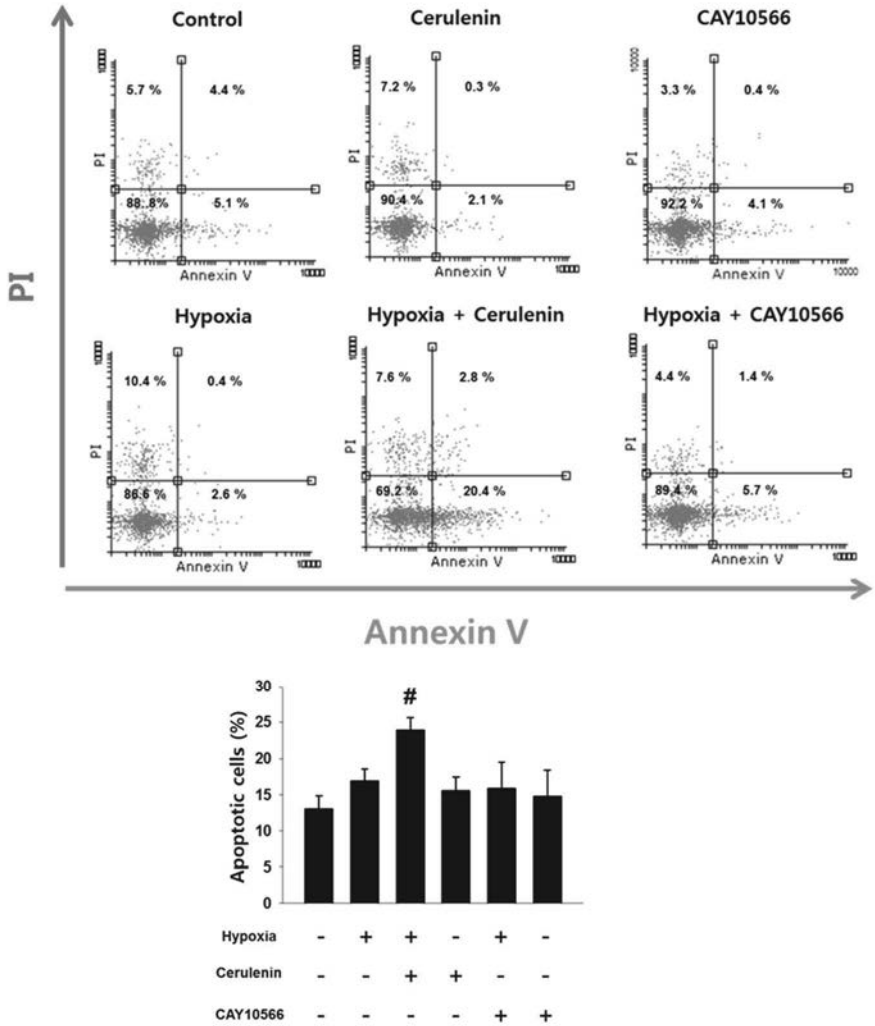

Figure 43. Role of hypoxia-induced FASN and SCD1 in UCB-hMSC survival. Cells were pretreated with cerulenin (10 μM) or CAY10566 (100 μM) for 30 min prior to hypoxia for 48 h. Apoptotic cells were detected by annexinV/PI analysis. Data are presented as a mean ± S.E. *n=4.* * indicates $p < 0.05$ vs. control, # indicates $p < 0.05$ vs. hypoxia.

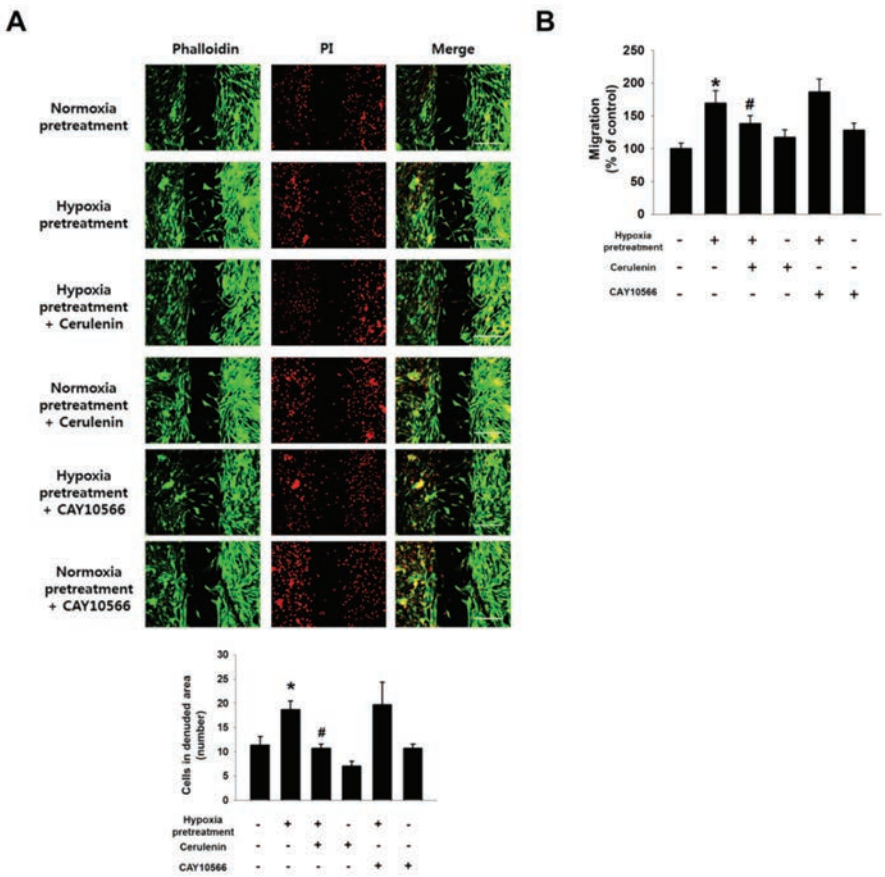

Figure 44. Role of hypoxia-induced FASN and SCD1 in UCB-hMSC migration. (A) Cells were plated in ibidi™ insert dish, and cerelenin (10 μM) or CAY10566 (100 μM) were pretreated to cells for 30 min prior to hypoxia pretreatment for 24 h. Migrated cells under normoxia for 24 h were immunostained with phalloidin and PI. $n=4$ (magnification×100). Scale bars, 200 μm. (B) Cell migration was measured by Oris™ migration assay. $n=8$. Data are presented as a mean ± S.E. * indicates $p < 0.05$ vs. normoxia pretreatment, # indicates $p < 0.05$ vs. hypoxia pretreatment.

3.7. Regulatory role of BNIP3-mediated ER stress in hypoxia-activated SREBP1

A SREBP1 has been reported as a major transcription factor regulating FASN expression in hypoxia (Lu et al., 2016). To confirm the role of SREBP1 in hypoxia-induced FASN, I pretreated fatostatin, a SREBP1 inhibitor. As shown in the figure 45, upregulation of *FASN* mRNA expression by hypoxia was abolished by pretreatment of fatostatin. Next, I checked the effect of BNIP3 silencing on expression of mature SREBP1 (68 kDa) in UCB-hMSCs under hypoxia to identify the mechanism involved in how BNIP3 induced by hypoxia regulates FASN expression. Interestingly, my data showed that mRNA expression of *SREBF1* increased by hypoxia was not affected by *BNIP3* siRNA transfection (Fig. 46A). However, the protein expressions of mature SREBP1 and FASN were inhibited by *BNIP3* siRNA transfection (Fig. 46B). In addition, silencing of BNIP3 expression also inhibited translocation of mature SREBP1 into the nucleus (Fig. 47A). There were no significant differences in HIF-1α expressions between groups treated with hypoxia or *BNIP3* siRNA (Fig. 47B). These results suggest BNIP3 silencing-regulated SREBP1 expression is transcription independent. I hypothesized excessive ROS production by BNIP3 silencing may be a regulator which leads to suppression of SREBP1/FASN pathway. To determine the effect of excessive

ROS production by BNIP silencing on ER stress, such as eukaryotic initiation factor 2 α (eIF-2α) and CCAAT-enhancer binding protein homologous protein (CHOP), expressions of mature SREBP1 and FASN, therefore, I pretreated low dose of NAC to BNIP3-silenced UCB-hMSCs prior to hypoxia treatment; the results confirmed that excessive ROS production induced by *BNIP3* siRNA transfection was decreased by low dose NAC pretreatment (Fig. 48A). As shown in the figure 48B, downregulated protein expressions of mature SREBP1 and FASN were recovered by NAC pretreatment. In addition, BNIP3 silencing further increased CHOP expression and eIF-2α phosphorylation, and decreased mTOR, S6K1, and S6 phosphorylations in UCB-hMSC under hypoxia (Figs. 49A and 49B). Low dose NAC pretreatment abolished augmentation of CHOP expression and eIF2α phosphorylation by BNIP3 silencing (Fig. 50A). I pretreated a ER stress inhibitor 4-phenylbutyrate (PBA) to *BNIP3* siRNA-transfected UCB-hMSCs under hypoxia to confirm the effect of endoplasmic reticulum (ER) stress augmentation on mature SREBP1 and FASN expression. And, I observed that suppressed expressions of mature SREBP1 and FASN were recovered by PBA pretreatment (Fig. 50B). Taken together, I suggest that the reduction of ROS by BNIP3 in hypoxia induces SREBP1 maturation and FASN expression through the suppression of ER stress and activation of mTOR/S6K1/S6 pathway.

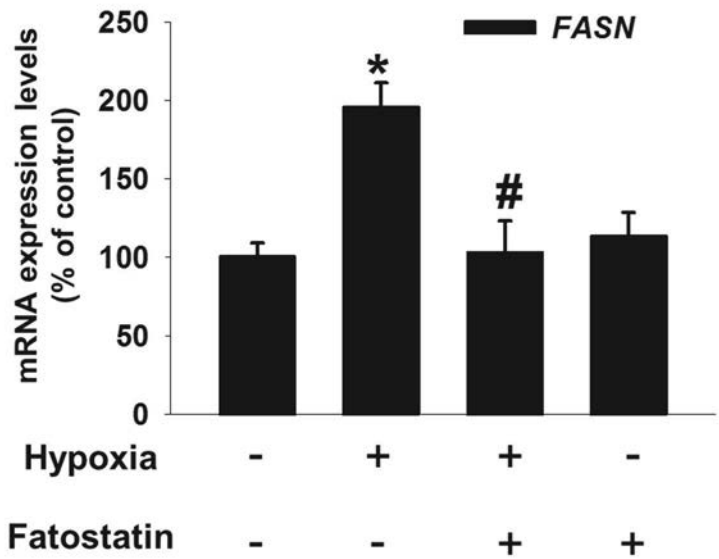

Figure 45. Role of SREBP1 in hypoxia-induced FASN expression. (A) UCB-hMSCs were pretreated with fatostatin (10 μM) for 30 min prior to hypoxia treatment for 24 h. The mRNA expression of *FASN* was analyzed by qPCR. $n=6$.

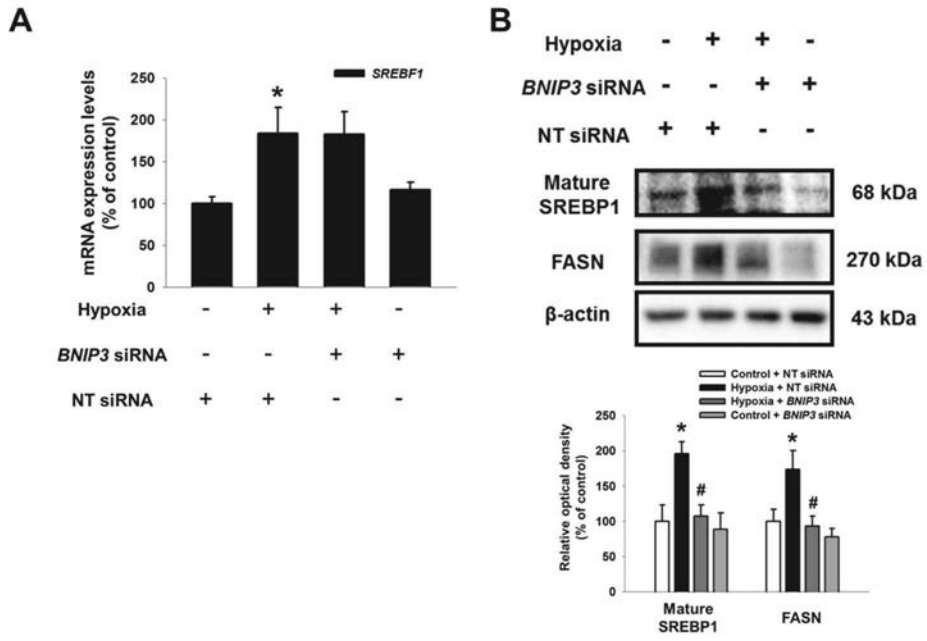

Figure 46. Effect of BNIP3 knock down on SREBP1 and FASN expressions in UCB-hMSCs under hypoxia. (A) UCB-hMSCs were transfected with *BNIP3* or NT siRNAs, incubated with hypoxia for 24 h. The mRNA expression of *SREBF1* was measured by qPCR. $n=6$. (B) The protein expressions of mature SREBP1, FASN, BNIP3 and β-actin were detected by western blot. $n=4$. Data are presented as a mean ± S.E $n=3$. * indicates $p < 0.05$ vs. control, # indicates $p < 0.05$ vs. hypoxia.

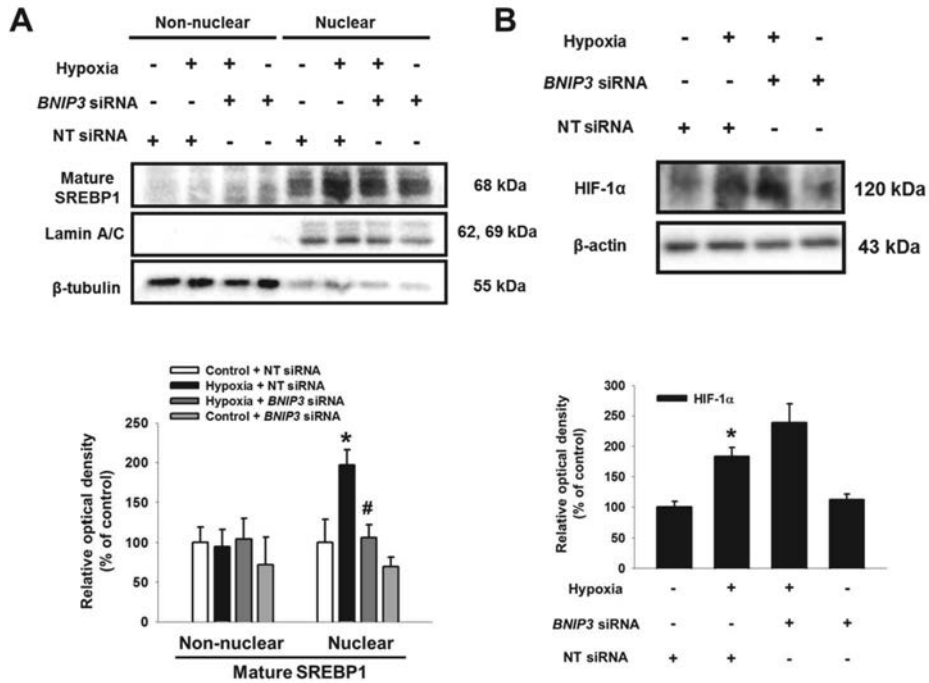

Figure 47. Effect of BNIP3 knock down on mature SREBP1 nuclear translocation and HIF-1α expressions in UCB-hMSCs under hypoxia. (A) Mature SREBP1, lamin A/C and β-tubulin expressions in non-nuclear and nuclear fractionized samples were detected by western blot. *n=3.* (B) HIF-1α and β-actin expressions were analyzed by western blot. *n=4.* Data are presented as a mean ± S.E *n*=3. * indicates $p < 0.05$ vs. control, # indicates $p < 0.05$ vs. hypoxia.

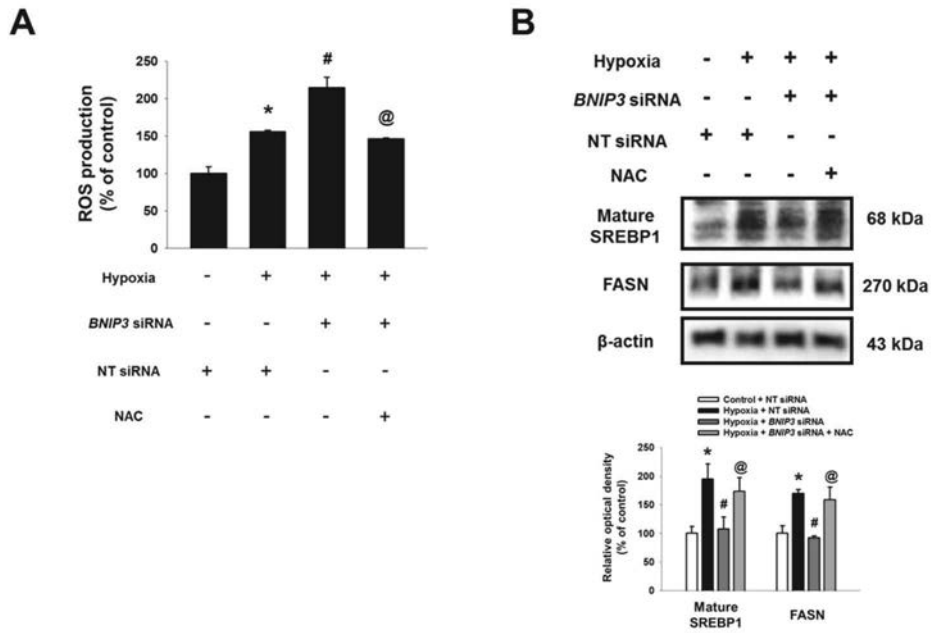

Figure 48. Effect of BNIP3 silencing on SREBP1 maturation, FASN expression. (A) UCB-hMSCs were transfected with *BNIP3* or NT siRNAs, and pretreated with NAC (500 uM) prior to hypoxia treatment for 48 h. ROS production level was measured. n=8. (B) *BNIP3* or NT siRNAs-transfected UCB-hMSCs were pretreated with NAC (500 uM) prior to hypoxia for 48 h. Mature SREBP1, FASN, BNIP3, and β-actin expressions were detected by western blot. n=3. Data are presented as a mean $\pm$ S.E. * indicates $p < 0.05$ vs. control, # indicates $p < 0.05$ vs. hypoxia, @ indicates $p < 0.05$ vs. *BNIP3* siRNA-transfected UCB-hMSCs with hypoxia.

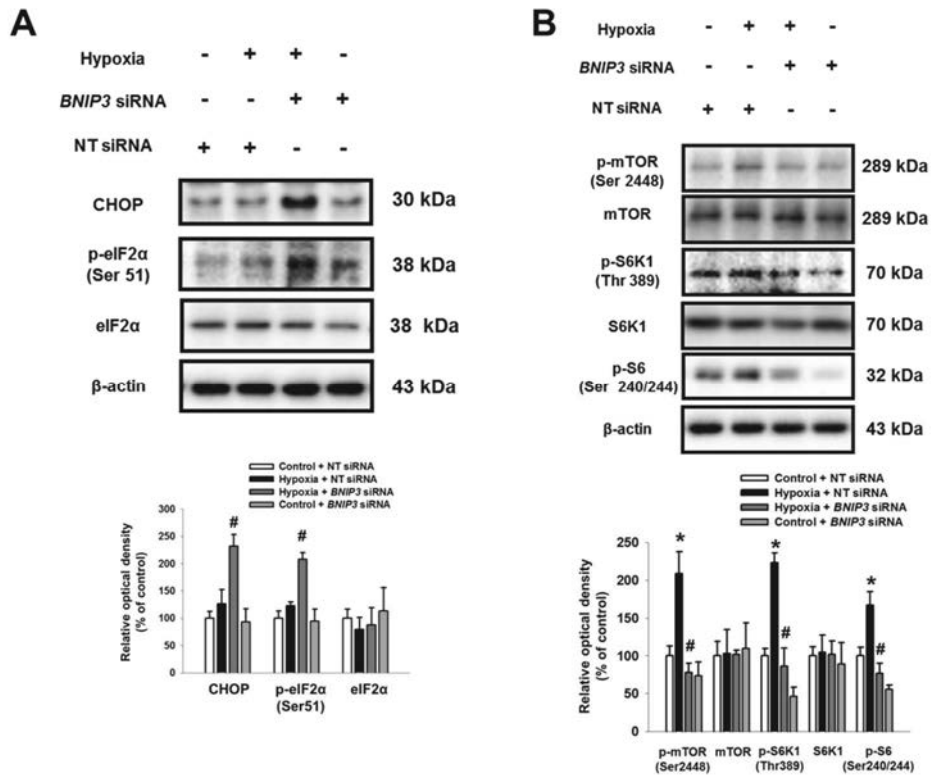

Figure 49. Effect of BNIP3 silencing on ER stress markers and mTOR signaling. (A, B) UCB-hMSCs were transfected with *BNIP3* or NT siRNAs, incubated with hypoxia for 48 h. CHOP, p-eIF2α, eIF2α, p-mTOR, mTOR, p-S6K1 (Thr389), S6K1, p-S6 and β-actin expressions were shown. $n=4$. Data are presented as a mean $\pm$ S.E. $*$ indicates $p < 0.05$ vs. control, # indicates $p < 0.05$ vs. hypoxia, @ indicates $p < 0.05$ vs. *BNIP3* siRNA-transfected UCB-hMSCs with hypoxia.

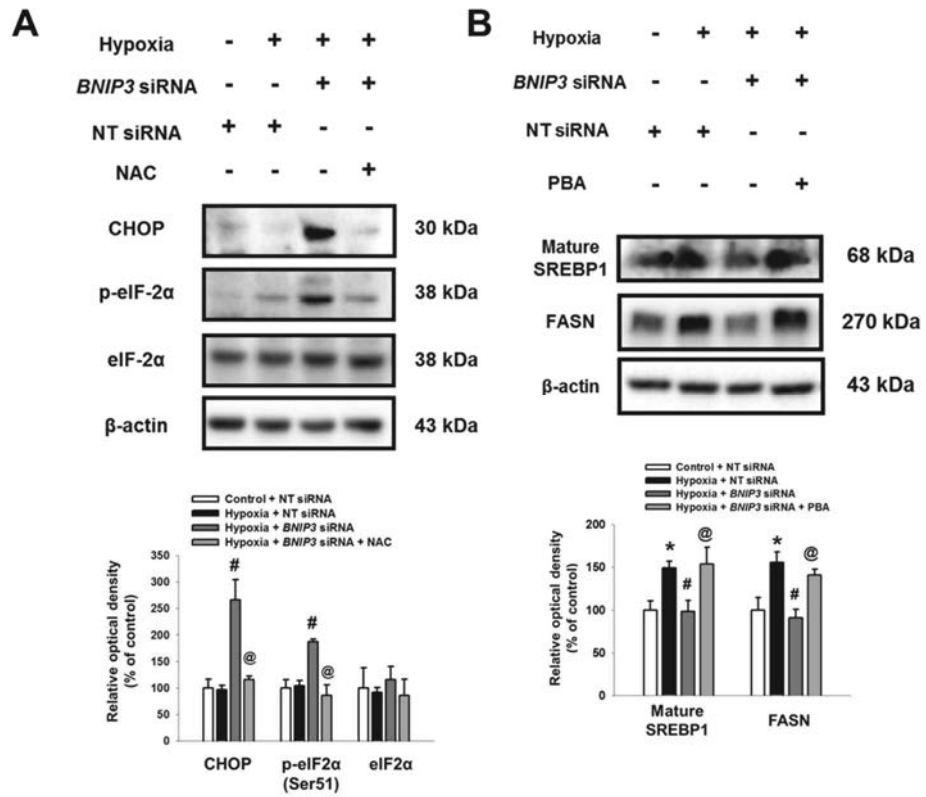

Figure 50. Regulatory role of ER stress induction by BNIP3 knock down in SREBP1 and FASN expressions. (A, B) *BNIP3* or NT siRNAs-transfected UCB-hMSCs were pretreated with NAC (500 μM) or PBA (100 μM) for 1 h prior to hypoxia treatment for 48 h. (A) The expressions of CHOP, p-eIF2α, eIF2α and β-actin were detected by western blot. $n=4$. (B) Mature SREBP1, FASN and β-actin expressions were shown. Data are presented as a mean $\pm$ S.E. * indicates $p < 0.05$ vs. control, # indicates $p < 0.05$ vs. hypoxia, @ indicates $p < 0.05$ vs. *BNIP3* siRNA-transfected UCB-hMSCs with hypoxia.

3.8. Role of BNIP3-induced PA production on survival and migration of UCB-MSCs under hypoxia

My previous study reported that PA produced by FASN is a major FFA regulating hypoxia-induced UCB-hMSC functions (Lee et al., 2015). Therefore, I investigated the effect of palmitic acid (PA), a FASN major lipid metabolite, on apoptosis and migration to confirm the role of BNIP3-induced FASN in UCB-hMSC function under hypoxia. As shown in figure 51A, protein expressions of cleaved caspase-3 and cleaved caspase-9 in UCB-hMSCs under hypoxia were increased by *BNIP3* siRNA transfection but decreased by PA pretreatment. Trypan blue exclusion cell viability assay and annexinV/PI double staining flow cytometry results showed that the decrease in cell viability and increase in the number of apoptotic cells by BNIP3-silenced UCB-hMSCs under hypoxia were reversed by PA pretreatment (Figs. 51B and 51C). Moreover, I found that BNIP3 silencing did not increase the number of apoptotic of UCB-hMSCs under normoxia (Fig. 51C). Next, I also investigated the effect of BNIP3 silencing and PA on F-actin polymerization regulatory protein. As shown in figure 52A, phosphorylation of cofilin-1 at Ser3 residue was upregulated by hypoxia pretreatment, but abolished by *BNIP3* siRNA transfection. PA pretreatment recovered the inhibitory effects of BNIP3 silencing in terms of cofilin-1 phosphorylation and F-actin expression in

UCB-hMSCs (Fig. 52A). Consistent with those results, the ibidi™ insert dish and Oris™ migration assay results showed that downregulated migration of BNIP3-silenced UCB-hMSCs by hypoxia pretreatment was partially recovered by PA pretreatment (Figs. 52B and 52C). My results indicate that exogenous PA rescues reduction of survival and migration by BNIP3 silencing in UCB-hMSCs under hypoxia.

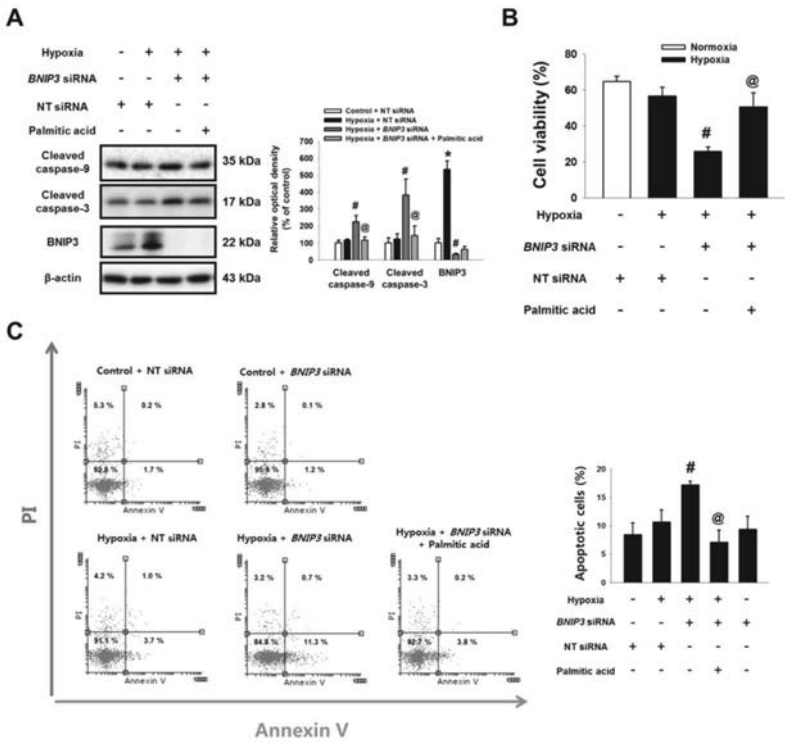

Figure 51. Anti-apoptotic effect of PA on BNIP3-silenced UCB-hMSCs. (A) The PA (20 μM) pretreated to UCB-hMSC transfected with *BNIP3* or NT siRNAs, and then cells were incubated with hypoxia for 48 h. The expressions of cleaved caspase-9, cleaved caspase-3, BNIP3 and β-actin were analyzed by western blot. *n=4.* (B) Cell viability was measured by trypan blue exclusion assay. *n=6.* (C) Apoptosis was assessed by AnnexinV/PI staining. *n=4.* Data are presented as a mean ± S.E. * indicates $p < 0.05$ vs. control, # indicates $p < 0.05$ vs. hypoxia, @ indicates $p < 0.05$ vs. *BNIP3* siRNA-transfectecd UCB-hMSC with hypoxia.

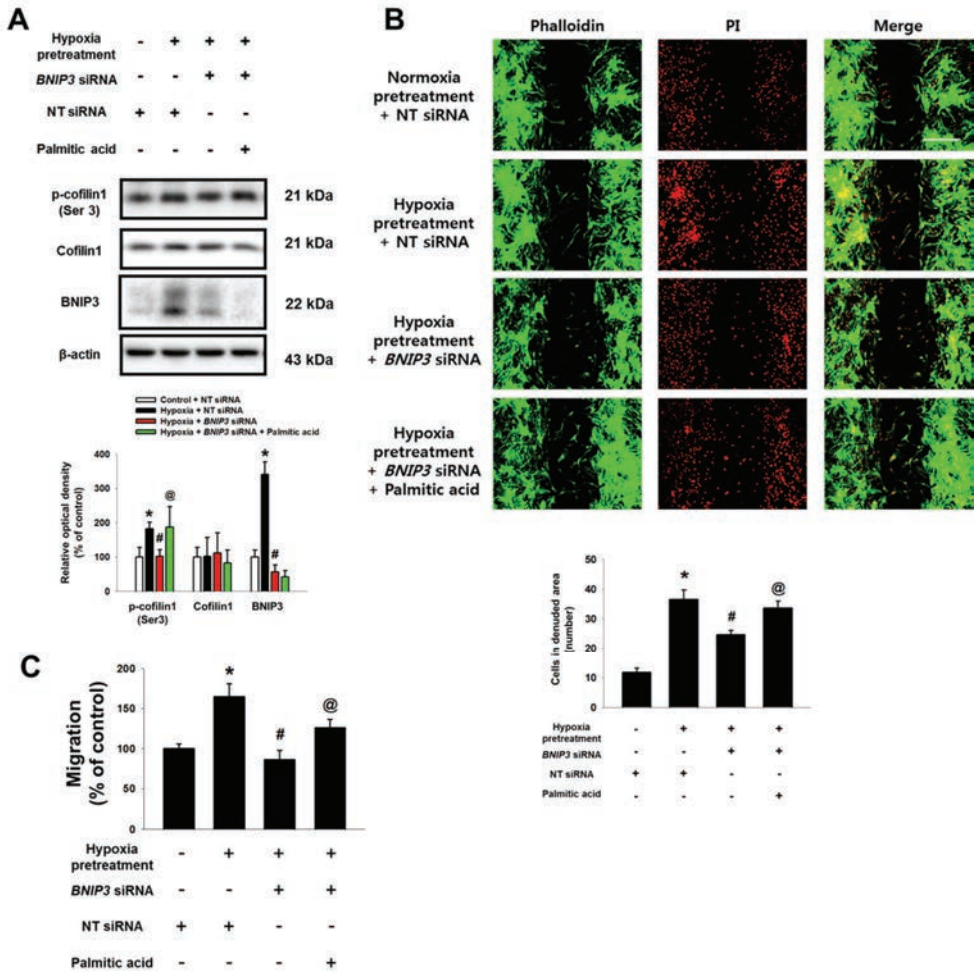

Figure 52. Effect of PA on BNIP3-silenced UCB-hMSC migration under hypoxia. (A) Cells transfected with *BNIP3* or NT siRNAs were pretreated with PA (20 μM) prior to hypoxia for 24 h. And, then cells were incubated with normoxia for 24 h. The expressions of p-cofilin1, cofilin1, BNIP3 and β-actin were detected by western blot. *n=4.* (B) Migrated UCB-hMSCs were immunostained with phalloidin and PI. *n=4* (magnification×100). Scale bars, 200 μm. (C) Cell migration was assessed by using luminometer with

Oris™ migration assay. $n=8$. Data are presented as a mean ± S.E. * indicates $p < 0.05$ vs. normoxia pretreatment, # indicates $p < 0.05$ vs. hypoxia pretreatment, @ indicates $p < 0.05$ vs. *BNIP3* siRNA-transfectecd UCB-hMSC with hypoxia pretreatment.

3.9. Role of BNIP3 on therapeutic potential of UCB-MSCs under hypoxia

Furthermore, I confirmed the effect of BNIP3 expression regulated by hypoxia pretreatment and PA on mouse skin wound healing with UCB-hMSC transplantation. Eight days after skin wound surgery, the wound area of mice was reduced to a significantly great extent in UCB-hMSCs with hypoxia. In addition, the wound area of mice given *BNIP3* siRNA-silenced UCB-hMSCs with hypoxia pretreatment was larger than that of mice given UCB-hMSCs with hypoxia or *BNIP3* siRNA-transfected UCB-hMSCs with pretreatments of hypoxia and PA (Fig. 53A). Meanwhile, my results showed that there was no statistical significance of the difference between wound area of mice given UCB-hMSCs and that of mice given *BNIP3* siRNA-transfected UCB-hMSCs. A histological evaluation at 12 days after skin wound surgery showed the wound bed to be completely covered by transplantations of UCB-hMSCs with hypoxia pretreatment and of *BNIP3* siRNA-transfected UCB-hMSCs with pretreatments of hypoxia and PA (Fig. 53B). In addition, the transplantation of UCB-hMSCs with hypoxia pretreatment showed re-epithelization as well as wound closure at the wound site. The re-epithelization histological scoring results showed that the re-epithelization score of transplantation of hypoxia-pretreated UCB-hMSCs is the highest among all

experimental groups. Re-epithelization score of the mice given *BNIP3* siRNA-transfected UCB-hMSCs with hypoxia and PA was higher than that of mice given *BNIP3* siRNA-transfected UCB-hMSCs with hypoxia pretreatment. There was no statistical significance between groups treated with vehicle or UCB-hMSCs alone. I further investigated the effect of BNIP3 regulation by pretreatment of either hypoxia or PA on angiogenesis capacity and survival of transplanted UCB-hMSCs. My results showed that transplantation of UCB-hMSCs with hypoxia pretreatment increased blood vessel formation and the amount of pan-endothelial marker CD31, myofibroblast marker α-smooth muscle actin (α-SMA)-positive and human nuclear antigen (HNA)-positive cells at the wound site compared to transplantation of UCB-hMSCs alone. In addition, angiogenesis capacity and survival rate of *BNIP3* siRNA-transfected UCB-hMSCs with hypoxia pretreatment was lower than those of UCB-hMSCs with hypoxia pretreatment and *BNIP3* siRNA-transfected UCB-hMSCs with hypoxia and PA (Figs. 54A-56). Overall, these findings indicate that decreased wound healing capacity of hypoxia-pretreated UCB-hMSCs by BNIP3 silencing is recovered by PA pretreatment.

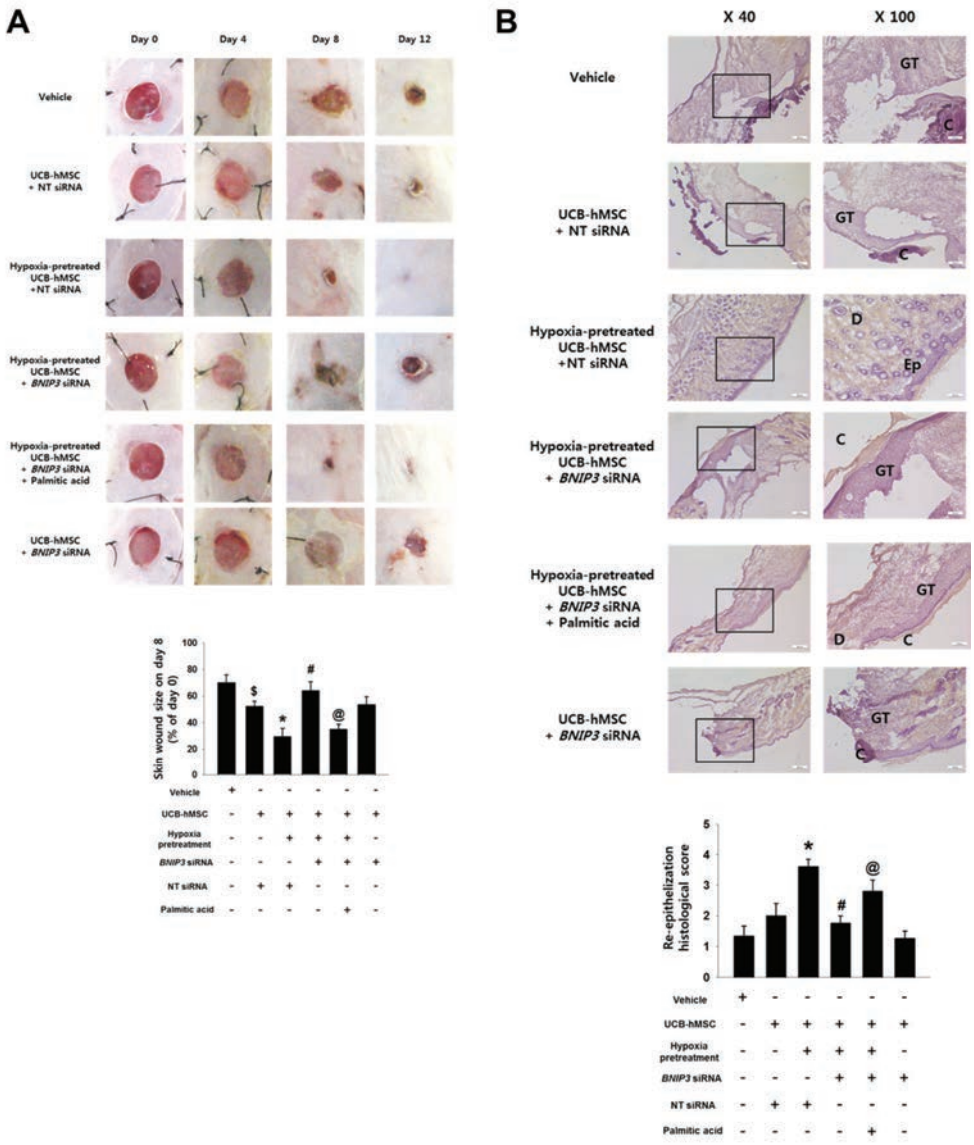

Figure 53. Role of PA in mouse skin wound healing by BNIP3-silenced UCB-hMSCs. (A) Representative gross wound images were acquired at post injection days 0, 4, 8, 12. Skin wound sizes at day 8 was compared with wound size at day 0. *n=5.* (B) Tissue slide samples were stained with hematoxylin and eosin. Low and

high magnified Histological gross images are shown in the left and right panels, respectively. Scale bars, 260 μm (magnification $\times$40) and 100 μm (magnification $\times$100). *n=5.* Data are presented as a mean $\pm$ S.E. $ indicates $p < 0.05$ vs. vehicle group, * indicates $p < 0.05$ vs. UCB-hMSC group given NT siRNA, # indicates $p < 0.05$ vs. UCB-hMSC group given NT siRNA with hypoxia pretreatment, @ indicates $p < 0.05$ vs. UCB-hMSC group given *BNIP3* siRNA with hypoxia pretreatment.

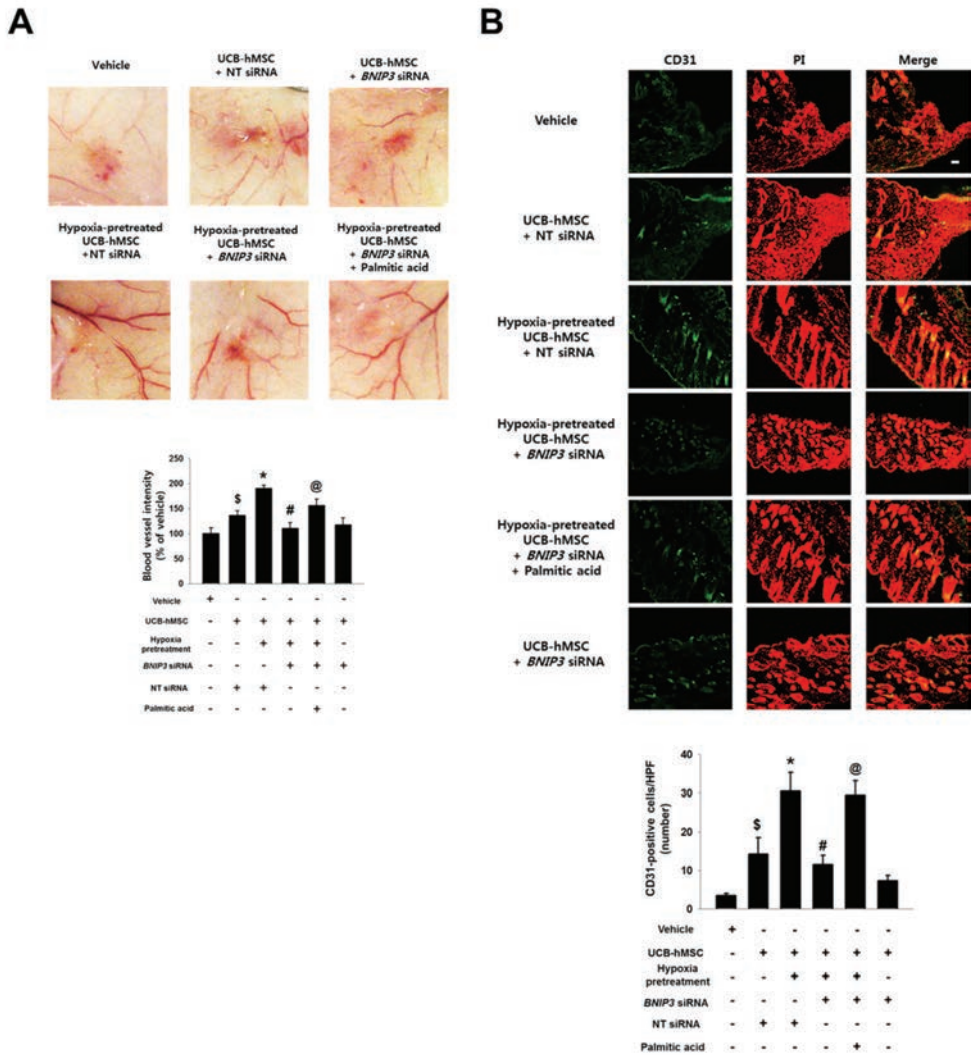

Figure 54. Effect of BNIP3-silenced UCB-hMSCs transplantation and PA on blood vessel formation and CD31 expression in mouse skin wound healing model. (A) Representative images of blood vessels in skin wounds on day 12. Vessel density was analyzed by using ImageJ program (bottom panel). *n=5.* (B) Histological tissue samples were immune-stained with CD31-specific antibodie and PI for counterstaining. The number of CD31-positive cells in high

power field (HPF) was analyzed by using Metamorph software. Scale bars, 100 μm (magnification $\times$100). *n=5.* Data are presented as a mean $\pm$ S.E. $ indicates $p < 0.05$ vs. vehicle group, * indicates $p < 0.05$ vs. UCB-hMSC group given NT siRNA, # indicates $p < 0.05$ vs. UCB-hMSC group given NT siRNA with hypoxia pretreatment, @ indicates $p < 0.05$ vs. UCB-hMSC group given *BNIP3* siRNA with hypoxia pretreatment.

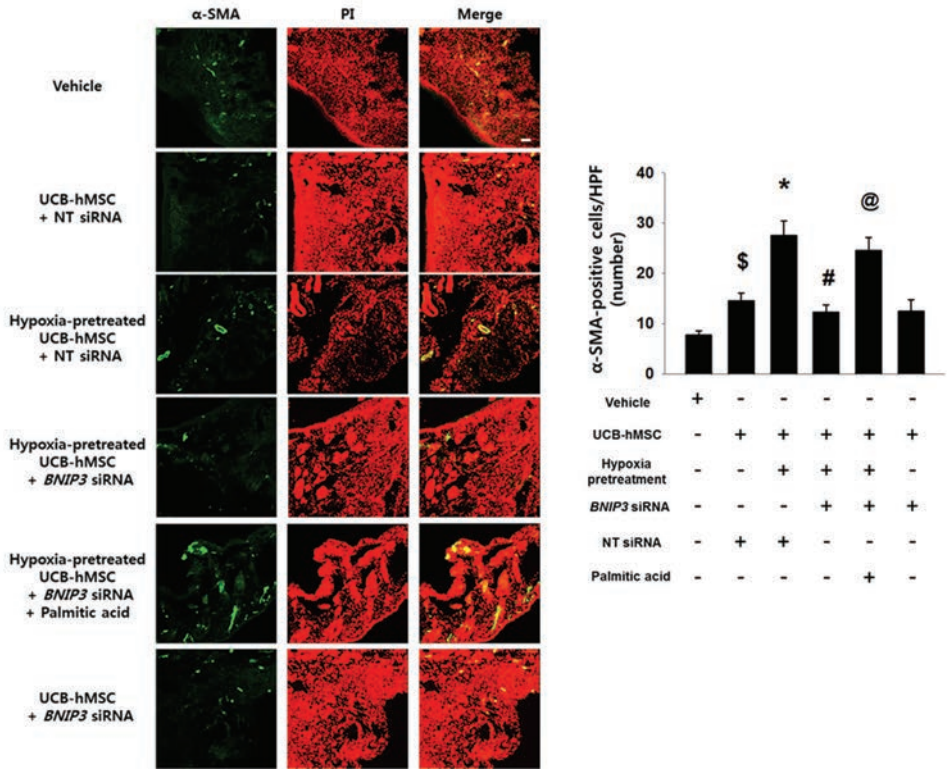

Figure 55. Effect of BNIP3-silenced UCB-hMSCs transplantation and PA on α-SMA expressions in mouse skin wound healing model. (A) Histological tissue samples were immune-stained with α-SMA specific antibodies and PI for counterstaining. The number of α-SMA-positive cells in HPF was analyzed by using Metamorph software. Scale bars, 100 μm (magnification $\times$100). $n=5$. Data are presented as a mean $\pm$ S.E.M. \$ indicates $p < 0.05$ vs. vehicle group, * indicates $p < 0.05$ vs. UCB-hMSC group given NT siRNA, # indicates $p < 0.05$ vs. UCB-hMSC group given NT siRNA with hypoxia pretreatment, @ indicates $p < 0.05$ vs. UCB-hMSC group given *BNIP3* siRNA with hypoxia pretreatment.

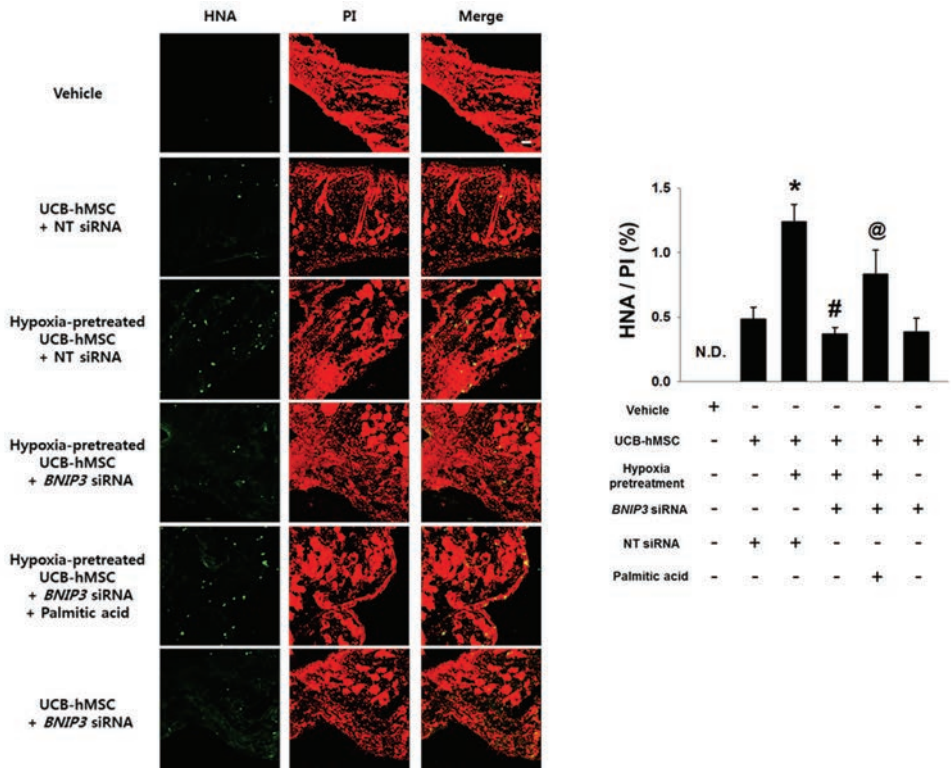

Figure 56. Effect of BNIP3-silenced UCB-hMSCs transplantation and PA on HNA expressions in mouse skin wound healing model. (A, B) Histological tissue samples were immune-stained with HNA-specific antibodies and PI for counterstaining. HNA-positive cells in total cells were analyzed by using Metamorph software. Scale bars, 100 μm (magnification $\times$100). $n=5$. Data are presented as a mean $\pm$ S.E.M. \$ indicates $p < 0.05$ vs. vehicle group, * indicates $p < 0.05$ vs. UCB-hMSC group given NT siRNA, # indicates $p < 0.05$ vs. UCB-hMSC group given NT siRNA with hypoxia pretreatment, @ indicates $p < 0.05$ vs. UCB-hMSC group given *BNIP3* siRNA with hypoxia pretreatment.

4. DISCUSSION

The present study highlights the mechanism controlling mitophagy in hypoxia and the relevance of mitophagy in the regulation of lipid metabolism and therapeutic functions, such as apoptosis, migration, and wound repair of UCB-hMSCs under hypoxia (Fig 57). Although PINK1 and NIX were increased by hypoxia, my results suggest that BNIP3 is a major mitophagy regulator stimulated by hypoxia in UCB-hMSCs, and it has a critical role in regulation of UCB-hMSC functions. There are several previous reports showing mitophagy induced by hypoxia via PINK1, NIX, BNIP3, and FUNDC1, but which factor is important for hypoxia-induced mitophagy appeared to be cell type-specific (Bellot et al., 2009; Liu et al., 2012b). Interestingly, my results showed hypoxia suppressed FUNDC1 expression. Although several investigators reported that FUNDC1 is associated with hypoxia-induced mitophagy, the effect of hypoxia on FUNDC1 expression is controversial, and the exact mechanism by which hypoxia regulates FUNDC1 expression has not been fully described (Chen et al., 2017; Liu et al., 2012b; Liu et al., 2014b). BNIP3 has been known as a non-selective mitophagy regulator removing healthy and unhealthy mitochondria mediated by interaction of the LC3 interacting region motif with LC3 (Zhu et al., 2013). Consistent with previous results,

my current results showed an increase in co-localization of COX4- and BNIP3-positive regions with LC3B. I also presented results showing that BNIP3 controls mitochondrial quality through the regulation of mtROS and mitochondrial membrane potential in hypoxia. It has been reported that mitophagy induced by BNIP3 and NIX removes damaged mitochondria and protects against ROS accumulation (Tracy et al., 2007; Zhang et al., 2008). In addition, dysregulation of the redox system and ROS accumulation directly link to stem cell apoptosis (Ito & Suda. 2014). The role of BNIP3 in cell death is debated, although it is reported that BNIP3 is a BH-3 only protein like other pro-apoptotic BCL-2 family members. Many researchers have reported that BNIP3 contributes to hypoxia-induced cell death through various mechanisms (Burton & Gibson. 2009; Qi et al., 2012). But, there is another report showing a protective effect of BNIP3 induction (Moriyama et al., 2017). Consistent with those findings, my results showed silencing of BNIP3 induced UCB-hMSC apoptosis. Therefore, further investigations using various types of stem cells are required to obtain more complete elucidation of the role of BNIP3 in stem cell functions under hypoxia.

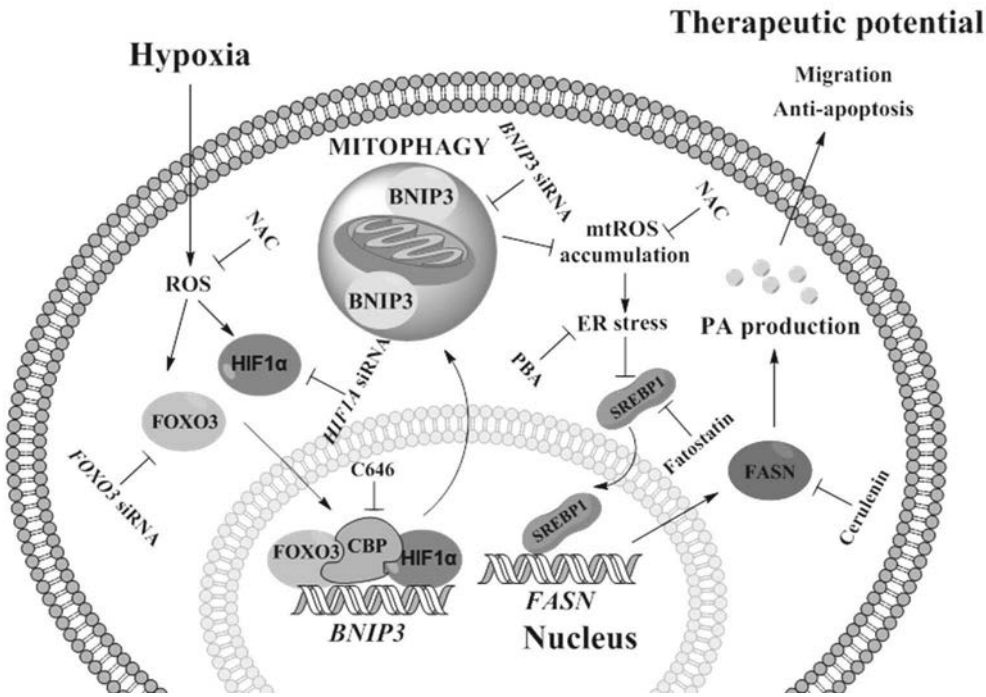

Figure 57. The schematic model for mechanism involved in the role of BNIP3 induced by hypoxia in UCB-hMSC therapeutic potential. Hypoxia stimulates BNIP3 expression through the formation of HIF-1α, FOXO3, CBP complex in the nucleus leading to BNIP3-dependent mitophagy. BNIP3 silencing induces accumulation of mitochondrial ROS (mtROS), associated with ER stress augmentation. Augmented ER stress suppresses SREBP1 protein expression and nuclear translocation followed by inhibition of FASN-mediated PA production. PA rescues decreased therapeutic potential including migration and anti-apoptosis by BNIP3 silencing in UCB-hMSCs under hypoxia.

Present study focused on identifying the molecular mechanism involved in how HIF-1α and FOXO3 contribute to BNIP3 transcription in UCB-hMSCs under hypoxia. My results showed both HIF-1α and FOXO3 expressions upregulated by hypoxia contribute to BNIP3 transcription. Notably, BNIP3 expression induced by hypoxia was mostly suppressed by *HIF1A* siRNA transfection, but also partially suppressed by *FOXO3* siRNA transfection. These results suggest the possibility of HIF-1α acting as an upstream regulator of FOXO3 in terms of BNIP3 regulation under hypoxia. Previous studies investigating the mechanism of FOXO3 regulation by hypoxia demonstrated that HIF-1α induced by oxidative stress stimulates FOXO3 expression (Bakker et al., 2007; Zhang et al., 2013). In addition, it has been reported that cooperation of HIF-1α with FOXO3 is required for high-level transcription of *BNIP3* mRNA by hypoxia (Chinnadurai et al., 2008). I hypothesized that there may be a molecule that mediates their cooperative action on BNIP3 expression. In addition, my results demonstrated that CBP acts as a transcriptional co-activator interacting with HIF-1α and FOXO3 in the nucleus, and is closely associated with the binding of HIF-1α and FOXO3 to the *BNIP3* gene promoter region indicating an epigenetic action of CBP for *BNIP3* mRNA transcription. CBP/p300 has recruitment sites for physical interaction with various transcription factors including HIF-1α and FOXOs (Calnan et al., 2008; Freedman et al., 2002).

Acetylation of histone by CBP/p300 neutralizes the positive charge of lysine residue, leading to an increase in the DNA accessibility of transcription factors (Jin et al., 2011; Legube et al., 2003). Moreover, CBP/p300 directly increases HIF-1α stability and FOXO3 activity through acetylation (Daitoku et al., 2011; Geng et al., 2012; van der Heide et al., 2005). Taken together, I propose that CBP induces transcriptional synergism between HIF-1α and FOXO3; an effect that is required for BNIP3 expression under hypoxia.

My present study highlights a critical role for the BNIP3 as a lipid metabolism regulator in UCB-hMSCs under hypoxia. Based on my results, hypoxia-induced BNIP3 regulates mRNA expressions of *FASN* and *SCD1*, which are involved in *de novo* synthesis of saturated and unsaturated long-chain FFAs. I used cerulenin and CAY10566 to distinguish the role of FASN and SCD1 regulated by BNIP3 in migration induced by hypoxia pretreatment and survival under hypoxia in UCB-hMSCs. Intriguingly, my results showed that migration and survival of UCB-hMSCs under hypoxia are regulated by FASN, not by SCD1. There have been several previous reports investigating the role of lipogenesis-regulating enzymes in stem cell regulation. For example, FASN-dependent lipogenesis is highly active in adult NSCs and progenitor cells that are associated with adult neurogenesis (Knobloch et al., 2013). FASN inhibition by cerulenin suppressed proliferation and migration as well as

stemness marker expression in glioma stem cell (Yasumoto et al., 2016). In addition, SCD1 has a tumor suppressive role in survival of leukemia stem cells and eliminates undifferentiated tumorigenic pluripotent stem cells (Ben-David et al., 2014; Zhang et al., 2012). Taken together, those findings suggest that different stem cell types have different levels of sensitivity to saturated and unsaturated long-chain FFAs. However, further investigation of the role of SCD1 upregulation by hypoxia in the stem cell is required to provide insight into lipid metabolism of stem cells under hypoxia. Meanwhile, there is a previous study reporting that the loss of BNIP3 increased FASN expression and lipid synthesis in hepatocytes due to ROS accumulation (Glick et al., 2012), which is inconsistent with my results. The difference between results is believed to be due to cell type and physiological condition differences like degree of ROS accumulation. Indeed, present study suggested both hypoxia and BNIP3 silencing stimulate ROS accumulation, but BNIP3 silencing caused severe ROS accumulation, which may lead to suppression of anti-apoptosis, migration and FFA production.

My results further indicate that the regulatory role of BNIP3 in ROS accumulation is associated with SREBP1/FASN pathway dependent lipogenesis in UCB-hMSCs under hypoxia. There are several reports showing the mechanism of regulation of SREBP1 expression. Previous studies suggested that SREBP1 expression is

regulated by HIF-1α and mTORC1 (Furuta et al., 2008a; Porstmann et al., 2008). In addition, I previously demonstrated that SREBP1 expression is mainly induced by HIF1α as an upstream regulator, but not mTOR, in UCB-hMSCs under hypoxic condition (Lee et al., 2015). SREBP1 consists of two isoforms of *SREBF1* gene, such as SREBP1a and SREBP1c. Previous reports presented that SREBP1c expression is responsible under hypoxic condition, which is associated with de novo lipogenesis (Garcia-Fuentes et al., 2015; Na et al., 2011). Although both SREBP1a and SREBP1c are involved in lipid metabolism (Horton et al., 2003; Shimano et al., 1996), most of previous studies present a SREBP-1c as a major regulator of FASN expression (Gao et al., 2015; Oem et al., 2008). Those previous findings indicate that SREBP-1c is a major regulator for FASN-induced lipogenesis in UCB-hMSCs under hypoxia.

Present study showed that the excessive ROS production by BNIP3 silencing decreased SREBP1 and FASN expressions. I pretreated NAC to suppress the ROS production potentiated by BNIP3 silencing. In my results, NAC pretreatment increased SREBP1 and FASN expressions reduced by BNIP3 silencing, and decreased ER stress markers expressions potentiated by BNIP3 silencing. In particular, I observed that BNIP3-silenced UCB-hMSCs under hypoxia still have high levels of HIF-1α protein and *SREBF1* mRNA, although BNIP3 silencing suppressed expressions

of mature SREBP1 and FASN as well as FFA production. Furthermore, I observed that augmentation of ER stress by oxidative stress significantly suppressed SREBP1 and FASN expressions. Two mechanisms involved in how hypoxia induces ER stress have been reported; one is driven by downregulation of Ero1 oxidase and the other involves induction of PERK signaling by GSK-3β activated by oxidative stress (Hotokezaka et al., 2009; Ramming et al., 2012). Previous reports demonstrated that the chronic and excessive ER stress inactivates mTORC1 signaling, which leads to translational inhibition (Guan et al., 2014; Kato et al., 2012). Indeed, I confirmed suppression of hypoxia-activated mTORC1 signaling in BNIP3-silenced UCB-hMSCs. Taken together, I present that NAC prevents against the ER stress-induced translational inhibition by BNIP3 silencing, which leads to induction of SREBP1 and FASN expressions.

There is ample evidence showing that enhancement of migration and anti-apoptosis is a potential therapeutic strategy in regenerative medicine using MSCs (He et al., 2009; Veevers-Lowe et al., 2011). My study results indicate PA, a major product of FASN, is a crucial lipid metabolic factor involved in UCB-hMSC migration and anti-apoptosis. Previous reports showed that PA stimulates migration through plasminogen activator inhibitor-1 expression and F-actin rearrangement mediated by Cdc42 (Byon et al., 2009; Puthanveetil et al., 2011). My previous and present

results demonstrate that enhancement of migratory ability of UCB-hMSCs under hypoxia is involved in F-actin polymerization via cofilin-1 phosphorylation and RhoA activation, not via Rac1 and Cdc42 (Lee et al., 2015). Meanwhile, several investigators have reported on the effect of PA on cell survival, and it seems to be dose-dependent (Beeharry et al., 2004; Oh et al., 2010). Although present study showed PA pretreatment recovers UCB-hMSC apoptosis under hypoxia, additional investigation revealing the mechanism involved in PA regulation of apoptosis of UCB-hMSCs under hypoxia is needed. It is clear that activation of GPR40 has key roles in calcium influx, thereby inducing a cAMP level increase, which drives anti-apoptotic effects (Verma et al., 2014). Furthermore, I present *in vivo* evidence that BNIP3-induced UCB-hMSCs transplantation by hypoxia pretreatment or PA accelerates myoblast switch and blood vessel formation, as well as the skin wound healing process. A phenotypic switch of fibroblasts toward myofibroblasts via myofibroblast development has been reported as a representative characteristic of wound repair and maturation (Hinz. 2007; Siebert et al., 2011). Although transplanted UCB-hMSCs at the wound site are exposed to hypoxia, due to low density of vascular distribution, BNIP3 silencing of UCB-hMSCs with normoxia pretreatment did not significantly affect this process. It is implied that BNIP3 may contribute to the survival of transplanted UCB-hMSCs in the initial wound-healing phase. In

addition, I observed that PA recovers the reduced regenerative capacity and survival of BNIP3-silenced UCB-hMSCs with hypoxia pretreatment. It has been shown that the tissue regenerative effect associated with transplantation of MSCs is induced by a paracrine effect rather than by cell replacement, and dynamic migration of transplanted cells into the wound site has been correlated with repair process initiation and the immune modulatory process (Granero-Molto et al., 2009; Kwon et al., 2013). Consequently, these results indicate that BNIP3 expression and PA production induced by hypoxia have critical roles in the regulation of migration and survival in transplanted UCB-hMSCs, thereby determining the therapeutic efficacy of UCB-hMSC transplantation with hypoxia pretreatment. There are many reports showing the effect of PA in cell functions, but it appears dose-dependent (Gillet et al., 2015; Lee et al., 2015; Menendez et al., 2004). A previous report showed high concentration of PA (above 100 μM) induced cell death in a dose-dependent manner (Gunaratnam et al., 2013). Transplanted cells into the healthy or obese or diabetes patients are exposed to high PA (120-220 μM) microenvironment compared to *in vitro* culture medium which does not contain PA (Bell et al., 2006; Jensen et al., 1989). Based upon those findings, I proposed that high PA microenvironment in obese or diabetic patients may decrease therapeutic efficiency of UCB-hMSCs transplantation. However, my previous report presented that PA pretreatment increased

proliferation and migration via activation of mTORC1 signaling in UCB-hMSCs under hypoxia (Lee et al., 2015). Therefore, I provide PA as an inducer or a signal molecule for enhancing the therapeutic potential of cell prior to UCB-hMSCs transplantation.

CHAPTER III

Protective effect of GPAT1 induction by O-GlcNAcylation on hypoxia-induced mESCs apoptosis

Manuscript is published in *Cell Death Dis*. 2016 24;7:e2158

1. INTRODUCTION

Stem cells in the body are exposed to low oxygen pressure due to the physiological distribution of vessels (Simon & Keith. 2008). This hypoxic niche for stem cells is essential to maintain the metabolic characteristics of stem cells (Ito & Suda. 2014). Thus, describing the oxygen nature of this stem cell niche is important for elucidating stem cell regulation. Oxygen signaling is a major determinant of cell fate–controlling cellular processes. Control of oxygen signaling in stem cells has the potential to regulate embryonic development, cell cultivation, cell reprogramming, and transplantation in regenerative medicine (Forsyth et al., 2006; Simon & Keith. 2008; Song et al., 2010; Theus et al., 2008; Yoshida et al., 2009). There are many reports showing the effects of hypoxia on various kinds of stem cells, and it has been shown that hypoxia has a paradoxical role in stem cell behaviors and cell fate regulation related to stem cell type, ageing, and oxygen concentration (Csete. 2005; Forsyth et al., 2006; Holbrook et al., 2002; Kumar et al., 2015). Studies of mechanisms by which stem cells function under hypoxia, and how they are regulated, have been undertaken. Several investigators recently reported that hypoxia–mediated stem cell metabolic alteration is associated with stem cell

function; as a result, interest in the interaction between hypoxia and stem cell metabolism is growing (Lee et al., 2015; Teslaa et al., 2015). However, which metabolic factors are important for stem cell fate under hypoxia have not been elucidated.

O-GlcNAcylation is affected by cellular nutrient status and extra-cellular stresses including hypoxia (Hart et al., 2007; Wells et al., 2001)-(Love et al., 2005). A hypoxia-induced glycolytic switch primarily stimulates HBP flux, which induces O-GlcNAcylation signaling (Guillaumond et al., 2013). O-GlcNAcylation is catalyzed by OGT to add N-acetyl glucosamine to the Ser or Thr residues of proteins (Dorfman et al., 1955; Ghosh et al., 1960; Marshall et al., 1991). O-GlcNAcylation acts as an essential factor for controlling physiological processes including migration, proliferation, and survival in stem cells, and recently it was considered as a potential strategy for use in stem cell therapy (Jeon et al., 2013; Shafi et al., 2000; Zafir et al., 2013). In addition, as many human metabolic diseases such as diabetes and cancer are attributed to aberrant O-GlcNAcylation, unraveling HBP-mediated O-GlcNAc signaling is important in the development of practical strategies for metabolic diseases treatment. For example, Liu *et al.* showed that glucosamine-mediated O-GlcNAcylation induced resistance to tissue damage resulting from ischemic injury and provided cardio-protection in an animal model (Liu et al., 2006). Furthermore, O-GlcNAcylation interacts with other nutrient

metabolic pathways such as lipogenesis, gluconeogenesis, and glycogen synthesis (Hardiville et al., 2014; Ruan et al., 2013; Wells et al., 2001). Among these metabolic pathways, lipid metabolism is reported to have a central role in controlling stem cell fate (Folmes et al., 2013; Ito et al., 2012). Collectively, these results suggest that O-GlcNAcylation can be a useful tool for use in cellular metabolic regulation, and identification of an O-GlcNAcylation-regulating potential lipid metabolic factor, which is important for stem cell regulation, may suggest metabolic approaches potentially useful in stem cell therapy.

ESCs are distinctive in that they have a self-renewal capacity, exhibit pluripotency to enable differentiation into cellular derivatives of three lineages, and may be used as a representative *in vitro* model in the study of early embryo development, pluripotent stem cell physiology, and clinical applications (Chambers. 2004; Murry et al., 2008; O'Shea. 2004). Despite the clinical limitation associated with ESCs and the possibility of cancer formation, several studies into the therapeutic effects of ESCs in regenerative medicine have been reported. Indeed, administrations of human or mouse ESCs has induced a paracrine effect and improved damaged cell functions (Hodgson et al., 2004; Laflamme et al., 2007; Lee et al., 2011). However, despite the benefit of ESCs in regenerative medicine, ESC apoptosis remains an impediment to ESC applications using hypoxia (Arnaboldi et al., 2005; Khan et al., 2007; Koay et al.,

2008). Thus, researchers are investigating ways to minimize ESC apoptosis and control ESC fate under hypoxia. In this study, I used glucosamine to induce O-GlcNAcylation. Therefore, my study investigated the role of O-GlcNAcylation via glucosamine (GlcN) which is recognized as a HBP activator (Pouwels et al., 2001) in lipid metabolism and in protection of mouse ESC (mESC) apoptosis under hypoxia.

2. MATERIALS & METHODS

2.1. Materials

Cells from a mESC line (ES-E14TG2a) were provided by the American Type Culture Collection (Manassas, VA). Fetal bovine serum was purchased from HyClone (Logan, UT). The Bcl-2, Bax, caspase-3, caspase-9, Sp1, cytochrome c, COX4, β-tubulin, Oct 3/4, nanog, β-actin, and Lamin A/C antibodies were acquired from Santa Cruz Biotechnology (Dallas, TX). The RL-2, Glycerol-3-phosphate acyltransferase 1 (GPAT1), and ALG10 antibodies were obtained from abcam (Cambridge, MA). Mammalian target of rapamycin (mTOR), p-mTOR (Ser2448), S6K1, p-S6K1 (Thr 389), 4EBP1, and p-4EBP1 (Thr37/46) antibodies were purchased from Cell Signaling Technology (Beverly, MA). HRP-conjugated rabbit anti-mouse and goat anti-rabbit secondary antibodies were acquired from Thermo Fisher (Waltham, MA), whereas HRP-conjugated rabbit anti-goat secondary antibody was obtained from Santa Cruz Biotechnology. Rapamycin, D-glucosamine, PUGNAc, N-acetyl D-glucosamine (GlcNAc), tunicamycin, LPA, palmitic acid, oleic acid, mithramycin A, pertussis toxin (Ptx), SN-50 and BrdU) were purchased from Sigma-Aldrich (St. Louis, MO). The OGT inhibitor ST045849 was obtained from Timtec (Newark, DE).

siRNA for *Gpat1* and NT siRNA were acquired from Dharmacon (Lafayette, CO). PI and Alexa fluor 488-conjugated secondary antibodies were purchased from Life technologies (Gaithersburg, MD). All experiments were performed with 6-10 passages of the tested cells.

2.2. mESC culture

The mESCs were cultured with 15% FBS, 1% antibiotic mixture, 5 ng/mL mouse LIF, and high glucose Dulbeco's essential medium (DMEM; Gibco, Grand Island, NY). The cells were grown on 6-well plates or in 35 or 60 mm culture dishes in an incubator maintained at 37° C with 5% CO_2. After 48 h of cell culture, cells were washed twice with PBS) and placed in DMEM-supplemented culture medium with 5% serum replacement, 1% antibiotics, and 5 ng/mL LIF (SR-medium). After cells were incubated 24 h for mESC synchronization, cells were washed twice with PBS and placed in SR-medium with agents.

2.3. Hypoxia treatment

The detailed protocol for hypoxia is described in Materials & Methods section of CHAPTER I.

2.4. Mouse skin flap model

All procedures using animals followed the National Institutes of Health Guidelines for the Humane Treatment of Animals and were performed under Institutional Animal Care and Use Committee-approved protocols at Seoul National University (SNU-150508-4). Mice were housed in a standard animal facility maintained on a 12 h light/dark cycle and within a room temperature range of 20-25° C. Eight-week-old male Institute for Cancer Research mice were anesthetized with 2% isoflurane in oxygen/nitrous oxide mixtures. A previously described skin flap model procedure was performed (Basu et al., 2014; de Carvalho et al., 2005; Morimoto et al., 2014). Experimental animals were divided into seven groups: vehicle-injected wild type mice (group 1, n=6); mESC transplantation mice that received mESC pretreated with either NT siRNA alone (group 2, n=6) or NT siRNA and 10 μM glucosamine (group 3, n=6); mice that received mESC pretreated with gpat1 siRNA and 10 μM glucosamine (group 4, n=6); mice that received 10 μM glucosamine with vehicle (group 5, n=6); mice that received mESC pretreated with 0.1 μM LPA (group 6, n=6); and mice that received 0.1 μM LPA with vehicle (group 7, n=6). After shaving off the hair, a 4 cm × 1 cm skin flap template on the dorsal surface of the mouse was traced by using a surgical marker. The surgical

procedure for flap creation was performed under aseptic conditions. A full-thickness skin flap was elevated for 30 min. For treatment, 100 μL of a PBS and matrigel (BD Biosciences, NJ) mixture containing vehicle or mESCs (n=1 × 10^6) with either glucosamine or LPA was injected into the dermis at the center of the skin flap. The flap was then sutured back to its original position by a simple interrupted suturing technique using 3-0 silk non-absorbable sutures. Transplanted mESCs were pretreated with BrdU (2 μM). All flap images were acquired at the same distance from the subject (30 cm) with a digital camera system (D50; Nikon, Tokyo, Japan). At post-injection day 12, all mice were euthanized and 1.5 cm × 0.5 cm tissue samples in the central part of the skin flap were excised and collected (Fig. 6A). Collected tissues were embedded in O.C.T compound (Sakura Finetek, Torrance, CA) and frozen. Embedded samples were sliced (10 μm thick), and underwent hematoxylin and eosin (H&E) and immunohistochemical staining. Sliced samples for IHC analysis were immunostained with BrdU and PI. Immunostained cells were visualized by using fluorescence microscopy (Olympus, Tokyo, Japan), and the images were analyzed by using MetaMorph software (Universal Imaging, West Chester, PA). Visual assessment of skin flap necrotic areas was performed by using ImageJ software (developed by Wayne Rasband, National Institutes of Health, Bethesda, MD; available at http://rsb.info.nih.gov/ij/). Dark areas with scabs in a skin flap were

considered necrotic. To determine the portion of the skin flap that was necrotic, I used the formula: Necrotic area in skin flap = necrotic area of flap area / area of total flap ×100.

2.5. Western blot analysis

The detailed protocol for hypoxia is described in Materials & Methods section of CHAPTER I.

2.6. Nuclear and non-nuclear fraction preparation

The detailed protocol for nuclear fractionation is described in Materials & Methods section of CHAPTER I.

2.7. Isolation of mitochondria

The detailed protocol for mitochondrial isolation is described in Materials & Methods section of CHAPTER II.

2.8. Immunoprecipitation

The detailed protocol for immunoprecipitation is described in Materials & Methods section of CHAPTER II.

2.9. mRNA isolation and reverse PCR

The mESC RNA was extracted by using the RNeasy Plus Mini Kit (QIAGEN, Valencia, CA). Extracted RNA (1 μg) was reverse-transcripted with a Maxime RT premix kit (iNtRON Biotechnology, Sungnam, Korea). The cDNA was amplified with the sense and antisense primers of *Gpat*1 and β-actin.

2.10. Real-time PCR

Expressions of the *Fasn, Acc1, Cpt1a, Cpt1b, Magl, Gpat1, Gpat2, Gpat3, Gpat4, Scd1, Scd2, Scd3, Scd4, Lpaatα, Lpaatβ, Lpaatδ, Lpaatε, and Actb* genes were detected by using a Rotor-Gene 6000 real-time thermal cycling system (Corbett Research, Mortlake, Australia) with a QuantiMix SYBR kit (Phile Korea Technology, Daejeon, Korea), mRNA primers, and 1 μg of the cDNA sample. Data were analyzed by using the manufacture's software (Corbett Research). Melting curve analysis was used to confirm the identity and specificity of the PCR products. Normalization was performed by using β-actin as the endogenous control. Primer sequences used in experiments are described in Table 7.

Table 7. Sequences of primers used for PCR.

Gene\	Identification	Sequence (5'-3')	Size (bp)
Fasn	Sense	GATGCCATTCCAGGTAAATG	147
	Antisense	CCAGAGGAAGTCAGATGATAG	
Cpt1a	Sense	TGTGGACCTGCATTCCTTCC	301
	Antisense	CAGGTGCTGGTGCTTTTCAC	
Cpt1b	Sense	CGAGAACTCGTACCAAGTA	301
	Antisense	TTGGAGGTCTTGTTTCTTATG	
Magl	Sense	GCAGAGTGAGGGAGAGAGGA	293
	Antisense	TGCGCCCCAAGGTCATATTT	
Gpat1	Sense	GGTTTGGGACTTGCACGTTC	327
	Antisense	GTGCCTTGTGTGCGTTTCAT	
Gpat2	Sense	GCTAGGTGAATGTAGTGTTG	329
	Antisense	TCAATAGGCTCAGTGTATGT	
Gpat3	Sense	AGGTTCTCCTCCGAAGAGCT	352
	Antisense	GAGAGGTGTGATTGGCGACA	
Gpat4	Sense	GCCCTACACCAACGGAATCA	197
	Antisense	GCTCCTCTGCCGAGAATCTC	
Scd1	Sense	TTGGCTAGCTATCTCTGCGC	289
	Antisense	GGCCGGCATGATGATAGTCA	
Scd2	Sense	CTTTCAACATAGCGCGCCTC	263
	Antisense	GCCTCTCCAGTCCTGCAATT	
Scd3	Sense	GAAGCACCCATGTTGTATAG	283
	Antisense	GAAGCACCCATGTTGTATAG	
Scd4	Sense	TACCGCTGGCACATCAACTT	277
	Antisense	AGACCATGTACCCTCCCCTC	
Lpaat-α	Sense	CTCGACCTGCTTGGAATG	237
	Antisense	GGAGCCATTGTGGTTTCT	
Lpaat-β	Sense	CATGATGGGTCTCATGGAAA	325
	Antisense	GTAGAAGGAAGAGAAAGACGAG	
Lpaat-δ	Sense	ATGCCTTTCAGGAGGAATAC	206
	Antisense	CATGGAGGCCATACAGAAG	
Lpaat-ε	Sense	CACCATCCATGACTGAGTTT	197
	Antisense	CCCAGGAAATTTGTTTCTTCTT	
β-actin	Sense	GCAGGAGTACGATGAGTCCG	239
	Antisense	ATCCTGAGTCAAAAGCGCCA	

2.11. Small interfering RNA transfection

Prior to transplantation or hypoxia treatment, siRNAs specific for *Gpat1* or NT siRNA as a negative control were transfected to mESCs for 24 h with HiPerfect transfection reagent (QIAGEN) according to the manufacturer's description. Each transfected siRNA's concentration was 25 nM. The siRNA sequences are described in Table 8.

Table 8. Sequences of siRNAs used for gene silencing.

Target gene	Sequence 5'-3'
Gpat1	CCACAUACUGUCUCGUGAA
	GGUGAGGAGCAGCGAGAUU
	CGUACAUCGCCUCGGGCAA
	CUUAUCACCAGGACGGAAA
Non-targeting	UAGCGACUAAACACAUCAA
	UAAGGCUAUGAAGAGAUAC
	AUGUAUUGGCCUGUAUUAG
	AUGAACGUGAAUUGCUCAA

2.12. Trypan blue exclusion cell viability assay

The detailed protocol for trypanblue exclusion cell viability assay is described in Materials & Methods section of CHAPTER I.

2.13. Annexin V/PI fluorescence-activated cell sorter (FACS) analysis

The detailed protocol for annexin V/PI FACS analysis is described in Materials & Methods section of CHAPTER I.

2.14. Intracellular ROS detection

The detailed protocol for ROS measurement is described in Materials & Methods section of CHAPTER II.

2.15. Immunofluorescence staining

The detailed protocol for immunofluorescence staining is described in Materials & Methods section of CHAPTER I.

2.16. Live Cell Imaging

The detailed protocol for live cell imaging is described in Materials & Methods section of CHAPTER I.

2.17. [^{3}H]-thymidine incorporation

The detailed protocol for [^{3}H]−thymidine incorporation is described in Materials & Methods section of CHAPTER I.

2.18. Statistical analysis

All experimental data are summarized as a mean ± standard error. Differences among experimental groups were tested by using ANOVA. To compare some treatment group means with either control or hypoxia treatment means, the Bonferroni−Dunn test was performed. A test result with a p value < 0.05 was considered significant.

3. RESULTS

3.1. Effect of hypoxia on O-GlcNAcylation and survival in mESCs

To investigate the effect of hypoxia on intracellular ROS production of mESCs, I performed DCF-DA staining assays. Intracellular ROS production in mESCs under hypoxia for 24 h increased to 156% of that in the normoxia control (Fig. 58A). To examine the effect of hypoxia on mESCs survival, mESCs were incubated under hypoxic condition for various durations (0-72 h). Anti-apoptotic protein Bcl-2 expression level decreased in a time-dependent manner after 12 h of hypoxia. But, hypoxia increased expression levels of Bax, cleaved caspase-9, and cleaved caspase-3 after 12 h of hypoxia (Fig. 58B). Viability of hypoxia-treated cells decreased in a time-dependent manner and was significantly lower than that of control cells during 24-72 h of hypoxia treatment (Fig. 58C). To confirm the role of glucosamine on O-GlcNAcylation in mESCs, I used RL-2 antibody specific for O-GlcNAc. Hypoxia treatment for 24 h slightly increased total O-GlcNAc level, and the maximum increase in O-GlcNAc level was observed in cells treated with 10 μM of glucosamine and hypoxia (Fig. 59A). As shown in figure 59B, the effect of another O-

GlcNAcylation activator GlcNAc was also similar to that of glucosamine.

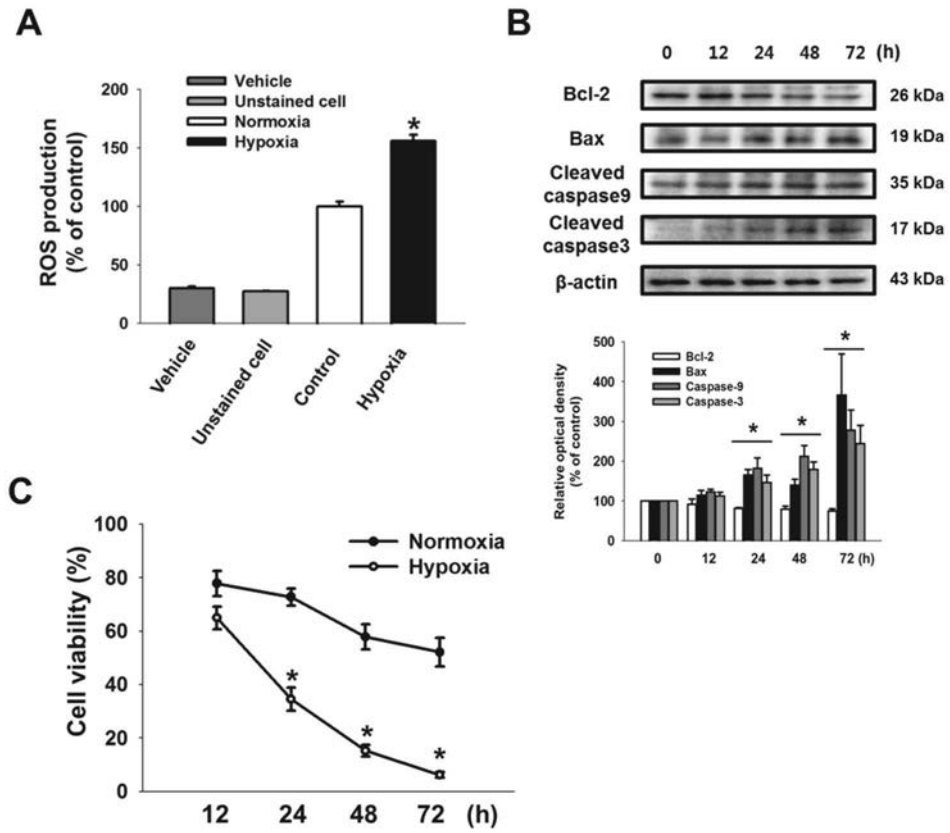

Figure 58. Effects of hypoxia on ROS production and apoptosis in mESCs. (A) Cells were exposed to hypoxa for 24 h, and then DCF-DA sensitive cellular ROS level was detected. n=6. * indicates $p < 0.05$ vs. normoxia control (B) Cells were exposed to hypoxic condition for 0-72 h. Bcl-2, Bax, cleaved caspase-9, and cleaved caspase-3 proteins were detected by western blotting. n=3. (C) Cell viability was measured directly using a Petroff-Hausser counting chamber. Data are reported as mean ± S.E of three independent experiments with duplex dishes. * indicates $p < 0.05$ vs. normoxia control.

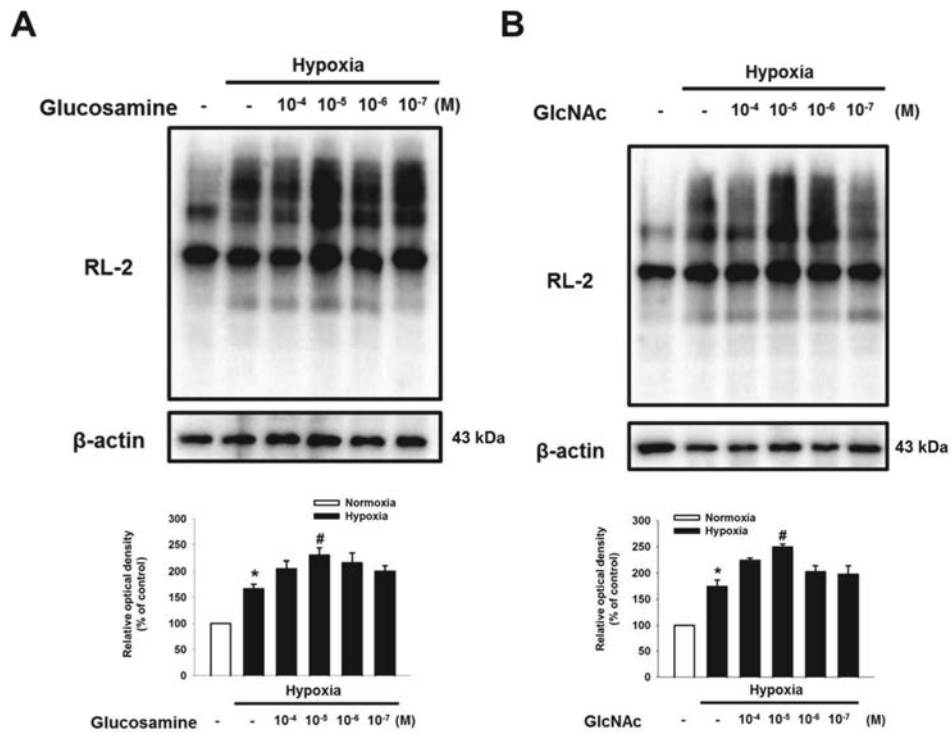

Figure 59. Effect of glucosamine and GlcNAc on O-GlcNAcylation in mESCs. (A, B) Cells were treated with various concentrations of glucosamine and GlcNAc (10-4 -10-7 M) for 30 min prior to hypoxia treatment. Glucosamine-pretreated cells were exposed to hypoxia for 24 h. And then, RL-2 and β-actin were detected by using western blotting. n=3. * indicates $p < 0.05$ vs. control, # indicates $p < 0.05$ vs. hypoxia treatment alone,

3.2. Effect of O-GlcNAcylation on mESC survival under hypoxia

To determine the effect of glucosamine on mESC survival, I examined cell viability after 24 h of hypoxic incubation with various concentrations of the glucosamine (10 mM to 1 μM). Hypoxia significantly decreased cell viability, but viability was recovered by 10 μM of glucosamine treatment (Fig. 60A). In addition, hypoxia decreased Bcl-2 expression and increased Bax, cleaved caspase-9, and cleaved caspase-3 expressions, results that were reversed by glucosamine treatment (Fig. 60B). Live cell imaging results showed that the size of mESC colonies with glucosamine under hypoxia was significantly larger than that of the hypoxia controls during 24-48 h incubation (Fig. 60C). Next, I investigated whether glucosamine-induced O-GlcNAcylation regulated mESC survival under hypoxia. Addition of the OGT inhibitor ST045849 decreased the previous glucosamine-increased cell viability (Fig. 61A). Consistent with this result, the glucosamine treatment reduced annexin V positive and PI positive mESCs under hypoxia, which was significantly inhibited by ST045849 addition (Fig. 61B).

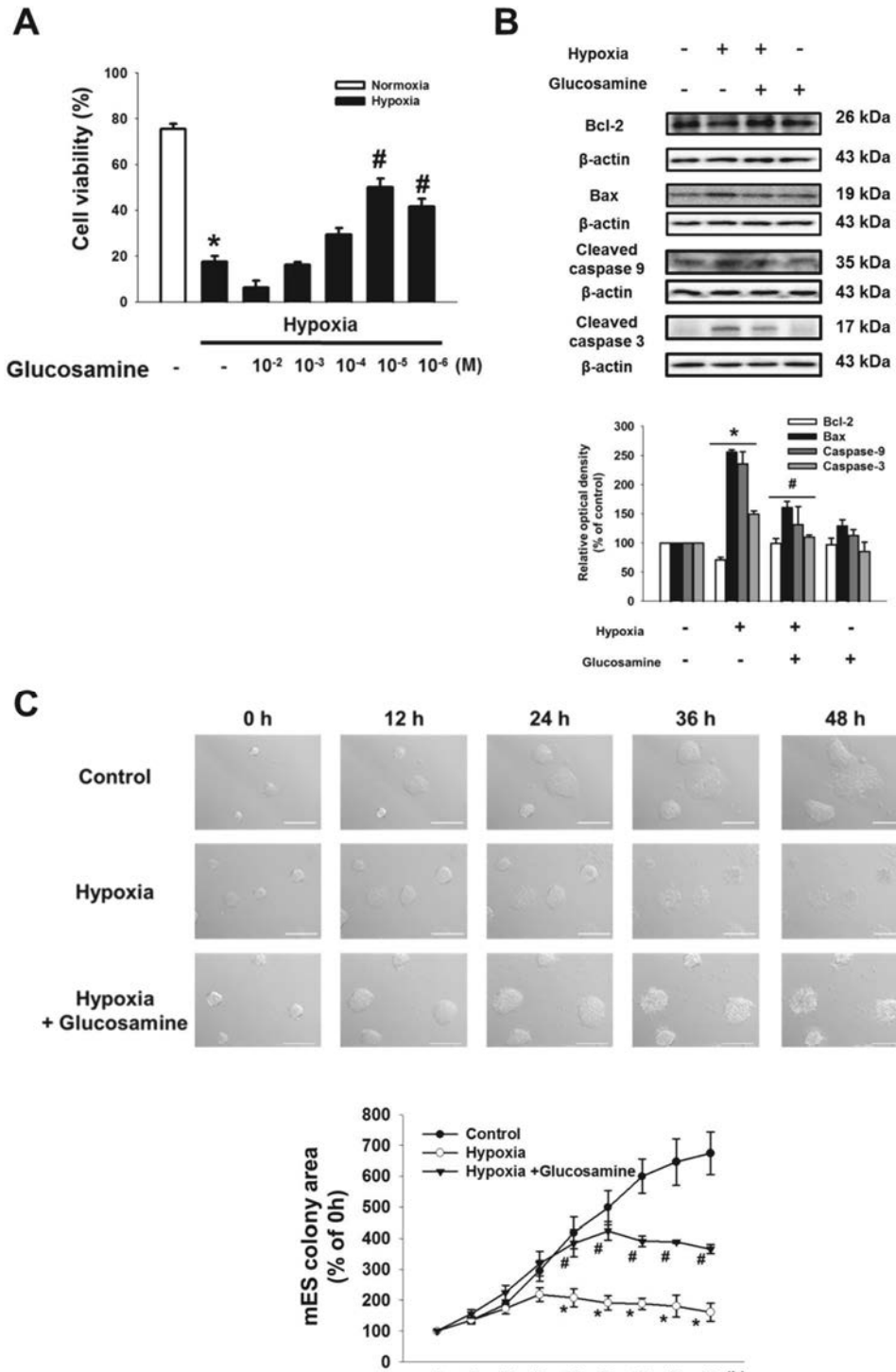
A
Cell viability (%)
Normoxia
Hypoxia
Hypoxia
Glucosamine - - 10-2 10-3 10-4 10-5 10-6 (M)
B
Hypoxia
Glucosamine
Bcl-2
β-actin
Bax
β-actin
Cleaved caspase 9
β-actin
Cleaved caspase 3
β-actin
26 kDa
43 kDa
19 kDa
43 kDa
35 kDa
43 kDa
17 kDa
43 kDa
Relative optical density (% of control)
Bcl-2
Bax
Caspase-9
Caspase-3
C
0 h
12 h
24 h
36 h
48 h
Control
Hypoxia
Hypoxia + Glucosamine
mES colony area (% of 0h)
Control
Hypoxia
Hypoxia +Glucosamine
0 6 12 18 24 30 36 42 48 (h)

Figure 60. Effect of glucosamine on mESCs apoptosis under hypoxia. (A) Cells were pretreated various concentrations of glucosamine (100 mM−1 μM). And then, cells were exposed to hypoxia for 24 h. Cell viability was detected using by trypan blue exclusion cell viability assay. n=6. * indicates $p < 0.05$ vs. normoxia control. (B) Cells were pretreated with glucosamine (10 μM) for 30 min prior to hypoxia treatment. After 24 h of hypoxic incubation, Bcl−2, Bax, cleaved caspase−9, cleaved caspase−3 and β−actin proteins were detected by western blotting. n=3. (C) mESCs colony size was acquired by using live cell imaging microscopy system. Scale bars=100 μm (magnification, × 200). n=3. * indicates $p < 0.05$ vs. control, and # indicates $p < 0.05$ vs. hypoxia treatment alone.

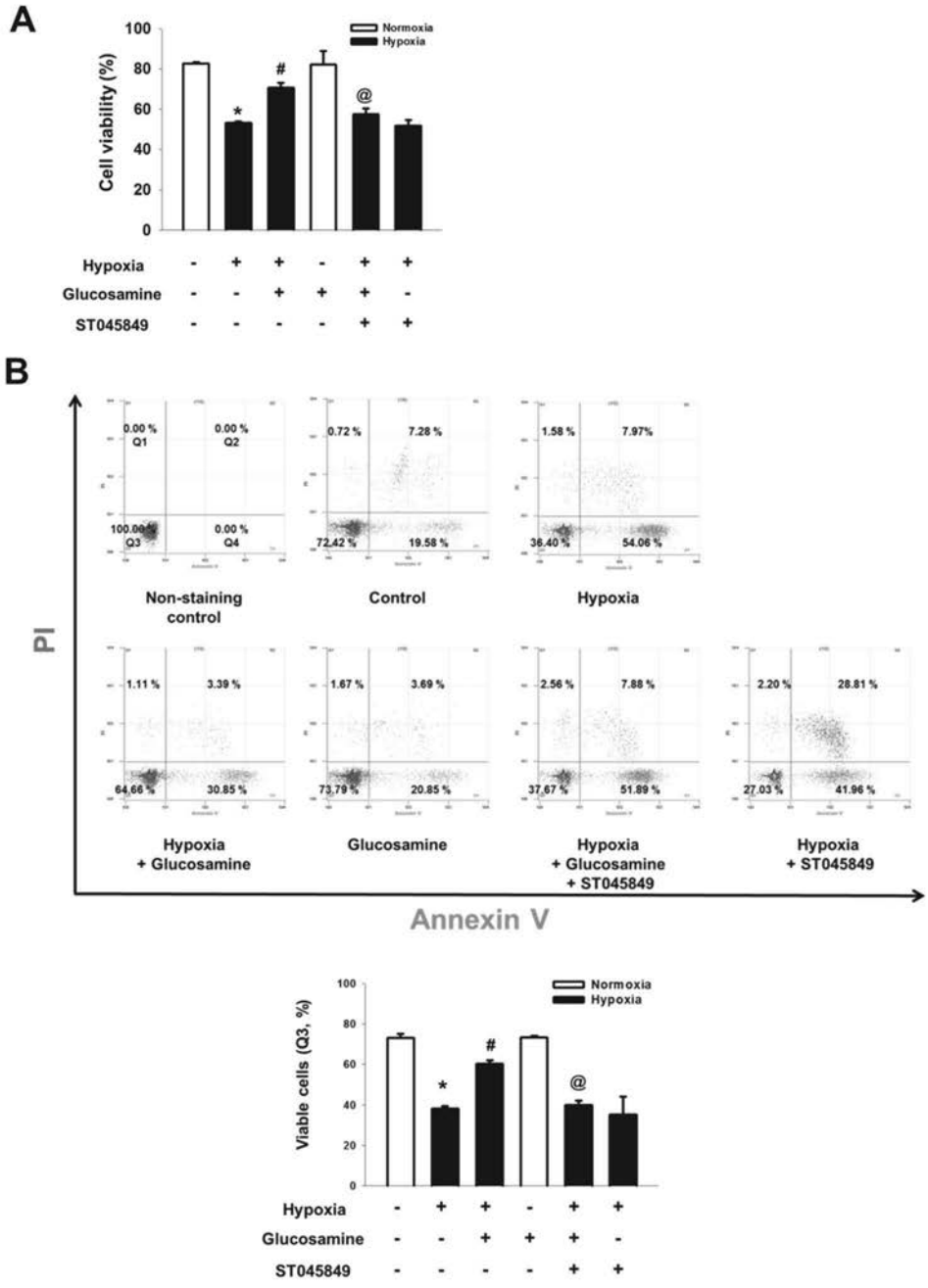
A
Normoxia
Hypoxia
Cell viability (%)
100
80
60
40
20
0
*
#
@
Hypoxia - + + - + +
Glucosamine - - + + + -
ST045849 - - - - + +
B
PI
Annexin V
0.00 %
Q1
0.00 %
Q2
100.00 %
Q3
0.00 %
Q4
Non-staining control
0.72 %
7.28 %
72.42 %
19.58 %
Control
1.58 %
7.97%
36.40 %
54.06 %
Hypoxia
1.11 %
3.39 %
64.66 %
30.85 %
Hypoxia + Glucosamine
1.67 %
3.69 %
73.79 %
20.85 %
Glucosamine
2.56 %
7.88 %
37.67 %
51.89 %
Hypoxia + Glucosamine + ST045849
2.20 %
28.81 %
27.03 %
41.96 %
Hypoxia + ST045849
Viable cells (Q3, %)
100
80
60
40
20
0
Normoxia
Hypoxia
*
#
@
Hypoxia - + + - + +
Glucosamine - - + + + -
ST045849 - - - - + +

Figure 61. Protective role of glucosamine-induced O-GlcNAcylation in mESCs apoptosis under hypoxia. (A) Cells were pretreated ST045849 (20 μM) for 30 min before treatment of glucosamine (10 μM) for 30 min. Subsequently, cells were exposed to hypoxia for 24 h. Cell viability were measured directly using a Petroff-Hausser cell counting chamber. n=6. (B) Cells were immunostained with FITC-conjugated annexin V antibody and PI, and analyzed by flow cytometry. Data are presented as a mean ± S.E. n=4. * indicates $p < .05$ vs. control, # indicates $p < 0.05$ vs. hypoxia treatment alone, and @ indicates $p < 0.05$ vs. hypoxia with glucosamine.

3.3. Effect of O-GlcNAcylation of Sp1 on GPAT1 expression

To determine the effect of hypoxia and glucosamine on lipid metabolic enzyme expressions in mESCs, I assessed mRNA expression levels of *Fasn*, *Acc1*, carnitine palmitoyltransferase 1a (*Cpt1a*), *Cpt1b*, monoacylglycerol lipase (*Magl*), *Gpat1*, *Gpat2*, *Gpat3*, *Gpat4*, *Scd1*, *Scd2*, *Scd3*, *Scd4*, lysophosphatidic acid acyltransferase α (*Lpaat*α), *Lpaat*β, *Lpaat*δ, and *Lpaat*ε. Hypoxia increased the mRNA expression levels of *Gpat1*, *Scd1*, *Lpaat*α, *Lpaat*δ, and *Lpaat*ε, whereas glucosamine treatment increased only *Gpat1* mRNA expression (Fig. 62A). Immunofluorescence staining results showed a 210% increase in the fluorescence intensity of GPAT1 in the glucosamine and hypoxia-treated mESCs and a 137% increase in the fluorescence intensity of GPAT1 in hypoxia-treated mESCs (Fig. 59B). Furthermore, glucosamine-induced GPAT1 expression was inhibited by ST045849 pretreatment (Fig. 63A). However, tunicamycin, a N-linked glycosylation inhibitor, did not affect glucosamine-induced GPAT1 expression of mESCs under hypoxia (Fig. 63B). As shown in figures 64 and 65A, hypoxia and glucosamine stimulated O-GlcNAcylation and nuclear translocation of Sp1. Nuclear translocation of Sp1 was regulated by the addition of ST045849 and the OGA inhibitor PUGNAc. After 24 h of hypoxia

and hypoxia with glucosamine treatments, fluorescence intensity of Sp1 in the PI-stained region increased to 129% and 193%, respectively. However, total fluorescence intensity of Sp1 was not affected by hypoxia and glucosamine treatment (Fig. 65B). In addition, pretreatment with the Sp1 inhibitor mithramycin A (1 μM) suppressed glucosamine-induced GPAT1 expression (Fig. 66A). However, the inhibition of SREBP1 activity by fatostatin pretreatment did not affect glucosamine-induced GPAT1 expression (Fig. 66B). Based on these results, I suggest that O-GlcNAyclation has a critical role in glucosamine-induced Sp1 nuclear translocation, which is followed by regulation of GPAT1 expression in mESCs under hypoxia.

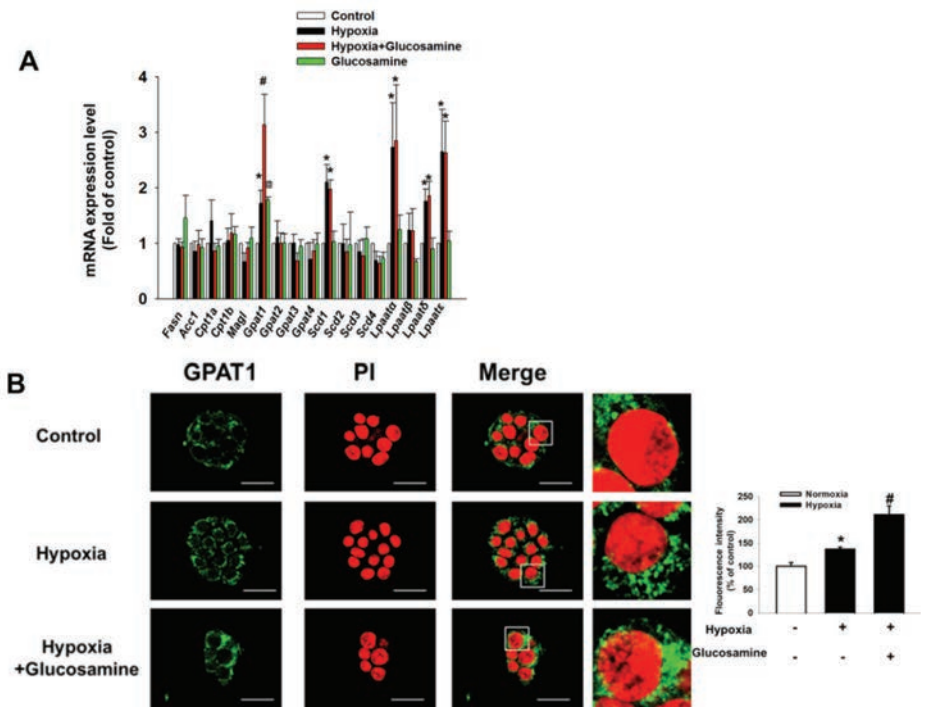

Figure 62. Effect of hypoxia and glucosamine on lipid metabolic enzymes expression. (A, B) Cells were pretreated with glucosamine (10 μM) for 30 min prior to hypoxia treatment. And then, cells were exposed to hypoxia for 24 h. (A) The mRNA expression levels of *Fasn, Acc1, Cpt1a, Cpt1b, Magl, Gpat1, Gpat2, Gpat3, Gpat4, Scd1, Scd2, Scd3, Scd4, Lpaatα, Lpaatβ, Lpaatδ, Lpaatε, and β-actin* mRNA were measured by using real-time PCR. Each mRNA expression was normalized by *β-actin* mRNA expression level. n=6. (B) Cells were immune-stained with GPAT1 antibody and PI. n=3. Data are presented as a mean ± S.E Scale bars = 25 μm (magnification, × 800). * indicates $p < 0.05$ vs. control, # indicates $p < 0.05$ vs. hypoxia treatment alone,

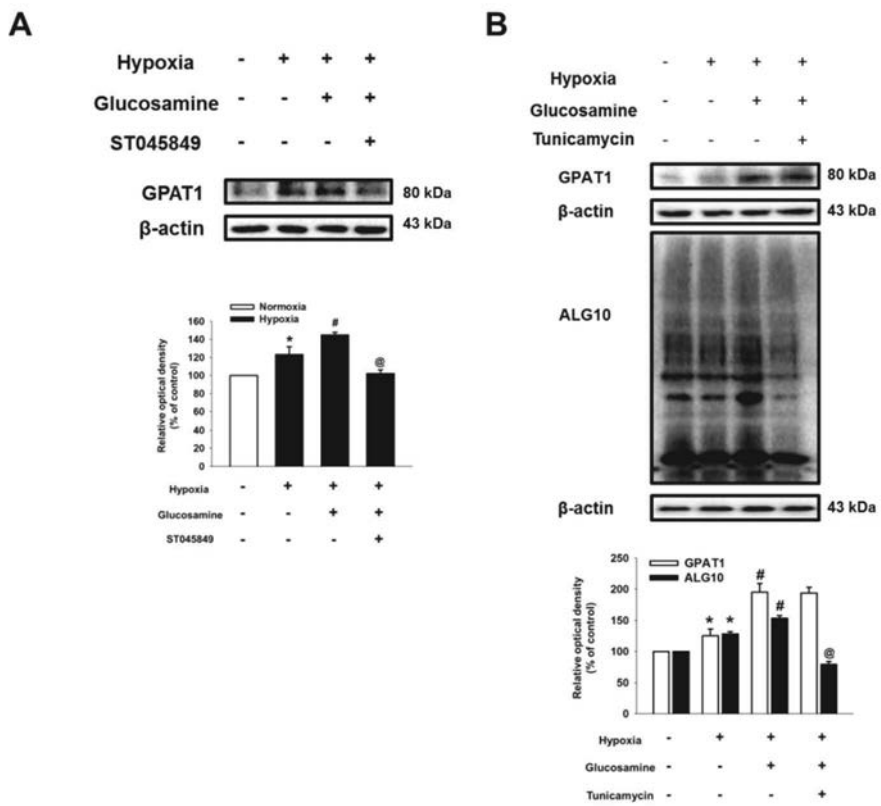

Figure 63. Role of glucosamine-induced O-GlcNAcylation in GPAT1 expression. (A, B) Cells were pretreated with ST045849 (20 μM) or tunicamycin (0.1 μg/ml) for 30 min prior to glucosamine treatment (10 μM) for 30 min, and then cells were exposed to hypoxia for 24 h. (A) GPAT1 protein and β-actin expressions were measured by using western blotting. n=3. (B) Total N-linked glycosylation (ALG10), GPAT1, and β-actin were detected by using western blotting. n=3 * indicates $p < 0.05$ vs. control, # indicates $p < 0.05$ vs. hypoxia treatment, and @ indicates $p < 0.05$ vs. hypoxia with glucosamine.

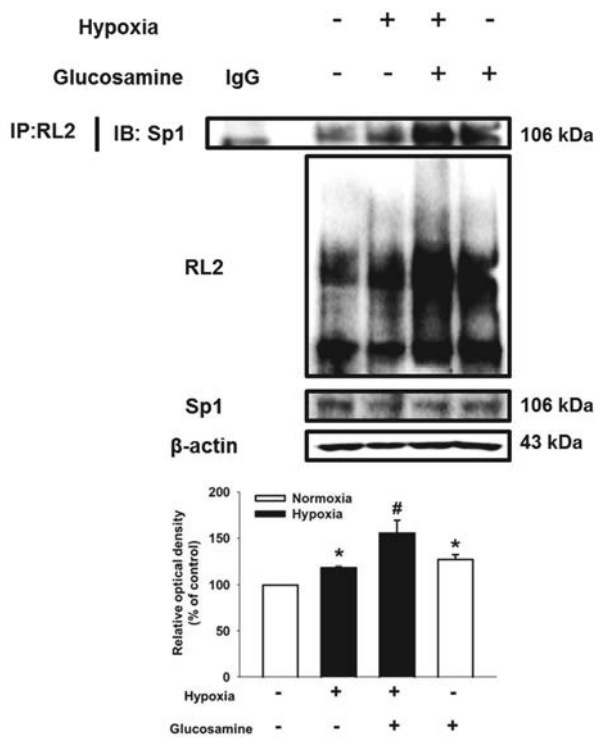

Figure 64. Effect of glucosamine on O-GlcNAcylation of Sp1 in mESCs under hypoxia. (A) Cells were pretreated with glucosamine (10 μM) for 30 min prior to hypoxia treatment. (A) RL-2, Sp1, and β-actin protein expressions were detected by western blotting. n=3. Error bars are presented as a mean ± S.E. n=3. Scale bars = 25 μm (magnification, × 800). * indicates $p < 0.05$ vs. control, # indicates $p < 0.05$ vs. hypoxia treatment alone.

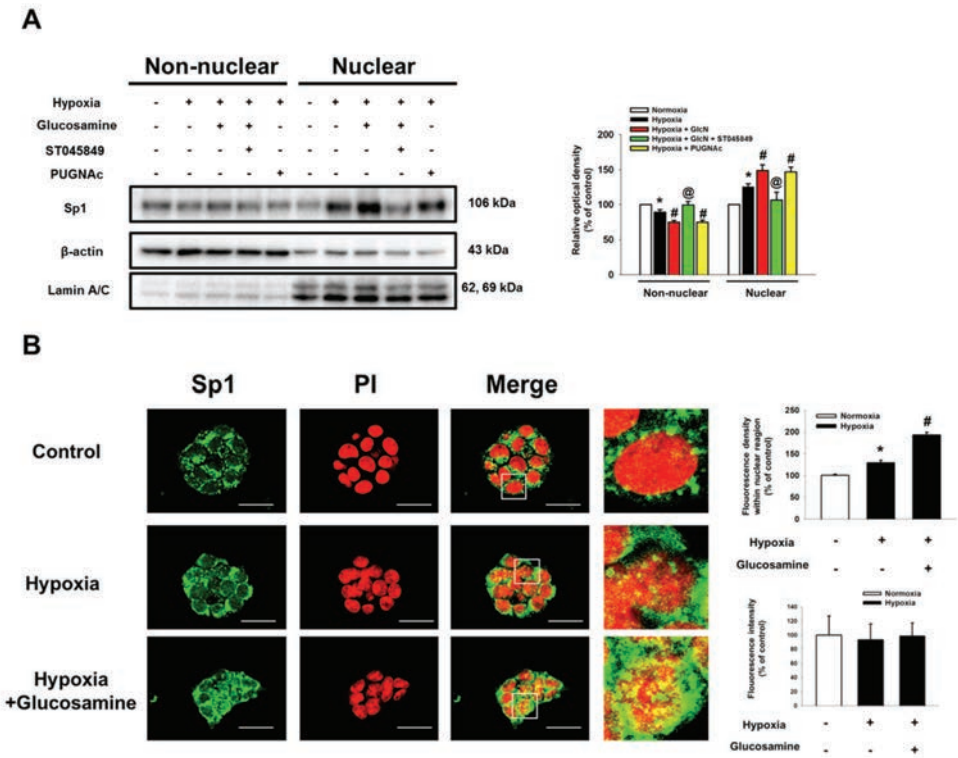

Figure 65. Role of glucosamine-induced O-GlcNAcylation of Sp1 in nuclear translocation of Sp1. (A) Cells were pretreated with ST045849 (20 μM) or PUGNAc (10 μM) prior to glucosamine (10 μM) treatment, and then cell were exposed to hypoxia for 24 h. Harvested cells were fractionized into non-nuclear and nuclear fractions. Sp1, β-actin, and lamin A/C were detected by western blotting. n=3. (B) GPAT1 was detected by immunostaining with GPAT1 antibody. Error bars are presented as a mean ± S.E. n=3. Scale bars = 25 μm (magnification, × 800). * indicates $p < 0.05$ vs. control, # indicates $p < 0.05$ vs. hypoxia treatment alone, and @ indicates $p < 0.05$ vs. hypoxia with glucosamine.

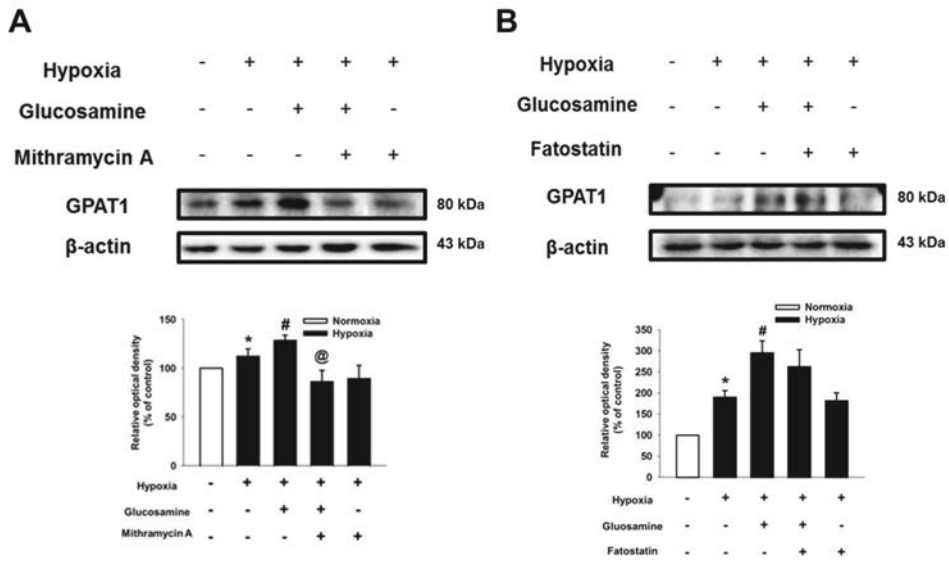

Figure 66. Role of Sp1 and SREBP1 in glucosamine-induced GPAT1 expression. (A) Cells were pretreated mithramycin A (1 μM) for 30 min prior to glucosamine (10 μM) treatment for 30 min. Subsequently, cells were exposed to hypoxia for 24 h. Total protein was extracted, and blotted with GPAT1. n=3. (B) Cells were pretreated with fatostatin (1 μM) prior to glucosamine (10 μM) treatment. And then cells were exposed to hypoxia for 24 h. Total proteins were extracted, and blotted with GPAT1 and β-actin specific antibodies. n=3. * indicates $p < 0.05$ vs. control, # indicates $p < 0.05$ vs. hypoxia treatment alone, and @ indicates $p < 0.05$ vs. hypoxia with glucosamine.

3.4. Role of GPAT1 in mESC apoptosis under hypoxia

Next, to determine the effect of lipid metabolic enzyme's metabolites on mESC survival under hypoxia, I performed cell viability assays after mESC pretreatment with palmitic acid, oleic acid, and LPA. As shown in figure 67, the survival effect of LPA was stronger than that of other substrates in mESCs under normoxia or hypoxia. Subsequently, I treated mESCs with glucosamine and *Gpat1*-specific siRNA to assess the role of GPAT1 on mESC survival under hypoxia. Silencing of GPAT1 expression decreased Bcl-2 expression, but increased Bax, cleaved caspase-9, and cleaved caspase-3 expressions (Fig. 68A). I performed trypan blue exclusion cell viability assays and annexin V/PI FACS analysis to elucidate further the role of GPAT1. The cell viability of *Gpat1* siRNA with glucosamine pretreatment was similar to that of hypoxia-treated mESCs (Fig. 68B and 68C). In addition, hypoxia and glucosamine-induced GPAT1 didn't affect undifferentiation markers Oct3/4 and nanog expressions (Fig 69). These results indicate that glucosamine-induced GPAT1 upregulation in hypoxia significantly affects mESC survival.

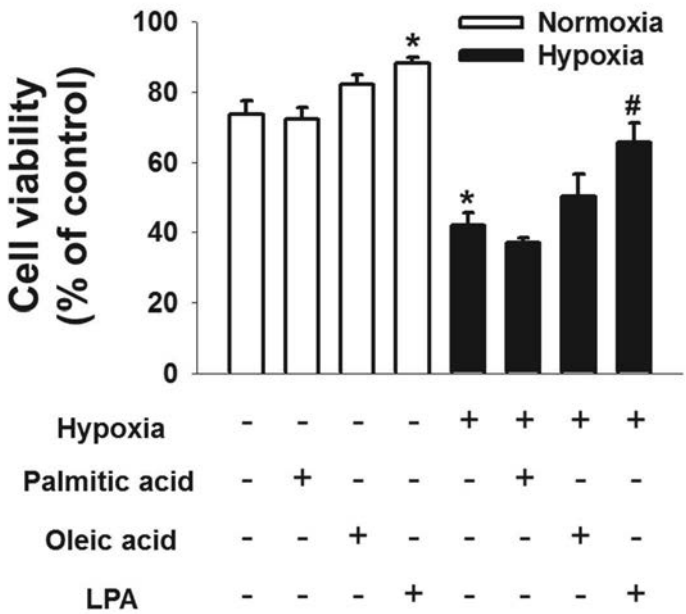

Figure 67. Effect of lipid metabolites on mESCs apoptosis under hypoxia. Cells were pretreated with palmitic acid (10 μM), oleic acid (10 μM), and LPA (0.1 μM) prior to hypoxia treatment for 24 h. Cell viability was measured with trypan blue exclusion assay. Error bars are showed as a mean ± S.E. n=6. * indicates $p < .05$ vs. control, # indicates $p < 0.05$ vs. hypoxia treatment.

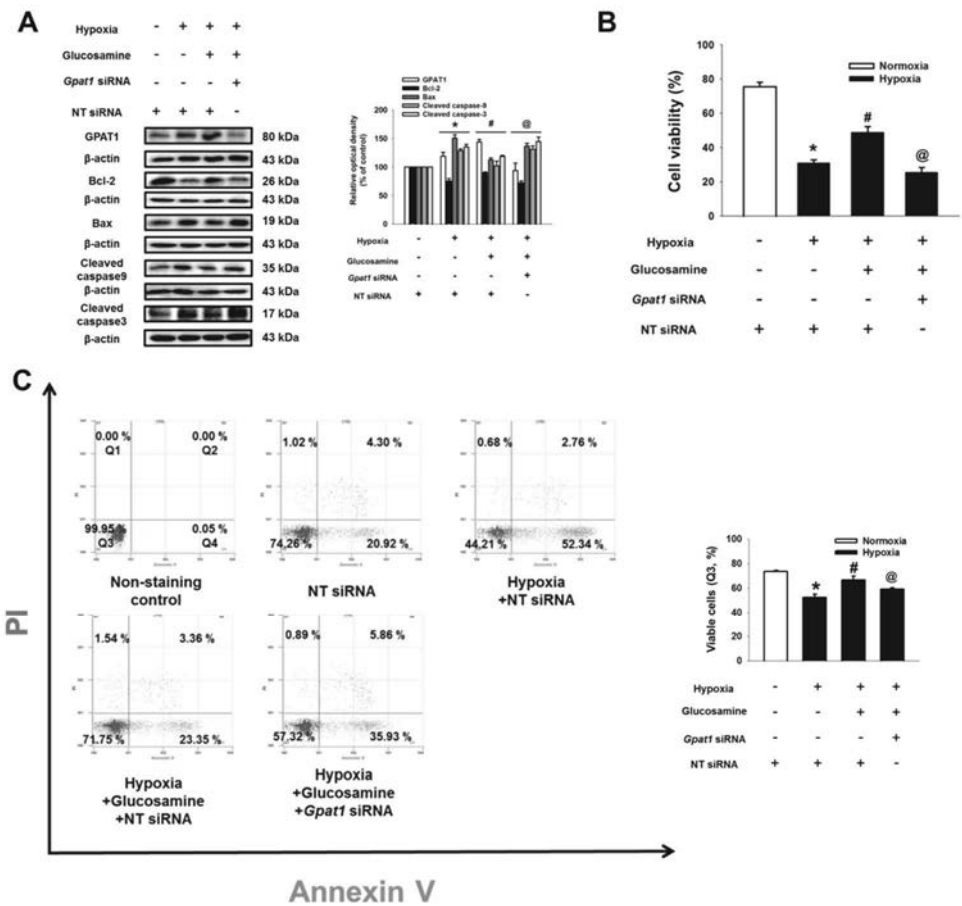

Figure 68. Role of GPAT1 in mESCs apoptosis under hypoxia. (A) Cells were transfected with *Gpat1* and NT siRNAs for 24 h prior to glucosamine (10 μM) treatment for 30 min, and then cells were exposed to hypoxia for 24 h. Expressions of GPAT1, Bcl-2, Bax, caspase-9, caspase-3, and β-actin are shown. n=3. (B) Cell viability was measured directly by trypan blue exclusion assay using counting chamber. n=6. (D) Viable cells were measured by using annexin V/PI flow cytometry analysis. n=4. * indicates $p < 0.05$ vs. control, # indicates $p < 0.05$ vs. hypoxia treatment alone,

and @ indicates $p < 0.05$ vs. hypoxia with glucosamine.

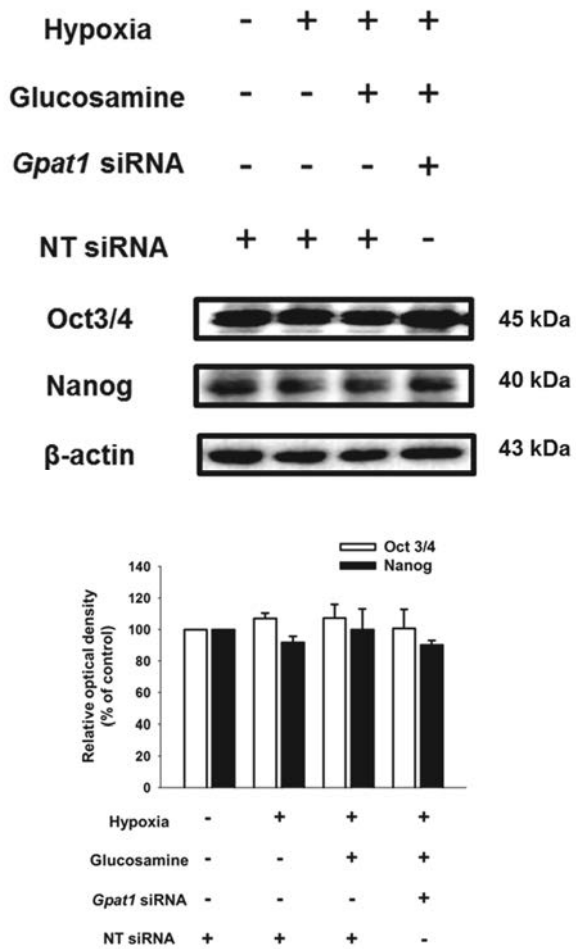

Figure 69. Role of GPAT1 in Oct3/4 and Nanog expressions in mESCs apoptosis under hypoxia. Cells were transfected with *Gpat1* and NT siRNA. And then, cells were exposed to hypoxia for 24 h. Total proteins were extracted, and blotted with Oct3/4, nanog and β-actin specific antibodies. n=3.

3.5. Role of glucosamine-induced GPAT1 in mTOR activation and apoptosis in mESCs under hypoxia

Subsequently, I investigated the detailed signaling pathway by which GPAT1 induces mESC survival under hypoxia. As shown in Fig. 70, glucosamine treatment phosphorylated mTOR, which was blocked by *Gpat1* siRNA transfection. I confirmed that glucosamine treatment increased Bcl-2 expression, and decreased Bax, cleaved caspase-9 expressions and cytochrome c release, which were reversed by 10 nM of mTOR inhibitor rapamycin pretreatment (Fig 71A and 71B). In addition, glucosamine treatment increased [^{3}H]-thymidine incorporation level of mESCs under hypoxia, which was blocked by rapamycin addition (Fig. 71C).

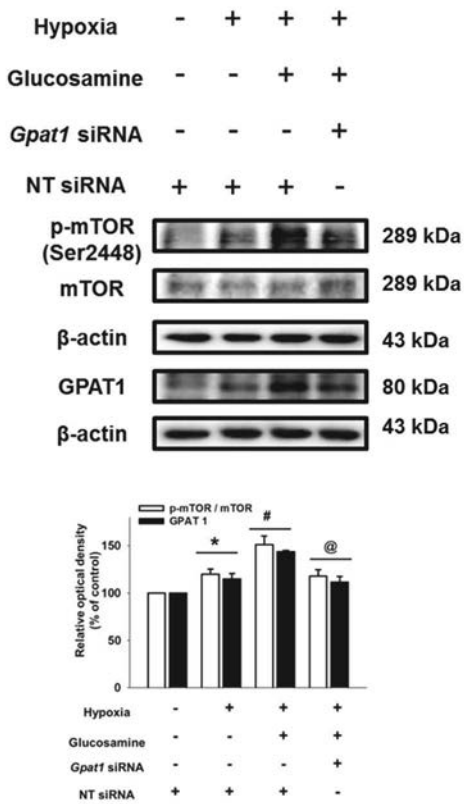

Figure 70. Role of glucosamine-induced GPAT1 in mTOR phosphorylation in mESCs under hypoxia. (A) Cells were transfected with *Gpat1* and NT siRNA for 24 h prior to glucosamine (10 μM) for 30 min. Subsequently, cells were exposed to hypoxia treatment for 24 h. Harvested samples are lysed, and p-mTOR, GPAT1, and β-actin protein expressions were measured by using western blotting. n=3. * indicates $p < 0.05$ vs. control, # indicates $p < 0.05$ vs. hypoxia treatment, and @ indicates $p < 0.05$ vs. hypoxia with glucosamine.

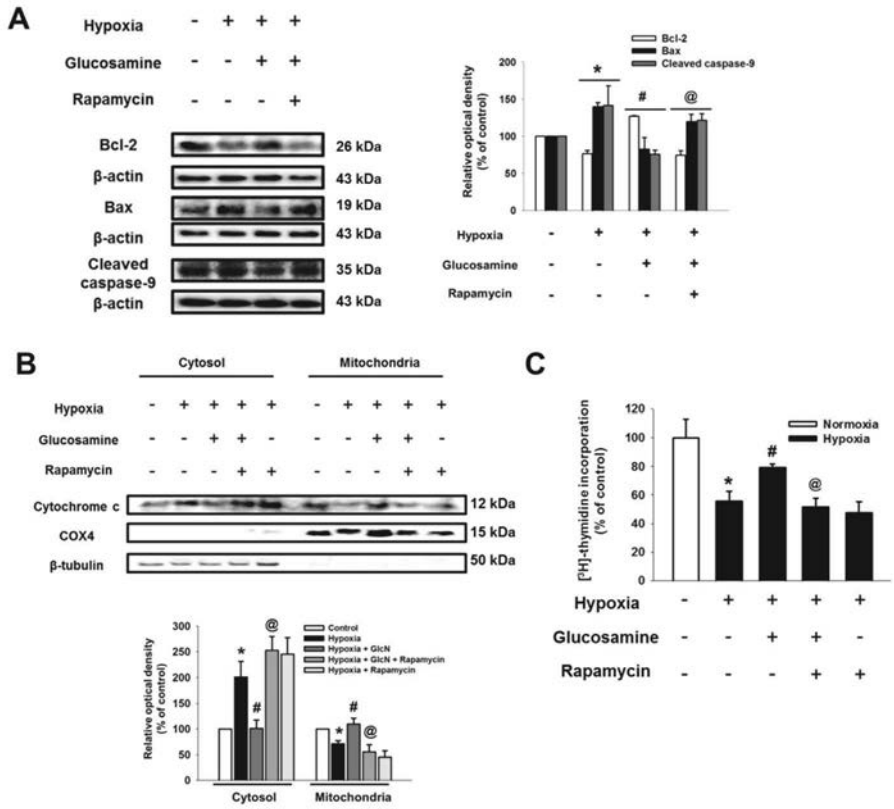

Figure 71. Involvement of mTOR in GPAT1-induced anti-apoptosis of mESCs under hypoxia. (A) Cells were pretreated with rapamycin (10 nM) or glucosamine (10 μM) prior to hypoxia for 24 h. Expressions of Bcl-2, Bax, cleaved caspase-9, and β-actin are shown. n=3. (B) Cytochrome c, COX4 and β-tubulin in the cytosolic and mitochondrial fraction were detected by western blot. (C) Cells were pulsed with 1 μCi of [^{3}H]-thymidine for 1 h prior to counting. Data are reported as a mean ± S.E. n=6. * indicates $p < 0.05$ vs. control, # indicates $p < 0.05$ vs. hypoxia treatment, and @ indicates $p < 0.05$ vs. hypoxia with glucosamine.

3.6. Effect of LPA on mTOR activation and survival in mESCs under hypoxia

Next, I treated LPA to determine the role of GPAT1 metabolite in mESC apoptosis under hypoxia. I examined cell viability after 24 h of hypoxic incubation with various concentrations of LPA (1 nM – 1 μM). The 0.1 and 1 μM LPA pretreatments increased significantly the cell viability of mESCs under hypoxia (Fig. 72A). In addition, hypoxia and hypoxia with LPA pretreatment increased phosphorylations of mTOR and mTOR substrates (S6K1 and 4EBP1). The LPA-induced phosphorylation of mTOR and mTOR substrates were suppressed by pretreatment with the LPA receptor inhibitor Ptx (Fig. 72B). After hypoxia and hypoxia with LPA treatment, the fluorescence intensity of p-mTOR in mESC colonies increased to 187% and 342%, respectively (Fig. 72C). Treatment with LPA increased Bcl-2 expression and decreased Bax, cleaved caspase-9, and cleaved caspase-3 expressions, which were reversed by rapamycin addition (Fig. 73A). Cell viability assay and annexin V/PI FACS analysis results showed that rapamycin treatment reduced LPA-induced mESC survival (Figs. 73B and 73C). In addition, I performed several experiments to identify the role of NF-κB in mESC apoptosis under hypoxia. I found that LPA increased phosphorylation (Ser 536) of NF-κB, the activation marker (Fig. 74A). However, NF-κB inhibitor SN-50 didn't

affect LPA-induced survival effect on mESCs under hypoxia (Fig. 74B). Based on these results, I suggest that LPA activates the mTOR pathway, resulting in mESC survival under hypoxia.

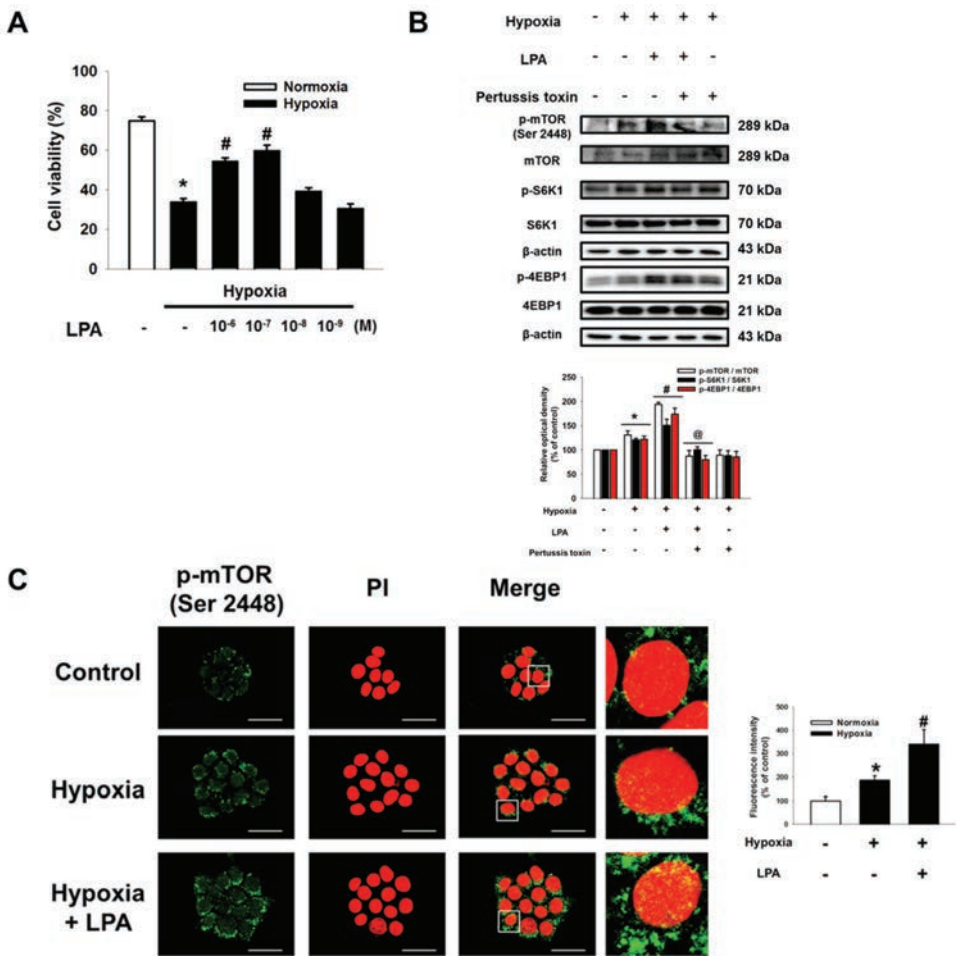

Figure 72. Effect of LPA on mTOR phosphorylation and survival of mESCs under hypoxia. (A) Cells were pretreated with various concentrations of LPA (10^{-6} M−10^{-9} M) prior to hypoxia for 24 h. Cell viability was measured by trypan blue exclusion assay. n=6. (B) Cells were pretreated with pertussis toxin (100 ng/ml) for 30 min prior to LPA treatment (0.1 μM) for 30 min. Cells were exposed to hypoxia treatment for 24 h. Total samples were blotted with p−mTOR, mTOR, p−S6K1, S6K1, p−4EBP1, 4EBP1, and β−actin.

n=3 (C) p-mTOR was immuno-stained with p-mTOR antibody, and counter-stained with PI. n=3. Data are presented as a mean ± S.E. * indicates $p < 0.05$ vs. control, # indicates $p < 0.05$ vs. hypoxia treatment alone, and @ indicates $p < 0.05$ vs. hypoxia with LPA.

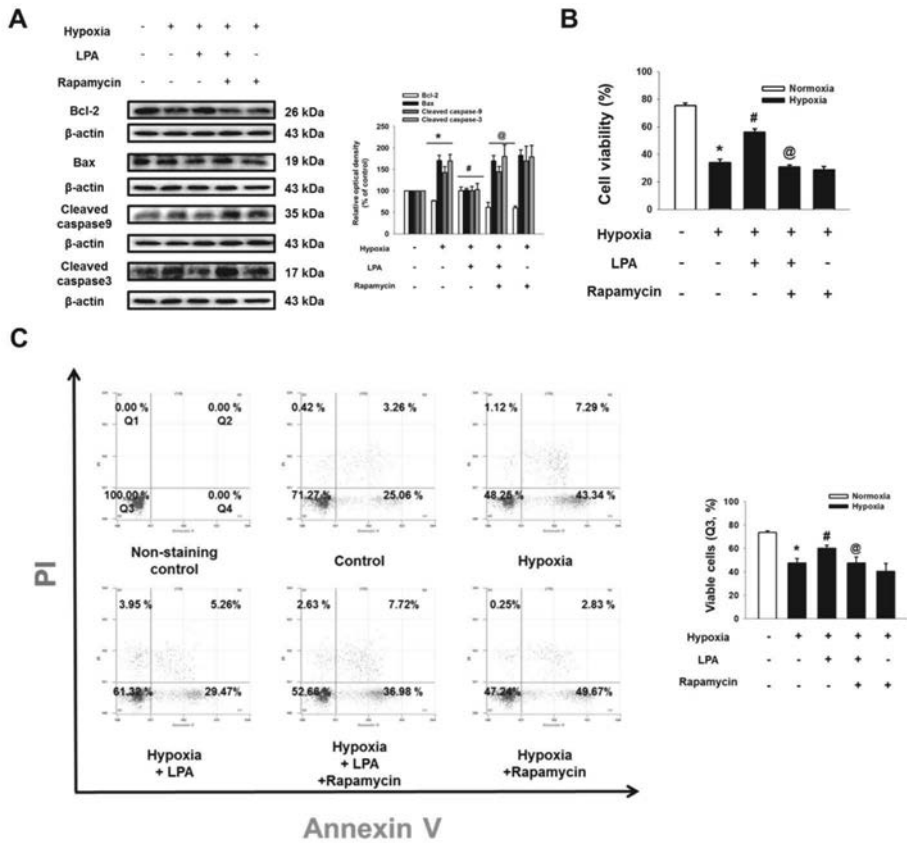

Figure 73. Protective role of LPA-activated mTOR in apoptosis of mESCs under hypoxia. (A) Cells were pretreated with rapamycin (10 nM) or LPA (0.1 μM) prior to hypoxia for 24 h. Samples were blotted with Bcl-2, Bax, cleaved caspase-9, cleaved caspase-3, and β-actin. n=3. (B) Cell viability was measured by using cell counter. n=6. (C) Viable cells were measured by flow cytometry analysis. n=4. Data are presented as a mean ± S.E. * indicates p < 0.05 vs. control, # indicates p < 0.05 vs. hypoxia, and @ indicates p < 0.05 vs. hypoxia with LPA.

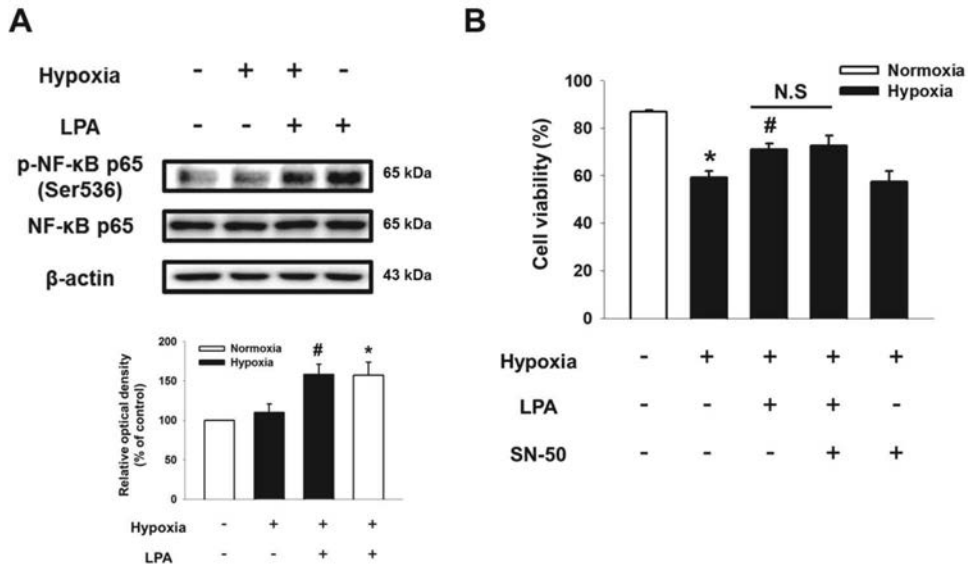

Figure 74. Role of NF-κB phosphorylation in LPA-induced survival of mESCs under hypoxia. (A) The mESCs were treated with hypoxia or LPA. And then, p-NF-κB p65 (S536), NF-κB p65 and β-actin were detected by using western blotting. n=3. (B) Measurement of cell viability was performed by trypan blue exclusion cell viability assay. Cells were pretreated with SN-50 (1 μM) prior to LPA (0.1 μM) for 30 min. Subsequently, cells were exposed to 24 h of hypoxia. Data are presented as a mean ± S.E. n=6. * indicates $p < 0.05$ vs. control, and # indicates $p < 0.05$ vs. hypoxia treatment alone. N.S indicates not statistically significant.

3.6. Role of GPAT1 on mESC survival and skin flap survival

I performed mouse skin flap surgery to test the protective roles of glucosamine and GPAT1 on transplanted mESC survival (Fig. 75A). An extended necrotic area in the central and distal part of the flap appeared in the vehicle, glucosamine, and LPA control groups. The necrotic area of the NT siRNA-transfected mESCs group was smaller than that of vehicle group. The necrotic region in the skin flap was reduced to a significantly greater extent in NT siRNA-transfected mESCs with either glucosamine or LPA than that in the NT siRNA-transfected mESCs group. However, the necrotic area of the *Gpat1* siRNA-transfected mESCs with glucosamine treatment group was larger than that of the NT siRNA-transfected mESCs with glucosamine treatment group (Fig. 75B). Histological evaluation, via H&E staining, showed an intact epithelial layer in the NT siRNA-transfected mESCs with glucosamine or LPA treatments, which indicates that mESCs with glucosamine treatment can stimulate skin flap survival under hypoxia conditions (Fig. 76A). Immunohistochemistry results showed that glucosamine and LPA significantly increased the number of BrdU-positive mESCs in the skin flap. The number of *Gpat1* siRNA-transfected mESCs in the glucosamine treatment group was similar to that in the NT siRNA-transfected mESCs alone group (Fig. 76B).

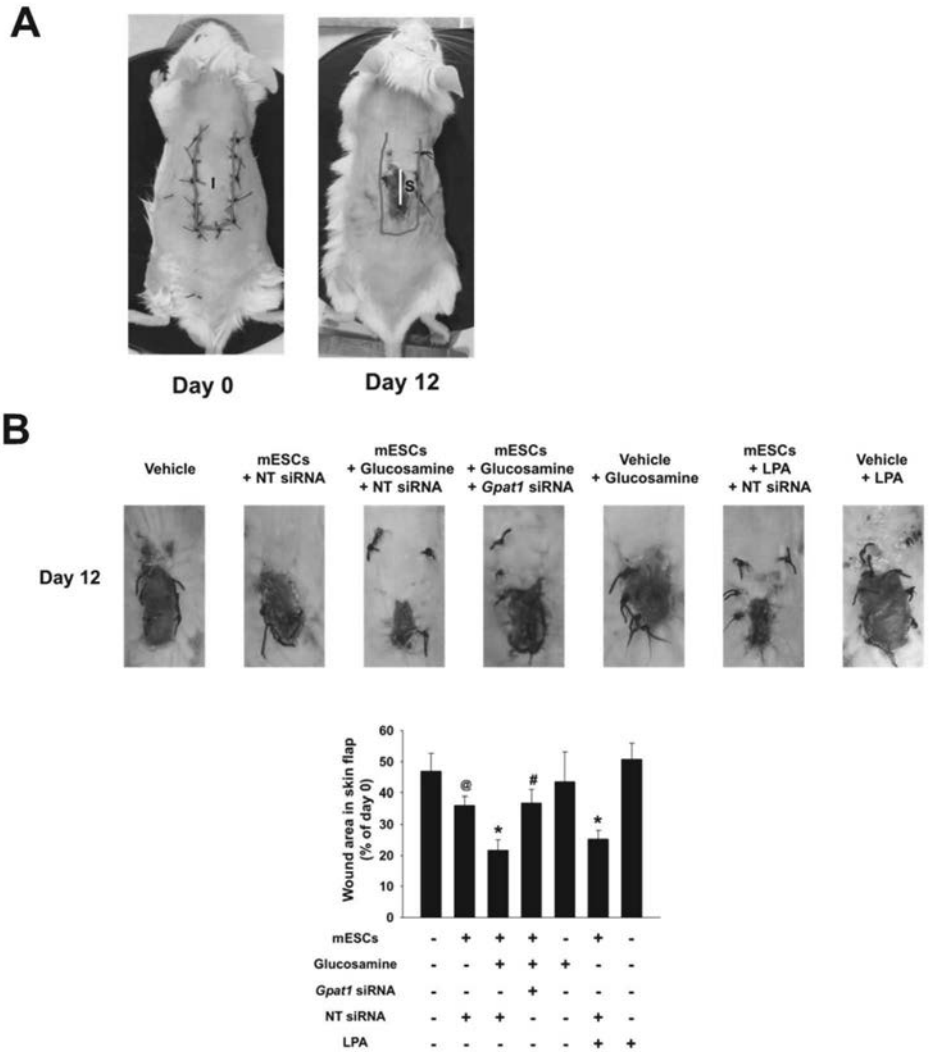

Figure 75. Role of glucosamine-induced GPAT1 in skin necrosis. (A) NT siRNA transfected cells are injected in the center region (I) of the flap. At post-injection day 12, all tissue samples (S) including injection site in are excised and collected. (B) Representative gross images of skin flap were obtained at day 12 after flap surgery. Necrotic area in skin flap was analyzed by using

ImageJ software. Error bars indicate a mean ± S.E. n=5. * indicates $p < 0.05$ vs. mESCs group, and # indicates $p < 0.05$ vs. mESCs with glucosamine group.

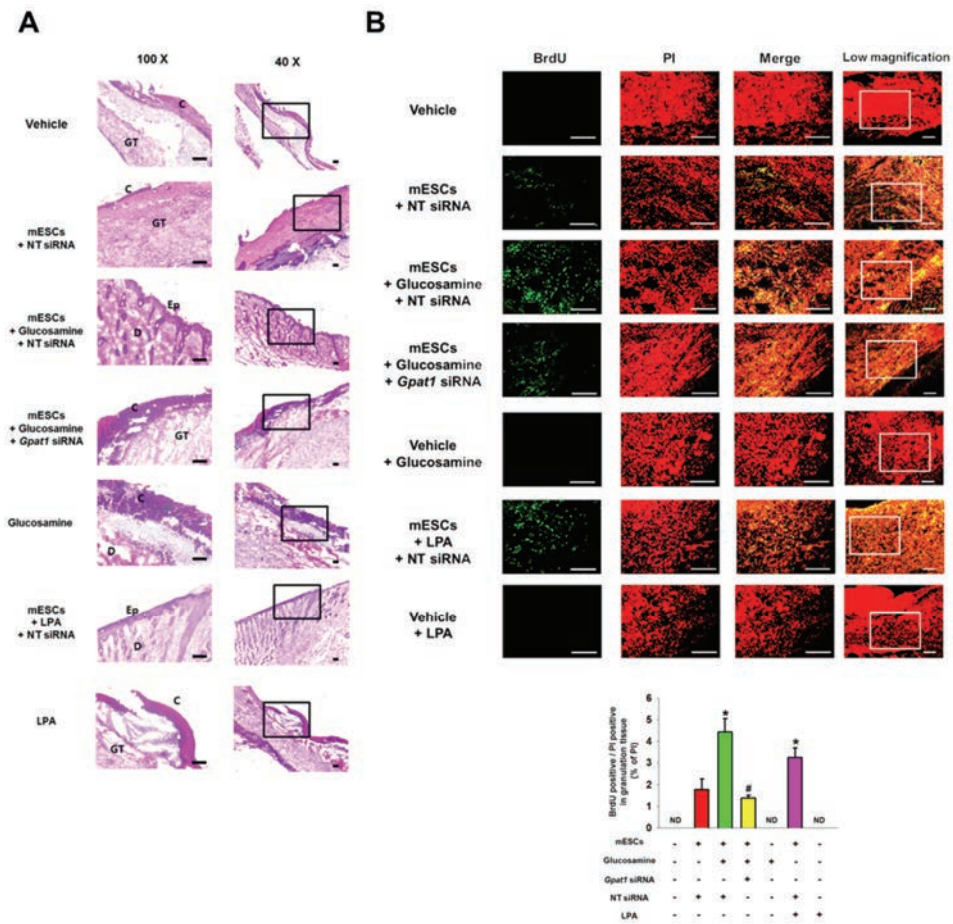

Figure 73. Role of GPAT1 in mESCs survival in the mouse skin flap model. (A) Tissue samples were stained with hematoxylin and eosin. Scale bars, 100 μm (magnification, $\times$40 and $\times$100). (B) BrdU and PI stained cells were analyzed by using MetaMorph software. Scale bars, 200 μm (magnification, $\times$100 and $\times$200). * indicates $p < 0.05$ vs. mESCs group, and # indicates $p < 0.05$ vs. mESCs with glucosamine group. ND, not detected. Abbreviations: C, crust; Ep, epidermis; D, dermis; GT, granulated tissue.

4. DISCUSSION

The results of the present investigation demonstrate the role of GPAT1 expression via augmented O-GlcNAcylation of Sp1 in mESC survival under hypoxia (Fig. 77). Although the effect of hypoxia on stem cell survival is not elucidated fully (Forsyth et al., 2006; Theus et al., 2008), I observed that increasing the exposure of mESC to hypoxia resulted in duration-dependent apoptosis. Mishra *et al.* reported that an increase in the Bax/Bcl-2 ratio is essential for caspase-9 mediated mitochondrial apoptosis under hypoxia (Mishra et al., 2006). In this study, hypoxia and glucosamine treatments increased O-GlcNAc level, and glucosamine augmented O-GlcNAcylation suppressed hypoxia-induced mESC apoptosis. In support of my results, there are several reports that glucosamine activates HBP flux and has a protective role via O-GlcNAcylation in other types of cells including cardiomyocytes and retinocytes (Chen et al., 2015; Linington et al., 1990; Pouwels et al., 2001). Moreover, my previous study established that glucosamine induces OGT expression, which is followed by an increase in O-GlcNAc levels in mESCs (Jeon et al., 2014). However, a high dose (>1 mM) of glucosamine did not induce the mESC protective effect. There are several reports showing that a high level of glucosamine-induced HBP activation

generates excess ROS, leading to apoptosis (Lima et al., 2012; Singh et al., 2007). In addition, there are several reports suggesting that O-GlcNAc signaling contributes to undifferentiation and self-renewal (Jang et al., 2012; Speakman et al., 2014). Furthermore, several reports suggest that hypoxia-induced O-GlcNAc signaling regulates metabolic alteration as well as survival responses against noxious stimuli in stem cells (Ferrer et al., 2014; Gutierrez-Uzquiza et al., 2012; Song et al., 2014). These results indicate the need to clarify the interaction of O-GlcNAc signaling-mediated cell survival with metabolic alteration. Based upon current and past results, I suggest that O-GlcNAcylation is a key factor in maintaining of stem cell populations *in vivo*.

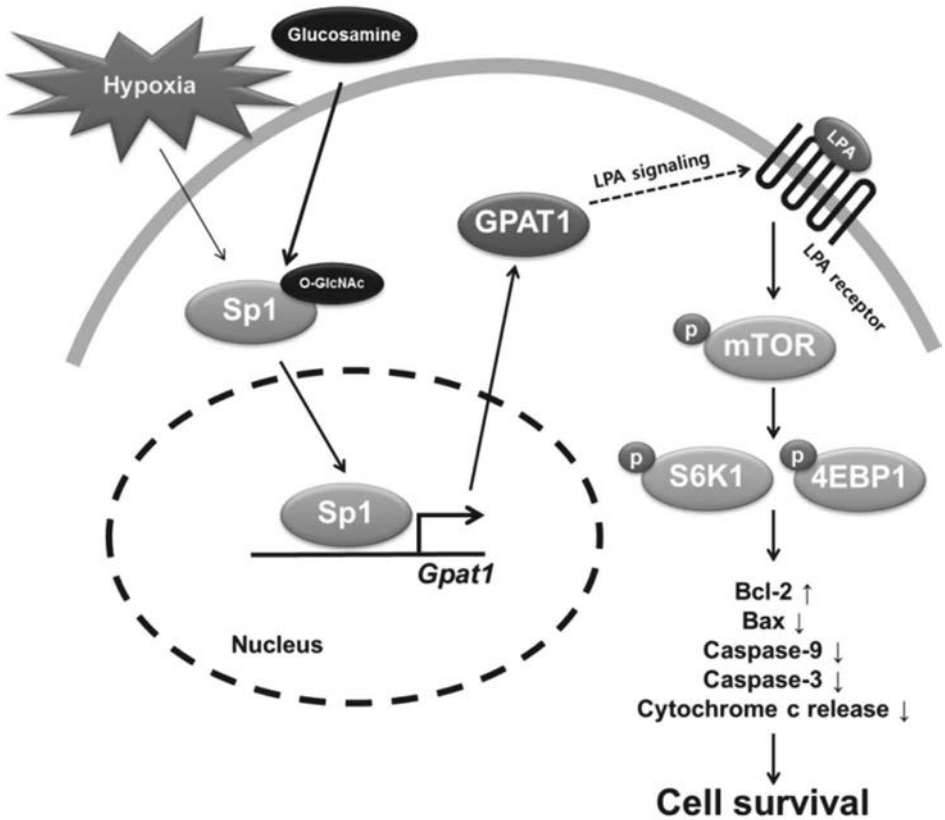

Figure 77. The proposed model for signaling pathways involved in glucosamine-induced mESCs survival under hypoxia. Glucosamine stimulates O-GlcNAcylation of Sp1 to activate GPAT1 gene transcription. Induction of GPAT1 activates LPA receptor, leads to mTOR phosphorylation-mediated anti-apoptosis in mESCs under hypoxia.

There are several recent reports on the interaction between lipid metabolic alteration by hypoxia and stem cell regulation. Indeed, several researchers have reported that hypoxia modulates lipid metabolic processes including fatty acid synthesis and β-oxidation (Furuta et al., 2008a; Rankin et al., 2009). My present study shows that hypoxia increased levels of metabolic enzymes that contribute to fatty acid and bio-lipid metabolite production and phosphatidic acid signaling. These lipid metabolites have been reported to have the ability to control stem cell functions such as migration, proliferation, and survival (Ben-David et al., 2013; Foster. 2013; Pebay et al., 2007). In addition, alteration of lipid metabolic enzymes profiles by hypoxia appears stem cell type-specific. My previous paper reported that hypoxia predominantly increased FASN in human mesenchymal stem cells (hMSCs), which regulates hMSC proliferation and migration (Lee et al., 2015). Uri *et al.* reported that SCD1 inhibition eliminated undifferentiated human ESCs selectively, but my previous study showed that SCD1 inhibition did not affect hMSC proliferation (Ben-David et al., 2013). Taken together, these results indicate a difference in lipid sensitivity between stem cell types. In particular, it is noteworthy that glucosamine upregulates GPAT1 expression through O-GlcNAcylation, which plays an important role in mESC survival under hypoxia. GPAT1 is a lipid metabolic enzyme localized at the mitochondrial outer membrane and is a major form of four GPAT

isotypes (Coleman et al., 2004; Gonzalez-Baro et al., 2007). GPAT1 metabolizes glycerol-3-phosphate with long chain fatty acyl-CoA to form LPA (Sul et al., 1998). Although no reports have demonstrated a role of GPAT1 in stem cells, several investigators have reported that GPAT1 is a factor potentially controlling various cellular processes such as lipid metabolism, mitochondrial dynamics, apoptosis, and proliferation in other cell types (Hammond et al., 2007; Ohba et al., 2013; Wendel et al., 2013). Further investigation into GPAT1's effect and the detailed mechanism for that effect in stem cells will provide information important for stem cell regulation. As Sp1 is emerging as a potential therapeutic target in metabolic diseases, interest in its effect on metabolic and nutritional regulation is increasing (Liu et al., 2012a; Solomon et al., 2008; Zhang et al., 2014). Furthermore, Sp1 is a transcription factor binding to the human GPAT1 promoter and regulating gene expression (Chen et al., 1997b; Sul & Wang. 1998). In addition, there are several reports suggesting that a HBP flux-mediated protective effect is induced via O-GlcNAcylation of specific proteins (Champattanachai et al., 2007; Schaffer et al., 2000). Moreover, O-GlcNAcylation of Sp1 is important for its subcellular localization, stabilization, and transcriptional regulation (Goldberg et al., 2000; Kudlow. 2006; Solomon et al., 2008). Taken together, these findings indicate that Sp1 regulation by O-GlcNAcylation can be a practical approach to metabolic regulation of stem cell fate.

Furthermore, my results demonstrate that O-GlcNAcylation-mediated GPAT1 expression significantly suppresses hypoxia-induced mESC mitochondrial apoptosis and increases proliferation via mTOR activation, which may suggest that glucosamine-induced resistance against hypoxia is attributed to GPAT1 signaling-mediated mTOR activation. The GPAT1 metabolite LPA has been reported as a potential bioactive lipid molecule that can modulate stem cell function (Costa et al., 2013; Dottori et al., 2008; Liu et al., 2009a; Ortlepp et al., 2013). You *et al.* reported that LPA activates the mTOR pathway via an LPA receptor-mediated ERK activation pathway (You et al., 2012). In addition, there are reports that mTOR is a nutrient-sensing molecule and can regulate stem cell survival (Kumar et al., 2014; Mungamuri et al., 2006; Zhou et al., 2007). A previous study reported that AKT/mTOR pathway activation increased the expression of anti-apoptotic proteins Bcl-2 and Bcl-xL, resulting in cell survival and growth. This result suggests that there may be interaction between GPAT1 signaling-mediated mTOR activation and apoptosis-related protein expression (Marinov et al., 2009). In this study, I demonstrated that glucosamine-induced GPAT1 expression increased mESC survival after transplantation; moreover, it prevented ischemia-induced flap necrosis *in vivo* in an animal model.

GENERAL CONCLUSION

Present study showed that hypoxia-regulated lipid metabolic enzymes expression has a critical role in proliferation, migration and survival of UCB-hMSCs and mESCs. According to previous reports, the control of lipid metabolism plays a key role in the regulation of stem cell fate. In addition, other investigators suggested that application of lipid metabolites such as essential FAs is a safe and practical approach to stem cell therapy (Kang et al., 2014). My study also revealed that lipid metabolites production induced by hypoxia and lipid metabolites treatment improve the proliferation, migration and survival of UCB-hMSC and mESCs. Moreover, O-GlcNAcylation induction and BNIP3-mediated mitophagy as key regulators for lipid metabolic enzyme expression in stem cells under hypoxia.

My study demonstrated that hypoxia activates HIF-1α/FASN/mTORC1 signaling pathway enhancing the UCB-hMSC proliferation and migration. This finding suggests that FASN-dependent mTORC1 signaling activation is a major signaling pathway which links hypoxia-induced lipogenesis to proliferation and migration of UCB-hMSCs. In addition, palmitic acid stimulates UCB-hMSCs proliferation and migration via mTORC1 activation, thereby producing cell proliferation and migration levels are similar to those obtained from hypoxia treatment. Similary, recent

investigators presented that FASN-dependent lipogenesis is critical factor for determining stemenss of ESCs and iPSCs (Wang et al., 2017; Yasumoto et al., 2016). Therefore, previous and present studies suggest that FASN is a prospective candidate which has a potential as part of novel strategies for regenerative treatments that use stem cells.

Next, my study revealed that BNIP3-mediated mitophagy occurs via ROS-dependent HIF-1α and FOXO3 activation, which are critical for SREBP1/FASN-dependent lipogenesis, migration and anti-apoptosis of UCB-hMSCs. Moreover, there are several evidence showing the key role of mitophagy in lipid metabolic regulation provides physiological implication and therapeutic potential of mitophagy-regulated lipid metabolism (Glick et al., 2012; Hamacher-Brady et al., 2016). Based upon those findings, present study suggests that BNIP3-dependent mitophagy induced by hypoxia can be a potential candidate for efficient lipid metabolic conversion and physiological regulation of stem cells exposed to hypoxia.

Furthermore, I demonstrated that glucosamine-induced O-GlcNAcylation of Sp1 stimulates GPAT1 expression, which plays a protective role in the survival of mESCs under hypoxia. To my knowledge, this is the first detailed identification of signaling pathways that allows glucosamine-induced O-GlcNAcylation to

control lipid metabolic alteration and provide cytoprotection against hypoxia in stem cells; thus, suggesting that lipid metabolic regulation via O-GlcNAcylation could be a novel strategy for improving the survival rate of ESCs. Consistent with my results, recent studies suggested the O-GlcNAcylation as a critical mediator of nutritional status to regulate key metabolic pathways (Ferrer et al., 2016). Also, elevation of O-GlcNAcylation by OGT stimulates SREBP1, which leads to lipogenesis and cell survival (Sodi et al., 2017). Previous and present evidences present a regulatory role of O-GlcNAcylation-regulated lipid metabolism in stem cell fate. Moreover, further investigation into the identification of key metabolic pathways regulated by O-GlcNAcylation that can regulate stem cell fate may hold additional promise for various stem cell applications.

In conclusion, present study demonstrated that 1) hypoxia-induced FASN expression activates mTORC1 signaling, which leads to proliferation and migration of UCB-hMSCs, 2) hypoxia-induced BNIP3-dependent mitophagy stimulates lipogenesis, migration and anti-apoptosis of UCB-hMSCs, and 3) the enhancement of O-GlcNAc signaling by glucosamine protects against apoptosis of mESCs through GPAT1 expression (Fig. 78).

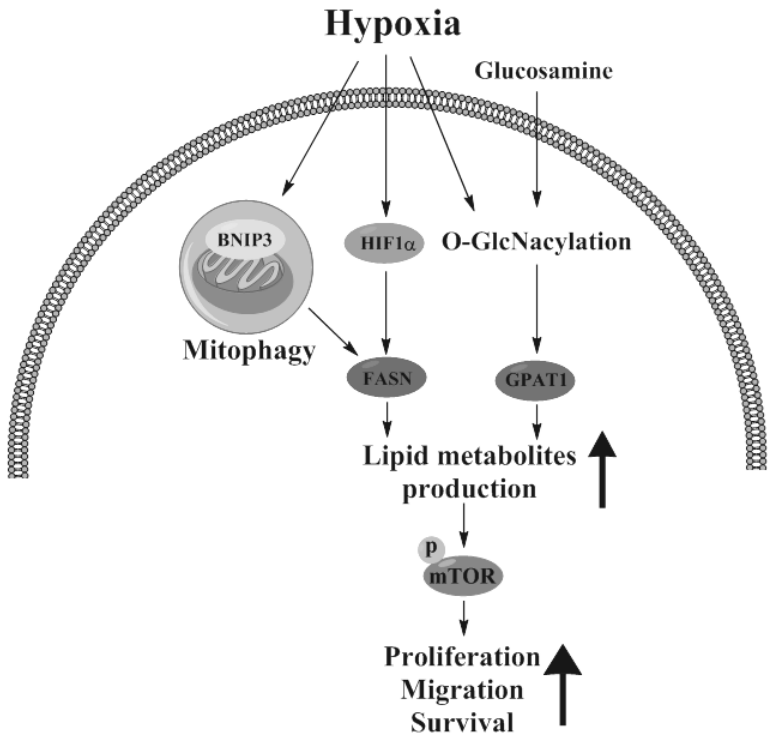

Figure 78. A schematic model summarizing the proposed pathway in the upregulation of proliferation, migration and survival of stem cells by hypoxia-induced FASN and GPAT1 expressions. Hypoxia-induced HIF1α stimulates FASN-dependent lipogenesis, which is critical for UCB-hMSC proliferation and migration via mTOR pathway. BNIP3-dependent mitophagy induced by hypoxia regulates the FASN-dependent lipogenesis, subsequently leads to mTOR-dependent migration and survival of UCB-hMSCs. Glucosamine-mediated O-GlcNAcylation enhances hypoxia-induced GPAT1 expression, leads to mTOR-mediated survival of mESCs

REFERENCES

Abdollahi H., Harris LJ., Zhang P., McIlhenny S., Srinivas V., Tulenko T., and DiMuzio PJ. (2011). The role of hypoxia in stem cell differentiation and therapeutics. J Surg Res. 165, 112-117.

Abecassis I., Olofsson B., Schmid M., Zalcman G., and Karniguian A. (2003). RhoA induces MMP-9 expression at CD44 lamellipodial focal complexes and promotes HMEC-1 cell invasion. Exp Cell Res. 291, 363-376.

Ader I., Brizueαla L., Bouquerel P., Malavaud B., and Cuvillier O. (2008). Sphingosine kinase 1: a new modulator of hypoxia inducible factor 1α during hypoxia in human cancer cells. Cancer Res. 68, 8635-8642.

Arnaboldi PM., Behr MJ., and Metzger DW. (2005). Mucosal B cell deficiency in IgA-/- mice abrogates the development of allergic lung inflammation. J Immunol. 175, 1276-1285.

Asahara T., Takahashi T., Masuda H., Kalka C., Chen D., Iwaguro H., Inai Y., Silver M., and Isner JM. (1999). VEGF contributes to postnatal neovascularization by mobilizing bone marrow-derived endothelial progenitor cells. EMBO J. 18, 3964-3972.

Baird D., Feng Q., and Cerione RA. (2005). The Cool-2/α-Pix protein mediates a Cdc42-Rac signaling cascade. Curr Biol. 15, 1-10.

Bakker WJ., Harris IS., and Mak TW. (2007). FOXO3a is activated in response to hypoxic stress and inhibits HIF1-induced apoptosis via regulation of CITED2. Mol Cell. 28, 941-953.

Basu G., Downey H., Guo S., Israel A., Asmar A., Hargrave B., and Heller R. (2014). Prevention of distal flap necrosis in a rat random skin flap model by gene electro transfer delivering VEGF(165) plasmid. J Gene Med. 16, 55-65.

Beeharry N., Chambers JA., and Green IC. (2004). Fatty acid protection from palmitic acid-induced apoptosis is lost following PI3-kinase inhibition. Apoptosis. 9, 599-607.

Bell JA., Volpi E., Fujita S., Cadenas JG., and Rasmussen BB. (2006). Dysregulation of muscle fatty acid metabolism in type 2 diabetes is independent of malonyl-CoA. Diabetologia. 49, 2144-2152.

Bellot G., Garcia-Medina R., Gounon P., Chiche J., Roux D., Pouyssegur J., and Mazure NM. (2009). Hypoxia-induced autophagy is mediated through hypoxia-inducible factor induction of BNIP3 and BNIP3L via their BH3 domains. Mol Cell Biol. 29, 2570-2581.

Ben-David U., Biran A., Scaffidi P., Herold-Mende C., Boehringer M., Meshorer E., and Benvenisty N. (2014). Elimination of undifferentiated cancer cells by pluripotent stem cell inhibitors. J Mol Cell Biol. 6, 267-269.

Ben-David U., Gan QF., Golan-Lev T., Arora P., Yanuka O., Oren

YS., Leikin-Frenkel A., Graf M., Garippa R., Boehringer M., Gromo G., and Benvenisty N. (2013). Selective elimination of human pluripotent stem cells by an oleate synthesis inhibitor discovered in a high-throughput screen. Cell Stem Cell. 12, 167-179.

Beneteau M., Pizon M., Chaigne-Delalande B., Daburon S., Moreau P., De Giorgi F., Ichas F., Rebillard A., Dimanche-Boitrel MT., Taupin JL., Moreau JF., and Legembre P. (2008). Localization of Fas/CD95 into the lipid rafts on downmodulation of the phosphatidylinositol 3-kinase signaling pathway. Mol Cancer Res. 6, 604-613.

Bigarella CL., Liang R., and Ghaffari S. (2014). Stem cells and the impact of ROS signaling. Development. 141, 4206-4218.

Blenis J. (2017). TOR, the Gateway to Cellular Metabolism, Cell Growth, and Disease. Cell. 171, 10-13.

Boomsma RA., and Geenen DL. (2012). Mesenchymal stem cells secrete multiple cytokines that promote angiogenesis and have contrasting effects on chemotaxis and apoptosis. PLoS One. 7, e35685.

Boulter E., Estrach S., Garcia-Mata R., and Feral CC. (2012). Off the beaten paths: alternative and crosstalk regulation of Rho GTPases. FASEB J. 26, 469-479.

Bradford MM. (1976). A rapid and sensitive method for the quantitation of microgram quantities of protein utilizing the principle of protein-dye binding. Anal Biochem. 72, 248-254.

Brustovetskii NN., Dedukhova VN., Egorova MV., Mokhova EN., and Skulachev VP. (1991). Uncoupling of oxidative phosphorylation by fatty acids and detergents suppressed by ATP/ADP antiporter inhibitors]. Biokhimiia. 56, 1042-1048.

Burgess RJ., Agathocleous M., and Morrison SJ. (2014). Metabolic regulation of stem cell function. J Intern Med. 276, 12-24.

Bursch W., Karwan A., Mayer M., Dornetshuber J., Frohwein U., Schulte-Hermann R., Fazi B., Di Sano F., Piredda L., Piacentini M., Petrovski G., Fesus L., and Gerner C. (2008). Cell death and autophagy: cytokines, drugs, and nutritional factors. Toxicology. 254, 147-157.

Burton TR., and Gibson SB. (2009). The role of Bcl-2 family member BNIP3 in cell death and disease: NIPping at the heels of cell death. Cell Death Differ. 16, 515-523.

Byon CH., Hardy RW., Ren C., Ponnazhagan S., Welch DR., McDonald JM., and Chen Y. (2009). Free fatty acids enhance breast cancer cell migration through plasminogen activator inhibitor-1 and SMAD4. Lab Invest. 89, 1221-1228.

Calnan DR., and Brunet A. (2008). The FoxO code. Oncogene. 27, 2276-2288.

Cao R., Zhao X., Li S., Zhou H., Chen W., Ren L., Zhou X., Zhang H., and Shi R. (2014). Hypoxia induces dysregulation of lipid metabolism in HepG2 cells via activation of HIF-2α. Cell Physiol Biochem. 34, 1427-1441.

Chambers I. (2004). The molecular basis of pluripotency in mouse embryonic stem cells. Cloning Stem Cells. 6, 386-391.

Champattanachai V., Marchase RB., and Chatham JC. (2007). Glucosamine protects neonatal cardiomyocytes from ischemia-reperfusion injury via increased protein-associated O-GlcNAc. Am J Physiol Cell Physiol. 292, C178-187.

Chen G., Ray R., Dubik D., Shi L., Cizeau J., Bleackley RC., Saxena S., Gietz RD., and Greenberg AH. (1997a). The E1B 19K/Bcl-2-binding protein Nip3 is a dimeric mitochondrial protein that activates apoptosis. J Exp Med. 186, 1975-1983.

Chen S., Nagy PL., and Zalkin H. (1997b). Role of NRF-1 in bidirectional transcription of the human GPAT-AIRC purine biosynthesis locus. Nucleic Acids Res. 25, 1809-1816.

Chen YJ., Huang YS., Chen JT., Chen YH., Tai MC., Chen CL., and Liang CM. (2015). Protective effects of glucosamine on oxidative-stress and ischemia/reperfusion-induced retinal injury. Invest Ophthalmol Vis Sci. 56, 1506-1516.

Chen Z., Liu L., Cheng Q., Li Y., Wu H., Zhang W., Wang Y., Sehgal SA., Siraj S., Wang X., Wang J., Zhu Y., and Chen Q. (2017). Mitochondrial E3 ligase MARCH5 regulates FUNDC1 to fine-tune hypoxic mitophagy. EMBO Rep. 18, 495-509.

Chieng-Yane P., Bocquet A., Letienne R., Bourbon T., Sablayrolles S., Perez M., Hatem SN., Lompre AM., Le Grand B., and David-Dufilho M. (2011). Protease-activated receptor-1

antagonist F 16618 reduces arterial restenosis by downregulation of tumor necrosis factor α and matrix metalloproteinase 7 expression, migration, and proliferation of vascular smooth muscle cells. J Pharmacol Exp Ther. 336, 643-651.

Chinnadurai G., Vijayalingam S., and Gibson SB. (2008). BNIP3 subfamily BH3-only proteins: mitochondrial stress sensors in normal and pathological functions. Oncogene. 27 Suppl 1, S114-127.

Choi H., Merceron C., Mangiavini L., Seifert EL., Schipani E., Shapiro IM., and Risbud MV. (2016). Hypoxia promotes noncanonical autophagy in nucleus pulposus cells independent of MTOR and HIF1A signaling. Autophagy. 12, 1631-1646.

Chourasia AH., and Macleod KF. (2015). Tumor suppressor functions of BNIP3 and mitophagy. Autophagy. 11, 1937-1938.

Cipolleschi MG., Marzi I., Santini R., Fredducci D., Vinci MC., D'Amico M., Rovida E., Stivarou T., Torre E., Dello Sbarba P., Stecca B., and Olivotto M. (2014). Hypoxia-resistant profile implies vulnerability of cancer stem cells to physiological agents, which suggests new therapeutic targets. Cell Cycle. 13, 268-278.

Coleman RA., and Lee DP. (2004). Enzymes of triacylglycerol synthesis and their regulation. Prog Lipid Res. 43, 134-176.

Costa M., Sourris K., Lim SM., Yu QC., Hirst CE., Parkington HC., Jokubaitis VJ., Dear AE., Liu HB., Micallef SJ., Koutsis K., Elefanty AG., and Stanley EG. (2013). Derivation of endothelial cells from human embryonic stem cells in fully defined medium enables

identification of lysophosphatidic acid and platelet activating factor as regulators of eNOS localization. Stem Cell Res. 10, 103-117.

Covello KL., Kehler J., Yu H., Gordan JD., Arsham AM., Hu CJ., Labosky PA., Simon MC., and Keith B. (2006). HIF-2α regulates Oct-4: effects of hypoxia on stem cell function, embryonic development, and tumor growth. Genes Dev. 20, 557-570.

Csete M. (2005). Oxygen in the cultivation of stem cells. Ann N Y Acad Sci. 1049, 1-8.

Currie E., Schulze A., Zechner R., Walther TC., and Farese RV, Jr., (2013). Cellular fatty acid metabolism and cancer. Cell Metab. 18, 153-161.

Daitoku H., Sakamaki J., and Fukamizu A. (2011). Regulation of FoxO transcription factors by acetylation and protein-protein interactions. Biochim Biophys Acta. 1813, 1954-1960.

Dall C., Khan M., Chen CA., and Angelos MG. (2016). Oxygen cycling to improve survival of stem cells for myocardial repair: A review. Life Sci. 153, 124-131.

de Carvalho EN., Ferreira LM., de Carvalho NA., Alba LE., and Liebano RE. (2005). Viability of a random pattern dorsal skin flap, in diabetic rats. Acta Cir Bras. 20, 225-228.

Di Meo S., Reed TT., Venditti P., and Victor VM. (2016). Role of ROS and RNS Sources in Physiological and Pathological Conditions. Oxid Med Cell Longev. 2016, 1245049.

Dimarino AM., Caplan AI., and Bonfield TL. (2013). Mesenchymal

stem cells in tissue repair. Front Immunol. 4, 201.

Doi H., Kitajima Y., Luo L., Yan C., Tateishi S., Ono Y., Urata Y., Goto S., Mori R., Masuzaki H., Shimokawa I., Hirano A., and Li TS. (2016). Potency of umbilical cord blood- and Wharton's jelly-derived mesenchymal stem cells for scarless wound healing. Sci Rep. 6, 18844.

Dorfman A., Roseman S., Moses FE., Ludowieg J., and Mayeda M. (1955). The biosynthesis of hyaluronic acid by group A Streptococcus. II. Origin of the N-acetylglucosamine moiety. J Biol Chem. 212, 583-591.

Dottori M., Leung J., Turnley AM., and Pebay A. (2008). Lysophosphatidic acid inhibits neuronal differentiation of neural stem/progenitor cells derived from human embryonic stem cells. Stem Cells. 26, 1146-1154.

Dunn L., Prosser HC., Tan JT., Vanags LZ., Ng MK., and Bursill CA. (2013). Murine model of wound healing. J Vis Exp. e50265.

Eliasson P., and Jonsson JI. (2010). The hematopoietic stem cell niche: low in oxygen but a nice place to be. J Cell Physiol. 222, 17-22.

Ezashi T., Das P., and Roberts RM. (2005). Low O_2 tensions and the prevention of differentiation of hES cells. Proc Natl Acad Sci U S A. 102, 4783-4788.

Feng CC., Lin CC., Lai YP., Chen TS., Marthandam Asokan S., Lin JY., Lin KH., Viswanadha VP., Kuo WW., and Huang CY. (2016).

Hypoxia suppresses myocardial survival pathway through HIF-1α-IGFBP-3-dependent signaling and enhances cardiomyocyte autophagic and apoptotic effects mainly via FoxO3a-induced BNIP3 expression. Growth Factors. 34, 73-86.

Ferrer CM., Lynch TP., Sodi VL., Falcone JN., Schwab LP., Peacock DL., Vocadlo DJ., Seagroves TN., and Reginato MJ. (2014). O-GlcNAcylation regulates cancer metabolism and survival stress signaling via regulation of the HIF-1 pathway. Mol Cell. 54, 820-831.

Ferrer CM., Sodi VL., and Reginato MJ. (2016). O-GlcNAcylation in Cancer Biology: Linking Metabolism and Signaling. J Mol Biol. 428, 3282-3294.

Filippi MD., Szczur K., Harris CE., and Berclaz PY. (2007). Rho GTPase Rac1 is critical for neutrophil migration into the lung. Blood. 109, 1257-1264.

Fillmore N., Huqi A., Jaswal JS., Mori J., Paulin R., Haromy A., Onay-Besikci A., Ionescu L., Thebaud B., Michelakis E., and Lopaschuk GD. (2015). Effect of fatty acids on human bone marrow mesenchymal stem cell energy metabolism and survival. PLoS One. 10, e0120257.

Flynn A., Barry F., and O'Brien T. (2007). UC blood-derived mesenchymal stromal cells: an overview. Cytotherapy. 9, 717-726.

Folmes CD., Park S., and Terzic A. (2013). Lipid metabolism greases the stem cell engine. Cell Metab. 17, 153-155.

Forsyth NR., Musio A., Vezzoni P., Simpson AH., Noble BS., and McWhir J. (2006). Physiologic oxygen enhances human embryonic stem cell clonal recovery and reduces chromosomal abnormalities. Cloning Stem Cells. 8, 16-23.

Foster DA. (2013). Phosphatidic acid and lipid-sensing by mTOR. Trends Endocrinol Metab. 24, 272-278.

Frank M., Duvezin-Caubet S., Koob S., Occhipinti A., Jagasia R., Petcherski A., Ruonala MO., Priault M., Salin B., and Reichert AS. (2012). Mitophagy is triggered by mild oxidative stress in a mitochondrial fission dependent manner. Biochim Biophys Acta. 1823, 2297-2310.

Freedman SJ., Sun ZY., Poy F., Kung AL., Livingston DM., Wagner G., and Eck MJ. (2002). Structural basis for recruitment of CBP/p300 by hypoxia-inducible factor-1 α. Proc Natl Acad Sci U S A. 99, 5367-5372.

Furuta E., Pai SK., Zhan R., Bandyopadhyay S., Watabe M., Mo YY., Hirota S., Hosobe S., Tsukada T., Miura K., Kamada S., Saito K., Iiizumi M., Liu W., Ericsson J., and Watabe K. (2008a). Fatty acid synthase gene is upregulated by hypoxia via activation of Akt and sterol regulatory element binding protein-1. Cancer Res. 68, 1003-1011.

Furuta E., Pai SK., Zhan R., Bandyopadhyay S., Watabe M., Mo YY., Hirota S., Hosobe S., Tsukada T., Miura K., Kamada S., Saito K., Iiizumi M., Liu W., Ericsson J., and Watabe K. (2008b). Fatty

acid synthase gene is upregulated by hypoxia via activation of Akt and sterol regulatory element binding protein-1. Cancer Res. 68, 1003-1011.

Gao F., Chiu SM., Motan DA., Zhang Z., Chen L., Ji HL., Tse HF., Fu QL., and Lian Q. (2016). Mesenchymal stem cells and immunomodulation: current status and future prospects. Cell Death Dis. 7, e2062.

Gao LL., Li M., Wang Q., Liu SA., Zhang JQ., and Cheng J. (2015). HCBP6 modulates triglyceride homeostasis in hepatocytes via the SREBP1c/FASN pathway. J Cell Biochem. 116, 2375-2384.

Garcia-Fuentes E., Santiago-Fernandez C., Gutierrez-Repiso C., Mayas MD., Oliva-Olivera W., Coin-Araguez L., Alcaide J., Ocana-Wilhelmi L., Vendrell J., Tinahones FJ., and Garrido-Sanchez L. (2015). Hypoxia is associated with a lower expression of genes involved in lipogenesis in visceral adipose tissue. J Transl Med. 13, 373.

Gasic GP. (1994). Basic-helix-loop-helix transcription factor and sterol sensor in a single membrane-bound molecule. Cell. 77, 17-19.

Genbacev O., Zhou Y., Ludlow JW., and Fisher SJ. (1997). Regulation of human placental development by oxygen tension. Science. 277, 1669-1672.

Geng H., Liu Q., Xue C., David LL., Beer TM., Thomas GV., Dai MS., and Qian DZ. (2012). HIF1α protein stability is increased by

acetylation at lysine 709. J Biol Chem. 287, 35496-35505.

Ghosh S., Blumenthal HJ., Davidson E., and Roseman S. (1960). Glucosamine metabolism. V. Enzymatic synthesis of glucosamine 6-phosphate. J Biol Chem. 235, 1265-1273.

Gillet C., Spruyt D., Rigutto S., Dalla Valle A., Berlier J., Louis C., Debier C., Gaspard N., Malaisse WJ., Gangji V., and Rasschaert J. (2015). Oleate abrogates palmitate-induced lipotoxicity and proinflammatory response in human bone marrow-derived mesenchymal stem cells and osteoblastic cells. Endocrinology. 156, 4081-4093.

Glick D., Zhang W., Beaton M., Marsboom G., Gruber M., Simon MC., Hart J., Dorn GW, 2nd., Brady MJ., and Macleod KF. (2012). BNip3 regulates mitochondrial function and lipid metabolism in the liver. Mol Cell Biol. 32, 2570-2584.

Goldberg HJ., Scholey J., and Fantus IG. (2000). Glucosamine activates the plasminogen activator inhibitor 1 gene promoter through Sp1 DNA binding sites in glomerular mesangial cells. Diabetes. 49, 863-871.

Golks A., Tran TT., Goetschy JF., and Guerini D. (2007). Requirement for O-linked N-acetylglucosaminyltransferase in lymphocytes activation. EMBO J. 26, 4368-4379.

Gonzalez-Baro MR., Lewin TM., and Coleman RA. (2007). Regulation of triglyceride metabolism. II. Function of mitochondrial GPAT1 in the regulation of triacylglycerol biosynthesis and insulin

action. Am J Physiol Gastrointest Liver Physiol. 292, G1195-1199.

Granero-Molto F., Weis JA., Miga MI., Landis B., Myers TJ., O'Rear L., Longobardi L., Jansen ED., Mortlock DP., and Spagnoli A. (2009). Regenerative effects of transplanted mesenchymal stem cells in fracture healing. Stem Cells. 27, 1887-1898.

Gu W., Hong X., Potter C., Qu A., and Xu Q. (2017). Mesenchymal stem cells and vascular regeneration. Microcirculation. 24,

Guan BJ., Krokowski D., Majumder M., Schmotzer CL., Kimball SR., Merrick WC., Koromilas AE., and Hatzoglou M. (2014). Translational control during endoplasmic reticulum stress beyond phosphorylation of the translation initiation factor eIF2α. J Biol Chem. 289, 12593-12611.

Guertin DA., and Sabatini DM. (2007). Defining the role of mTOR in cancer. Cancer Cell. 12, 9-22.

Guillaumond F., Leca J., Olivares O., Lavaut MN., Vidal N., Berthezene P., Dusetti NJ., Loncle C., Calvo E., Turrini O., Iovanna JL., Tomasini R., and Vasseur S. (2013). Strengthened glycolysis under hypoxia supports tumor symbiosis and hexosamine biosynthesis in pancreatic adenocarcinoma. Proc Natl Acad Sci U S A. 110, 3919-3924.

Gulhati P., Bowen KA., Liu J., Stevens PD., Rychahou PG., Chen M., Lee EY., Weiss HL., O'Connor KL., Gao T., and Evers BM. (2011). mTORC1 and mTORC2 regulate EMT, motility, and metastasis of colorectal cancer via RhoA and Rac1 signaling

pathways. Cancer Res. 71, 3246-3256.

Gunaratnam K., Vidal C., Boadle R., Thekkedam C., and Duque G. (2013). Mechanisms of palmitate-induced cell death in human osteoblasts. Biol Open. 2, 1382-1389.

Gutierrez-Uzquiza A., Arechederra M., Bragado P., Aguirre-Ghiso JA., and Porras A. (2012). p38α mediates cell survival in response to oxidative stress via induction of antioxidant genes: effect on the p70S6K pathway. J Biol Chem. 287, 2632-2642.

Hamacher-Brady A., and Brady NR. (2016). Mitophagy programs: mechanisms and physiological implications of mitochondrial targeting by autophagy. Cell Mol Life Sci. 73, 775-795.

Hammerling BC., Najor RH., Cortez MQ., Shires SE., Leon LJ., Gonzalez ER., Boassa D., Phan S., Thor A., Jimenez RE., Li H., Kitsis RN., Dorn Ii GW., Sadoshima J., Ellisman MH., and Gustafsson AB. (2017). A Rab5 endosomal pathway mediates Parkin-dependent mitochondrial clearance. Nat Commun. 8, 14050.

Hammond LE., Albright CD., He L., Rusyn I., Watkins SM., Doughman SD., Lemasters JJ., and Coleman RA. (2007). Increased oxidative stress is associated with balanced increases in hepatocyte apoptosis and proliferation in glycerol-3-phosphate acyltransferase-1 deficient mice. Exp Mol Pathol. 82, 210-219.

Hardiville S., and Hart GW. (2014). Nutrient regulation of signaling, transcription, and cell physiology by O-GlcNAcylation. Cell Metab. 20, 208-213.

Harrison JS., Rameshwar P., Chang V., and Bandari P. (2002). Oxygen saturation in the bone marrow of healthy volunteers. Blood. 99, 394.

Hart GW., Housley MP., and Slawson C. (2007). Cycling of O-linked β-N-acetylglucosamine on nucleocytoplasmic proteins. Nature. 446, 1017-1022.

Hart GW., Slawson C., Ramirez-Correa G., and Lagerlof O. (2011). Cross talk between O-GlcNAcylation and phosphorylation: roles in signaling, transcription, and chronic disease. Annu Rev Biochem. 80, 825-858.

Hay N., and Sonenberg N. (2004). Upstream and downstream of mTOR. Genes Dev. 18, 1926-1945.

He A., Jiang Y., Gui C., Sun Y., Li J., and Wang JA. (2009). The antiapoptotic effect of mesenchymal stem cell transplantation on ischemic myocardium is enhanced by anoxic preconditioning. Can J Cardiol. 25, 353-358.

Henningson CT, Jr.., Stanislaus MA., and Gewirtz AM. (2003). 28. Embryonic and adult stem cell therapy. J Allergy Clin Immunol. 111, S745-753.

Hinz B. (2007). Formation and function of the myofibroblast during tissue repair. J Invest Dermatol. 127, 526-537.

Hodgson DM., Behfar A., Zingman LV., Kane GC., Perez-Terzic C., Alekseev AE., Puceat M., and Terzic A. (2004). Stable benefit of embryonic stem cell therapy in myocardial infarction. Am J Physiol

Heart Circ Physiol. 287, H471-479.

Holbrook NJ., and Ikeyama S. (2002). Age-related decline in cellular response to oxidative stress: links to growth factor signaling pathways with common defects. Biochem Pharmacol. 64, 999-1005.

Honda A., Hirose M., and Ogura A. (2009). Basic FGF and Activin/Nodal but not LIF signaling sustain undifferentiated status of rabbit embryonic stem cells. Exp Cell Res. 315, 2033-2042.

Hornberger TA., Sukhija KB., Wang XR., and Chien S. (2007). mTOR is the rapamycin-sensitive kinase that confers mechanically-induced phosphorylation of the hydrophobic motif site Thr(389) in p70(S6k). FEBS Lett. 581, 4562-4566.

Horton JD., Shah NA., Warrington JA., Anderson NN., Park SW., Brown MS., and Goldstein JL. (2003). Combined analysis of oligonucleotide microarray data from transgenic and knockout mice identifies direct SREBP target genes. Proc Natl Acad Sci U S A. 100, 12027-12032.

Horwitz EM., Prockop DJ., Fitzpatrick LA., Koo WW., Gordon PL., Neel M., Sussman M., Orchard P., Marx JC., Pyeritz RE., and Brenner MK. (1999). Transplantability and therapeutic effects of bone marrow-derived mesenchymal cells in children with osteogenesis imperfecta. Nat Med. 5, 309-313.

Hotokezaka Y., van Leyen K., Lo EH., Beatrix B., Katayama I., Jin G., and Nakamura T. (2009). αNAC depletion as an initiator of ER

stress-induced apoptosis in hypoxia. Cell Death Differ. 16, 1505-1514.

Hou Z., Zhang J., Schwartz MP., Stewart R., Page CD., Murphy WL., and Thomson JA. (2013). A human pluripotent stem cell platform for assessing developmental neural toxicity screening. Stem Cell Res Ther. 4 Suppl 1, S12.

Hu JK., Du W., Shelton SJ., Oldham MC., DiPersio CM., and Klein OD. (2017). An FAK-YAP-mTOR signaling axis regulates stem cell-based tissue renewal in mice. Cell Stem Cell. 21, 91-106 e106.

Huang J., Nguyen-McCarty M., Hexner EO., Danet-Desnoyers G., and Klein PS. (2012). Maintenance of hematopoietic stem cells through regulation of Wnt and mTOR pathways. Nat Med. 18, 1778-1785.

Hudson CC., Liu M., Chiang GG., Otterness DM., Loomis DC., Kaper F., Giaccia AJ., and Abraham RT. (2002). Regulation of hypoxia-inducible factor 1α expression and function by the mammalian target of rapamycin. Mol Cell Biol. 22, 7004-7014.

Humar R., Kiefer FN., Berns H., Resink TJ., and Battegay EJ. (2002). Hypoxia enhances vascular cell proliferation and angiogenesis in vitro via rapamycin (mTOR)-dependent signaling. FASEB J. 16, 771-780.

Iglesias-Bartolome R., Patel V., Cotrim A., Leelahavanichkul K., Molinolo AA., Mitchell JB., and Gutkind JS. (2012). mTOR inhibition prevents epithelial stem cell senescence and protects from

radiation-induced mucositis. Cell Stem Cell. 11, 401-414.

Ito K., Carracedo A., Weiss D., Arai F., Ala U., Avigan DE., Schafer ZT., Evans RM., Suda T., Lee CH., and Pandolfi PP. (2012). A PML-PPAR-σ pathway for fatty acid oxidation regulates hematopoietic stem cell maintenance. Nat Med. 18, 1350-1358.

Ito K., Hirao A., Arai F., Matsuoka S., Takubo K., Hamaguchi I., Nomiyama K., Hosokawa K., Sakurada K., Nakagata N., Ikeda Y., Mak TW., and Suda T. (2004). Regulation of oxidative stress by ATM is required for self-renewal of haematopoietic stem cells. Nature. 431, 997-1002.

Ito K., and Suda T. (2014). Metabolic requirements for the maintenance of self-renewing stem cells. Nat Rev Mol Cell Biol. 15, 243-256.

Jacinto E., Loewith R., Schmidt A., Lin S., Ruegg MA., Hall A., and Hall MN. (2004). Mammalian TOR complex 2 controls the actin cytoskeleton and is rapamycin insensitive. Nat Cell Biol. 6, 1122-1128.

Jang H., Kim TW., Yoon S., Choi SY., Kang TW., Kim SY., Kwon YW., Cho EJ., and Youn HD. (2012). O-GlcNAc regulates pluripotency and reprogramming by directly acting on core components of the pluripotency network. Cell Stem Cell. 11, 62-74.

Jang YY., and Sharkis SJ. (2007). A low level of reactive oxygen species selects for primitive hematopoietic stem cells that may reside in the low-oxygenic niche. Blood. 110, 3056-3063.

Jensen MD., Haymond MW., Rizza RA., Cryer PE., and Miles JM. (1989). Influence of body fat distribution on free fatty acid metabolism in obesity. J Clin Invest. 83, 1168-1173.

Jeon JH., Suh HN., Kim MO., and Han HJ. (2013). Glucosamine-induced reduction of integrin β4 and plectin complex stimulates migration and proliferation in mouse embryonic stem cells. Stem Cells Dev. 22, 2975-2989.

Jeon JH., Suh HN., Kim MO., Ryu JM., and Han HJ. (2014). Glucosamine-induced OGT activation mediates glucose production through cleaved Notch1 and FoxO1, which coordinately contributed to the regulation of maintenance of self-renewal in mouse embryonic stem cells. Stem Cells Dev. 23, 2067-2079.

Jin Q., Yu LR., Wang L., Zhang Z., Kasper LH., Lee JE., Wang C., Brindle PK., Dent SY., and Ge K. (2011). Distinct roles of GCN5/PCAF-mediated H3K9ac and CBP/p300-mediated H3K18/27ac in nuclear receptor transactivation. EMBO J. 30, 249-262.

Joshi A., and Kundu M. (2013). Mitophagy in hematopoietic stem cells: the case for exploration. Autophagy. 9, 1737-1749.

Jung SY., Jeon HK., Choi JS., and Kim YJ. (2012). Reduced expression of FASN through SREBP-1 downregulation is responsible for hypoxic cell death in HepG2 cells. J Cell Biochem. 113, 3730-3739.

Jung YH., Lee SJ., Oh SY., Lee HJ., Ryu JM., and Han HJ. (2015).

Oleic acid enhances the motility of umbilical cord blood derived mesenchymal stem cells through EphB2-dependent F-actin formation. Biochim Biophys Acta. 1853, 1905-1917.

Kang JX., Wan JB., and He C. (2014). Concise review: Regulation of stem cell proliferation and differentiation by essential fatty acids and their metabolites. Stem Cells. 32, 1092-1098.

Kang S., Han J., Song SY., Kim WS., Shin S., Kim JH., Ahn H., Jeong JH., Hwang SJ., and Sung JH. (2015). Lysophosphatidic acid increases the proliferation and migration of adiposederived stem cells via the generation of reactive oxygen species. Mol Med Rep. 12, 5203-5210.

Kato H., Nakajima S., Saito Y., Takahashi S., Katoh R., and Kitamura M. (2012). mTORC1 serves ER stress-triggered apoptosis via selective activation of the IRE1-JNK pathway. Cell Death Differ. 19, 310-320.

Keith B., and Simon MC. (2007). Hypoxia-inducible factors, stem cells, and cancer. Cell. 129, 465-472.

Khan WS., Adesida AB., and Hardingham TE. (2007). Hypoxic conditions increase hypoxia-inducible transcription factor 2α and enhance chondrogenesis in stem cells from the infrapatellar fat pad of osteoarthritis patients. Arthritis Res Ther. 9, R55.

Kim SJ., Zhang Z., Saha A., Sarkar C., Zhao Z., Xu Y., and Mukherjee AB. (2010a). ω-3 and ω-6 fatty acids suppress ER- and oxidative stress in cultured neurons and neuronal progenitor

cells from mice lacking PPT1. Neurosci Lett. 479, 292-296.

Kim YS., Kwon JS., Hong MH., Kim J., Song CH., Jeong MH., Cho JG., Park JC., Kang JC., and Ahn Y. (2010b). Promigratory activity of oxytocin on umbilical cord blood-derived mesenchymal stem cells. Artif Organs. 34, 453-461.

Knobloch M., Braun SM., Zurkirchen L., von Schoultz C., Zamboni N., Arauzo-Bravo MJ., Kovacs WJ., Karalay O., Suter U., Machado RA., Roccio M., Lutolf MP., Semenkovich CF., and Jessberger S. (2013). Metabolic control of adult neural stem cell activity by Fasn-dependent lipogenesis. Nature. 493, 226-230.

Koay EJ., and Athanasiou KA. (2008). Hypoxic chondrogenic differentiation of human embryonic stem cells enhances cartilage protein synthesis and biomechanical functionality. Osteoarthritis Cartilage. 16, 1450-1456.

Kofoed H., Sjontoft E., Siemssen SO., and Olesen HP. (1985). Bone marrow circulation after osteotomy. Blood flow, pO2, pCO2, and pressure studied in dogs. Acta Orthop Scand. 56, 400-403.

Krishnamurthy P., Ross DD., Nakanishi T., Bailey-Dell K., Zhou S., Mercer KE., Sarkadi B., Sorrentino BP., and Schuetz JD. (2004). The stem cell marker Bcrp/ABCG2 enhances hypoxic cell survival through interactions with heme. J Biol Chem. 279, 24218-24225.

Kudlow JE. (2006). Post-translational modification by O-GlcNAc: another way to change protein function. J Cell Biochem. 98, 1062-1075.

Kuhajda FP., Jenner K., Wood FD., Hennigar RA., Jacobs LB., Dick JD., and Pasternack GR. (1994). Fatty acid synthesis: a potential selective target for antineoplastic therapy. Proc Natl Acad Sci U S A. 91, 6379-6383.

Kumar D., Shankar S., and Srivastava RK. (2014). Rottlerin induces autophagy and apoptosis in prostate cancer stem cells via PI3K/Akt/mTOR signaling pathway. Cancer Lett. 343, 179-189.

Kumar S., and Ashraf M. (2015). Tadalafil, a Phosphodiesterase Inhibitor Protects Stem Cells over Longer Period Against Hypoxia/Reoxygenation Injury Through STAT3/PKG-I Signaling. Stem Cells Dev. 24, 1332-1341.

Kurihara Y., Kanki T., Aoki Y., Hirota Y., Saigusa T., Uchiumi T., and Kang D. (2012). Mitophagy plays an essential role in reducing mitochondrial production of reactive oxygen species and mutation of mitochondrial DNA by maintaining mitochondrial quantity and quality in yeast. J Biol Chem. 287, 3265-3272.

Kwon YW., Heo SC., Jeong GO., Yoon JW., Mo WM., Lee MJ., Jang IH., Kwon SM., Lee JS., and Kim JH. (2013). Tumor necrosis factor-α-activated mesenchymal stem cells promote endothelial progenitor cell homing and angiogenesis. Biochim Biophys Acta. 1832, 2136-2144.

Laflamme MA., Chen KY., Naumova AV., Muskheli V., Fugate JA., Dupras SK., Reinecke H., Xu C., Hassanipour M., Police S., O'Sullivan C., Collins L., Chen Y., Minami E., Gill EA., Ueno S., Yuan

C., Gold J., and Murry CE. (2007). Cardiomyocytes derived from human embryonic stem cells in pro-survival factors enhance function of infarcted rat hearts. Nat Biotechnol. 25, 1015-1024.

Laplante M., and Sabatini DM. (2009). mTOR signaling at a glance. J Cell Sci. 122, 3589-3594.

Lavrentieva A., Majore I., Kasper C., and Hass R. (2010). Effects of hypoxic culture conditions on umbilical cord-derived human mesenchymal stem cells. Cell Commun Signal. 8, 18.

Le Blanc K., Tammik L., Sundberg B., Haynesworth SE., and Ringden O. (2003). Mesenchymal stem cells inhibit and stimulate mixed lymphocyte cultures and mitogenic responses independently of the major histocompatibility complex. Scand J Immunol. 57, 11-20.

Lee DE., Ayoub N., and Agrawal DK. (2016). Mesenchymal stem cells and cutaneous wound healing: novel methods to increase cell delivery and therapeutic efficacy. Stem Cell Res Ther. 7, 37.

Lee HJ., Ryu JM., Jung YH., Oh SY., Lee SJ., and Han HJ. (2015). Novel pathway for hypoxia-induced proliferation and migration in human mesenchymal stem cells: Involvement of HIF-1α, FASN, and mTORC1. Stem Cells. 33, 2182-2195.

Lee KB., Choi J., Cho SB., Chung JY., Moon ES., Kim NS., and Han HJ. (2011). Topical embryonic stem cells enhance wound healing in diabetic rats. J Orthop Res. 29, 1554-1562.

Legube G., and Trouche D. (2003). Regulating histone

acetyltransferases and deacetylases. EMBO Rep. 4, 944-947.

Li M., Yu J., Li Y., Li D., Yan D., Qu Z., and Ruan Q. (2010). CXCR4 positive bone mesenchymal stem cells migrate to human endothelial cell stimulated by ox-LDL via SDF-1α/CXCR4 signaling axis. Exp Mol Pathol. 88, 250-255.

Li N., Yan YL., Fu S., Li RJ., Zhao PF., Xu XY., Yang JP., and Damirin A. (2017). Lysophosphatidic acid enhances human umbilical cord mesenchymal stem cell viability without differentiation via LPA receptor mediating manner. Apoptosis. 11, 1296-1309.

Liang R., and Ghaffari S. (2014). Stem cells, redox signaling, and stem cell aging. Antioxid Redox Signal. 20, 1902-1916.

Liew A., and O'Brien T. (2012). Therapeutic potential for mesenchymal stem cell transplantation in critical limb ischemia. Stem Cell Res Ther. 3, 28.

Lima VV., Spitler K., Choi H., Webb RC., and Tostes RC. (2012). O-GlcNAcylation and oxidation of proteins: is signalling in the cardiovascular system becoming sweeter? Clin Sci (Lond). 123, 473-486.

Lin W., Wadlington NL., Chen L., Zhuang X., Brorson JR., and Kang UJ. (2014). Loss of PINK1 attenuates HIF-1α induction by preventing 4E-BP1-dependent switch in protein translation under hypoxia. J Neurosci. 34, 3079-3089.

Linington C., and Hohlfeld R. (1990). T-cell mediated autoimmunity: molecular interactions and therapeutic implications. J

Autoimmun. 3, 501-506.

Liu H., Wang Z., Yu S., and Xu J. (2014a). Proteasomal degradation of O-GlcNAc transferase elevates hypoxia-induced vascular endothelial inflammatory responsedagger. Cardiovasc Res. 103, 131-139.

Liu J., Li T., Yang D., Ma R., Moran TH., and Smith WW. (2012a). Synphilin-1 alters metabolic homeostasis in a novel Drosophila obesity model. Int J Obes (Lond). 36, 1529-1536.

Liu J., Pang Y., Chang T., Bounelis P., Chatham JC., and Marchase RB. (2006). Increased hexosamine biosynthesis and protein O-GlcNAc levels associated with myocardial protection against calcium paradox and ischemia. J Mol Cell Cardiol. 40, 303-312.

Liu L., Feng D., Chen G., Chen M., Zheng Q., Song P., Ma Q., Zhu C., Wang R., Qi W., Huang L., Xue P., Li B., Wang X., Jin H., Wang J., Yang F., Liu P., Zhu Y., Sui S., and Chen Q. (2012b). Mitochondrial outer-membrane protein FUNDC1 mediates hypoxia-induced mitophagy in mammalian cells. Nat Cell Biol. 14, 177-185.

Liu L., Luo Y., Chen L., Shen T., Xu B., Chen W., Zhou H., Han X., and Huang S. (2010). Rapamycin inhibits cytoskeleton reorganization and cell motility by suppressing RhoA expression and activity. J Biol Chem. 285, 38362-38373.

Liu L., Sakakibara K., Chen Q., and Okamoto K. (2014b). Receptor-mediated mitophagy in yeast and mammalian systems. Cell Res. 24, 787-795.

Liu L., Yu Q., Lin J., Lai X., Cao W., Du K., Wang Y., Wu K., Hu Y., Zhang L., Xiao H., Duan Y., and Huang H. (2011). Hypoxia-inducible factor-1α is essential for hypoxia-induced mesenchymal stem cell mobilization into the peripheral blood. Stem Cells Dev. 20, 1961-1971.

Liu X., Hou J., Shi L., Chen J., Sang J., Hu S., Cong X., and Chen X. (2009a). Lysophosphatidic acid protects mesenchymal stem cells against ischemia-induced apoptosis in vivo. Stem Cells Dev. 18, 947-954.

Liu Y., Thyagarajan B., Lakshmipathy U., Xue H., Lieu P., Fontes A., MacArthur CC., Scheyhing K., Rao MS., and Chesnut JD. (2009b). Generation of platform human embryonic stem cell lines that allow efficient targeting at a predetermined genomic location. Stem Cells Dev. 18, 1459-1472.

Llevadot J., Murasawa S., Kureishi Y., Uchida S., Masuda H., Kawamoto A., Walsh K., Isner JM., and Asahara T. (2001). HMG-CoA reductase inhibitor mobilizes bone marrow--derived endothelial progenitor cells. J Clin Invest. 108, 399-405.

Love DC., and Hanover JA. (2005). The hexosamine signaling pathway: deciphering the "O-GlcNAc code". Sci STKE. 2005, re13.

Lowe C., Gillespie GA., and Pike JW. (1995). Leukemia inhibitory factor as a mediator of JAK/STAT activation in murine osteoblasts. J Bone Miner Res. 10, 1644-1650.

Lu H., Gao Z., Zhao Z., Weng J., and Ye J. (2016). Transient

hypoxia reprograms differentiating adipocytes for enhanced insulin sensitivity and triglyceride accumulation. Int J Obes (Lond). 40, 121-128.

Lubas WA., Frank DW., Krause M., and Hanover JA. (1997). O-Linked GlcNAc transferase is a conserved nucleocytoplasmic protein containing tetratricopeptide repeats. J Biol Chem. 272, 9316-9324.

Luckashenak N., Wahe A., Breit K., Brakebusch C., and Brocker T. (2013). Rho-family GTPase Cdc42 controls migration of Langerhans cells in vivo. J Immunol. 190, 27-35.

Ma XM., Yoon SO., Richardson CJ., Julich K., and Blenis J. (2008). SKAR links pre-mRNA splicing to mTOR/S6K1-mediated enhanced translation efficiency of spliced mRNAs. Cell. 133, 303-313.

Mammucari C., Milan G., Romanello V., Masiero E., Rudolf R., Del Piccolo P., Burden SJ., Di Lisi R., Sandri C., Zhao J., Goldberg AL., Schiaffino S., and Sandri M. (2007). FoxO3 controls autophagy in skeletal muscle in vivo. Cell Metab. 6, 458-471.

Marinov M., Ziogas A., Pardo OE., Tan LT., Dhillon T., Mauri FA., Lane HA., Lemoine NR., Zangemeister-Wittke U., Seckl MJ., and Arcaro A. (2009). AKT/mTOR pathway activation and BCL-2 family proteins modulate the sensitivity of human small cell lung cancer cells to RAD001. Clin Cancer Res. 15, 1277-1287.

Marshall S., Bacote V., and Traxinger RR. (1991). Discovery of a

metabolic pathway mediating glucose-induced desensitization of the glucose transport system. Role of hexosamine biosynthesis in the induction of insulin resistance. J Biol Chem. 266, 4706-4712.

Marzi I., Cipolleschi MG., D'Amico M., Stivarou T., Rovida E., Vinci MC., Pandolfi S., Dello Sbarba P., Stecca B., and Olivotto M. (2013). The involvement of a Nanog, Klf4 and c-Myc transcriptional circuitry in the intertwining between neoplastic progression and reprogramming. Cell Cycle. 12, 353-364.

Matsushima M., Fujiwara T., Takahashi E., Minaguchi T., Eguchi Y., Tsujimoto Y., Suzumori K., and Nakamura Y. (1998). Isolation, mapping, and functional analysis of a novel human cDNA (BNIP3L) encoding a protein homologous to human NIP3. Genes Chromosomes Cancer. 21, 230-235.

Menendez JA., and Lupu R. (2007). Fatty acid synthase and the lipogenic phenotype in cancer pathogenesis. Nature Reviews Cancer. 7, 763-777.

Menendez JA., Mehmi I., Atlas E., Colomer R., and Lupu R. (2004). Novel signaling molecules implicated in tumor-associated fatty acid synthase-dependent breast cancer cell proliferation and survival: Role of exogenous dietary fatty acids, p53-p21WAF1/CIP1, ERK1/2 MAPK, p27KIP1, BRCA1, and NF-κB. Int J Oncol. 24, 591-608.

Mikkola HK., Klintman J., Yang H., Hock H., Schlaeger TM., Fujiwara Y., and Orkin SH. (2003). Haematopoietic stem cells retain

long-term repopulating activity and multipotency in the absence of stem-cell leukaemia SCL/tal-1 gene. Nature. 421, 547-551.

Mishra OP., Randis T., Ashraf QM., and Delivoria-Papadopoulos M. (2006). Hypoxia-induced Bax and Bcl-2 protein expression, caspase-9 activation, DNA fragmentation, and lipid peroxidation in mitochondria of the cerebral cortex of newborn piglets: the role of nitric oxide. Neuroscience. 141, 1339-1349.

Mitalipov S., and Wolf D. (2009). Totipotency, pluripotency and nuclear reprogramming. Adv Biochem Eng Biotechnol. 114, 185-199.

Mohyeldin A., Garzon-Muvdi T., and Quinones-Hinojosa A. (2010). Oxygen in stem cell biology: a critical component of the stem cell niche. Cell Stem Cell. 7, 150-161.

Morimoto A., Tomita S., Imanishi M., Shioi G., Kihira Y., Izawa-Ishizawa Y., Takaku M., Hashimoto I., Ikeda Y., Nakanishi H., and Tamaki T. (2014). Overexpressed HIF-2α in endothelial cells promotes vascularization and improves random pattern skin flap survival. Plast Reconstr Surg Glob Open. 2, e132.

Moriyama M., Moriyama H., Uda J., Kubo H., Nakajima Y., Goto A., Morita T., and Hayakawa T. (2017). BNIP3 upregulation via stimulation of ERK and JNK activity is required for the protection of keratinocytes from UVB-induced apoptosis. Cell Death Dis. 8, e2576.

Moschella PC., Rao VU., McDermott PJ., and Kuppuswamy D.

(2007). Regulation of mTOR and S6K1 activation by the nPKC isoforms, PKCε and PKCσ, in adult cardiac muscle cells. J Mol Cell Cardiol. 43, 754-766.

Mungamuri SK., Yang X., Thor AD., and Somasundaram K. (2006). Survival signaling by Notch1: mammalian target of rapamycin (mTOR)-dependent inhibition of p53. Cancer Res. 66, 4715-4724.

Murakami M., Ichisaka T., Maeda M., Oshiro N., Hara K., Edenhofer F., Kiyama H., Yonezawa K., and Yamanaka S. (2004). mTOR is essential for growth and proliferation in early mouse embryos and embryonic stem cells. Mol Cell Biol. 24, 6710-6718.

Murry CE., and Keller G. (2008). Differentiation of embryonic stem cells to clinically relevant populations: lessons from embryonic development. Cell. 132, 661-680.

Na TY., Lee HJ., Oh HJ., Huh S., Lee IK., and Lee MO. (2011). Positive cross-talk between hypoxia inducible factor-1α and liver X receptor α induces formation of triglyceride-loaded foam cells. Arterioscler Thromb Vasc Biol. 31, 2949-2956.

Novak I., and Dikic I. (2011). Autophagy receptors in developmental clearance of mitochondria. Autophagy. 7, 301-303.

O'Shea KS. (2004). Self-renewal vs. differentiation of mouse embryonic stem cells. Biol Reprod. 71, 1755-1765.

Oem JK., Jackel-Cram C., Li YP., Zhou Y., Zhong J., Shimano H., Babiuk LA., and Liu Q. (2008). Activation of sterol regulatory element-binding protein 1c and fatty acid synthase transcription by

hepatitis C virus non-structural protein 2. J Gen Virol. 89, 1225-1230.

Oh SR., Sul OJ., Kim YY., Kim HJ., Yu R., Suh JH., and Choi HS. (2010). Saturated fatty acids enhance osteoclast survival. J Lipid Res. 51, 892-899.

Ohba Y., Sakuragi T., Kage-Nakadai E., Tomioka NH., Kono N., Imae R., Inoue A., Aoki J., Ishihara N., Inoue T., Mitani S., and Arai H. (2013). Mitochondria-type GPAT is required for mitochondrial fusion. EMBO J. 32, 1265-1279.

Ohta Y., Hartwig JH., and Stossel TP. (2006). FilGAP, a Rho- and ROCK-regulated GAP for Rac binds filamin A to control actin remodelling. Nat Cell Biol. 8, 803-814.

Ortlepp C., Steudel C., Heiderich C., Koch S., Jacobi A., Ryser M., Brenner S., Bornhauser M., Brors B., Hofmann WK., Ehninger G., and Thiede C. (2013). Autotaxin is expressed in FLT3-ITD positive acute myeloid leukemia and hematopoietic stem cells and promotes cell migration and proliferation. Exp Hematol. 41, 444-461 e444.

Palomaki S., Pietila M., Laitinen S., Pesala J., Sormunen R., Lehenkari P., and Koivunen P. (2013). HIF-1α is upregulated in human mesenchymal stem cells. Stem Cells. 31, 1902-1909.

Papandreou I., Cairns RA., Fontana L., Lim AL., and Denko NC. (2006). HIF-1 mediates adaptation to hypoxia by actively downregulating mitochondrial oxygen consumption. Cell Metab. 3,

187-197.

Pebay A., Bonder CS., and Pitson SM. (2007). Stem cell regulation by lysophospholipids. Prostaglandins Other Lipid Mediat. 84, 83-97.

Peterson TR., Laplante M., Thoreen CC., Sancak Y., Kang SA., Kuehl WM., Gray NS., and Sabatini DM. (2009). DEPTOR is an mTOR inhibitor frequently overexpressed in multiple myeloma cells and required for their survival. Cell. 137, 873-886.

Porstmann T., Santos CR., Griffiths B., Cully M., Wu M., Leevers S., Griffiths JR., Chung YL., and Schulze A. (2008). SREBP activity is regulated by mTORC1 and contributes to Akt-dependent cell growth. Cell Metab. 8, 224-236.

Pouwels MJ., Jacobs JR., Span PN., Lutterman JA., Smits P., and Tack CJ. (2001). Short-term glucosamine infusion does not affect insulin sensitivity in humans. J Clin Endocrinol Metab. 86, 2099-2103.

Puthanveetil P., Wang Y., Zhang D., Wang F., Kim MS., Innis S., Pulinilkunnil T., Abrahani A., and Rodrigues B. (2011). Cardiac triglyceride accumulation following acute lipid excess occurs through activation of a FoxO1-iNOS-CD36 pathway. Free Radic Biol Med. 51, 352-363.

Qi Y., Tian X., Liu J., Han Y., Graham AM., Simon MC., Penninger JM., Carmeliet P., and Li S. (2012). Bnip3 and AIF cooperate to induce apoptosis and cavitation during epithelial morphogenesis. J

Cell Biol. 198, 103-114.

Qiao C., Xu W., Zhu W., Hu J., Qian H., Yin Q., Jiang R., Yan Y., Mao F., Yang H., Wang X., and Chen Y. (2008). Human mesenchymal stem cells isolated from the umbilical cord. Cell Biol Int. 32, 8-15.

Rajabi MA., and Rajabi F. (2007). The effect of estrogen on wound healing in rats. Pak J Med Sci. 23, 349-352.

Ramirez-Bergeron DL., and Simon MC. (2001). Hypoxia-inducible factor and the development of stem cells of the cardiovascular system. Stem Cells. 19, 279-286.

Ramming T., and Appenzeller-Herzog C. (2012). The physiological functions of mammalian endoplasmic oxidoreductin 1: on disulfides and more. Antioxid Redox Signal. 16, 1109-1118.

Rankin EB., Rha J., Selak MA., Unger TL., Keith B., Liu Q., and Haase VH. (2009). Hypoxia-inducible factor 2 regulates hepatic lipid metabolism. Mol Cell Biol. 29, 4527-4538.

Rexach JE., Clark PM., Mason DE., Neve RL., Peters EC., and Hsieh-Wilson LC. (2012). Dynamic O-GlcNAc modification regulates CREB-mediated gene expression and memory formation. Nat Chem Biol. 8, 253-261.

Rey S., Luo W., Shimoda LA., and Semenza GL. (2011). Metabolic reprogramming by HIF-1 promotes the survival of bone marrow-derived angiogenic cells in ischemic tissue. Blood. 117, 4988-4998.

Richard VR., Leonov A., Beach A., Burstein MT., Koupaki O.,

Gomez-Perez A., Levy S., Pluska L., Mattie S., Rafesh R., Iouk T., Sheibani S., Greenwood M., Vali H., and Titorenko VI. (2013). Macromitophagy is a longevity assurance process that in chronologically aging yeast limited in calorie supply sustains functional mitochondria and maintains cellular lipid homeostasis. Aging (Albany NY). 5, 234-269.

Rocheteau P., Chatre L., Briand D., Mebarki M., Jouvion G., Bardon J., Crochemore C., Serrani P., Lecci PP., Latil M., Matot B., Carlier PG., Latronico N., Huchet C., Lafoux A., Sharshar T., Ricchetti M., and Chretien F. (2015). Sepsis induces long-term metabolic and mitochondrial muscle stem cell dysfunction amenable by mesenchymal stem cell therapy. Nat Commun. 6, 10145.

Rosner M., Siegel N., Valli A., Fuchs C., and Hengstschlager M. (2010). mTOR phosphorylated at S2448 binds to raptor and rictor. Amino Acids. 38, 223-228.

Ruan HB., Singh JP., Li MD., Wu J., and Yang X. (2013). Cracking the O-GlcNAc code in metabolism. Trends Endocrinol Metab. 24, 301-309.

Ryu JM., Baek YB., Shin MS., Park JH., Park SH., Lee JH., and Han HJ. (2014). Sphingosine-1-phosphate-induced Flk-1 transactivation stimulates mouse embryonic stem cell proliferation through S1P1/S1P3-dependent β-arrestin/c-Src pathways. Stem Cell Res. 12, 69-85.

Ryu JM., and Han HJ. (2015a). Autotaxin-LPA axis regulates

hMSC migration by adherent junction disruption and cytoskeletal rearrangement via LPAR1/3-dependent PKC/GSK3β/β-catenin and PKC/Rho GTPase pathways. Stem Cells. 33, 819-832.

Ryu JM., Lee HJ., Jung YH., Lee KH., Kim DI., Kim JY., Ko SH., Choi GE., Chai, II., Song EJ., Oh JY., Lee SJ., and Han HJ. (2015b). Regulation of Stem Cell Fate by ROS-mediated Alteration of Metabolism. Int J Stem Cells. 8, 24-35.

Samartsev VN., Belosludtsev KN., Chezganova SA., and Zeldi IP. (2002). Effect of ethanol on the palmitate-induced uncoupling of oxidative phosphorylation in liver mitochondria. Biochemistry (Mosc). 67, 1240-1247.

Sarbassov DD., Guertin DA., Ali SM., and Sabatini DM. (2005). Phosphorylation and regulation of Akt/PKB by the rictor-mTOR complex. Science. 307, 1098-1101.

Saxton RA., and Sabatini DM. (2017). mTOR Signaling in Growth, Metabolism, and Disease. Cell. 169, 361-371.

Schaffer SW., Croft CB., and Solodushko V. (2000). Cardioprotective effect of chronic hyperglycemia: effect on hypoxia-induced apoptosis and necrosis. Am J Physiol Heart Circ Physiol. 278, H1948-1954.

Scherz-Shouval R., and Elazar Z. (2011). Regulation of autophagy by ROS: physiology and pathology. Trends Biochem Sci. 36, 30-38.

Schneider A., Younis RH., and Gutkind JS. (2008). Hypoxia-

induced energy stress inhibits the mTOR pathway by activating an AMPK/REDD1 signaling axis in head and neck squamous cell carcinoma. Neoplasia. 10, 1295-1302.

Schofield R. (1978). The relationship between the spleen colony-forming cell and the haemopoietic stem cell. Blood Cells. 4, 7-25.

Scholz G., Jandus C., Zhang L., Grandclement C., Lopez-Mejia IC., Soneson C., Delorenzi M., Fajas L., Held W., Dormond O., and Romero P. (2016). Modulation of mTOR signalling triggers the formation of stem cell-like memory T cells. EBioMedicine. 4, 50-61.

Schosserer M., Reynoso R., Wally V., Jug B., Kantner V., Weilner S., Buric I., Grillari J., Bauer JW., and Grillari-Voglauer R. (2015). Urine is a novel source of autologous mesenchymal stem cells for patients with epidermolysis bullosa. BMC Res Notes. 8, 767.

Shafi R., Iyer SP., Ellies LG., O'Donnell N., Marek KW., Chui D., Hart GW., and Marth JD. (2000). The O-GlcNAc transferase gene resides on the X chromosome and is essential for embryonic stem cell viability and mouse ontogeny. Proc Natl Acad Sci U S A. 97, 5735-5739.

Shi D., Li X., Chen H., Che N., Zhou S., Lu Z., Shi S., and Sun L. (2014). High level of reactive oxygen species impaired mesenchymal stem cell migration via overpolymerization of F-actin cytoskeleton in systemic lupus erythematosus. Pathol Biol (Paris). 62, 382-390.

Shimano H., Horton JD., Hammer RE., Shimomura I., Brown MS., and Goldstein JL. (1996). Overproduction of cholesterol and fatty acids causes massive liver enlargement in transgenic mice expressing truncated SREBP-1a. J Clin Invest. 98, 1575-1584.

Siebert N., Xu W., Grambow E., Zechner D., and Vollmar B. (2011). Erythropoietin improves skin wound healing and activates the TGF-β signaling pathway. Lab Invest. 91, 1753-1765.

Simon MC., and Keith B. (2008). The role of oxygen availability in embryonic development and stem cell function. Nat Rev Mol Cell Biol. 9, 285-296.

Singh LP., Cheng DW., Kowluru R., Levi E., and Jiang Y. (2007). Hexosamine induction of oxidative stress, hypertrophy and laminin expression in renal mesangial cells: effect of the anti-oxidant α-lipoic acid. Cell Biochem Funct. 25, 537-550.

Smith AG. (2001). Embryo-derived stem cells: of mice and men. Annu Rev Cell Dev Biol. 17, 435-462.

Sodi VL., Bacigalupa ZA., Ferrer CM., Lee JV., Gocal WA., Mukhopadhyay D., Wellen KE., Ivan M., and Reginato MJ. (2017). Nutrient sensor O-GlcNAc transferase controls cancer lipid metabolism via SREBP-1 regulation. Oncogene. Epub ahead of print. doi: 10.1038/onc.2017.395.

Solomon SS., Majumdar G., Martinez-Hernandez A., and Raghow R. (2008). A critical role of Sp1 transcription factor in regulating gene expression in response to insulin and other hormones. Life Sci.

83, 305-312.

Song C., Song C., and Tong F. (2014). Autophagy induction is a survival response against oxidative stress in bone marrow-derived mesenchymal stromal cells. Cytotherapy. 16, 1361-1370.

Song H., Cha MJ., Song BW., Kim IK., Chang W., Lim S., Choi EJ., Ham O., Lee SY., Chung N., Jang Y., and Hwang KC. (2010). Reactive oxygen species inhibit adhesion of mesenchymal stem cells implanted into ischemic myocardium via interference of focal adhesion complex. Stem Cells. 28, 555-563.

Sowter HM., Ratcliffe PJ., Watson P., Greenberg AH., and Harris AL. (2001). HIF-1-dependent regulation of hypoxic induction of the cell death factors BNIP3 and NIX in human tumors. Cancer Res. 61, 6669-6673.

Speakman CM., Domke TC., Wongpaiboonwattana W., Sanders K., Mudaliar M., van Aalten DM., Barton GJ., and Stavridis MP. (2014). Elevated O-GlcNAc levels activate epigenetically repressed genes and delay mouse ESC differentiation without affecting naive to primed cell transition. Stem Cells. 32, 2605-2615.

Suda T., Arai F., and Hirao A. (2005). Hematopoietic stem cells and their niche. Trends Immunol. 26, 426-433.

Suh HN., Lee YJ., Kim MO., Ryu JM., and Han HJ. (2014). Glucosamine-induced Sp1 O-GlcNAcylation ameliorates hypoxia-induced SGLT dysfunction in primary cultured renal proximal tubule cells. J Cell Physiol. 229, 1557-1568.

Sul HS., and Wang D. (1998). Nutritional and hormonal regulation of enzymes in fat synthesis: studies of fatty acid synthase and mitochondrial glycerol-3-phosphate acyltransferase gene transcription. Annu Rev Nutr. 18, 331-351.

Sun K., Zhang Y., D'Alessandro A., Nemkov T., Song A., Wu H., Liu H., Adebiyi M., Huang A., Wen YE., Bogdanov MV., Vila A., O'Brien J., Kellems RE., Dowhan W., Subudhi AW., Jameson-Van Houten S., Julian CG., Lovering AT., Safo M., Hansen KC., Roach RC., and Xia Y. (2016). Sphingosine-1-phosphate promotes erythrocyte glycolysis and oxygen release for adaptation to high-altitude hypoxia. Nat Commun. 7, 12086.

Teslaa T., and Teitell MA. (2015). Pluripotent stem cell energy metabolism: an update. EMBO J. 34, 138-153.

Theus MH., Wei L., Cui L., Francis K., Hu X., Keogh C., and Yu SP. (2008). In vitro hypoxic preconditioning of embryonic stem cells as a strategy of promoting cell survival and functional benefits after transplantation into the ischemic rat brain. Exp Neurol. 210, 656-670.

Thomson JA., Itskovitz-Eldor J., Shapiro SS., Waknitz MA., Swiergiel JJ., Marshall VS., and Jones JM. (1998). Embryonic stem cell lines derived from human blastocysts. Science. 282, 1145-1147.

Tracy K., and Macleod KF. (2007). Regulation of mitochondrial integrity, autophagy and cell survival by BNIP3. Autophagy. 3,

616-619.

Unzek S., Zhang M., Mal N., Mills WR., Laurita KR., and Penn MS. (2007). SDF-1 recruits cardiac stem cell-like cells that depolarize in vivo. Cell Transplant. 16, 879-886.

Vadysirisack DD., and Ellisen LW. (2012). mTOR activity under hypoxia. Methods Mol Biol. 821, 45-58.

van der Heide LP., and Smidt MP. (2005). Regulation of FoxO activity by CBP/p300-mediated acetylation. Trends Biochem Sci. 30, 81-86.

Vazquez-Martin A., Van den Haute C., Cufi S., Corominas-Faja B., Cuyas E., Lopez-Bonet E., Rodriguez-Gallego E., Fernandez-Arroyo S., Joven J., Baekelandt V., and Menendez JA. (2016). Mitophagy-driven mitochondrial rejuvenation regulates stem cell fate. Aging (Albany NY). 8, 1330-1352.

Veevers-Lowe J., Ball SG., Shuttleworth A., and Kielty CM. (2011). Mesenchymal stem cell migration is regulated by fibronectin through $\alpha 5\beta 1$-integrin-mediated activation of PDGFR-β and potentiation of growth factor signals. J Cell Sci. 124, 1288-1300.

Veigel D., Wagner R., Stubiger G., Wuczkowski M., Filipits M., Horvat R., Benhamu B., Lopez-Rodriguez ML., Leisser A., Valent P., Grusch M., Hegardt FG., Garcia J., Serra D., Auersperg N., Colomer R., and Grunt TW. (2015). Fatty acid synthase is a metabolic marker of cell proliferation rather than malignancy in ovarian cancer

and its precursor cells. Int J Cancer. 136, 2078-2090.

Ventura FV., Ruiter JP., Ijlst L., Almeida IT., and Wanders RJ. (1995). Inhibition of oxidative phosphorylation by palmitoyl-CoA in digitonin permeabilized fibroblasts: implications for long-chain fatty acid β-oxidation disorders. Biochim Biophys Acta. 1272, 14-20.

Verma MK., Sadasivuni MK., Yateesh AN., Neelima K., Mrudula S., Reddy M., Smitha R., Biswas S., Chandravanshi B., Pallavi PM., Oommen AM., Jagannath MR., and Somesh BB. (2014). Activation of GPR40 attenuates chronic inflammation induced impact on pancreatic β-cells health and function. BMC Cell Biol. 15, 24.

Wagner W., Wein F., Seckinger A., Frankhauser M., Wirkner U., Krause U., Blake J., Schwager C., Eckstein V., Ansorge W., and Ho AD. (2005). Comparative characteristics of mesenchymal stem cells from human bone marrow, adipose tissue, and umbilical cord blood. Exp Hematol. 33, 1402-1416.

Wallace DC. (2005). A mitochondrial paradigm of metabolic and degenerative diseases, aging, and cancer: a dawn for evolutionary medicine. Annu Rev Genet. 39, 359-407.

Wang K., Zhang T., Dong Q., Nice EC., Huang C., and Wei Y. (2013). Redox homeostasis: the linchpin in stem cell self-renewal and differentiation. Cell Death Dis. 4, e537.

Wang L., Zhang T., Wang L., Cai Y., Zhong X., He X., Hu L., Tian S., Wu M., Hui L., Zhang H., and Gao P. (2017). Fatty acid synthesis is critical for stem cell pluripotency via promoting mitochondrial

fission. EMBO J. 36, 1330-1347.

Wang M., Yang Y., Yang D., Luo F., Liang W., Guo S., and Xu J. (2009). The immunomodulatory activity of human umbilical cord blood-derived mesenchymal stem cells in vitro. Immunology. 126, 220-232.

Wang R., Dillon CP., Shi LZ., Milasta S., Carter R., Finkelstein D., McCormick LL., Fitzgerald P., Chi H., Munger J., and Green DR. (2011). The transcription factor Myc controls metabolic reprogramming upon T lymphocyte activation. Immunity. 35, 871-882.

Wang S., Jiang B., Zhang T., Liu L., Wang Y., Wang Y., Chen X., Lin H., Zhou L., Xia Y., Chen L., Yang C., Xiong Y., Ye D., and Guan KL. (2015). Correction: Insulin and mTOR pathway regulate hdac3-mediated deacetylation and activation of PGK1. PLoS Biol. 13, e1002287.

Weissman IL., Anderson DJ., and Gage F. (2001). Stem and progenitor cells: origins, phenotypes, lineage commitments, and transdifferentiations. Annu Rev Cell Dev Biol. 17, 387-403.

Wells L., Gao Y., Mahoney JA., Vosseller K., Chen C., Rosen A., and Hart GW. (2002). Dynamic O-glycosylation of nuclear and cytosolic proteins: further characterization of the nucleocytoplasmic β-N-acetylglucosaminidase, O-GlcNAcase. J Biol Chem. 277, 1755-1761.

Wells L., Vosseller K., and Hart GW. (2001). Glycosylation of

nucleocytoplasmic proteins: signal transduction and O-GlcNAc. Science. 291, 2376-2378.

Wendel AA., Cooper DE., Ilkayeva OR., Muoio DM., and Coleman RA. (2013). Glycerol-3-phosphate acyltransferase (GPAT)-1, but not GPAT4, incorporates newly synthesized fatty acids into triacylglycerol and diminishes fatty acid oxidation. J Biol Chem. 288, 27299-27306.

Wu H., and Chen Q. (2015). Hypoxia activation of mitophagy and its role in disease pathogenesis. Antioxid Redox Signal. 22, 1032-1046.

Wu W., Lin C., Wu K., Jiang L., Wang X., Li W., Zhuang H., Zhang X., Chen H., Li S., Yang Y., Lu Y., Wang J., Zhu R., Zhang L., Sui S., Tan N., Zhao B., Zhang J., Li L., and Feng D. (2016a). FUNDC1 regulates mitochondrial dynamics at the ER-mitochondrial contact site under hypoxic conditions. EMBO J. 35, 1368-1384.

Wu Y., Chen K., Liu X., Huang L., Zhao D., Li L., Gao M., Pei D., Wang C., and Liu X. (2016b). Srebp-1 Interacts with c-Myc to Enhance Somatic Cell Reprogramming. Stem Cells. 34, 83-92.

Xiang X., Zhao J., Xu G., Li Y., and Zhang W. (2011). mTOR and the differentiation of mesenchymal stem cells. Acta Biochim Biophys Sin (Shanghai). 43, 501-510.

Xie M., and Roy R. (2012a). Increased levels of hydrogen peroxide induce a HIF-1-dependent modification of lipid metabolism in AMPK compromised *C. elegans* dauer larvae. Cell

Metab. 16, 322-335.

Yang SE., Ha CW., Jung M., Jin HJ., Lee M., Song H., Choi S., Oh W., and Yang YS. (2004). Mesenchymal stem/progenitor cells developed in cultures from UC blood. Cytotherapy. 6, 476-486.

Yang X., and Qian K. (2017). Protein O-GlcNAcylation: emerging mechanisms and functions. Nat Rev Mol Cell Biol. 18, 452-465.

Yang X., Su K., Roos MD., Chang Q., Paterson AJ., and Kudlow JE. (2001). O-linkage of N-acetylglucosamine to Sp1 activation domain inhibits its transcriptional capability. Proc Natl Acad Sci U S A. 98, 6611-6616.

Yasumoto Y., Miyazaki H., Vaidyan LK., Kagawa Y., Ebrahimi M., Yamamoto Y., Ogata M., Katsuyama Y., Sadahiro H., Suzuki M., and Owada Y. (2016). Inhibition of fatty acid synthase decreases expression of stemness markers in glioma stem cells. PLoS One. 11, e0147717.

Ying QL., Nichols J., Chambers I., and Smith A. (2003). BMP induction of Id proteins suppresses differentiation and sustains embryonic stem cell self-renewal in collaboration with STAT3. Cell. 115, 281-292.

Yoshida Y., Takahashi K., Okita K., Ichisaka T., and Yamanaka S. (2009). Hypoxia enhances the generation of induced pluripotent stem cells. Cell Stem Cell. 5, 237-241.

You JS., Frey JW., and Hornberger TA. (2012). Mechanical stimulation induces mTOR signaling via an ERK-independent

mechanism: implications for a direct activation of mTOR by phosphatidic acid. PLoS One. 7, e47258.

Zafir A., Readnower R., Long BW., McCracken J., Aird A., Alvarez A., Cummins TD., Li Q., Hill BG., Bhatnagar A., Prabhu SD., Bolli R., and Jones SP. (2013). Protein O-GlcNAcylation is a novel cytoprotective signal in cardiac stem cells. Stem Cells. 31, 765-775.

Zhang H., Bosch-Marce M., Shimoda LA., Tan YS., Baek JH., Wesley JB., Gonzalez FJ., and Semenza GL. (2008). Mitochondrial autophagy is an HIF-1-dependent adaptive metabolic response to hypoxia. J Biol Chem. 283, 10892-10903.

Zhang H., Li H., Ho N., Li D., and Li S. (2012). Scd1 plays a tumor-suppressive role in survival of leukemia stem cells and the development of chronic myeloid leukemia. Mol Cell Biol. 32, 1776-1787.

Zhang S., Zhao Y., Xu M., Yu L., Zhao Y., Chen J., Yuan Y., Zheng Q., and Niu X. (2013). FoxO3a modulates hypoxia stress induced oxidative stress and apoptosis in cardiac microvascular endothelial cells. PLoS One. 8, e80342.

Zhang X., Yang R., Jia Y., Cai D., Zhou B., Qu X., Han H., Xu L., Wang L., Yao Y., and Yang G. (2014). Hypermethylation of Sp1 binding site suppresses hypothalamic POMC in neonates and may contribute to metabolic disorders in adults: impact of maternal dietary CLAs. Diabetes. 63, 1475-1487.

Zhao D., Yang J., and Yang L. (2017). Insights for oxidative stress and mTOR signaling in myocardial ischemia/reperfusion injury under diabetes. Oxid Med Cell Longev. 2017, 6437467.

Zhou H., and Huang S. (2011). Role of mTOR signaling in tumor cell motility, invasion and metastasis. Curr Protein Pept Sci. 12, 30-42.

Zhou J., Su P., Wang L., Chen J., Zimmermann M., Genbacev O., Afonja O., Horne MC., Tanaka T., Duan E., Fisher SJ., Liao J., Chen J., and Wang F. (2009). mTOR supports long-term self-renewal and suppresses mesoderm and endoderm activities of human embryonic stem cells. Proc Natl Acad Sci U S A. 106, 7840-7845.

Zhou J., Wulfkuhle J., Zhang H., Gu P., Yang Y., Deng J., Margolick JB., Liotta LA., Petricoin E, 3rd., and Zhang Y. (2007). Activation of the PTEN/mTOR/STAT3 pathway in breast cancer stem-like cells is required for viability and maintenance. Proc Natl Acad Sci U S A. 104, 16158-16163.

Zhu Y., Massen S., Terenzio M., Lang V., Chen-Lindner S., Eils R., Novak I., Dikic I., Hamacher-Brady A., and Brady NR. (2013). Modulation of serines 17 and 24 in the LC3-interacting region of Bnip3 determines pro-survival mitophagy versus apoptosis. J Biol Chem. 288, 1099-1113.

국 문 초 록

저산소 유도 지질대사 효소 발현이 mTOR 신호에 의한 줄기세포 행동에 미치는 영향

The effect of hypoxia-induced lipid metabolic enzymes expression on mTOR signaling-regulated behavior of stem cells

서울대학교 대학원
수의학과 수의생명과학 전공
이 현 직
지도교수 한 호 재

저산소 환경에서 일어나는 영양소 대사 조절은 줄기세포의 항상성 유지와 세포 행동 조절을 위한 필수요소이다. 특히, 지질대사 및 지질대사체는 줄기세포의 에너지대사, 분화능, 증식능, 이주능 조절에

있어 중요한 역할을 담당한다. 이전 연구자들은 저산소 환경에서 유도되는 미토콘드리아 자가 탐식과 O-GlcNAc 수식화 신호가 대사조절과 밀접한 관련이 있음을 제시하였다. 하지만 미토콘드리아 자가 탐식과 O-GlcNAc 수식화 신호 조절이 저산소 환경에 노출된 줄기세포 지질대사와 이주능, 증식능, 세포사멸과 같은 행동 조절에 미치는 영향에 대해서는 자세히 알려져 있지 않다. 따라서 본 연구는 1) 줄기세포에서 저산소 환경이 지질대사 조절 효소 발현에 미치는 영향과 지질대사체에 의한 세포 행동 조절 효과를 조사하고, 2) 저산소 환경에 의해 조절되는 미토콘드리아 자가 탐식 및 O-GlcNAc 수식화 신호가 지질대사 조절 효소 발현에 미치는 영향 및 관련 기전을 규명하기 위해 수행되었다. 결과는 아래와 같다.

1. 저산소 처리는 줄기세포의 증식능과 이주능을 증가시켰으며, 지방산 합성 효소인 FASN의 발현을 증가시켰다. FASN 억제제 처리는 저산소 환경에 의해 증가된 줄기세포 증식능을 감소시켰다. 이외에도 저산소 환경은 HIF-1α/SREBP1 경로활성을 통한 FASN 발현과 mTOR의 인산화(Ser2481, Ser2448)를 증가시켰으며, 이는 FASN 억제제 전처리에 의해 감소되었다. FASN 또는 mTOR 억제제 전처리는 저산소 처리에 의해 증가되었던 줄기세포의 증식능과 이주능을 억제시켰다. 저산소 처리는 세포주기 조절 단백질의 발현과 세포골격 조절 단백질의 발현 및 활성을 촉진시켰으며, 이는 mTORC1 신호 조절 단백질인 RAPTOR 발현 억제에 의해 감소되었다. 따라서 저산소 환경은 HIF-1α/SREBP1 신호경로 활성을 통해서 FASN 발현을 유도하며, 이는 mTORC1 신호 활성을 통하여 줄기세포의 증식능과 이주능을 촉진시켰다.

2. 저산소 처리는 줄기세포내 미토콘드리아 표지 단백질 발현을 감소시켰으며, 미토콘드리아 자가 탐식 조절 단백질인 BNIP3의 발현을 증가시켰다. BNIP3 발현 억제는 저산소 환경에 의해 유도되는 줄기세포의 미토콘드리아 자가탐식 작용을 억제시켰으며, 세포 생존율과 이주능을 감소시켰다. 저산소 환경에 의해 활성화된 HIF-1α와 FOXO3 신호경로는 BNIP3의 전사를 증가시켰다. 또한 BNIP3의 발현 유도는 SREBP1/FASN 의존성 자유지방산 생성과 mTOR의 활성을 촉진시켰다. 마우스 상처치유 모델에서 BNIP3 발현이 억제된 줄기세포에 저산소 전처리 후 상처치유 모델에 이식은 저산소 전처리 줄기세포 단독 처리군에 비해 상처치유 효과, 이식세포 생착률을 감소시켰으며, 이는 팔미트산 전처리에 의해 회복되었다. 따라서 저산소 환경에 의해 유도된 BNIP는 미토콘드리아 자가 탐식 작용을 조절하는 주요 단백질로서 저산소 환경에서 유도되는 FASN 매개의 지방산 합성을 증가시키고 줄기세포의 이주능과 생존율을 향상시켰다.

3. 저산소 처리는 마우스 배아줄기세포의 생존율을 시간의존적으로 감소시켰다. O-GlcNAc 유도체 글루코사민 처리는 세포내 O-GlcNAc 수식화신호를 유의적으로 항진시켰으며, 저산소 처리에 의한 세포자멸사를 억제시켰다. 또한 글루코사민 처리는 저산소 처리에 의해 유도된 Sp1의 O-GlcNAc 수식화와 핵내 이동을 촉진시켜 GPAT1의 발현을 증가시켰다. GPAT1 발현 억제는 글루코사민 처리에 의한 mTOR 인산화와 세포 생존율을 감소시켰으며, 이는 GPAT1의 대사산물인 LPA 처리에 의하여 회복되었다. 마우스 피부허혈 모델에서 글루코사민이 전처리된 마우스 배아줄기세포의 이식은 세포 생착률과 피부 생활률을 증가시켰지만, 이는 GPAT1 발현 억제에 의해

감소되었다. 따라서 글루코사민을 이용한 마우스 배아줄기세포내 O-GlcNAc 수식화 항진은 GPAT1 매개의 mTOR 활성을 통해서 허혈성 손상에 의한 세포자멸사를 억제시켰다.

결론적으로 1) 저산소 환경에 의해 유도되는 HIF-1α/FASN/mTORC1 신호는 인간 제대혈 중간엽줄기세포의 증식능, 이주능, 생존율을 향상시키는 중요한 신호경로이다. 2) BNIP3는 저산소 환경에 노출된 줄기세포의 지방산 합성과 이주능 및 세포 사멸을 조절하는 주요 미토콘드리아 자가 탐식인자이다. 3) 글루코사민에 의한 O-GlcNAc 수식화 신호 항진은 GPAT1 발현을 유도해 마우스 배아줄기세포의 허혈성 손상을 감소시켰다. 이러한 연구 결과는 저산소 유도 지질대사에 기반한 줄기세포 행동 조절의 기초자료를 제시함으로써 향후 세포치료제 개발에 활용될 수 있을 것이다.

주요어: 줄기세포, 저산소 환경, 지방산 합성, O-GlcNAc 수식화, 미토콘드리아 자가 탐식, FASN, GPAT1, BNIP3

학번: 2013-21541